PhD

3rd CYCLE

FCUP
UA
2025

U.PORTO

Self-burning of Coal Mining Wastes Environmental and Ecotoxicological Approaches

Aracelis del Carmen Narayan Rajnauth

FC

U.PORTO
FACULDADE DE CIÊNCIAS
UNIVERSIDADE DO PORTO

universidade de aveiro
theoria poiesis praxis

Self-burning of Coal Mining Wastes Environmental and Ecotoxicological Approaches

Aracelis del Carmen Narayan Rajnauth
Doctoral Program in Earth Sciences
Faculty of Sciences of the University of Porto and University of Aveiro
2025

U.PORTO
FACULDADE DE CIÊNCIAS
UNIVERSIDADE DO PORTO

universidade de aveiro
theoria poiesis praxis

PhD

Self-burning of Coal Mining Wastes Environmental and Ecotoxicological Approaches

Aracelis del Carmen Narayan Rajnauth

Thesis carried out as part of the Doctoral Program in Earth Sciences

Department of Geosciences, Environment and Spatial Plannings

2025

Supervisor
Deolinda Maria dos Santos Flores Marcelo da Fonseca, Full Professor, Faculty of Sciences of the University of Porto

Co-supervisor
Jorge Manuel Espinha Marques, Assistant Professor, Faculty of Sciences of the University of Porto

Co-supervisor
Sara Cristina Ferreira Marques Antunes, Associate Professor, Faculty of Sciences of the University of Porto

“…Om gurur brahmā gurur vishṇu gurur devo maheśvarah

Gurureva param brahma tasmai śrī gurave namah…”

To my roots, Carmen and Harry,

To my flower and fruit, Cristina and Manuelito,

To my strong stem, Manuel,

The loves of my life…

Acknowledgements

To my Hindu Gods: Brahma, Shiva and Vishnu, for giving me the strength and conviction.

To the University of Porto for allowing me to study for this PhD.

To Dr Deolinda Flores, thank you for accepting to be my guide on this journey. Your knowledge, experience, and patience open my eyes and mind to a new story in my life.

To Dr Jorge Espinha, I don´t have enough words to express my gratitude. You were the first person I contacted, and from that moment until now, you have been unconditional. I learned a lot during the fieldwork and while writing my thesis, your guidance helped me understand the processes and dynamics of hydropedology.

To Dr Sara Antunes, Thanks for the opportunity to work with you and your excellent team. Through the work carried out in the laboratory, I was able to rediscover my passion for my role as a chemist. When I mentioned that I wanted to work in ecotoxicology, what I had in mind was phytoremediation. But getting to know you made me see a world of possibilities within this area. Thank you for your patience, positivity, and encouragement when I needed it most.

To Barbara Diogo, Mariana Costa, Patricia Santos, and Paulo Ferreira, for their support in the lab and during the sampling campaign.

To my family: Manuel, my husband, who had to deal with my bad mood, loved me and helped me; thank you for your patience during this journey. Without you, I am nothing… My kids, Cristina and Manuelito, the loves of my life, always support me, encourage me, and love me…

To my brother and sister: Damelis Narayan and Wilfredo Narayan

To my dear and loving Friends: Alcis Pereira and Gerlys Doural

To my friends: Sonia, Marcelo, Alfredo, Ana and Sandra, my new family…

This research was supported by the “SHS: Soil health surrounding former mining areas: characterisation, risk analysis, and intervention” Project, financed by NORTE-45-2020-75-SISTEMA DE APOIO À INVESTIGAÇÃO CIENTÍFICA E TECNOLÓGICA - “PROJETOS ESTRUTURADOS DE I&D” - HORIZONTE EUROPA, Ref. NORTE-01-0145-FEDER-000056 and framed within the ICT G3 activities (UIDB/04683/2020 and UIDP/04683/2020).

Resumo

A autocombustão de resíduos de carvão (RMC) resultantes da atividade mineira constitui um problema ambiental complexo, envolvendo não apenas a emissão de substâncias perigosas, mas também a alteração dos solos e dos ecossistemas circundantes. A escombreira da mina do Fojo entrou em ignição em 2017, na sequência de fogos florestais, tendo sido extinta em 2019, após a remobilização dos materiais da escombreira, associada à utilização de um agente de arrefecimento misturado com água e, posteriormente, cobertos com material lítico de natureza inerte. No âmbito do desenvolvimento desta Tese de Doutoramento procedeu-se à investigação os impactes ambientais das escombreiras de resíduos de carvão que sofreram autocombustão na área de Fojo, localizada na Bacia Carbonífera do Douro (Portugal), através de uma abordagem geoambiental e ecotoxicológica integrada.

A estratégia adotada consistiu, em primeiro lugar, em caracterizar os resíduos resultantes da atividade mineira de carvão através de análises petrográficas, mineralógicas e geoquímicas, a fim de determinar a sua composição, modo de ocorrência e diferenças resultantes da transformação induzida pela combustão. Em seguida, foram exploradas as alterações na estrutura do solo, retenção de água, condutividade hidráulica, dinâmica de nutrientes e metais através das propriedades hidropedológicas dos solos afetados pelos resíduos que sofreram autocombustão. Posteriormente, os efeitos dos lixiviados derivados dos resíduos de carvão e do solo foram avaliados através de uma abordagem ecotoxicológica, utilizando um conjunto de espécies bioindicadoras para determinar os riscos potenciais para os ecossistemas aquáticos e terrestres.

A área de deposição dos resíduos resultantes da atividade mineira do carvão na região do Fojo foi dividida em seis zonas: solo a montante da escombreira (US), resíduos resultantes da atividade mineira do carvão que não sofreram combustão (UCW), resíduos resultantes da atividade mineira do carvão que sofreram combustão (BCW), material misto (MBW), camada de cobertura do solo queimado (CL) e solo a jusante da escombreira, do sentido de drenagem (DS). As áreas US e DS são zonas sem acumulação de resíduos mineiros.

A caracterização destes resíduos mineiros, a vitrinite é o grupo maceral predominante, na fração orgânica, com valores de refletância mais elevados observados em UCW, sugerindo material termicamente inalterado. Os resíduos de BCW e MBW exibiram sinais de transformação a alta temperatura, tais como oxidação de pirite framboidal de

reação, vacúolos de desvolatilização e, pontualmente, carbono pirolítico. A microscopia eletrónica de varrimento revelou um conjunto de minerais distintos, entre os tipos de resíduos, pirite, óxidos de ferro, zircão, rútilo, xenótimo (fosfato de Y com Dy e Gd) e também monazite (fosfato de Ce com La e Nd), esta por vezes contendo Th e U. Foram, ainda, identificadas partículas de cinábrio, galena, florencite (fosfato de Ce com Al), arsenopirite e também um sulfato de Ag. A assinatura geoquímica é idêntica entre as amostras que sofreram combustão e as áreas que contêm material de mistura. No entanto, quando comparadas com resíduos mineiros não afetados por combustão, denotam um enriquecimento em Fe, Na, S, As, Bi, Sc, Sr, Th, ∑LREE. As amostras afetadas por combustão apresentaram empobrecimentos nos elementos Ca, Mn, Hf, Co, Ni, Pb, Mo e Zr quando comparadas com as amostras de materiais que não sofreram efeitos pirolíticos. A distribuição dos elementos vestigiais foi inferida usando ferramentas estatísticas, identificando frações geoquímicas associadas a aluminossilicatos, carbonatos, fosfatos e sulfuretos. Relativamente à concentração de hidrocarbonetos aromáticos policíclicos (PAH), os de baixa massa molecular ocorrem em concentrações elevadas tanto nos resíduos queimados quanto nos não queimados, com evidências de enriquecimento pirolítico e de deposição subsequente nos solos florestais a montante após as operações de extinção da combustão.

Foram investigadas as alterações hidropedológicas da escombreira de resíduos de extração de carvão do Fojo. Aplicou-se uma abordagem integradora, que começou pela delimitação de zonas hidropedológicas com base nas observações de campo dos fatores de formação do solo. Em cada zona, os perfis de solo foram descritos segundo as suas características morfológicas e os horizontes minerais mais superficiais foram amostrados para análise da geoquímica de elementos potencialmente tóxicos e mineralogia. Foram também efetuadas medições de campo da condutividade hidráulica não saturada, do teor de água do solo e da hidrofobicidade. Foi avaliado o potencial de lixiviação dos solos e determinadas as assinaturas hidrogeoquímicas. Os resultados revelaram diferenças significativas entre as zonas hidropedológicas, incluindo variações no desenvolvimento do perfil do solo, na composição mineral e na geoquímica de elementos potencialmente tóxicos, bem como uma condutividade hidráulica não saturada mais elevada e um aumento da lixiviação de iões maiores e dos referidos elementos nas áreas influenciadas pela atividade mineira. Uma análise de componentes principais confirmou, ainda, a existência de padrões distintos, concordantes com o zonamento hidropedológico. Os resultados destacam o papel significativo dos regimes hidropedológicos no transporte de poluentes e na vulnerabilidade da água subterrânea à poluição em áreas mineiras abandonadas.

Bioensaios realizados com *Aliivibrio fischeri*, *Daphnia magna*, *Lemna minor* e *Lactuca sativa* revelaram sensibilidades específicas de cada espécie, sendo *A. fischeri* e *L. sativa* as espécies mais sensíveis. A toxicidade observada foi associada a valores de pH baixos, altas concentrações de Fe, Mn, NO_2^- e outros iões, com evidências de efeitos sinérgicos envolvendo PAH. A toxicidade mais elevada foi observada nos elutriados de UCW e nalgumas amostras de solo florestal, indicando o potencial de contaminação difusa por vias atmosféricas e hidrológicas. Esses resultados enfatizam a necessidade de estratégias integradas de avaliação de risco que considerem não apenas a contaminação por metais, mas também o papel dos contaminantes orgânicos e suas interações.

Em geral, os resultados revelaram que, apesar da baixa concentração de metais-traço no lixiviado, certos materiais, particularmente resíduos não queimados (UW) e solos florestais a montante (US), exibiram toxicidade significativa. Isso sugere que outros fatores, notadamente a presença de contaminantes orgânicos, como hidrocarbonetos aromáticos policíclicos (PAH), podem desempenhar um papel crítico na toxicidade. Além disso, as evidências indicam que a extinção da combustão e a deposição atmosférica de subprodutos dessa combustão contribuíram para a contaminação dos solos circundantes.

Este estudo destaca a importância de estratégias abrangentes de avaliação de risco que considerem parâmetros geoquímicos e ecotoxicológicos em ambientes pós-mineração. As descobertas contribuem para uma melhor compreensão dos impactes dos resíduos resultantes da atividade mineira de carvão em Portugal e apoiam o desenvolvimento de medidas de monitorização e de remediação mais eficazes.

Palavras-chave: Resíduos mineiros de carvão, Autocombustão, Petrologia, Mineralogia, Geoquímica, Pedologia, Ecotoxicologia, espécies-padrão.

Abstract

The self-burning of coal mining waste (CMW) is a complex environmental problem, involving not only the emission of hazardous substances, but also changes to the surrounding soil and ecosystems. The Fojo mine waste dump caught fire in 2017 following forest fires and was extinguished in 2019 after the waste dump materials were remobilised using a cooling agent mixed with water and subsequently covered with inert lithic material. This doctoral thesis investigated the environmental impacts of coal waste dumps that underwent self-burning in the Fojo area, located in the Douro Carboniferous Basin (Portugal), through an integrated geo-environmental and ecotoxicological approach.

The strategy adopted consisted, first, of characterising the waste resulting from coal mining through petrographic, mineralogical and geochemical analyses, in order to determine its composition, mode of occurrence and differences resulting from combustion-induced transformation. Second, changes in soil structure, water retention, hydraulic conductivity, nutrient dynamics, and metal content were explored through the hydropedological properties of soils affected by waste that had undergone self-burning. Subsequently, the effects of leachates derived from coal waste and soil were assessed using an ecotoxicological approach, employing a set of bioindicator species to determine the potential risks to both aquatic and terrestrial ecosystems.

The Fojo coal mining waste disposal area was divided into six different zones: uphill soil (US), unburned coal waste (UCW), burned coal waste (BCW), mixed burned coal waste (MBW), cover layer (CL), and downhill soil (DS). The US and DS areas are surrounding areas without coal mining waste.

The results reveal that vitrinite is the predominant maceral group in the organic fraction of mining waste, with higher reflectance values observed in UCW, suggesting thermally unaltered material. The BCW and MBW showed signs of high-temperature transformation, such as oxidation of framboidal pyrite, devolatilisation vacuoles and, occasionally, pyrolytic carbon. Scanning electron microscopy revealed a set of distinct minerals among the types of waste, including pyrite, iron oxides, zircon, rutile, xenotime (Y phosphate with Dy and Gd) and also monazite (Ce phosphate with La and Nd), the latter sometimes containing Th and U. Particles of cinnabar, galena, florencite (Ce phosphate with Al), arsenopyrite and also Ag sulphate were also identified. The geochemical signature is identical between the samples that underwent combustion and the areas containing mixed material. However, when compared to mining residues not affected by combustion, they show enrichment in Fe, Na, S, As, Bi, Sc, Sr, Th, ∑LREE.

The samples affected by combustion showed depletion of the elements Ca, Mn, Hf, Co, Ni, Pb, Mo and Zr when compared to samples of materials that did not undergo pyrolytic effects. The distribution of trace elements was inferred using statistical tools, identifying geochemical fractions associated with aluminosilicates, carbonates, phosphates and sulphides. Regarding the concentration of polycyclic aromatic hydrocarbons (PAH), those with low molecular mass occur in high concentrations in both burned and unburned residues, with evidence of pyrolytic enrichment and subsequent deposition in uphill soils after combustion extinguishing operations.

The changes in the hydropedological conditions of the Fojo coal mining waste pile was investigated. An integrative approach was applied, beginning with the delineation of hydropedological zones based on field observations of soil-forming factors. Within each zone, soil profiles were characterised by their morphological features, and upper mineral horizons were sampled for mineralogical and potentially toxic elements (PTE) geochemistry. In addition, field measurements of unsaturated hydraulic conductivity, soil water content, and hydrophobicity were conducted. The hydrogeochemistry of soil leachates was assessed, and the leaching potential of the soils was evaluated. The results revealed significant differences among the hydropedological zones, including variations in the soil profile development, mineral composition, and Potentially Toxic Elements geochemistry, as well as higher unsaturated hydraulic conductivity and increased leaching of major ions and of the mentioned elements in areas influenced by coal mining activity. A Principal Component Analysis further confirmed the existence of distinct patterns aligned with the hydropedological zoning. These findings highlight the significant role of hydropedological regimes in the transport of pollutants and the vulnerability of groundwater to pollution in abandoned mining areas.

Bioassays conducted with *Aliivibrio fischeri*, *Daphnia magna*, *Lemna minor* and *Lactuca sativa* revealed species-specific sensitivities, with *A. fischeri* and *L. sativa* being the most responsive species. Toxicity observed was linked to low pH, high concentrations of Fe, Mn, NO_2^-, and other ions, with evidence of synergistic effects involving PAH. The highest toxicity was observed in eluates from UCW and some uphill soil samples, indicating the potential for diffuse contamination through atmospheric and hydrological pathways. These results emphasise the need for integrated risk assessment strategies that consider not only metal contamination but also the role of organic contaminants and their interactions.

Overall, the results revealed that despite the relatively low concentration of trace metals in the leachate, certain materials, particularly unburned waste (UW) and uphill soils (US),

exhibited significant toxicity. This suggests that other factors, notably the presence of organic contaminants such as polycyclic aromatic hydrocarbons (PAH), may play a critical role in toxicity. Furthermore, evidence suggests that the extinction of combustion and atmospheric deposition of combustion by-products contributed to the contamination of surrounding soils.

This study highlights the importance of comprehensive risk assessment strategies that take into account geochemical and ecotoxicological parameters in post-mining environments. The findings contribute to a better understanding of the legacy impacts of coal mining waste in Portugal and support the development of more effective monitoring and remediation measures.

Keywords: Coal mining waste, Self-burning, Petrology, Mineralogy, Geochemistry, Pedology, Ecotoxicology, standard species.

Table of Contents

List of Tables

List of Figures

List of Abbreviations

AMD	ACID MINE DRAINAGE
ANOVA	ANALYSIS OF VARIANCE
APA	PORTUGUESE ENVIRONMENTAL AGENCY
ASTM	AMERICAN SOCIETY FOR TESTING AND MATERIALS
BCW	BURNED COAL WASTE
BCWDC	BURNED COAL WASTE FROM THE DOURO COALFIELD
CANOCO	CANONICAL COMMUNITY ORDINATION
CAT	CATALASE
CDF	CANONICAL DISCRIMINANT FUNCTION
CEMUP	MATERIALS CENTRE OF THE UNIVERSITY OF PORTO
CSF	SEGMENTED FLOW INSTRUMENT
CIZ	CENTRAL IBERIAN ZONE
CL	COVER LAYER
CMW	COAL MINING WASTE
CO	CARBON MONOXIDE
CO_2	CARBON DIOXIDE
DCB	DOURO CARBONIFEROUS BASIN
DC	DOURO COALFIELD
DC_{COAL}	THE COAL FROM THE DOURO COALFIELD
DC_{LITHO}	THE LITHOLOGY FROM THE DOURO COALFIELD
DS	DOWNHILL SOIL
EC	ELECTRIC CONDUCTIVITY
EC_{50}	EFFECTIVE CONCENTRATION 50%
EDM	EMPRESA DE DESENVOLVIMENTO MINEIRO
EF	ENRICHMENT FACTOR
EPA	ENVIRONMENTAL PROTECTION AGENCY
FAO	FOOD AND AGRICULTURE ORGANISATION
HMW	HEAVY MOLECULAR WEIGTH
HREE	HEAVY RARE EARTH ELEMENT
H_2S	HYDROGEN SULPHUR
ICCP	INTERNATIONAL COMMITTEE FOR COAL AND ORGANIC PETROLOGY
ICP-OES/MS	INDUCTIVELY COUPLED PLASMA OPTICAL EMISSION/MASS SPECTROMETRY
IPB	IBERIAN PYRITE BELT

IPMA	ATMOSPHERE AND OCEAN PORTUGUESE INSTITUTE
K	HYDRAULIC CONDUCTIVITY
LNEG	NATIONAL LABORATORY FOR GEOLOGY AND ENERGY
LMW	LOW MOLECULAR WEIGHT
LREE	LIGHT RARE EARTH ELEMENT
MBW	MIXED BURNED COAL WASTE
MDA	MALONDIALDEHYDE
MDI	MINI DISK INFILTROMETER
NE	NORTH EAST
NW	NORTH WEST
OECD	ORGANISATION FOR ECONOMIC CO-OPERATION AND DEVELOPMENT
OM	ORGANIC MATTER
PAH	POLYCYCLIC AROMATIC HYDROCARBONS
PCA	PRINCIPAL COMPONENT ANALYSIS
PTE	POTENTIALLY TOXIC ELEMENTS
PUFA	POLYUNSATURATED FATTY ACIDS
REE	RARE EARTH ELEMENTS
SE	SOUTH EAST
SEM-EDX	SCANNING ELECTRON MICROSCOPY-ENERGY DISPERSIVE X-RAY SPECTROMETRY
SHS	SOIL HEALTH SURROUNDING
SPAC	SOLUBLE, PARTICULATE, AND ADSORBED CARBON
SPC	SÃO PEDRO DA COVA
SPSS	STATISTICAL PACKAGE FOR THE SOCIAL SCIENCES
SO_X	SULPHUR OXIDES
TOC	TOTAL ORGANIC CARBON
UCW	UNBURNED COAL WASTE PILE
UCWDC	UNBURNED COAL WASTE FROM THE DOURO COALFIELD
US	UPHILL SOIL
USGS FLT	UNITED STATES GEOLOGICAL SURVEY FAULT
VOC_S	VOLATILE ORGANIC COMPOUNDS
WDPT	WATER DROP PENETRATION TIME
WHC	WATER HOLDING CAPACITY

Chapter 1. General Approach

1.1 Introduction

Coal mining waste (CMW) poses significant environmental and human health risks due to its potential for soil contamination, ecosystem disruption, and adverse effects on local populations. Understanding the physical, chemical, and biological behaviour of these materials is essential for the development of appropriate management strategies and the mitigation of their environmental footprint.

In the last century, many coal mines in Europe have been closed (Younger 2002). Indeed, coal production declined by 80% in 2022 compared to 1990 (Rouhani et al. 2024), leaving behind an important environmental legacy: coal mining waste (CMW). This waste management did not provide adequate environmental controls, and CMW has become a major pollution source in many countries (Adeniyi et al. 2022; Li et al. 2021; Ribeiro et al. 2013, 2016, 2020; Teodoro et al. 2021; Tiwary 2001).

The CMW is chemically heterogeneous, resulting from a mixture of coal mining fragments, operational mine residues, and hosting rocks (Gao et al. 2014; Modarres et al. 2015; Vo et al. 2022). The CMW is prone to particle breakage due to compaction, rapid degradation from wetting-drying cycles, and is susceptible to liquefaction when loosely deposited (Vo et al. 2022). The CMW is habitually dumped in landfill sites or incinerated, and its elemental composition depends on the surrounding geological setting, extraction methods, and beneficiation (García Giménez et al. 2016).

Once the CMW is exposed to atmospheric conditions, some waste oxidises and becomes more soluble and producing acid mine drainage (AMD), with mobilisation of solids particles and dissolved elements by water percolation and infiltration (Santos et al. 2023; Vo et al. 2002), as well as the mineralisation of new neoformed mineral products (Ribeiro et al. 2010b). At the same time, some waste particles are transported by wind and water, allowing different substances to leach into waterways and impact the local ecology (Ofori et al. 2023).

Effective CMW management requires a better understanding of fundamental behaviour, such as i) lixiviation due to weathering, which alters physical and chemical parameters; ii) the intrinsic properties of the original material; and iii) self-burning or spontaneous combustion processes (Skarżyńska 1995). Indeed, the self-burning process in CMW is considered the most dangerous environmental source for impact from CMW dumps. It is a critical factor, as it induces changes in the chemical and mineralogical composition, leads to the release of heat, the volatilisation of organic compounds (CO, CO_2, H_2S, SOx,

CH_4, volatile organic compound [VOC], polycyclic aromatic hydrocarbons [PAH], and phenols) (Flores et al. 2024), and the volatilisation, concentration, and mineralisation of inorganic elements (Ribeiro et al. 2010abc; Smoliński et al. 2021).

The pollutants are released into the atmosphere and deposited onto soil, vegetation, and freshwater. Other hazardous compounds remain in the waste material, where their concentrations can increase (Ribeiro et al. 2010 ab). The environmental impacts are only mentioned in the components of air, water bodies, and soils (Espinha Marques et al. 2021; Ribeiro et al. 2010 ab, 2011; Santos 2008; Santos et al. 2023). In some cases, it is mentioned that it could harm species, mainly vegetation, due to deterioration caused by the effects of self-burning and AMD. However, there is a lack of studies to provide evidence of the impacts of CMW on species (aquatic and terrestrial) and the behaviour of the leaches in soils.

The ecotoxicological impacts of CMW have not been explored, either in vegetation or in biota species. The environmental effects on soil, water bodies, and air have been studied; further research on species remains to be done.

1.2 Investigation Questions

The environmental legacy of coal mining waste activities continues to pose a significant risk, particularly in post-mining landscapes where residues are left exposed and unmanaged. Among these, self-burning CMW represent a specific and understudied threat due to the complex physicochemical transformations induced by spontaneous combustion processes. These transformations can lead to the formation of secondary minerals, the alteration of trace element speciation, and the generation of toxic compounds, such as polycyclic aromatic hydrocarbons (PAH), which possess an ecological risk.

In the Douro Carboniferous Basin (DCB), the Fojo site provides a representative case study of coal mining residues undergoing spontaneous combustion; however, little is known about their long-term environmental impacts. Existing research in similar contexts has often focused on either the geochemistry of altered materials or the environmental toxicity of leachates, but rarely integrates both within a landscape-scale perspective (Ribeiro et al 2010abc, 2011). This thesis addresses the gap by combining mineralogical and geochemical characterisation, hydropedological assessment, and ecotoxicological testing, thereby providing a holistic understanding of the fate and impact of the self-burning waste.

The findings are expected to support more informed risk assessment and management strategies in the former CMW area, especially in forested or semi-natural systems where monitoring is scarce. Furthermore, the interdisciplinary approach adopted here may serve as a framework for evaluating other legacy contaminants in post-industrial regions affected by spontaneous combustion processes.

The North of Portugal was associated with an important coal mining activity in the last two centuries. Portugal´s first coal exploration data dates back to 1773, and the leading coal mines were São Pedro de Cova and Pejão, located in the Douro Coalfield. These have been the most important coal producers, with many mines geographically dispersed along the Douro Carboniferous Basin. Coal mining activities, which ended in 1994, caused several impacts on the environment, one of which is the number of tailings, discarded material (mainly carbonaceous shales and lithic arenites), that was placed in many waste piles throughout the coalfield area (Ribeiro et al. 2010abc, 2011, 2012, 2013). Abandoned impacted areas, such as mines or industrial facilities, are common, and many exhibit high levels of environmental contamination.

In 2017, the Pejão coal mining area was affected by intense forest fires, and the Fojo waste dump began to burn. Since February 2018, the company Empresa de Desenvolvimento Mineiro, S.A. (EDM) has spent more than 1,600 k€ on efforts to extinguish the fire, focusing on the remobilisation of the coal waste material and using water and a cooling accelerator agent. This is a primary concern for soil and freshwater quality, as well as for ecotoxicological issues, since the effects of the cooling accelerator agent on fire extinction are uncertain and may impact entire ecosystems.

It is well known that the self-burning process of the CMW mobilises contaminants, such as particulate matter and gases, composed of organic and inorganic (e.g., potentially toxic elements) compounds, which may be emitted, released, or leached to soils, water, and atmosphere on the entire area and adjacent land. The coal self-burning can occur in piles where coal mining waste is deposited.

In the Douro Coalfield, specifically in the São Pedro da Cova (SPC) area, which includes coal mining waste from SPC, Midões and Lomba, there were reported petrographic, mineralogic, and geochemical descriptions (Ribeiro et al. 2010a, 2011), PAH (Ribeiro et al. 2012), and the effects of CMW lixiviate in soils and hydropedological features (Espinha Marques et al. 2021; Santos et al. 2023). On the other hand, the Pejão area was studied for nanomineral formation and was carried out a characterisation of the CMW in the Serrinha waste dump (Ribeiro et al. 2010bc), the CMW in Germunde and

Fojo (Ribeiro et al. 2022), freshwater systems (Santos 2008), and other coal waste dump sites (Ribeiro et al. 2011).

The Fojo coal mining waste dump has undergone its first general characterisation by Ribeiro et al. (2022). However, there is a gap in the information; a more detailed study is necessary to understand the interaction between the different types of coal waste, the cooling agent, and the site-specific soil material. At the same time, the environmental impacts of the CMW dumps on the soils, the runoff and/or infiltration of the AMD lixiviate into the soil layers, and the effects of these lixiviate on aquatic and terrestrial species need to be understood.

Characterising the CMW and the environmental impact are essential tools for managing and avoiding possible environmental issues that affect species and human health. The petrological, geochemical, and mineralogical characteristics of CMW, with and without combustion, in the mines of São Pedro da Cova, Lomba, Midões, and Serrinha were studied (Ribeiro et al 2010abc; Ribeiro et al 2011), as well as the effects on soils in São Pedro da Cova (Espinha Marques et al. 2021; Santos et al. 2023), however, the effects of the leachates on standard species are unknown.

The environmental impacts potentially associated with coal mining and self-burning include air pollution from gas emissions and particle dispersion; contamination of soil, surface water, and groundwater due to the mobilisation of solid particles, leaching of hazardous elements, dissolution of newly formed minerals, and deposition of airborne particles; landslides and mass movements triggered by weathering agents and combustion in coal waste piles; and damage to vegetation caused by acid drainage and the combustion process.

Based on these considerations, this thesis explores the following research questions:

1.- Are there differences in the petrographic, mineralogical, and geochemical features between the unburned, burned, and mixed coal mining waste in the Fojo CMW dump?

2.- Do the petrographic, mineralogical, and geochemical characteristics of the coal mining waste from the Fojo dump align with those from the SPC area and the Serrinha CMW dump? If not, what distinguishes them?

3.- Has the use of a cooling agent caused any alteration in the petrography, mineralogy, or geochemical composition of the coal mining waste?

4.- Are there changes in the hydropedological properties of the soils by the disposal of the coal mining waste in the Fojo CMW dump? Does the coal mining waste from the

Fojo dump exhibit hydropedological features and behaviours similar to those of the SPC area? What are the key differences?

5.- Could leachates from coal mining waste be toxic to aquatic and terrestrial species? What are the principal parameters affecting this toxicity? Which major or trace elements appear most toxic, and by what mechanisms? Could these species serve as indicators of coal mining waste toxicity?

1.3 Main Goal

The thesis is part of the Soil Health Surrounding Former Mining Areas: characterisation, risk analysis, and intervention (SHS) project, which analyses mining waste, soils, and waters impacted by mining activity. This thesis aims to evaluate the environmental consequences of self-burning coal mining waste from the Fojo site through an integrated petrographic, geochemical, pedological, and ecotoxicological framework.

By combining these complementary lines of evidence, the research aims to enhance the current understanding of the environmental risks posed by altered coal mining residues and their potential pathways of contaminant transfer within forested and semi-rural ecosystems.

To achieve the main goal, the following specific tasks were performed:

- The determination of the geochemical, petrographic, and mineralogical composition of the coal waste materials and the elements' mode of occurrence to identify the changes induced by the combustion process and the use of the cooling accelerator agent in the fire extinction.
- The assessment of changes in the hydropedological conditions due to the coal waste deposition and self-burning.
- The assessment of the ecotoxicological effects of water leachates from burned, unburned, mixed coal mining waste materials and soils in a multi-species (the bacteria *Aliivibrio fischeri*, the microcrustacean *Daphnia Magna*, the macrophyte *Lemna minor*, and the terrestrial plant *Lactuca sativa*) standard approach.

1.4 Thesis Structure

The thesis is presented in a typical format, with the goals achieved in a structure of six chapters to help readers understand the methodology, results, and discussion of coal mining waste characterisation, the impacts on soil hydropedological features, and the effects of the coal mining waste lixiviate on aquatic and terrestrial species. Each chapter has its reference.

Chapter 1. General Approach. This chapter provides an introduction to coal mining waste, outlines the purpose of the thesis, and presents the main objectives. Moreover, it defines the research and justifies questions, as well as the need for and importance of the study in terms of pollution effects.

Chapter 2. **State-of-the-art and the study area environmental settings.** This chapter provides a comprehensive review of the environmental impacts associated with coal mining waste. It contains the studies conducted in the Douro Coalfield for coal mining waste, where the geochemical, petrographic, and mineralogical characterisation of both burned and unburned waste material was performed. At the same time, the study area's environmental features are mentioned, with special emphasis on its geological settings. A geological characterisation, hydropedology, and ecotoxicology are summarily framed.

Chapter 3. The Fojo Coal Mining Waste Characterisation: Petrography, Mineralogy and Geochemistry. This chapter describes the methodology, results, discussion, and final remarks regarding the petrological, geochemical, and mineralogical (SEM) features of the coal mining waste, including burned, unburned, and mixed materials from the Fojo coal mining waste dump site. The polycyclic aromatic hydrocarbon (PAH) was measured in the different types of CMW. It also discusses and compares the results with others research already conducted at the Douro Coalfield.

Chapter 4. Hydropedology Characterisation of the Fojo Coal Mining Waste Deposition Area. The hydropedological features of the coal mining waste, including burned, unburned, mixed materials and surrounding soils (upper and down soils), are examined in this chapter. The outcomes of hydropedological aspects from rainy and sunny seasons are contrasted and discussed. It examines the enrichment from the CMW disposal area in the down soils as well as the chemical concentration of the major and trace elements in the leachates from the CMW in the waste dump area.

Chapter 5. Ecotoxicological Effects of the Coal Mining Waste Elutriate in Aquatic and Terrestrial Species. This chapter focuses on the ecotoxicological outcomes of the impact on standard species following exposure to elutriates from the soils of the burned, unburned, and mixed coal mining waste study area, as well as the cover layer. A series of bioassays was carried out using species from various trophic levels and endpoints, including acute assays (immobilisation/mortality of *Daphnia magna),* microtox assays (bioluminescence inhibition of the bacterium *Aliivibrio fischeri*), growth inhibition assay (*Lemna minor)*, and seed germination bioassay (*Lactuca sativa)*. Total chlorophyll content, CAT, and MDA were assessed for *L. minor* and *L. sativa*. Furthermore, biometric

parameters and morphological changes in early plant growth were measured for the terrestrial species *L. sativa* after exposure to the different waste and soil elutriates.

Chapter 6. **Conclusions**. The findings from Chapters 3, 4, and 5 are compiled and integrated from a multifactor perspective. It refers to the final remarks of the research performed, highlighting the key elements and selecting significant subjects for further study in relevant fields.

Chapter 2. Coal Mining Waste Environmental Impacts, Background Studies, and Environmental Settings of the Fojo Waste Pile.

2.1 Introduction

Coal mining in northern Portugal has played a significant role in the region's industrial development, particularly during the 20th century (Ribeiro 2020a). The exploitation of coal deposits was concentrated in the Douro Coalfield, particularly in São Pedro da Cova and Pejão, where anthracite coal was primarily extracted for energy production and industry (Alves Dias et al. 2018; Costa et al. 2022; Sousa and Rodrigues 2025). These operations contributed to local economic growth but also left a lasting legacy of environmental degradation that persists to this day. Coal mining in this region has left a lasting environmental impact, with waste dumps posing risks to soil, water, and ecosystems (Ribeiro and Flores 2021). The anthracite coal extracted in this region is predominantly of Carboniferous age and occurs in sedimentary rock formations composed mainly of breccias, sandstones, siltstones, shale and coal layers (Pinto de Jesus 2003). Mining activities in the area generate large volumes of waste materials, including unburned coal residues, combustion by-products, and mixed deposits. In some locations, these residues were deposited directly onto the ground or into old mining pits without adequate environmental control measures, resulting in the formation of Technosols and alteration of natural soil profiles (Espinha Marques et al. 2021, 2024).

Although most of the mines have ceased operation since the late 20th century, the remnants of coal-related activities remain visible in the landscape. The abandoned residues, often exposed to atmospheric agents, pose a long-term environmental risk due to their potential to release contaminants through leaching and surface runoff. In recent years, growing attention has been given to the characterisation and environmental monitoring of these residues. Yet, many aspects of their impact remain insufficiently understood, particularly in their interaction with local soils and biota. This chapter reviews the primary environmental challenges associated with burned and unburned coal mining waste, focusing primarily on the characterisation of the material, its impact on soil, and the limited information available on biodiversity. Some authors have noted increasing concern about the importance of coal mining waste pollution to the environment over the last 10-15 years, especially in the Douro Coalfield (Espinha Marques et al. 2021, 2024; Monteiro et al. 2024; Ribeiro et al. 2010abc, 2011, 2012, 2013, 2015, 2022; Ribeiro and Flores 2021; Santos et al. 2023ab; Teodoro et al. 2021). The focus on sustainable

management and restoration of the soil and surrounding environment at the coal waste pile is crucial for conserving biodiversity, maintaining aesthetic quality, and promoting human health (Amrani et al. 2020; Pactwa et al. 2020).

2.2. Environmental and Ecological Impacts of Anthracite Coal Waste

Coal to energy will be the major energy source for the foreseeable future and has been a major global resource for at least the past 250 years (Chinh et al. 2007; Hassi and Gasii 2024; Meegoda et al. 2011; Welch et al. 2021). When the coal trade had come to dominate regional economies in mining districts, its negative impacts came to be accepted as a necessary byproduct of generating coal-based wealth. However, at the same time, coal mining has a long-lasting effect on the landscape, ecosystem, and sociocultural and economic considerations (Giri et al. 2014). Coal production has important economic and social benefits; however, it generates large amounts of coal mine spoils and waste rocks, which oxidise under atmospheric conditions and release metal(loid)-rich effluents to the surrounding environment. It has only been since large-scale mine closures began to take place in the major coal-mining economies of the developed world during the last few decades that the negative impacts of coal mining have once more been deemed unacceptable (Younger 2004).

The coal waste generated is often disposed of without proper care in the environment, which serves as an active source of coal mine drainage generation, severely contaminating soil, surface water, and groundwater, and endangering the local ecosystems (Komnitsas et al. 2001; Younger 2004). One of the effects of anthracite coal waste is the proliferation of acid mine drainage (AMD), which is characterised by a low pH and high dissolved metal(loid) concentrations (Bott et al. 2012). The environmental impacts arising from coal mining activities are fundamentally attributable to the exposure of reduced earth materials (mainly coal, pyrite, siderite, and ankerite) to the oxidising power of the Earth’s atmosphere. The consequences range from the spontaneous combustion of coal to the release of acidic waters from pyrite oxidation (Younger 2004). Toxic substances are inherently present in coal mining waste, e.g., metal(loid)s such as iron (Fe), mercury (Hg), arsenic (As), lead (Pb), zinc (Zn), and cadmium (Cd) (Guha-Roy 1991). These potential toxic elements leach out of the stored waste piles and contaminate the immediate environment (Giri et al. 2014). Additionally, biodiversity, particularly the more sensitive types, declines. For example, macroinvertebrate family richness declined by 65 % and abundance by 90 % when coal waste was discharged into a freshwater system. Indeed, electrical conductivity (EC) changed to 11 times higher, and Zn concentration shifted to 24 times higher (Belmer et al. 2014).

The major environmental impacts of coal mining include changes in soil stratification, reduced biotic diversity, and alterations to the structure and functioning of ecosystems, which ultimately influence water and nutrient dynamics, as well as trophic interactions. Land degradation due to coal mining is the cumulative effect of air and water pollution, degradation of soil quality, and loss of biodiversity (Shankar et al. 1993). The process works through a cycle known as the land degradation cycle. The magnitude and impact of mining on the environment vary from mineral to mineral and also depend on the potential of the surrounding environment to attenuate the adverse effects of mining, such as the geographical disposition of mineral deposits (Giri et al. 2014). Acidic water adversely affects the soil environment by making the soil acidic and rich in inorganic components, while being poor in organic content. Deterioration of soil quality has severely affected the crop growth and yield in the area, mainly due to high concentrations of hydrogen ions, which inactivate most enzyme systems, restrict respiration, and impede root uptake of salts and water by plants. It also leads to deficiencies in nitrogen, phosphorus, calcium, magnesium, molybdenum, boron, iron, and manganese, as well as increased toxicity.

The deposition of coal waste in dumps can be compared to the effects of surface coal mining on various environmental impacts, including ecosystem losses, landscape alteration, soil degradation, and changes to surface and groundwater quality and quantity. Additionally, toxic compounds such as potential toxic elements (PTE), radioactive elements, polycyclic aromatic hydrocarbons (PAH), and other organic contaminants are released into the environment, ultimately affecting the health of ecosystems and the general population (Rouhani et al. 2023). Natural recovery in mine spoils is a very slow process, which may take about 200 years of natural succession on mine-degraded land for the total nutrient pool recovery to the level of native forest, the uphill soil. The first step in any restoration program is to protect the disturbed habitat and communities from being further wasted. This is followed by accelerating the re-vegetation process to increase biodiversity and stabilise nutrient cycling. As a result of natural succession by planting desirable plant species on mine degraded land, a self-sustaining ecosystem may be developed quickly. Bad disposal of coal-dump wastes represents significant environmental concerns due to their potential influence on the atmosphere, river sediments, soils, and surface and groundwater in the surrounding areas (Civeira et al. 2016).

The process of spontaneous combustion of coal and coal waste involves the emission of gases, condensation of inorganic and organic species in vents, and leachability (Querol et al. 2011). Moreover, coal waste from self-burning can have a negative impact

on the environment through air pollution, greenhouse gas emissions, and soil and water contamination (Ribeiro 2020b; Ribeiro et al. 2020). In abandoned areas with coal mining waste piles, self-burning occurs through oxidation processes as air passes into the coal waste. Under certain conditions, this phenomenon is widespread, even in modern-day mining, as coal can spontaneously ignite through an exothermic process, which may be accelerated by catalytic compounds (e.g., water, pyrite). The hypothesis holds that oxygen will be absorbed into the material if the active molecule sides of flammable materials are exposed to air, such as in porous coal. This fact could induce a series of heterogeneous surface reactions, whose rates rise exponentially with temperature as a function of oxygen content in the coal deposits (Civeira et al. 2016). It is reported that self-burning in an anthracite coal waste pile leads to geochemical changes in surrounding soils, including increased levels of potentially toxic elements and polycyclic aromatic hydrocarbons, as well as the formation of secondary organic pollutants, such as chlorinated aromatics and light sulphur compounds (Nádudvari et al. 2018; Santos et al. 2023ab).

Self-burning in coal waste leads to oxidative and thermal alterations of organic and mineral matter; a petrographic classification system is necessary to monitor and manage these changes (Misz-Kennan et al. 2020). For organic compounds, when a combustion reaction occurs, carbon, hydrocarbons, and other organic material are oxidised, mostly converting into CO_2 (carbon dioxide) and CO (carbon monoxide). Suppose the combustion is incomplete, due to a lack of oxygen. In that case, it can also produce volatile organic compounds (VOCs) and polycyclic aromatic hydrocarbons (PAH), which are toxic and persistent in the environment. Additionally, the majority of organic compounds are easily oxidisable organic matter that burns away, thereby reducing the total organic content of the material. So, the residual material (ashes) becomes richer in inorganic content. On the other hand, thermal transformation decomposes some minerals at high temperatures (e.g., carbonates like $CaCO_3$, which can release CO_2 and leave CaO). New mineral phases can form due to heat and reactions between existing minerals (formation of oxides and/or silicates). Some metal(loid)s become more mobile at high temperatures, like Pb, As, Cd, Zn; they can volatilise and then condense. Additionally, metal(loid) enrichment can occur as the organic material burns off, resulting in an increase in the relative concentration of metal(loid)s in the solid residue. In some cases, new mineral phases can trap metal(loid)s (e.g., forming stable oxides). Still, in other cases, they can become bioavailable and more dangerous if they migrate to soil and freshwater systems.

Studies have shown that coal waste elutriates contain potentially toxic elements like Al, Pb, Cd, Ni, and Zn, which adversely affect aquatic and terrestrial species (Diogo et al. 2023a; Narayan et al. 2024). While coal piles and waste runoff contain complex mixtures of metals, salts, and organics, with As, Cd, and Se identified as potentially problematic components for aquatic biota (Hall et al. 1982). On the other hand, the effects of coal combustion residues are accumulated by adult amphibians and transfer some contaminants to terrestrial systems (Rowe 2014). Anthracite coal waste has been reported to have limited waterborne acute toxicity to aquatic species despite high native polycyclic aromatic compound content (Meyer et al. 2013). Coal mine wastewater can have acute and sub-chronic toxic effects on aquatic invertebrate and vertebrate species, particularly affecting their morphological properties. Effects were observed following the sub-chronic exposures (Lanctôt et al. 2016). For coal ash, the exposure of freshwater snails to leachates caused delays in embryonic development and reduced juvenile shell growth. Additionally, it resulted in a decrease in adult fecundity, with a particular emphasis on clutch and egg deposition (Frankel et al. 2023). Furthermore, coal ash deposition can cause oral deformities in tadpoles that reduce their grazing ability and growth (Christopher et al. 1996).

2.3. Previous Studies for Coal Mining Waste in the Douro Carboniferous Basin

In the Douro Coalfield (DC), extensive research has been conducted to characterise the petrographic, mineralogical, and geochemical properties of coal mining waste (CMW) (Ribeiro et al. 2010abc, 2011, 2012, 2013, 2015, 2022; Ribeiro and Flores 2021). Moreover, soil samples from both burned and unburned CMW were studied at disposal sites, including São Pedro da Cova (SPC), Lomba, Midões, and Serrinha (Espinha Marques et al. 2021, 2024; Santos et al. 2023ab). Additionally, the composition, combustion temperature at the burning pile, the minerals formed around vents in burning zones (coal fire gas minerals), the geochemical composition, and mineralogical transformation have been reported (Ribeiro et al. 2010a, b).

The CMW exhibited high heterogeneity in macroscopic characterisation due to the varying lithologies and techniques employed for material extraction. The samples consisted mainly of lithic fragments, including black shales and sandstones with variable particle size distributions and organic matter content. The material that had undergone combustion displayed distinctive reddish to greyish hues reflecting the thermal alteration processess (Misz et al. 2007; Ribeiro et al. 2010a, 2011). The coal associated with DC has a rank of anthracite A with vitrinite random reflectance ranging between 4 % and 6

% (Costa et al. 2022; Ribeiro et al. 2011; Ribeiro et al. 2022). The principal environmental impacts reported for the disposal site in DC are: i) atmospheric dispersion of particles; ii) self-burning of the waste pile; iii) landslides and mass movements in the coal waste pile; iv) mobilisation of material; v) leaching of elements; and vi) formation of acid drainage caused by weathering and/or oxidation process (Ribeiro et al. 2011).

On the north side of the DC, there are three mean coal mining waste piles (SPC, Lomba, and Midões) that were and/are in combustion. Ribeiro (2010abc, 2011) characterised these waste piles well that have been burning since their ignition caused by forest fires in 2005. For the SPC waste pile, the petrographic results indicate that vitrinite is the dominant maceral group, with the presence of inertinite (Ribeiro et al. 2010a, 2011). Organic and inorganic constituents from the unburned zone showed signs of weathering (e.g., cracks and fissures in maceral particles) (Ribeiro et al. 2010ab,2011). In samples of burned material, the organic matter appears to be strongly affected, exhibiting lower reflectance, more cracks and fissures, reduced anisotropy, devolatilisation vacuoles, and rims with lower reflectance. On the other hand, minerals exhibited the successive formation of different iron oxides, indicating the progression of the combustion process (Ribeiro et al. 2010a). Although the Lomba showed high heterogeneity, the unburned waste pile exhibited fresh organic matter with fewer signs of weathering. In contrast, in the burned samples, a few organic particles remained, visibly affected by the process. The other samples were partially burned, and the petrographic analysis revealed signs of pre-combustion (Ribeiro et al. 2010ab, 2011). At Midões waste pile, samples appeared not to have been burned entirely, as indicated by their grey colour and the presence of organic particles. The petrographic characteristics of these three areas in DC suggest that the coal mining waste pile has a lower reflectance than the fresh coal. The differences in reflectance values between the unburned and burned zones are attributed to weathering and combustion processes (Ribeiro et al. 2010a, 2011).

During the combustion of coal mining waste, the gas composition showed a broad mixture of aromatic and aliphatic hydrocarbons. The SPC waste pile had a more complex composition and the highest concentration than the Lomba coal waste pile, with benzene, toluene, ethylbenzene, pyridine, and xylenes as the main aromatic hydrocarbons, and hexane and ethane-isothiocyanate as the principal aliphatic compounds (Ribeiro et al. 2010a). Polycyclic aromatic hydrocarbons (PAH) were found in CMW burned and unburned material with petrogenic and pyrolytic origins for CMW from the DC (Ribeiro et al. 2012). The behaviour of the PAH in the CMW is described as follows: i) they can volatilize and enter the atmosphere, and re-precipitate in colder areas; ii) they could also be retained or adsorbed within the waste material; iii) migrate within

the waste piles where the more soluble compounds can be dissolved and migrate into surrounding areas (Ribeiro et al. 2012).

In the case of sites that pass through a combustion process, new minerals were reported; they could be formed by the thermal decomposition of clays and other minerals (e.g., pyrite) at around 900–1300 °C (Saxby 2000; Ribeiro et al. 2010a). Mining areas as SPC, Lomba, and Midões had in the unburned coal waste quartz, illite, mica (mainly muscovite), and, in many cases, pyrophyllite as the main minerals. Regarding the concentration of major and trace metal(loid)s, light rare earth element (LREE), and heavy rare earth element (HREE) for burned coal mining waste piles, Lomba samples were characterised by an enrichment in Co, Cr, Mn, Ni, V, and Zn. At the same time, SPC indicates an enrichment in Al, Fe, Ti, As, Cu, Pb, Li, Rb, Sr, and Zr (Ribeiro et al. 2010a). For the burned sample from the Germunde (PjB) and the Fojo coal waste dump (PjA), there is a slit enrichment for S, Ti, Cr, Cs, Nb, Ta, V, and W for PjA. In the case of PjB the following elements are concentrated after combustion Al, Ca, K, Mg, Na, P, Ti, Ba, Ga, Hf, Li, Nb, Sc, Sr, Ta, Th, Tl, U, V, Y, Zr, LREE, HREE (Ribeiro et al. 2022). The environmental impacts observed were leachates from CMW, neoformed minerals, a higher concentration of chemical elements in sediments and soils in the surrounding areas, and gas from vents, and the precipitation of two compounds, Sulphur and salammoniac (Pone et al. 2007; Ribeiro et al. 2010abc).

Another mining area characterised was the Serrinha CMW pile, located on the south side of the Douro River in the DC. The self-burning process did not occur at this coal mining pile, primarily because the conditions required for self-combustion were not present. In addition, unlike the other disposal sites, this pile was not affected by intense forest fires, which could otherwise have acted as an external ignition source and promoted combustion processes. The petrographic results showed that the maceral of the vitrinite group represents the organic fraction. The organic matter shows optical anisotropy and some cracks (Ribeiro et al. 2010b). Evidence of weathering included cracks in organic particles, the time of exposure, easy air access within the waste pile due to poor compaction, and material heterogeneity (Ribeiro et al. 2010b). The mineralogical composition of the Serrinha coal mining waste pile was principally quartz and clay minerals. Illite is the most abundant mineral, followed by quartz, muscovite, chlorite, and pyrophyllite, with traces of other minerals such as rutile, anatase, and jarosite (Ribeiro et al. 2010abc). The chemical composition of samples of CMW in Serrinha and coal from the DC has a higher content of almost all trace elements than the world coal composition (Swaine 1990; Ribeiro et al. 2010b). These elements in coal are associated with organic or mineral matter: silicates, sulphides, oxides, carbonates, phosphates, sulphates, etc

(Finkelman and Gross, 1999; Ribeiro et al 2010b; Suárez-Ruiz and Crelling 2008; Swaine 1990). The geochemical values showed that Al, Fe, and K dominate the major elements in the waste pile samples. In contrast, the other remaining elements (Ca, Mg, Na, S, and Ti) have concentrations of less than 1.0 % (Ribeiro et al. 2010b). Trace elements in leachates from Serrinha CMW include Cd, Co, Cu, Ni, and Zn. The percentages extracted show a major association with H_20-soluble compounds for elements, as shown by the following composition: Co>Mn>Cd>Zn>Ni>Cu. Metals associated with this phase are readily available and relatively mobile, allowing for biological uptake (Ribeiro et al. 2010b).

Other waste piles without fire influence were studied in the DC, in addition to Serrinha. One is located on the north side, near Midões, and the others are located on the south side of the DC, including Germunde, Fojo, Pejão Novo, Paraduça, Ervedal, Vale de Cana, Carvalhais, Rodelo, Sobrido, and Lameira. The geochemical composition exhibited high heterogeneity in the concentrations of major and trace elements, without a discernible common pattern. Indeed, the elements Ca, Cu, As, Ni, Pb, Fe, K, Mg, S, Co, Cs, Mn, and Sb exhibited higher concentrations. In contrast, P, Nb, Sn, Ta, and U showed lower values (Ribeiro et al. 2011).

The mode of occurrence is an important factor that is rarely considered by authors studying unburned and burned coal waste (Dai et al. 2014b,2021,2023; Finkelman 1981ab,2018). Since they can strongly influence their behaviour during weathering, leaching, combustion, etc, moreover, they can be of particular concern due to their potentially adverse effect on the environment during the utilisation and disposal of the waste products (Finkelman and Gross 1999; Ribeiro et al. 2011; Ribeiro and Flores 2021; Suárez-Ruiz and Crelling 2008; Swaine and Goodarzi 1995). The mode of occurrence of elements in coal waste reflects the thermal stability of their associated mineral phases. Before combustion, elements are primarily associated with thermally labile minerals such as sulphides, phosphates, and carbonates. During pyrolysis, these minerals are prone to decomposition or transformation at relatively low temperatures. After combustion, the remaining ash predominantly consists of refractory minerals, such as zircon, aluminosilicates, and thermally stable clay-derived phases. This shift indicates that the combustion process disrupts weaker chemical bonds, resulting in the preservation of only the most thermally resistant mineral associations.

On the other hand, soil pedogenesis directly influences the physical, chemical, and mineralogical properties of CMW. This can differentiate soil features, including the type of soil profile (Lilić et al. 2014). In particular, the pedological evolution of technosols from

CMW piles depends on how soil formation factors transform the original materials and may influence water circulation and pollutant transport in these porous materials (Espinha Marques et al. 2024). The occurrence of subsequent processes, such as coal waste self-burning, induces severe changes in the normal soil profile evolution and originates zones with distinct hydropedological features. As a result, the soil from coal waste piles may present high spatial contrast concerning the leaching of pollutants (Espinha Marques et al. 2021; Teodoro et al. 2021).

The presence of CMW has environmental impacts on soil, including the leaching of many elements and compounds from the waste piles, such as PTE and PAH (Espinha Marques et al. 2021). Some mining impacts on soils result from metals and metalloids (Li et al. 2014; Sahoo et al. 2016). Soil leaching is found to be one of the primary pathways for pollutant compounds to enter the environment (Dutta et al. 2018; Larson et al. 2018). Espinha Marques et al. (2021) identified and characterised changes induced by self-burning in technosols from the SPC coal waste pile by a comprehensive hydropedological assessment using geochemical, mineralogical, and hydrological data, showing that this type of soil is classified as Spolic Technosols (FAO, 2006). The soil features a weakly developed soil profile that is formed and includes two mineral horizons: the first one, a superficial layer, with accumulation of humified organic matter; and the second one, a horizon with none to very low humified organic matter content.

The technosol mineralogy results indicate that samples from the waste pile with normal pedogenesis composition is typical of a fine-grained siliciclastic material, dominated by quartz, muscovite, and feldspars, with pyrophyllite, kaolinite, anatase, jarosites, and opal A as accessory minerals, all of them usually present in these types of materials (Chaminé et al. 2003; Espinha Marques 2021,2024; Pinto de Jesus et al. 1997,2003; Ribeiro et al. 2015). Samples from the waste pile affected by self-burning showed substantial changes with the presence of Fe oxides (hematite) and sulphates (jarosites, accompanied by their Al isomorph alunites), as well as traces of sulphur (Espinha Marques et al. 2021). The CMW with normal pedogenesis and those affected by self-burning showed differences in the morphological features, geochemistry, mineralogy, and unsaturated hydraulic conductivity. Another feature to consider is the leaching from both burned and unburned coal waste, as well as the differences in the types of solubilised elements. The susceptibility of pollutants to leaching from the CMW pile depends on several factors, including the solubility and availability of the specific element, as well as its potential release. Additionally, drainage conditions may increase solubility and flow rates through materials containing pollutant-bearing minerals (Benerjee 2014). For SPC, no difference was observed between horizons for soil texture, structure, porosity, or weathering of rock

fragments (Espinha Marques et al. 2021). These authors commented that soil organic matter plays an important role in pollutant transport because PTE sorption on soil organic matter, forming organometallic substances, and this type of sorption is greater than the one that occurs on the mineral matrix (clay minerals, iron oxides, and hydroxides) (Lair et al. 2007).

For CMW with combustion, the behaviour shows that the normal pedologic evolution was interrupted by high temperatures, and the humified organic matter was destroyed. Geochemical and mineralogical transformations occurred, and due to the combined influence of self-burning and rainwater infiltration, three new layers were formed, exhibiting distinct hydropedological behaviour (Espinha Marques et al. 2021). The self-burning CMW in SPC created an environment where pollutants were leached, especially from the deeper layer, with acidic water percolating through the unsaturated zone. This environment is characterised by higher infiltration due to the absence of humified organic matter (Espinha Marques et al. 2021). Geochemistry analyses were done in the area by Teodoro et al. (2021) in SPC. They showed that several trace elements, Sb, Ba, U, As, V, Be, Cr, Mo, Pb, and Se, exceed the values proposed for soil contamination in agricultural areas. Samples located preferentially in urbanised regions, upstream of the mine, show a moderate concentration of As, Pb, Mo, Cu, Zn, Co, Ni, and Ag. In contrast, samples from the waste pile drainage basin showed an increase in V, Be, Cr, and Ta concentrations, supporting the idea that multiple types of contamination sources contribute differently to the concentration of PTE and other elements in soils (Teodoro et al. 2021).

Another study was performed by Santos et al. (2023) for the soils surrounding the self-burning waste pile in SPC. They focused the survey on the soil physicochemical and geochemical characteristics, comparing the elemental concentrations in the soils surrounding the mine with concentrations found in the waste pile. Arsenic, Cs, and Sb soil concentrations were significantly higher than the average European topsoil and world soils (APA 2019). Moreover, the authors also observed that other trace elements, such as Mo, Be, Cu, Pb, Zn, Sn, Th, and U, presented higher concentrations. The spatial distribution of magnetic susceptibility in the soils surrounding the waste pile was also studied. It seems to be controlled by pedogenetic factors. Based on spatial and statistical correlations, Cu, Pb, Zn, Cd, and Sn concentrate preferentially in urban areas on topographic hilltops, upstream of the waste pile. In this case, the elementary correlations suggest that the sources are typical urban anthropogenic activities, except that these elements may have originated in the mine waste pile.

For the DC, there is a gap regarding the effects of lixiviate or elutriate from these anthracite CMW on aquatic or terrestrial species. Despite the chemical contamination studied by several authors, there is a lack of knowledge on the toxicological effects of the coal mining waste leachates on species from different trophic levels. Most studies in ecotoxicology of coal waste, coal ash, and coal washery effluent were done on bituminous and sub-bituminous coal grades (Blinova and Dobrydina 2017; Maltby and Booth 1991; Simonin et al. 2021; Tiwary and Dhar 1994). Meanwhile, as anthracite coal lixiviate is more associated with inorganic elements than organic compounds (Espinha Marques 2021; Ribeiro and Flores 2021), it was decided to explore the behaviour and the ecotoxicological effects of the selected standard species *Allivibrio fischeri*, *Lemna minor*, *Daphnia magna*, and *Lactuca sativa* with wastewater effluents and acid mining drainage (AMD) that have a high load of potential toxic elements and low pH, similar feature of anthracite coal waste lixiviate.

The genotoxic effects of water samples from mining lakes were investigated using *Lemna minor*, which exhibited significant physiological and genotoxic effects, resulting in severe damage and decreased growth (Fomin et al. 2000). Ecotoxicity evaluations of industrial discharge waters and metallic solutions were conducted using *Lactuca sativa* and *Daphnia magna*. The results showed a difference in metal toxicity order, with more toxicity from discharges, and the species that was more sensitive was *D. magna* than *L. sativa* (Priac et al. 2014). On the other hand, AMD was tested in the *Daphnia* bioassay, showing high acute toxicity in Daphnia magna, as well as inducing strong phyto-, cyto-, and genotoxicity in *Allium cepa* roots. Short-term exposure to AMD inhibited duckweed growth and chlorophyll a content, while simultaneously promoting lipid peroxidation and DNA damage, despite duckweed's (*Lemna minor*) capability to upregulate antioxidative defence mechanisms. The results show that observed (geno)toxicity could be related to oxidative stress, most probably induced by toxic metal action. However, the influence of low pH as a contributing factor in the phytotoxicity of AMD cannot be excluded (Radić et al. 2014). Mining activities in the Portuguese sector of the Iberian Pyrite Belt (IPB) have been responsible for pollution of water, sediments, and biota, caused by acid mine drainage (AMD) from the tailing deposits. Aquatic bioassays evidenced the high ecotoxicity of the Água Forte water at that site, with very low EC50 values for *Vibrio fischeri* luminescence inhibition (<3.1 % v/v) and *Daphnia magna* 48-hour immobilisation/mortality assays (<6.3 % v/v) (Alvarenga et al. 2021).

2.4. Study Area Location and Environmental Setting

The study takes place in the Douro Carboniferous Basin, the largest outcrop of terrestrial Carboniferous coal-bearing deposits in Portugal (Eagar 1983; Fernandes et al. 1997; Lemos de Sousa and Wagner 1983; Wagner and Lemos de Sousa 1983), with a length of 53 km and a width ranging from 30 m to 250 m. The geographic limits of the DCB are São Pedro de Fins (Maia) and Janarde (S. Pedro do Sul) (Pinto de Jesus, 1987, 2001, 2003). In addition to many small mines, there were two principal centers of mining activity: The São Pedro da Cova and the Pejão mining areas. The importance of these centers was due to their economic and technological impacts and cultural significance. São Pedro da Cova was the main exploitation centre from the end of the 17th century (1795) until the middle of the 20th century. In contrast, Pejão was the principal activity centre from the 1940s until 1994, when the mine was finally closed (Custódio 2004). The Pejão mining area, also known as Couto Mineiro Pejão, is divided into three mines: Choupelo, Fojo, and Germunde. They are located south of the Douro River in the Castelo de Paiva area, Aveiro, northwest of Portugal. Castelo de Paiva county is situated between the natural regions of Beira and Douro littoral, approximately 50 km from Porto city. The entire municipality is located in the Douro River basin, which encompasses the sub-basins of the Arda, Paiva, and Sardoura Rivers (Gomes and Chaminé 2005).

The study area is situated in Póvoa, within the Raiva, Pedorido, and Paraíso parishes, in the Castelo de Paiva municipality, Aveiro District. The area is used as a coal waste disposal site. For this research, different map sheets were used: 134 of the military charter of Portugal (scale 1:25.000), sheet 13-B of the geological map of Portugal at scale 1:50.000 (Medeiros et al. 1964), and the mineral deposit map with geological base at scale 1:200.000 (Laboratório Nacional de Energia e Geologia [LNEG] 2013). The study area's geographic location is summarised in Table 2.1 and shown in Figure 2.1.

Table 2.1 Geographic coordinates of the Fojo coal mining waste disposal area

Study area	Location UTM	
Fojo mine coal waste piles	Longitude (W)	Latitude (N)
P1	-8.386532	41.041349
P2	-8.383368	41.041997
P3	-8.380865	41.040713
P4	-8.384081	41.039893

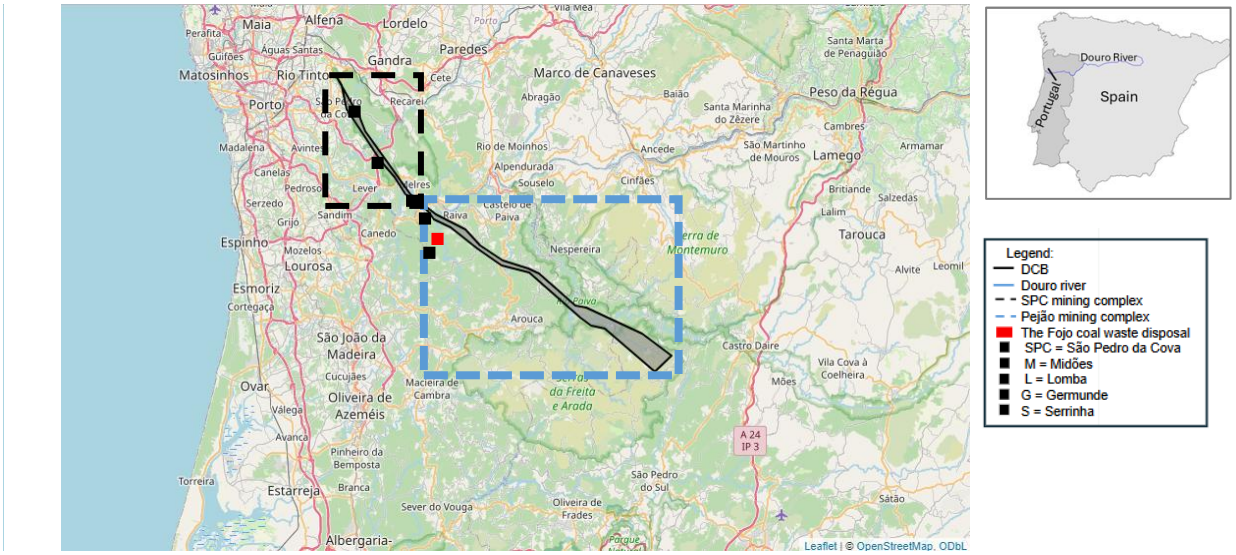

Figure 2.1 The Fojo coal mining waste disposal area geographic location in the Douro Coalfield

A wildfire in October 2017 ignited and subsequently combusted the Fojo waste pile material. Between 2017 and 2019, the company Empresa de Desenvolvimento Mineiro, S.A. (EDM) conducted an operation to control and extinguish coal waste combustion. This procedure involves remobilising the coal waste and applying a water mixture with a cooling accelerator agent. The Fojo coal mining waste disposal area is characterised by its proximity to the village centre and commercial eucalyptus plantations.

2.4.1 Geology

The Fojo coal waste disposal area is located in the Douro Coalfield, which is part of the Douro Carboniferous Basin (DCB). This basin is located in the Central Iberian Zone (CIZ), with a NW-SE orientation, covering an extension of 85 km in length and a narrow width of less than 1 km (Lemos de Sousa and Wagner, 1983; Pinto de Jesus, 2001, 2003). The basal strata of the DCB rest unconformably on Early Cambrian strata. The top of the DCB is cut by a reverse fault that placed the Early–Middle Palaeozoic formations of the Valongo Anticline structurally above the Lower Gzhelian coal measures of the DCB (Domingos et al. 1983; Lemos de Sousa 1984; Pinto de Jesus 2001, 2003; Pinto de Jesus and Lemos de Sousa 2003; Wagner et al. 1984).

Geologically, the base of the DCB all along the SW side rests over the Precambrian (Beiras Group). At the SE end, the contact is made over the Silurian beds. NE limits, for the top of the Douro Coalfield, is a reverse fault that cuts through the Carboniferous and sets the early Palaeozoic formations of the reverse limb of the Valongo Anticline over

the Douro Carboniferous Basin (Domingos et al. 1983; Lemos de Sousa 1984; Pinto de Jesus and Lemos de Sousa, 2003; Ribeiro et al. 2011; Wagner et al. 1984). The Douro Carboniferous Basin was formed during the Lower Gzhelian (Lower Stephanian C) as a pull-apart basin controlled by sinistral shear activity along the Douro-Beira Carboniferous Trough. Sedimentation was syntectonic, with depocentres migrating from NW to SE. The basin evolved into a foreland-style sedimentary system, characterised by alluvial fans at its margins, which supplied sediments to a palustrine/lacustrine environment. These deposits were later reworked by braided river systems flowing northwestwards.

The thermal evolution of the basin was significantly influenced by the emplacement of granitoid rocks, which, combined with subsidence, led to the coalification of organic matter, resulting in meta-anthracite rank coals. Late Variscan tectonic phases, characterised by NE-SW oriented stress and sinistral shear, generated thrust faults with piggy-back structures, duplexes, and triplexes. These movements caused rotation and microfolding in coal strata, particularly near major overthrust faults. The basin's structural complexity, including oblique faulting and cleavage development, indicates a shift from transcurrent sinistral NW-SE regimes during the Moscovian (Westphalian) to a transgressive sinistral regime with W-E compression by the lower Stephanian C. This tectonic framework underscores the interplay between sedimentation, magmatism, and deformation in the basin's evolution.

Figure 2.2 illustrates the different formations of the studied area, which are characterised by Palaeozoic rocks. The basement of the Douro Carboniferous Basin consists of metamorphic rocks that were deformed by the Variscan Orogeny. The lithological framework of the Douro Carboniferous Basin indicates extensive fluvial and swampy conditions, which facilitated the deposition of coal-bearing sequences comprising breccias, mudstones, siltstones, sandstones, and coal seams.

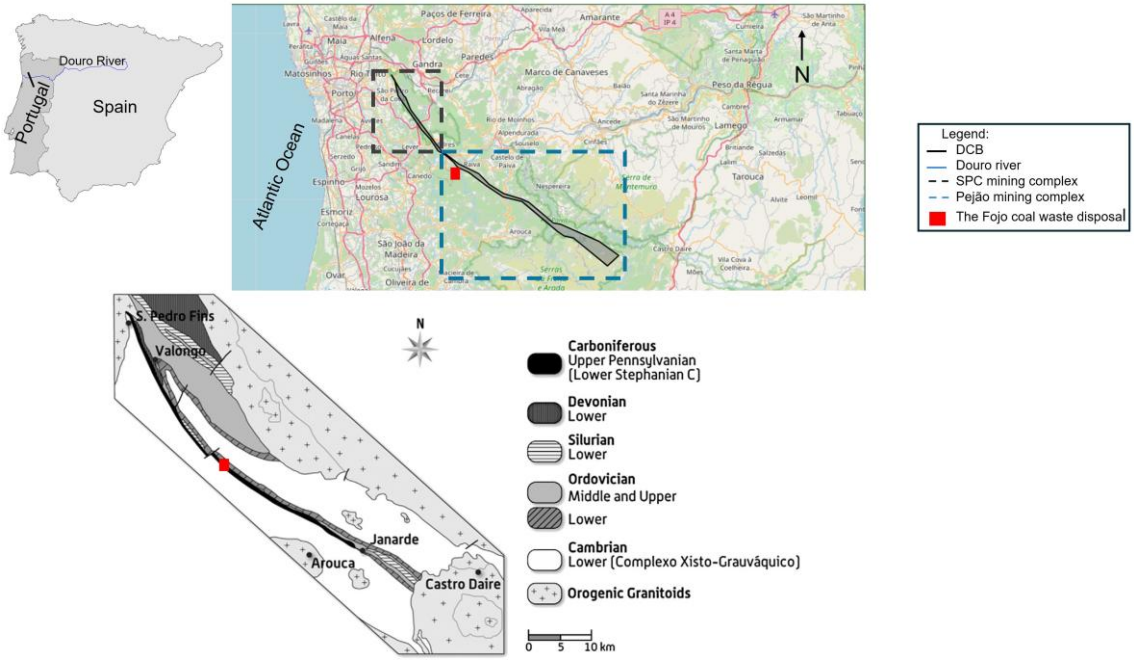

Figure 2.2 Geological setting of the Douro Coalfield (modified from Pinto de Jesus 2001; Ribeiro et al 2011).

2.4.2 Geomorphology

The Douro Carboniferous Basin's geomorphology has been closely linked to regional geology, tectonic settings, and erosional processes since the late Palaeozoic era. The basin, located mainly in northern Portugal (between Porto, Vila Real, and Bragança), is a Variscan (Hercynian) intermontane basin formed during the late Carboniferous. The DCB is part of the Iberian Massif, embedded within a crystalline basement of Precambrian and Palaeozoic rocks (Dias et al. 2013; Feio 2004; Ramos and Ramos 2020). The geomorphology reflects: i) tectonic controls bounded by faults and horst-graben, systems, where the faults (often reactivating Variscan structures) shape steep escarpments and lineaments; some parts of the basin show structural asymmetry due to differential uplift and fault displacement. ii) erosional surfaces and denudation, the landscape has been heavily eroded, especially during the Mesozoic and Cenozoic; planation surfaces dominate in some areas, especially over resistant lithologies; and denudation has exposed older basement rocks surrounding the preserved Carboniferous sediments (Correia 2016; Ferreira 1981; Ramos and Ramos 2020).

Three geomorphological types are identified: a) Residual hills and mesas, formed from erosion-resistant carboniferous sandstones and conglomerates; isolated hills and mesas indicate differential erosion, where harder layers resist weathering. b) Structural valleys

and Graben-like depressions, linear valleys aligned with fault systems; some parts of the basin are graben-like, with flanking fault scraps, and the valleys are filled with Carboniferous sediments and sometimes younger colluvial/alluvial deposits. c) Uplifted basement and fault scarps, surrounding gneiss and granite highlands form a sharp contrast; prominent fault scarps mark the limits of the Carboniferous sequences; ridges and stepped topography formed by tilting and erosion of sedimentary layers. The DCB´s geomorphology was shaped by syn-tectonic sedimentation, where sediment deposition co-occurred with tectonic activity (Ferreira 1996; Pais et al. 2013). At the same time, the basin transitioned from a transcurrent (strike-slip) regime to a transpressional (compressional) regime, leading to foreland-style basin development. Coalification was driven by geothermal heat from nearby granitoid intrusions, and the final structure of the basin was influenced by oblique thrusting, resulting in a complex deformed geometry with duplicated stratigraphic sequences (Fernandes et al. 1997).

A brief geological analysis of the Valongo Anticline is characterised by the remarkable lithological diversity, largely represented by Paleozoic metasedimentary formations. These geological units span a broad stratigraphic range, from the Precambrian and/or Cambrian to the Carboniferous period. This diversity is evident in lithological characteristics and reflected in the numerous geomorphological contrasts observed throughout the area. As a result, this setting naturally favours significant variability in hydraulic and hydrogeological parameters. The DCB encompasses the Valongo Anticline and its surrounding areas by marked topographic contrasts, which result from the long-term action of geomorphic agents acting upon Palaeozoic formations. The tectonic activity significantly enhanced the impact of these exogenous (geodynamic) processes, which took place during the Mesozoic and Cenozoic eras (Dias et al. 2013; Feio 2004; Ramos and Ramos 2020).

Currently, the region presents a phenomenon of topographic inversion, with an extensive valley running through the core of the Valongo Anticline, where the Shist-Greywacke complex is predominant. This inversion represents the most notable geomorphological feature of the region, although others, such as the prominent quartzite ridges, are also interesting. Around the quartzite ridges, in zones where Palaeozoic metasediments dominate, a series of planation surfaces can be observed, ranging in elevation from 70-210 m (Medeiros et al. 1964). Across these zones, a complex drainage network has developed, composed of the Leça and Douro rivers, including the Ferreira and Sousa rivers. This fluvial network is heavily influenced by fault systems associated with the late Variscan deformation phases (D3 and D4).

The highest altitudes are found within the granitic formations east of the anticline in Valongo and Paredes and the region between Castelo de Paiva and Arouca. Although these granites are not part of the Valongo Anticline itself, they play a prominent role in shaping the regional geomorphology. The Castelo da Paiva-Arouca region also exhibits pronounced topographic contrasts, where Ordovician quartzite ridges play a significant role, providing clear evidence of quartzite's greater resistance to erosion compared to surrounding rock types. The quartzite ridges outline an eroded anticline trending NW-SE. The western flank is defined mainly by the Flores and São Domingos Mountain ranges, while the eastern flank includes the ranges of Santa Iria, Banjas, and part of Serra da Boneca (Medeiros et al. 1964). Beyond the quartzite ridges, dense and tectonically controlled fluvial networks further shape the region's geomorphology. Notable among these are the Paiva, Ardena and Sardoura rivers. North of Castelo da Paiva, the Douro River dominates the landscape, which has carved a deep and narrow valley, showcasing the ongoing interaction between tectonic structure and fluvial erosion.

On the other hand, the north side of the DCB has relatively easy-to-recognise vast areas of marked flattening around the Douro River tributaries (Figure 2.3, black dots). In the south, in addition to the fact that the relief tends to be more rugged, with steeper slopes, there are generally higher elevations, which in some places exceed 700 m (Figure 2.3, blue dots).

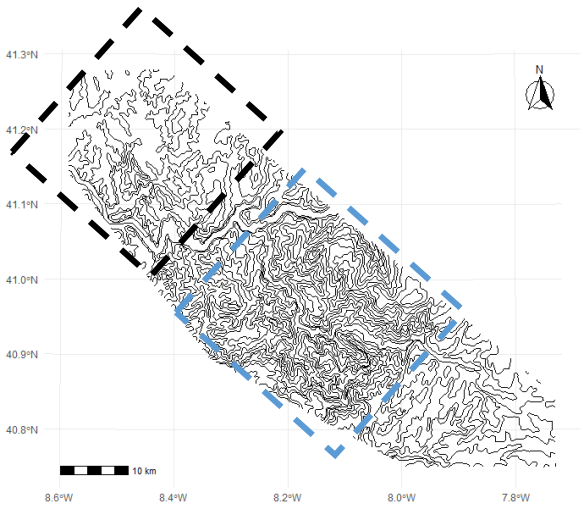

Figure 2.3 Spatial distribution of altimetry values (m) in the Douro Carboniferous Basin (DCB), showing the northern and southern sectors (adapted from Atlas do Ambiente 1985).

2.4.3 Climate

The Douro Carboniferous Basin (DCB) in northern Portugal is distributed in three municipalities: Porto, Aveiro, and Braga. It lies along the Douro River and includes the Douro Coalfield. The region generally falls under the Mediterranean climate (Csa/Csb) classification according to the Köppen-Geiger system (Mora and Vieira 2020). Still, it has Atlantic influences, particularly in the west, closer to the city of Porto. The climate of the DCB depends on various parameters such as temperature, precipitation, relative humidity, radiation index, and evaporation. For the climatological approach, the Environmental Atlas website data was used (Atlas do Ambiente 1980). The summary data was adapted for the context of the DCB and the study area, the Fojo coal mining waste disposal site. For the climatic characterisation of the region near Castelo de Paiva, data from the Paços de Ferreira weather station were considered more representative of the local climate. The period from 1955 to 1980 was used (Instituto de Meteorologia e Geofísica 1990). Additionally, precipitation data were obtained from the Sobrado de Paiva udometric station for the period 1951-1980 (Instituto de Meteorologia e Geofísica 1990).

According to the bioclimatic classification developed by Rivas-Martinez (1985), the municipality of Castelo de Paiva lies within the temperate oceanic meso-sub-Mediterranean bioclimatic zone. Observed data indicate a strong Atlantic influence, reflected in high relative humidity (79 % at 9 a.m. and 75 % at 6 p.m.) and a relatively low thermal amplitude, resulting in a moderate and fresh climate. Figure 2.4 represents the mean annual relative humidity (%) for Portugal, the DCB and the study area. In the DCB, the percentage of humidity increases from 70% to 85%, moving from south-west to north-west. According to the data from the Environment Atlas Website, the study area has an annual mean value of 80 % for the relative humidity. Additionally, the relative proximity to the sea, combined with the patch of vegetation, significantly contributes to the occurrence of high humidity values (Gonçalves 2013).

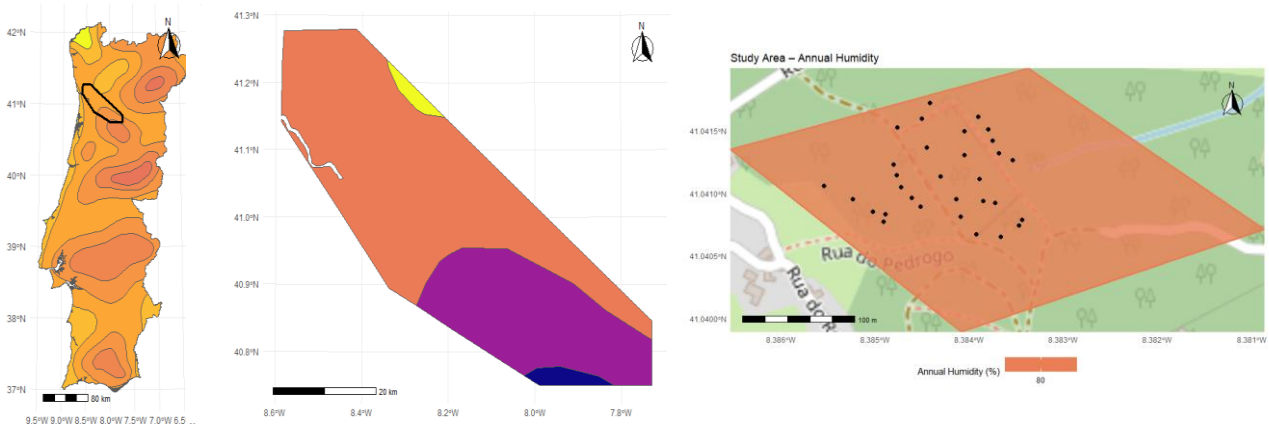

Figure 2.4 Relative humidity (%) for Portugal, DCB, and the Fojo coal mining waste disposal site (adapted from Atlas do Ambiente 1985).

Mediterranean influences are also evident, particularly in the seasonality of precipitation. According to data from the Sobrado de Paiva station, only 7.1% of the annual rainfall occurs between June and August, while 53.2% falls between December and March (Figure 2.5). The total annual precipitation is approximately 1355.8 mm, a value that coincides with the data from the Environment Atlas Website (Figure 2.6). In the DCB, there is a gradient of precipitation that goes from 1200 mm to 2400 mm, and it is reflected in the center of the DCB to the south and the north. Precipitation occurs frequently, on about 120 days per year, with a significant likelihood of heavy rainfall. Around 48 days per year record precipitation above 10 mm, mainly between October and March. Moreover, it arises in the month of April.

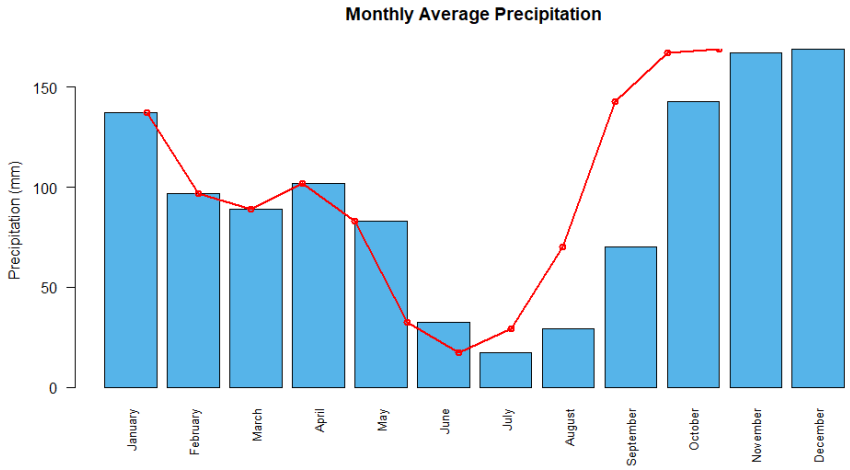

Figure 2.5 Annual precipitation (mm) for the climatic region Douro-Minho-Beira Litoral for 2022 (IPMA 2023).

The frequency of heavy rainfall (over 10 mm) is notable, approximately 48 days annually, spread across all months. Prevailing winds come predominantly from the southwest (23.6 %), followed by southeast (17.0 %) and northwest (13.2 %) directions. Other directions occur less frequently, indicating a relatively even wind distribution over the year. Calm periods also happen. Average wind speeds are relatively uniform across.

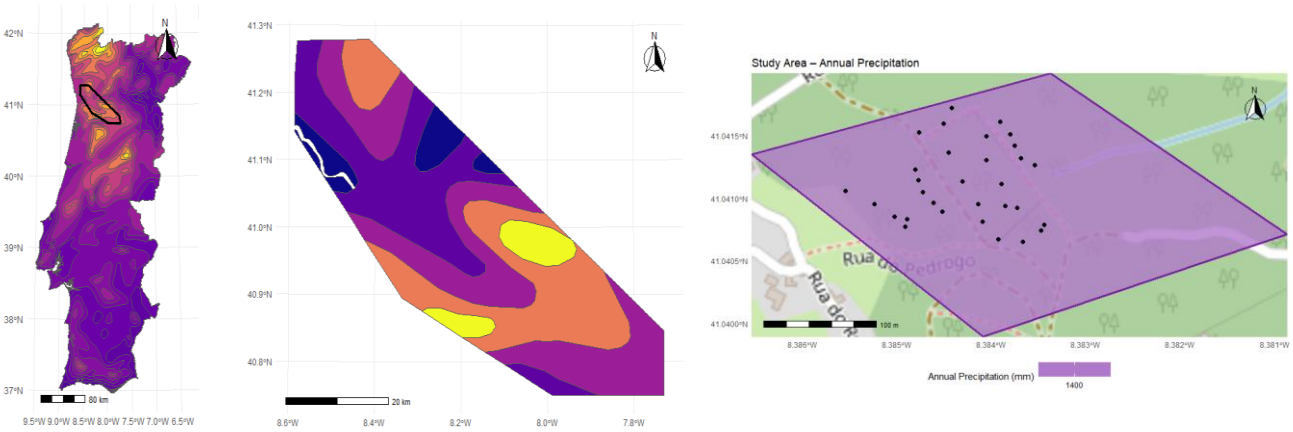

Figure 2.6 Annual precipitation (mm) in Portugal, the DCB and the study area during 1950-1980 period (adapted from Atlas do Ambiente 1985).

The average monthly temperature recorded at the Paços de Ferreira station is 13.0 ºC. July is the warmest month (19.3 ºC), while December and January are the coldest (7.4 ºC). The average maximum temperature is 26.1 ºC in August, and the average minimum is 2.7 ºC in December. Absolute recorded temperatures range from a maximum of 39.1 ºC in July to a minimum of -8.0 ºC in February. The area exhibits an evident Atlantic climatic influence, characterised by a low annual thermal amplitude of 11.9 °C. Summers are relatively hot, with around 57 days registering maximum temperatures above 25 ºC. In winter, there are approximately 30 days with minimum temperatures below 0 ºC (Green Plan, 2011). The climatological station of Porto-Pedra Rubas (IPMA 2023) showed a mean maximum temperature of 25 ºC between July and August, and a mean minimum of 10 ºC (Figure 2.7).

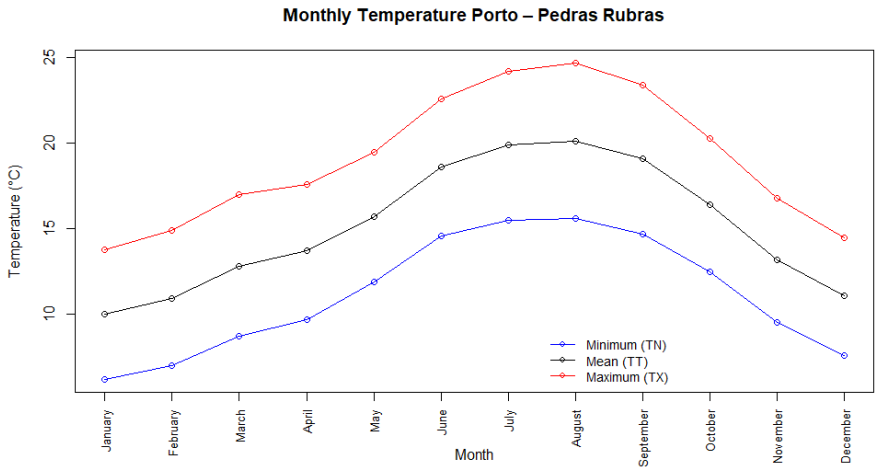

Figure 2.7 Annual temperature average (ºC) for the climatic region Douro-Minho-Beira Litoral for 2022 (IPMA 2023).

In the DCB, it is reported that the annual mean temperature oscillates between 10 ºC and 16 ºC (Figure 2.8), depending on the terrain height and solar radiation. Gonçalves (2013) stated that, the fact that the north regions of the DCB have higher average annual temperatures than the south areas are not, at the first glance, directly related to solar exposure (or the amount of radiation), as there are no considerable fluctuations in the amount of radiation between the DCB.

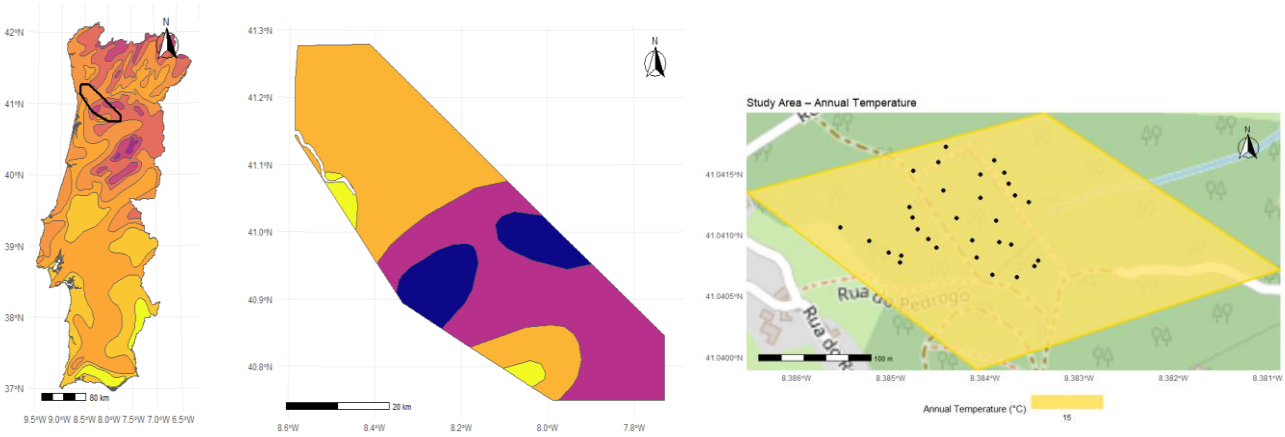

Figure 2.8 Annual Temperature variation (ºC) in Portugal, the DCB and the study area (adapted from Atlas do Ambiente 1985).

Evaporation is most significant during the hottest months, with an annual total of 971.5 mm (Green Plan 2011). The north of Portugal seems to have the highest evaporation rates, ranging from 700 mm to 800 mm in the DCB and 700 mm in the study area (Figure 2.9). An important aspect is the distribution of the higher evaporation rates, where on the north side of the DCB, it is observed on the east side and on the south side, it is observed

on the west side. This fact is associated with the main relief patterns in the DCB. Meanwhile, the difference in the mean evaporation is not very high, but it still shows a distinct pattern (Gonçalves 2013). A fragmented type of relief marks the south of the DCB, with practically no flattened areas.

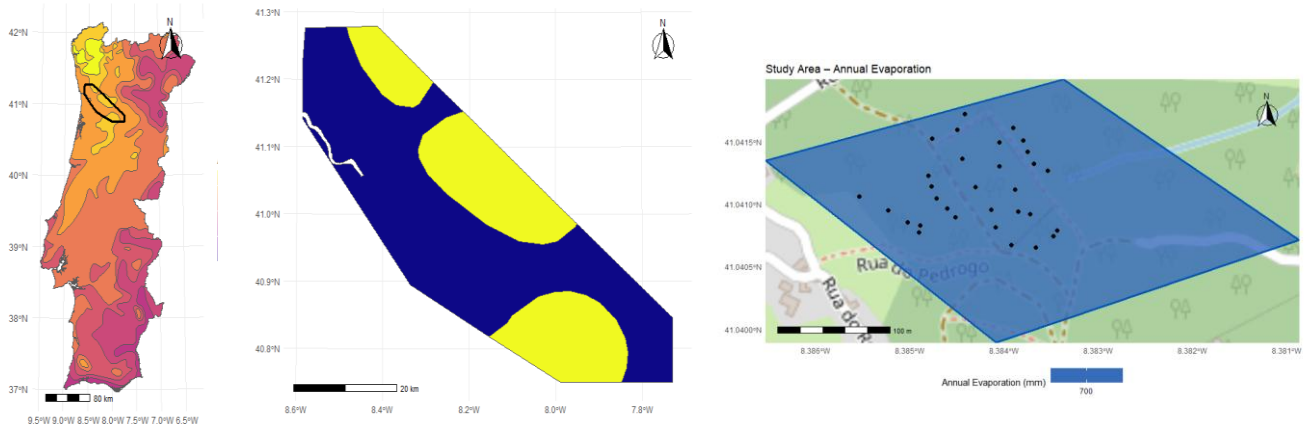

Figure 2.9 Annual evaporation average (mm) for Portugal, the DCB and the study area (adapted from Atlas do Ambiente 1985).

The difference in height between the north and south sites results in areas with reduced daily sun exposure, particularly during the winter months. In this context, climate conditions develop that are less favourable to the occurrence of significant temperature and evaporation peaks (Gonçalves 2013).

2.4.4 Soils

Portugal exhibits a wide diversity of soils, shaped by a complex interplay of climatic, geomorphological, and lithological conditions. The dominant soil classes include Cambisols, Fluvisols, Lithosols, Luvisols, Planosols, Podzols, Rankers, Regasols, Solonchaks, and Vertisols. These soils exhibit distinct morphological and chemical characteristics that govern their ecological function and suitability for land use. Cambisols are widely distributed across northern and central Portugal, having developed from various parent materials, including initial weathering and the formation of structure (IUSS Working Group WRB 2022). Their moderate fertility and depth make them suitable for forestry and pastureland.

The most representative soil types within the Douro coalfield include Cambisols, Regosols, Rankers, and Fluvisols. Cambisols are common in areas of moderate topography where pedogenesis has resumed over weathered metasedimentary substrates. Regosols dominate disturbed areas, including coal spoil heaps and eroded slopes, where profile development is in its incipient stage. Rankers are found in steeper terrains or regions dominated by resistant rock outcrops. Fluvisols occur in limited valley bottoms influenced by fluvial dynamics. The dominance of these soils reflects both the natural litho-geomorphological setting and the strong anthropogenic imprint of coal mining and self-burning processes, which continue to shape the pedological evolution of the region (Espinha Marques et al. 2021).

According to the World Reference Base for Soil Resources (WRB), the soils identified in the study area are primarily classified as technosols and regosols. Technosols dominate the zones directly associated with the coal waste pile, where the parent material consists wholly or partially of mining residues, either unburned (UCW), burned (BCW), or a heterogeneous mixture of both (MBW). These Technosols are poorly developed, often lacking an A horizon, and predominantly composed of coarse-textured materials. In contrast, Regosols are the original soil before the disposal of coal mining waste. These soils are derived from Carboniferous metasedimentary rocks and show shallow but identifiable profiles (Espinha Marques et al. 2024).

The Regosols are poorly developed mineral soils lacking significant horizon differentiation. They form on unconsolidated materials, such as colluvium or weathered rock fragments, and are typical of unstable or recently disturbed environments (FAO 2006). In coal-mining landscapes like São Pedro da Cova, Regosols form in spoil heaps and eroded slopes, where soil genesis is in its early stages of development.

2.4.5 Vegetation

The Portuguese Forest is an ancient ecosystem, characterised by deciduous trees in the north and evergreen trees in the south. In 2017, the area occupied by forests in mainland Portugal was 39.0 %, equivalent to 3,472,459 hectares. In the centre and north of the country, 57 % of the plant species are of European origin, and only 26 % are Mediterranean species (Silva 2024). In the northeast, oceanic influences are more pronounced, and evergreen species are replaced by deciduous trees that are better adapted to humid climates. The latitudinal layout of Portuguese territory gives rise to various areas of potential vegetation, the distribution of which is fundamentally based on temperature and rainfall. In northern Portugal, the Atlantic region is characterised by deciduous species typical of Oceanic Europe. The deciduous forest is primarily

composed of tall trees with large, broad leaves. The deciduous forest is a biome, but it is not restricted only to the temperate maritime climate. Mixed deciduous woodlands characterise the area, featuring species such as ash, sycamore, oak, beech, chestnut, linden, poplar, elm, birch, broom, heather, and brambles. However, some evergreen species, such as maritime pine, can also coexist, especially on mountain slopes (Silva 2024).

The vegetation in the study area, principally in the forest site at the uphill soil, is represented by the following species: *Pinus pinaster, Arbutus unedo, Eucalyptus, and Bryophyta*. For the coal mining waste disposal site, the species *Acacia dealbata* and *Eucalyptus globulus* were characteristic of the unburned site, the mixed material and the down soil (Narayan et al. 2024).

2.5. General Sampling Description

The study area was divided into six sites, depending on the location of the coal mining disposal and the type of coal mining waste. To answer the specific objectives of this thesis, 41 soil samples, including deposited coal mining waste, a covering layer of the burning coal waste site (CL) and the soils located uphill (US) and downhill (DS), were collected. On the site, coal mining waste with and without the combustion process was identified (BCW, UCW, respectively), as well as areas with a mix of these two types of coal waste and typical soil (MBW) (Figure 2.10).

Figure 2.10 The Fojo coal mining waste disposal area and the sample site location (Espinha Marques et al. 2024).

Representative soil samples of each site were distributed as follows: i) 5 soil samples for uphill soil (US1, US2, US3, US4, US5); ii) 5 soil samples for unburned coal mining waste (UCW1, UCW2, UCW3, UCW4, UCW5); iii) 10 soil samples for burned coal mining waste (BCW1, BCW2, BCW3, BCW4, BCW5, BCW6, BCW7, BCW8, BCW9, BCW10); iv) 10 soil samples for the covering layer (CL1, CL2, CL3, CL4, CL5, CL6, CL7, CL8, CL9, CL10); v) 6 soil samples for MBW (MBW1, MBW2, MBW3, MBW4, MBW5, MBW6); and vi) 5 soil samples for DS (DS1, DS2, DS3, DS4, DS5) (Figure 2.2). Table 2.1 specifies the number of samples between unburned, burned, and mixed material used for each analysis: i) geochemical, mineralogical and petrological characterisation, 21 samples; ii) the pedological study, 39 samples were analysed; and iii) 25 samples were used for the ecotoxicological essays.

Table 2.2 Sample identification for the petrographic, mineralogic, pedological characterisation and ecotoxicological studies

Sample	Characterisation						Ecotoxicological essays
		Mineralogy					
	Petrology	SEM-EDX	XRD	Geochemistry	PAH	Pedology	
US1	-	-	-	-	-	X	X
US2	-	-	X	-	-	X	-
US3	-	-	-	-	-	X	-
US4	-	-	X	-	X	X	X
US5	-	-	-	-	-	X	X
UCW1	-	-	-	X	X	X	X
UCW2	X	X	X	X	-	X	-
UCW3	-	-	-	X	-	X	X
UCW4	-	-	-	X	X	X	-
UCW5	X	X	X	X	X	X	X
MBW1	-	-	-	X	-	X	X
MBW2	-	-	X	X	-	X	X
MBW3	-	-	-	X	-	X	X
MBW4	X	X	-	X	-	X	X
MBW5	-	-	X	X	X	X	X
MBW6	-	-	-	X	-	X	X
BCW1	-	-	-	X	X	X	-
BCW2	-	-	-	X	-	X	-
BCW3	-	-	X	X	-	X	X
BCW4	-	-	-	X	-	X	X
BCW5	-	-	X	X	X	X	-
BCW6	-	-	X	X	-	X	-
BCW7	X	X	-	X	X	X	-
BCW8	-	-	-	X	-	X	X
BCW9	-	-	X	X	X	X	X
BCW10	X	X	-	X	-	X	X
CL1	-	-	-	-	-	X	-
CL2	-	-	-	-	-	X	-
CL3	-	-	X	-	-	X	X
CL4	-	-	-	-	-	X	X
CL5	-	-	X	-	-	X	-
CL6	-	-	X	-	-	X	-
CL7	-	-	-	-	-	X	-
CL8	-	-	-	-	-	X	X
CL9	-	-	X	-	-	X	X
CL10	-	-	X	-	-	X	X
DS1	-	-	-	-	-	-	X
DS2	-	-	X	-	X	-	-
DS3	-	-	X	-	-	X	X
DS4	-	-	-	-	-	X	-
DS5	-	-	X	-	-	X	X

The sample collection was conducted in July and August 2021, depending on the zoning of the study area, which was defined by soil mapping (Agroconsultores and Geometral 1995) and the World Reference Base for Soil Resources (FAO 2015). The soil (uphill and downhill) and CMW (burned, unburned, and mixed material) samples were taken at the heterogeneous area to a depth of 20 cm. Each soil sample was collected with a mass of around 1 kg and stored in polyethene bags. For US and DS, the first covering was removed before collecting the samples to avoid contamination from roots, leaves, and the first organic layer. At the laboratory, the soil samples were dried at room temperature until they were in equilibrium with the laboratory's humidity. After this period, the soil samples were homogenised to: i) the original sample without granulometric discrimination, separated into four quadrilles was used for petrological and geochemical analysis; ii) the original sample with granulometric separation smaller than 2 mm was

used for lixiviate chemical analysis; and iii) original samples with a granulometric separation smaller than 4 mm was used for ecotoxicological studies.

Chapter 3. The Fojo Coal Mining Waste Characterisation: Petrography, Mineralogy and Geochemistry

3.1 Introduction

The Fojo coal mining waste in the Douro Coalfield comprises rejected, unburned, and burned material by the effect of the combustion process that was subsequently extinguished by the remobilisation of the material and the application of water mixed with a cooling accelerator agent. The coal waste originated from the deposition of coal mining residues and is composed predominantly of different lithologies, such as carbonaceous shales and lithic arenites (Ribeiro et al. 2010ab; 2011, 2022), with variable quantities of anthracite A (ISO 11760, 2005).

The main objective of this chapter is to study the petrological, mineralogical, and geochemical composition of the mining residues of the Fojo coal mining waste, as well as the identification and quantification of the 16 priority PAH. Evaluate their source, affinity, and association.

3.2. Methodology

A total of 21 coal mining waste (CMW) samples were analysed, including five unburnt samples (UCW1, UCW2, UCW3, UCW4, UCW5), ten burned samples (BCW1, BCW2, BCW3, BCW4, BCW5, BCW6, BCW7, BCW8, BCW9, BCW10), and six mixed samples (MBW1, MBW2, MBW3, MBW4, MBW5, MBW6). The sampling sites are shown in Figure 3.1. Petrographic, mineralogy, and geochemical analyses were performed on these samples.

Five samples were selected for mineralogical analysis: two from the UCW site (UCW2 and UCW5), two from the BCW group (BCW7 and BCW10), and one from the MBW (MBW4). Polycyclic aromatic hydrocarbons (PAH) were also analysed in ten samples representing different types of coal mining waste and surrounding soils. These included one sample from uphill soil (US4), two from UCW (UCW1 and UCW4), four from BCW (BCW1, BCW5, BCW7, and BCW9), two from MBW (MBW1 and MBW5), and one from downhill soil (DS2).

Figure 3.1 Location (in orange) of the coal mining waste samples analysed for petrographic, mineralogic, and geochemical features.

3.1.1 Petrographic and Mineralogic Analyses

Petrographic studies were conducted on polished blocks prepared following standard procedures (ISO 7407-2, 2009) (Figure 3.2). The random and maximum vitrinite reflectance was determined using a Leica DM4000 microscope equipped with white light and fitted with “Discus-Fossil” software. Petrographic characterisation and vitrinite reflectance were performed following established standard procedures and International Committee for Coal and Organic Petrology (ICCP) recommendations (ISO 7404-5, 2009; ICCP, 1998, 2001). The ICCP classification system proposed by Misz-Kennan et al. (2020) was employed to identify the organic particles affected by self-burning in coal waste materials.

Figure 3.2 Coal mining waste sample, polished blocks for petrological analyses.

Scanning Electron Microscopy with Energy Dispersive X-ray spectrometry (SEM-EDX) analyses were performed at the University of Porto Materials Center (CEMUP) to complement the optical microscopy observations and provide further information for mineral identification and element mode of occurrence. The study of selected samples on polished blocks included observation under secondary electron and backscattered electron detection modes, as well as energy-dispersive X-ray (EDX) analysis, to determine their chemical compositions. The SEM-EDX analyses were performed using an FEI Quanta 400FEG environmental scanning electron microscope with a Genesis X4M energy-dispersive X-ray analyser. Before analysis, the polishing blocks were coated with a thin film of C by vapour deposition using the JEOL JEE-4X vacuum evaporation equipment.

3.1.2 Geochemical Analysis

Ash yield and moisture in the coal mining waste material were determined following ISO standards (ISO 1171, 2010; ISO 589, 2008). The geochemical analyses included inductively coupled plasma emission spectrometry/mass spectrometry (ICP-OES/MS) to determine the inorganic composition of major and trace elements in the studied samples after digestion with an acid solution of H_2O-HF-$HClO_4$-HNO_3. To ensure the quality of the data, reference materials, duplicates, and blanks were subject to analysis. The ICP-OES/MS analyses were conducted by Bureau Veritas Mineral Laboratories (Canada).

3.1.3 Polycyclic Aromatic Hydrocarbons (PAH)

Ten (10) samples were subjected to analysis, comprising two unburnt and six samples of burnt coal mining waste. These samples represent the diverse range of materials present within the study area. Each sample was pulverised to a particle size of 1 mm and extracted with a 1:1 acetone mixture using the Soxhlet method as described in the USEPA 3540 method (USEPA 1996). A 10 g portion of the test sample with 10 g of anhydrous sodium sulphate was placed in an extraction thimble. The samples were extracted for 24 hours at a rate of 4-6 cycles per hour. After the extraction of the samples,

the solvent vapour recovery was done, and the samples were concentrated to 2.0 mL with a gentle flow of N_2. Thereafter, sample cleaning was performed using silica gel cleanup (USEPA 3630C) and sulphur cleanup (USEPA 3660B). The 1g silica cartridges were conditioned by adding 4 mL of hexane for 5 min. Samples were then passed through and eluted with two 3 mL portions of hexane. With a gentle flow of N_2, the samples were concentrated to 1 mL and 2 g of cleaned copper powder was added. The sample extract is recovered and evaporated to dryness under a nitrogen stream. The residue was dissolved in 500 µL of acetonitrile, from which it was taken for analysis according to the procedure described by Borges et al. (2018).

3.1.4 Statistical Analysis

Chemical element concentration was correlated with ash yield, and the correlation was calculated using Pearson's coefficient to understand the mode of occurrence of each element and its association with the corresponding chemical group. Cluster analysis was used to understand the similarity or degree of separation between elements. Principal component analysis was used to project coal geochemistry data, maximising the variance of each dimension and highlighting the chemical elements with the most significant influence in the different samples. The significance level used was $\alpha = 0.05$, and the statistical software used was SPSS v29 and R. Ward's clustering methods utilised Statistics 14 software to aggregate chemical elements and understand geochemical affinity.

3.2 Results

3.2.1 Petrographic and Mineralogical Characterisation

A qualitative petrographic characterisation of the organic and mineral matter in the CMW was conducted. Table 3.1 presents the results of random and maximum vitrinite reflectance (Rr and Rmax). Thus, Rx range of 5.20 % to 6.23 % for BCW, 5.20 % to 7.61 % for UCW, and 5.29 % to 6.73 % for MBW (Table 3.1). In contrast, maximum vitrinite reflectance values range from 6.15 % to 7.05 % for BCW, 6.18 % to 7.84 % for UCW, and 6.53 % to 7.39 % for MBW (Table 3.1).

Table 3.1 Mean random (Rr) and maximum vitrinite (Rmax) reflectance data for Fojo CMW.

	Samples	Rr (%)	Rmax (%)
Unburned CMW	UCW1	5.60	6.34
	UCW2	6.34	6.81
	UCW3	5.53	6.66
	UCW4	5.19	6.18
	UCW5	7.61	7.84
Burned CMW	BCW1	5.49	6.72
	BCW2	5.58	6.57
	BCW3	5.41	6.71
	BCW4	5.40	6.72
	BCW5	5.20	6.15
	BCW6	5.38	6.50
	BCW7	5.96	6.84
	BCW8	5.36	6.58
	BCW9	5.38	6.58
	BCW10	6.23	7.05
Mixed CMW	MBW1	6.06	7.39
	MBW2	5.43	6.57
	MBW3	5.65	6.66
	MBW4	6.73	7.18
	MBW5	5.30	6.53
	MBW6	5.29	6.58

The petrographic analysis revealed that the samples are composed primarily of minerals, with quartz being the most prevalent (Figure 3.3A). The reddish or blue-greyish colour observed in the burned sample indicates the presence of iron oxides (Figure 3.3 B, C, and D). The latter two (C and D) indicate elevated temperatures resulting from the self-burning process. In the UCW sample, iron oxides are derived from the weathering of iron minerals, typically pyrite (Figure 3.3 E and F).

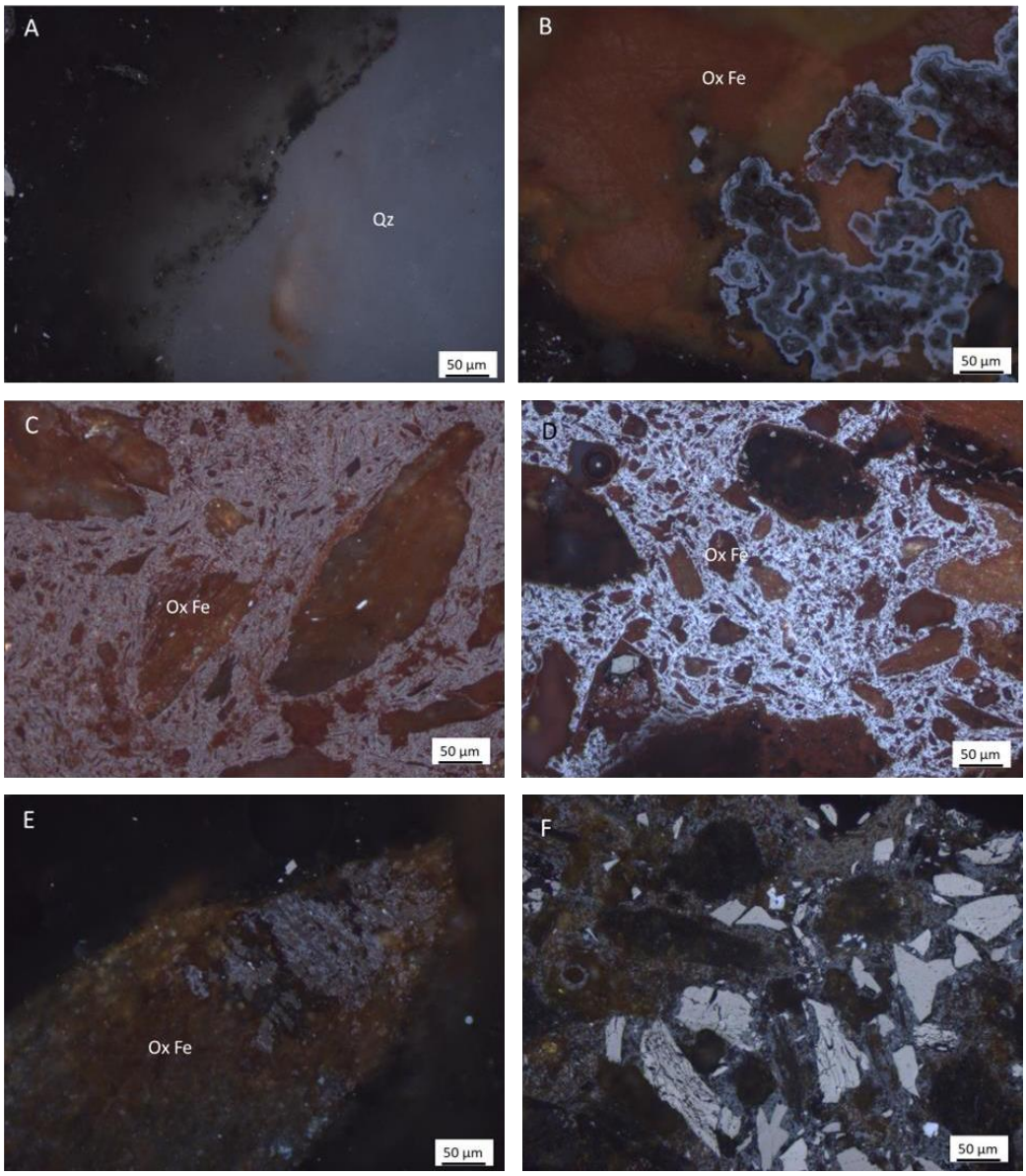

Figure 3.3 Minerals identification from photomicrographs: A) quartz (Qz); B) iron oxides (OxFe) reddish with self-burning signals to greyish blue; C) and D) matrix of iron oxides (OxFe) greyish blue; E) and F) iron oxides particle in a UCW.

In addition to the mineral fraction, the organic fraction comprises vitrinite, specifically collotelinite (Figure 3.4 A, C, and D) and collodetrinite (Figure 3.4 B). Inertinite particles, namely fusinite and semifusinite, were also identified (Figures 3.4 B and C, respectively).

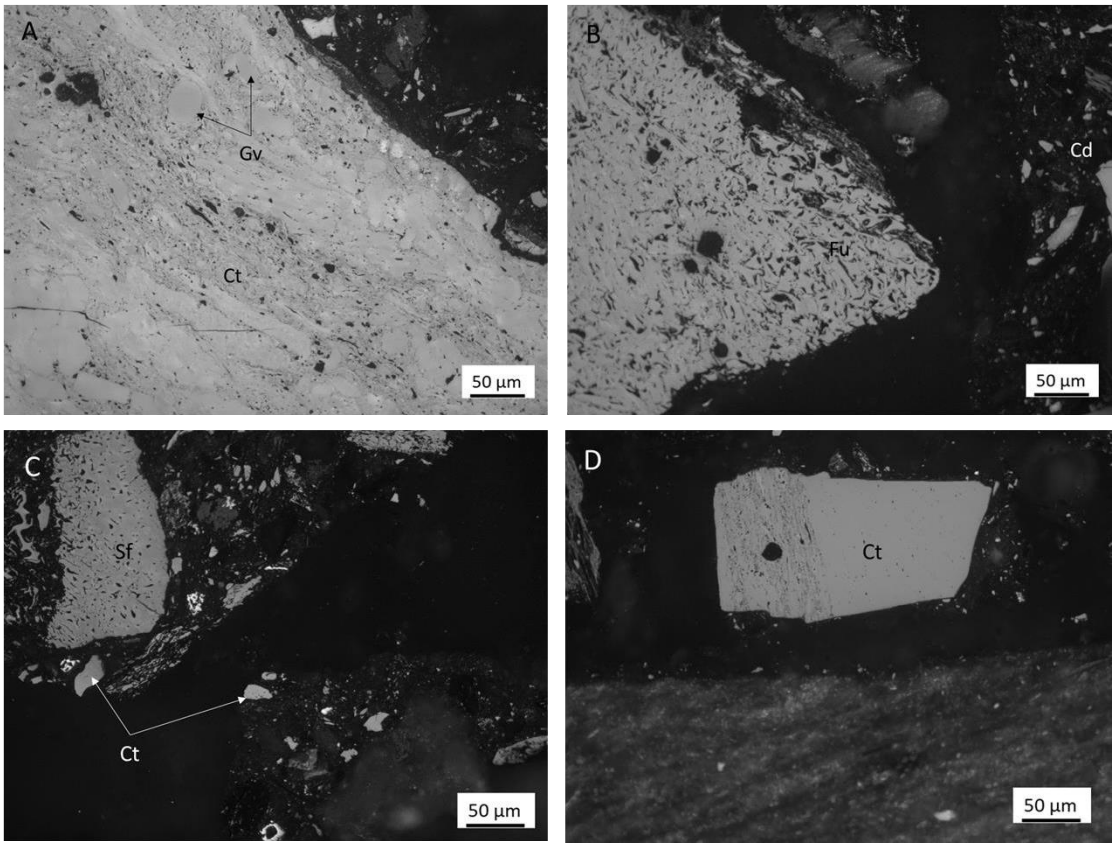

Figure 3.4 Photomicrographs of macerals present in the samples: A) Gelovritrinite (Gv) in collotelinite (Ct); B) Fusinite (Fu) and collodetrinite; C) Semifusinite (Sf) and collotelinite (Ct); D) Collotelinite (Ct).

It was also identified that organic particles with evidence of combustion were present in the samples. The petrographic features identified are cracks and dark reaction rims (Figure 3.5 A, B, C, and D), oxidation of framboidal pyrite (Figure 3.5 E), devolatilisation vacuoles (Figure 3.5 F) and pyrolytic carbon (Figure 3.5 G and H). These features were previously identified in other wastes that experience combustion in the Douro Coalfield, namely in the São Pedro da Cova, Lomba, and Midões waste piles (Ribeiro et al. 2010a).

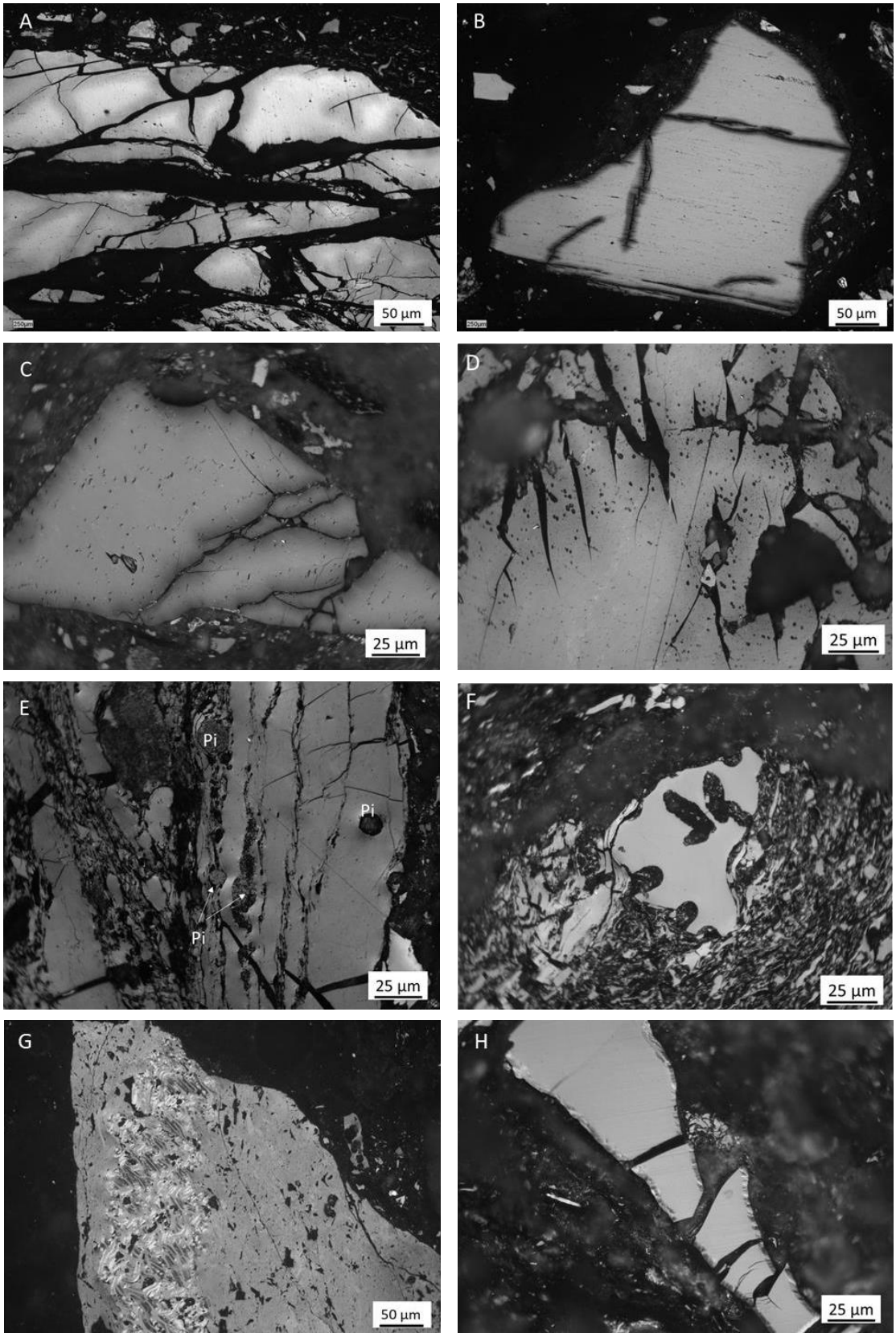

Figure 3.5 Photomicrographs of particles showing evidence of self-burning. A, B, C, and D – Particles with cracks and dark reaction rims; E – Oxidised framboidal pyrite (Pi); F – Particle with devolatilisation vacuoles; G and H – Particles with pyrolytic carbon.

In addition to these features, some particles were identified as reaction rims with higher reflectance (Figure 3.6). In anthracite, the brighter edges of higher reflectance rims are associated with lower combustion temperatures (Alpern and Maume 1969; Misz-Kennan et al. 2020). This may be related to the rapid cooling promoted by the coolant agent used to extinguish the fire, as these features were never observed in the other wastes that experienced combustion in the Douro Coalfield.

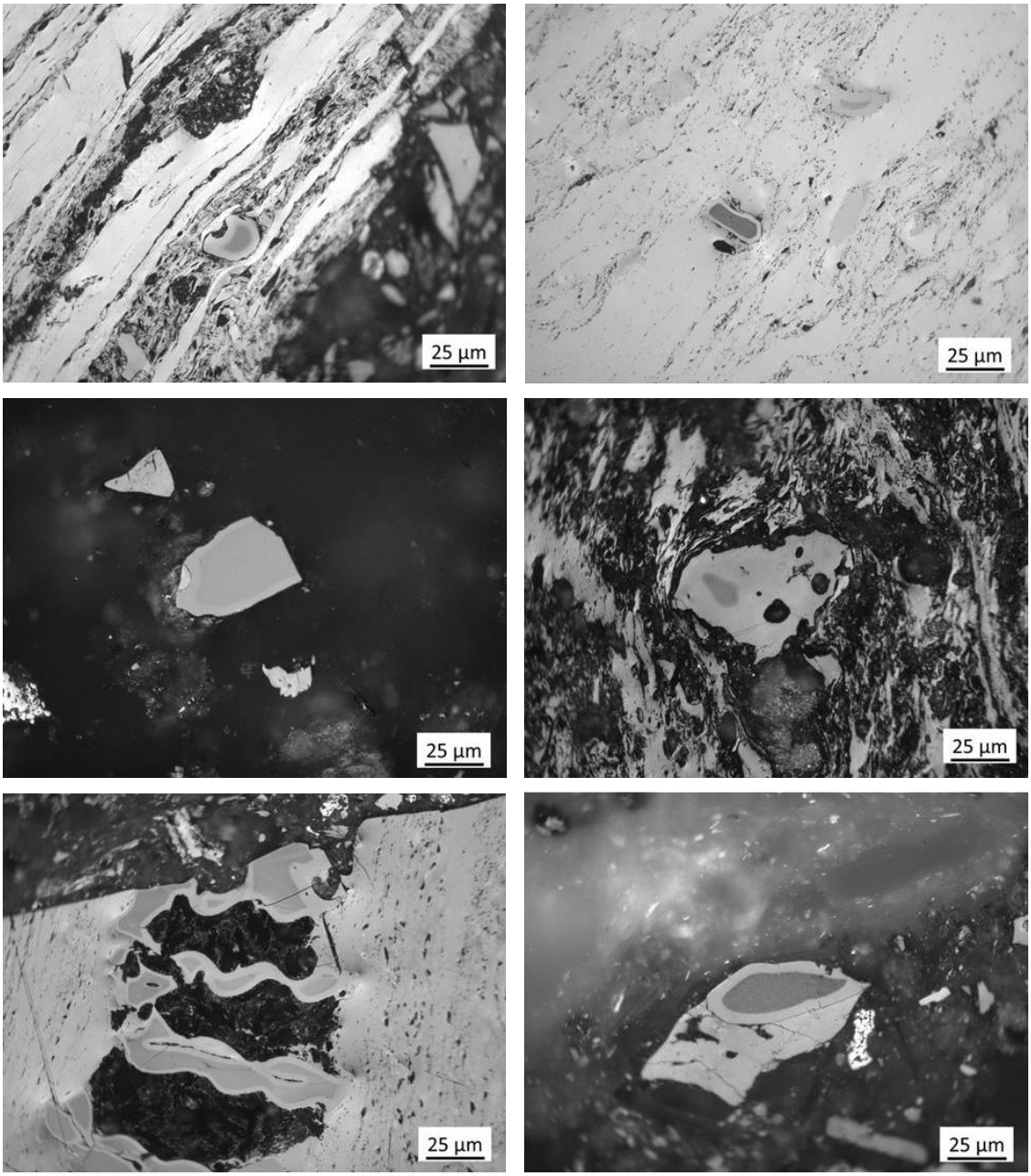

Figure 3.6 Photomicrographs of particles with brighter reaction rims.

Mineralogical analysis indicates that all samples contain zircon, rutile, xenotime, monazite, pyrite, and iron oxides (Figure 3.7).

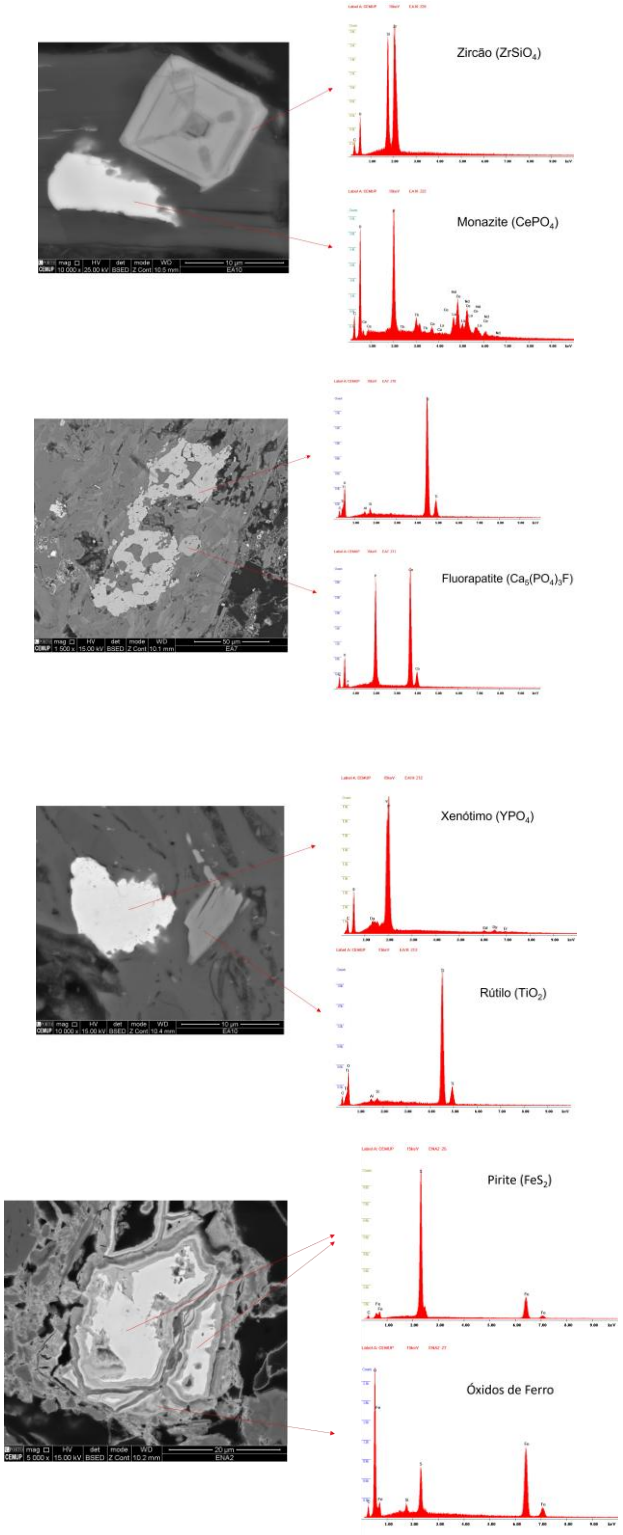

Figure 3.7 SEM image and EDS spectra for samples a) and c) BCW10; b) BCW7; and d) UCW2; this spectrum shows a pyrite particle associated with iron oxide.

In addition, the burned samples BCW10 and BCW7 contained cinnabar and galena (Figure 3.8).

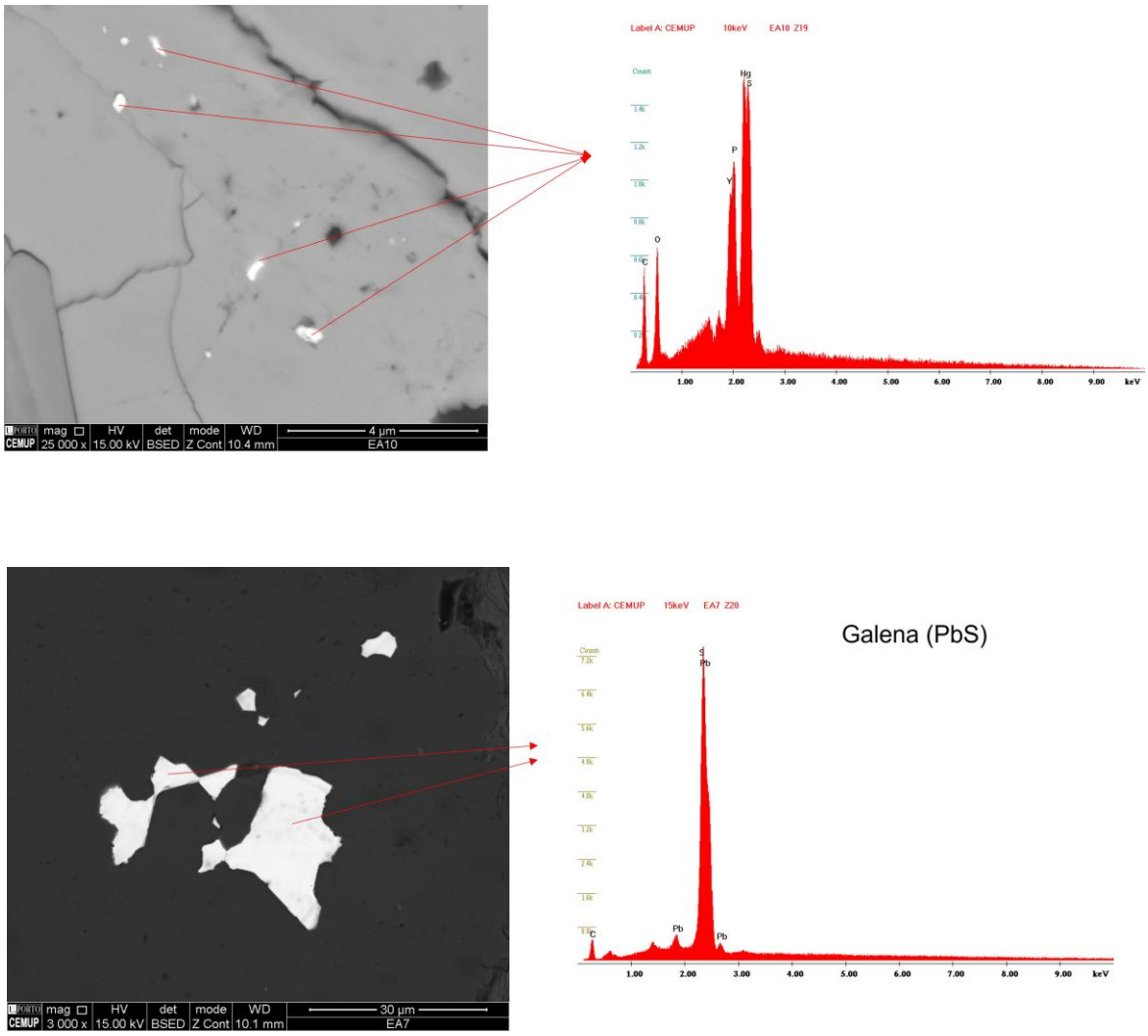

Figure 3.8 SEM image and EDS spectra for samples BCW10 and BCW7.

The unburnt samples were also identified as florencite, acanthite (silver sulphide), and arsenopyrite. Concurrently, a minor particle was discerned that may indicate cassiterite (Figure 3.9).

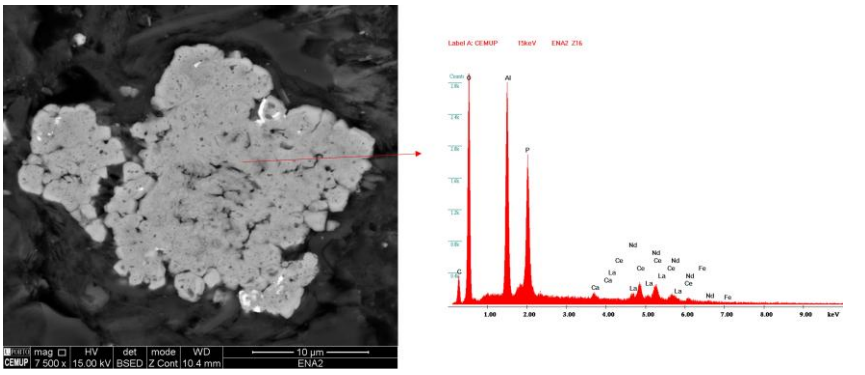

(a)

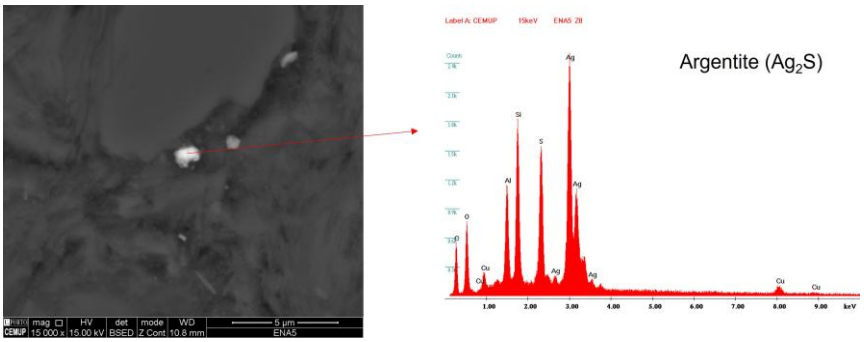

(b)

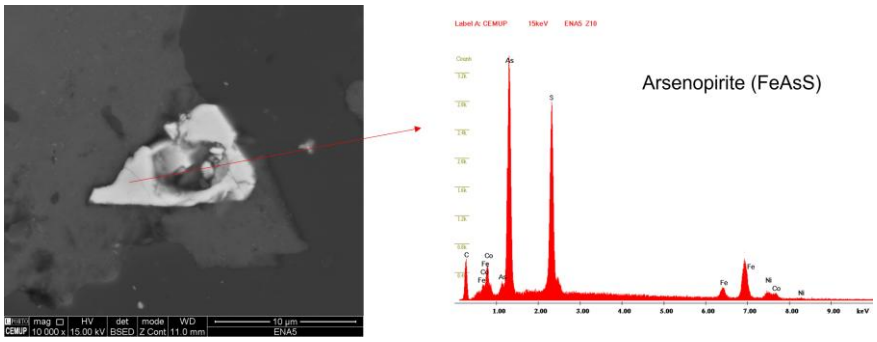

(c)

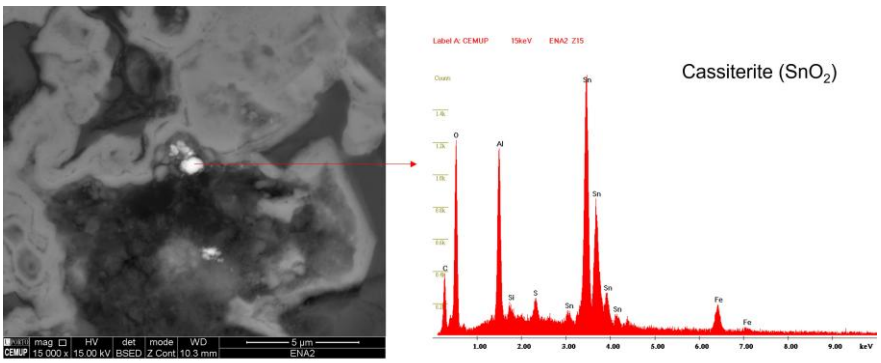

(d)

Figure 3.9 SEM image and EDS spectra for samples a) and d) UCW2; b) and c) UCW5.

3.2.2 Ash Yield and Geochemical Composition

3.2.2.1 Coal Waste Material Characterisation

To characterise the three types of coal waste, key geochemical parameters were analysed, including ash yield, pH, electrical conductivity (EC), and organic matter (OM) content. Table 3.2 summarises the average values of these parameters of each coal mining waste type. The ash yield is reported on a dry basis (db) for UCW, MBW, and BCW. The ash yield was notably higher in BCW compared to UCW, indicating significant mineral enrichment after combustion. BCW values range from 78.35 % to 91.20 %, MBW with a range of 77.00 % to 84.89 %, and UCW showed values from 71.36 % to 83.09 %. pH values for the three types of coal waste varied from 3.50 to 5.23 for UCW, 3.63 to 4.63 for BCW, and from 3.83 to 4.23 for MBW. These values indicate that the coal waste is strongly acidic. Electrical conductivity values for the three types of coal waste indicated high ion mobility. The highest range is UCW> BCW > MBW. OM content was highest in UCW and decreased in BCW and MBW, likely due to combustion-driven organic matter degradation.

Table 3.2 Ash yield on a dry basis (db) data, humidity, pH, electrical conductivity, and organic matter (OM) values for Fojo coal mining waste

	Samples	Ash (wt.%)	W (wt.%)	pH	Conductivity (µS/cm)	OM (%)
Unburned coal waste	UCW1	71.36	2.67	4.75	147.6	19.44
	UCW2	81.42	2.04	5.23	166.8	14.36
	UCW3	83.09	2.43	5.15	155.0	24.92
	UCW4	72.03	2.97	3.75	416.0	25.48
	UCW5	74.92	2.50	3.50	322.0	24.51
Burned coal waste	BCW1	83.52	2.11	3.97	148.3	10.7
	BCW2	83.01	2.25	4.10	235.0	9.99
	BCW3	82.79	2.15	4.08	179.3	7.77
	BCW4	84.32	1.98	4.28	103.3	11.36
	BCW5	79.36	2.4	3.63	248.0	14.49
	BCW6	85.13	1.93	4.01	133.7	9.89
	BCW7	78.35	2.17	3.73	357.0	15.81
	BCW8	86.22	1.81	4.16	211.3	7.23
	BCW9	78.43	2.39	4.13	208.7	4.49
	BCW10	91.2	1.53	4.63	100.6	4.69
Mixed burned coal waste	MBW1	77.00	2.08	3.83	208.3	9.03
	MBW2	83.77	1.80	4.10	255.0	12.95
	MBW3	84.89	1.61	4.04	238.7	7.93
	MBW4	84.83	1.90	4.23	107.7	11.24
	MBW5	84.48	2.04	3.97	202.3	11.64
	MBW6	82.00	2.09	3.90	269.7	11.52

Table 3.3 illustrates the major and trace elements present in UCW, BCW, and MBW material of the Fojo mining waste. The data are compared with the concentrations of these elements in the Douro Coalfield (DC) materials, including unburned coal waste piles (UCWDC) and burned coal waste piles (BCWDC), coal from the coalfield (DC_{coal}), and primary overlain lithologies (DC_{Litho}) used by Ribeiro et al. (2022). The rare earth elements (REE) are reported as the sum of the light REE (∑LREE: La, Ce, Pr, Nd, Sm) and the heavy REE (∑HREE: Eu, Gd, Tb, Dy, Ho, Er, Tm, Yb, Lu).

The higher values for the major elements were observed in the order Al > Fe > K. In contrast, the other major elements, Ca, Mg, Na, P, S, and Ti, exhibited concentrations below 1% for the unburned, burned, and mixed coal mining waste. The concentration of trace elements, ∑LREE and ∑HREE elements concentration in UCW exhibited the following pattern: Ba > Mn > Rb > LREE > V > Zr > Li > Cr > Zn > Sr > Pb > As > Cu > Ni > Ga > Cs > Sc > Th > Co > Y > ∑HREE > Sb > Nb > U > Be > Sn > Mo > Hf > W > Bi > Ta > Cd. In contrast, the pattern for BCW and MBW was Ba > ∑LREE > Rb > Mn > V > Sr > Cr > Li > Zr > Zn > As > Cu > Pb > Ga > Ni > Cs > Sc > Th > ∑HREE > Y > Sb > Nb > Co > Sn > U > Be > Mo > Hf > W > Bi > Ta > Cd.

The concentrations of major elements in the studied samples are lower than those reported for DCcoal, except for S, which is more similar to DC_{litho}. In contrast, trace element concentrations are typically lower than those reported for DC_{coal}. The mean concentration of major and trace elements in this study exhibited a comparable concentration to that observed in UCWDC, except for the following elements: Ag, Ba, Cd, Cr, Cs, Li, Sb, Sr, and Zr with lower concentrations, and higher concentrations for Co, Cu, Pb, and Rb. In the case of burned coal waste, a comparison with BCWDC, there is an enrichment for Fe, Mn, Ag, As, Cu, Pb, Sb, Sc, Zn, and ∑LREE, while the concentration for Ti, Cr, Cs, Li, Nb, Ni, Sr, Ta, U, W, and ∑HREE is lower.

Table 3.3 Major and trace element concentration for the three types of coal waste and comparison with the main value in the DC

	Unburned coal mining waste UCW (n=5)				Burned coal mining waste BCW(n=10)				Mixed coal mining waste MBW (n=6)							
	Mean	SD	Max	Min	Mean	SD	Max	Min	Mean	SD	Max	Min	*UCWDC	*BCWDC	**DC_{coal}	**DC_{Litho}
Al (%)	8.37	0.24	8.72	8.11	9.37	0.41	9.72	8.33	8.53	0.45	9.06	7.88	8.53	9.68	11.7	9.19
Ca (%)	0.11	0.08	0.24	0.03	0.06	0.01	0.09	0.04	0.06	0.01	0.08	0.05	0.09	0.05	0.32	0.05
Fe (%)	4.55	0.68	5.72	3.92	5.99	0.77	7.09	4.63	5.46	0.75	6.58	4.37	4.20	2.97	4.45	2.66
K (%)	2.38	0.10	2.45	2.20	2.61	0.09	2.73	2.45	2.44	0.11	2.55	2.24	2.33	2.31	2.55	2.47
Mg (%)	0.36	0.14	0.59	0.21	0.33	0.04	0.38	0.26	0.36	0.06	0.43	0.27	0.31	0.20	0.46	0.46
Na (%)	0.37	0.06	0.45	0.28	0.44	0.05	0.51	0.37	0.42	0.05	0.47	0.35	0.34	0.52	1.00	0.41
P (%)	0.08	0.01	0.09	0.08	0.08	0.01	0.10	0.07	0.07	0.02	0.09	0.05	0.10	0.06	0.22	0.03
S tot (%)	0.39	0.07	0.49	0.31	0.47	0.14	0.79	0.22	0.47	0.11	0.63	0.35	0.25	0.42	0.07	0.10
Ti (%)	0.25	0.03	0.27	0.21	0.24	0.02	0.29	0.21	0.25	0.02	0.27	0.23	0.29	0.41	0.58	0.40
Mn (mg/kg)	230	169	475	47.0	141	53.4	267	77.0	135	17.8	153	108	251	63.5	313	430
Ag (mg/kg)	366	100	543	304	260	47.2	367	220	215	38.3	277	177	226	182	n.a	n.a
As (mg/kg)	53.6	8.84	62.3	41.1	61.0	9.58	79.6	49.6	53.0	5.83	62.1	47.0	52.4	41.1	142	11.0
Ba (mg/kg)	453	19.4	480	431	550	58.3	653	446	502	45.9	550	437	521	549	1187	667
Be (mg/kg)	4.40	1.14	6.00	3.00	3.90	0.74	5.00	3.00	3.67	0.52	4.00	3.00	4.05	4.03	12.0	3.33
Bi (mg/kg)	0.71	0.07	0.80	0.64	0.85	0.16	1.22	0.71	0.61	0.13	0.79	0.46	0.69	0.77	1.77	0.22
Cd (mg/kg)	0.17	0.15	0.39	0.03	0.15	0.08	0.29	0.03	0.12	0.03	0.16	0.08	0.22	0.17	1.06	0.12
Co (mg/kg)	10.7	8.90	23.4	2.20	5.45	1.27	8.60	3.80	5.38	0.99	6.80	4.10	5.49	4.77	73.3	8.60
Cr (mg/kg)	87.4	11.8	108	79.0	91.4	6.40	102	81.0	89.3	3.20	94.0	85.0	119	142	184	85.7
Cs (mg/kg)	17.3	2.59	20.7	14.3	21.5	2.29	25.8	17.1	18.9	1.40	20.5	17.4	21.3	34.4	78.3	18.9
Cu (mg/kg)	51.5	21.0	75.7	30.4	50.7	7.83	62.8	41.3	49.2	7.76	57.6	39.1	36.7	32.5	131	8.85
Ga (mg/kg)	23.2	0.76	23.9	22.1	26.9	1.52	29.1	24.3	24.6	2.04	27.3	22.4	24.0	26.5	36.4	23.3
Hf (mg/kg)	2.59	0.25	3.00	2.33	2.05	0.32	2.78	1.58	1.82	0.34	2.19	1.22	3.11	3.17	3.01	3.89
In (mg/kg)	0.09	0.01	0.10	0.09	0.10	0.02	0.12	0.08	0.11	0.01	0.13	0.09	0.09	0.08	n.a	n.a
Li (mg/kg)	96.4	10.0	107	85.9	93.4	5.19	102	86.7	85.4	5.52	91.0	75.6	134.	175	497	155
Mo (mg/kg)	3.29	0.84	4.28	2.32	3.00	0.28	3.57	2.69	2.50	0.38	3.11	2.13	3.02	4.83	25.8	0.69

*UCWDC= main value of unburned coal waste for the Douro Coalfield

*BCWDC= main value of burned coal waste for the Douro Coalfield

**DC_{coal}= main value of the coal from the Douro Coalfield

**DC_{litho}= main value of the lithology in the Douro Coalfield

	Unburned coal mining waste UCW (n=5)				Burned coal mining waste BCW(n=10)				Mixed coal mining waste MBW (n=6)				*UCWDC	*BCWDC	**DC_{coal}	**DC_{Litho}
	Mean	SD	Max	Min	Mean	SD	Max	Min	Mean	SD	Max	Min				
Nb (mg/kg)	7.13	0.95	7.92	5.52	6.76	0.65	8.12	5.83	7.08	0.79	8.13	6.04	9.48	19.5	22.6	16.9
Ni (mg/kg)	29.4	16.8	54.4	12.7	22.0	3.40	29.5	16.2	20.8	3.33	24.8	15.0	31.8	30.7	438	39.0
Pb (mg/kg)	68.4	27.9	115	46.1	53.5	7.42	67.3	45.3	47.8	6.53	55.0	39.5	35.5	45.7	88.6	36.6
Rb (mg/kg)	143	9.95	157	131	158	9.19	167	138	140	11.8	156	125	136	147	164	121
Re (mg/kg)	0.005	0.001	0.006	0.005	0.003	0.002	0.006	0.002	0.004	0.002	0.006	0.002	0.005	0.006	n.a	n.a
Sb (mg/kg)	7.78	2.26	10.2	4.72	9.08	1.22	10.4	7.07	7.58	0.72	8.50	6.71	13.1	5.50	8.76	5.28
Sc (mg/kg)	13.5	1.29	15.6	12.5	16.8	1.39	18.6	15.0	15.1	1.37	16.3	13.2	12.6	13.7	20.8	14.0
Se (mg/kg)	2.22	0.48	2.90	1.70	1.78	0.28	2.20	1.30	1.65	0.40	2.40	1.20	1.97	1.28	n.a	n.a
Sn (mg/kg)	4.20	0.42	4.70	3.80	4.92	0.65	6.20	4.00	4.63	0.56	5.50	4.00	4.27	5.73	10.2	4.97
Sr (mg/kg)	73.2	15.9	90.0	50.0	113	20.0	139	78.0	105	10.9	121	90.0	96.4	169	568	103
Ta (mg/kg)	0.56	0.09	0.60	0.40	0.52	0.04	0.60	0.50	0.53	0.05	0.60	0.50	0.61	1.17	1.4	0.90
Te (mg/kg)	0.08	0.03	0.13	0.05	0.07	0.02	0.10	0.05	0.07	0.04	0.15	0.05	0.08	0.07	n.a	n.a
Th (mg/kg)	12.6	1.50	15.1	11.4	16.1	2.13	18.2	11.8	13.1	1.99	15.1	10.6	11.4	13.3	15.0	10.3
Tl (mg/kg)	1.24	0.06	1.28	1.14	0.07	0.19	0.10	0.05	0.07	0.04	0.15	0.05	1.49	1.36	n.a	n.a
U (mg/kg)	5.16	0.65	6.20	4.70	4.62	0.35	5.20	3.90	4.00	0.65	5.10	3.20	5.26	6.10	10.4	4.07
V (mg/kg)	115	6.06	121	106	127	8.60	143	119	117	6.24	126	111	117	127	321	118
W (mg/kg)	1.04	0.23	1.40	0.80	1.21	0.19	1.70	1.00	1.23	0.10	1.40	1.10	1.89	3.07	6.60	2.10
Y (mg/kg)	10.4	1.10	11.8	8.90	9.59	1.51	12.4	7.10	8.30	1.73	9.60	5.30	10.4	12.6	23.5	7.00
Zn (mg/kg)	74.4	49.5	151	26.4	68.4	18.7	110	45.4	66.6	6.61	75.9	58.5	53.6	33.2	215	65.2
Zr (mg/kg)	97.4	9.4	113	88.8	72.4	9.52	92.8	58.0	67.0	12.4	82.5	44.5	107	114	103	132
ΣLREE (mg/kg)	136	20.4	169	114	195	38.7	237	126	155	27.7	183	120	136	179	256	128
ΣHREE (mg/kg)	10.1	1.05	11.4	8.70	9.93	1.24	11.6	7.70	8.42	1.62	9.70	5.82	12.0	14.2	28.8	9.30
ΣREE (mg/kg)	146	21.3	180	123	241	39.7	247	135	164	29.1	193	127	149	193	285	138

*UCWDC= main value of unburned coal waste for the Douro Coalfield

*BCWDC= main value of burned coal waste for the Douro Coalfield

**DC_{coal}= main value of the coal from the Douro Coalfield

**DC_{litho}= main value of the lithology in the Douro Coalfield

3.2.2.2 Geochemical Association: Correlation and Grouping

In order to investigate the mode of occurrence of the elements in coal mining waste from the Fojo mine, an inorganic affinity with indirect analysis was conducted using the Pearson correlation coefficient ($r > 0.500$; $p < 0.05$) to determine the relationship between each chemical element and the ash yield, as well as the elements themselves (n = 21 samples). The correlation coefficients of the elements with the ash yield are presented in Table 3.4 for each type of coal waste and bulk coal waste. Indeed, the mobilisation or availability of the chemical elements will depend on their mode of occurrence (Dai et al. 2021)

For UCW, coal waste without combustion, some elements have a significant positive correlation with the ash yield ($r > 0.9$, $p < 0.05$): P, Mn, Cd, Co, Cu, Ni, U, and Zn. Indicating that these elements could be concentrated in the inorganic fraction before combustion. Besides, Mg has a high correlation ($r = 0.899$; $p = 0.04$). On the other hand, for the coal waste after the combustion, BCW, it is observed that these same elements have a negative correlation with the ash yield, indicating volatilisation or mobility after the combustion. In the case of MBW, the mixed material showed similarity with the BCW and the UCW.

When the Pearson correlation is performed to the bulk samples of coal waste, the elements that show a positive correlation with the ash yield are Al, Fe, K, Mg, Na, S, As, Ba, Bi, Cd, Cr, Cs, Cu, Ga, In, Nb, Rb, Sb, Sc, Sn, Sr, Th, Tl, V, W, Zn, and ΣLREE. The elements with a negative correlation are Ca, P, Ti, Mn, Ag, Be, Co, Hf, Li, Mo, Ni, Pb, Re, Se, Ta, Te, U, Y, Zr, and ΣHREE. The negative correlation could indicate mobilisation by solubility or loss by combustion for some elements and/or affinity with organic fraction (Dai et al. 2021; Dai et al. 2023; Finkelman et al. 2018).

Table 3.4 Major, trace and REE element affinities deduced from Pearson correlation coefficients between each element concentration and the percentage of ash yield.

	UCW		MBW		BCW		Coal waste	
	r	*p-value*	*r*	*p-value*	*r*	*p-value*	*r*	*p-value*
Al	-0.760	0.135	-0.623	0.186	-0.283	0.429	0.345	0.125
Ca	0.820	0.090	-0.731	0.099	-0.446	0.197	-0.241	0.294
Fe	0.368	0.541	0.162	0.760	-0.064	0.861	**0.544**	**0.011**
K	-0.373	0.536	-0.712	0.113	-0.078	0.830	0.389	0.081
Mg	**0.899**	**0.040**	**-0.850**	**0.032**	0.280	0.433	0.126	0.588
Na	0.550	0.340	-0.767	0.075	-0.194	0.592	**0.454**	**0.039**
P	**0.939**	**0.017**	0.032	0.953	-0.494	0.147	-0.097	0.677
S tot	-0.561	0.325	0.130	0.806	-0.549	0.100	0.018	0.937
Ti	-0.126	0.840	0.725	0.103	0.615	0.059	-0.028	0.904
Mn	**0.913**	**0.030**	-0.183	0.729	0.033	0.928	-0.089	0.702
Ag	-0.368	0.543	-0.639	0.172	-0.540	0.107	**-0.696**	**<0.001**
As	0.032	0.960	0.264	0.613	0.217	0.547	0.291	0.200
Ba	0.535	0.353	-0.410	0.420	0.233	0.517	**0.571**	**0.007**
Be	0.422	0.479	0.300	0.563	0.501	0.140	-0.021	0.930
Bi	-0.806	0.099	0.783	0.065	0.215	0.550	0.217	0.344
Cd	**0.962**	**0.009**	-0.674	0.142	-0.304	0.392	0.019	0.936
Co	**0.967**	**0.007**	-0.728	0.101	-0.143	0.694	-0.135	0.560
Cr	0.841	0.074	-0.416	0.412	0.613	0.060	**0.531**	**0.013**
Cs	-0.824	0.086	-0.769	0.074	0.161	0.657	0.364	0.105
Cu	**0.920**	**0.027**	-0.739	0.094	-0.153	0.673	0.169	0.463
Ga	-0.507	0.383	-0.463	0.355	0.204	0.571	**0.513**	**0.017**
Hf	0.864	0.059	-0.343	0.506	-0.403	0.248	**-0.540**	**0.011**

	UCW		MBW		BCW		Coal waste	
	r	*p-value*	*r*	*p-value*	*r*	*p-value*	*r*	*p-value*
In	0.011	0.986	0.690	0.130	0.095	0.795	0.404	0.069
Li	0.854	0.066	-0.654	0.159	-0.126	0.730	-0.117	0.613
Mo	-0.270	0.660	0.406	0.425	-0.302	0.396	-0.368	0.101
Nb	-0.226	0.715	0.685	0.133	0.612	0.060	0.006	0.980
Ni	**0.963**	**0.008**	**-0.951**	**0.004**	-0.180	0.618	-0.070	0.762
Pb	-0.591	0.294	0.748	0.088	-0.281	0.431	**-0.552**	**0.009**
Rb	-0.820	0.089	**-0.878**	**0.022**	-0.211	0.558	0.102	0.660
Re	-0.456	0.441	0.191	0.717	-0.135	0.710	-0.032	0.892
Sb	0.517	0.373	0.421	0.405	-0.062	0.866	0.332	0.141
Sc	0.608	0.277	-0.720	0.106	-0.006	0.987	**0.582**	**0.006**
Se	0.061	0.922	0.671	0.144	0.186	0.606	-0.330	0.144
Sn	0.446	0.452	0.807	0.052	0.338	0.339	**0.589**	**0.005**
Sr	0.631	0.254	-0.590	0.218	-0.023	0.950	**0.638**	**0.002**
Ta	-0.274	0.655	**0.882**	**0.020**	0.275	0.443	-0.195	0.396
Te	0.069	0.912	-0.102	0.848	-0.238	0.508	-0.148	0.523
Th	0.565	0.321	-0.621	0.188	-0.219	0.542	0.372	0.097
Tl	-0.458	0.438	0.172	0.744	0.015	0.966	**-0.837**	**<0.001**
U	**0.993**	**0.001**	-0.161	0.761	**-0.693**	**0.026**	-0.343	0.128
V	0.347	0.567	0.167	0.751	0.377	0.283	**0.504**	**0.020**
W	0.553	0.334	0.624	0.186	0.033	0.927	**0.469**	**0.032**
Y	0.654	0.231	-0.666	0.149	-0.419	0.228	-0.333	0.141
Zn	**0.960**	**0.009**	-0.563	0.245	-0.294	0.409	0.130	0.575
Zr	0.749	0.145	-0.399	0.433	-0.327	0.357	**-0.616**	**0.003**
ΣLREE	0.378	0.530	-0.685	0.133	-0.160	0.659	0.397	0.075
ΣHREE	0.716	0.174	-0.642	0.169	-0.424	0.222	-0.143	0.535

The major elements, Al, Na, K, P, S, Ti, Ca, and Mg, were correlated with ash yield. The results exhibited a positive pattern for Al, Na, K, and Mg. A very strong positive correlation is observed for these elements. However, a negative correlation is observed in the case of P and Ca, which could indicate an association with the organic fraction. Titanium and S did not show a clear correlation with the ash yield.

Additionally, Pearson correlation analysis was performed to evaluate the major, trace, and REE associations with key geochemical groups, including aluminosilicates (Al+Na+K), zircon minerals (Zr+Hf), phosphate (P), sulphur (S), carbonates (Ca+Mg), and rutile mineral (Ti). The results, summarised in Table 3.5, highlight statistically significant correlations (r) with p-values < 0.05, categorising elements according to their chemical group affinities. The aluminosilicate group (Al+Na+K): Elements exhibiting strong positive correlations with aluminosilicates include Al, K, Na, Ba, Cs, Ga, Rb, Sc, Sr, Th, Tl, V, ΣLREE, and ΣHREE, suggesting their predominant occurrence within silicate phases. In contrast, Se shows a strong negative correlation, indicating its exclusion from aluminosilicate-bearing fractions; this element is more closely associated with the organic fraction. Iron, P, S, As, Bi, Cr, Li, Re, Sb, Sn, U, and Y also display low positive correlations, suggesting a possible but weaker association with aluminosilicate phases. On the other hand, in the zircon mineral group (Zr+Hf), elements such as Fe, Mn, Ag, Co, Hf, Li, Ni, U, Y, and Zr exhibit strong positive correlations with Zr+Hf, suggesting a geochemical affinity with zircon mineral phases. Conversely, Tl, Sr, Sc, Cs, and Fe show strong negative correlations, implying their relative depletion in zircon-rich fractions. Several other elements, including Mg, P, Ti, Be, Cd, Cr, Cu, Mo, Nb, Pb, Se, Ta, Te, Zn, and ΣHREE, exhibit low positive correlations, indicating a weaker association with zircon minerals.

The elements with a strong positive correlation with the carbonates group include Ca, Mg, Mn, Be, Cd, Co, Cr, Cu, Li, Ni, Sb, Zn, and Zr, indicating their likely incorporation into this geochemical phase. Cs is the only element showing a strong negative correlation with the carbonates, suggesting its geochemical incompatibility with this group. Other elements, such as Na, P, Ti, Hf, Nb, Sr, Ta, Tl, U, W, Y, and ΣHREE, exhibit weak positive correlations, suggesting a potential but less pronounced association with carbonates. The phosphate group (P) is composed of elements that exhibit a significant positive correlation with phosphate. Ga, Li, and U showed a *p-value* < 0.05, reinforcing their preferential incorporation into phosphate minerals. Additionally, several elements, including Al, Ca, Fe, K, Na, S, Mn, Ag, As, Ba, Be, Bi, Cd, Co, Cr, Cu, Mo, Ni, Rb, Sb, Sc, Se, Sn, Sr, Th, Y, Zn, ΣLREE, and ΣHREE, exhibit weak positive correlations (*r* <

0.5), suggesting a possible but less definitive association with phosphate-bearing phases.

Elements such as Be, Nb, and Ta display a strong positive correlation with rutile minerals, implying their geochemical affinity with Ti-bearing minerals. Other elements exhibiting weaker positive correlations include Ca, Mg, Mn, Bi, Cr, In, Pb, Sn, Tl, V, W, and Zr, indicating a possible but less pronounced association with rutile phases. In the sulphide group, sulphur (S) shows a strong positive correlation exclusively with Fe, suggesting its association with sulphide or sulphate phases within the samples. Additionally, several elements, including Al, Na, P, As, Cs, Ga, In, Mo, Pb, Rb, Re, Sc, Se, Sn, Sr, Th, and ΣLREE, exhibit weaker positive correlations with sulphur, indicating a potential but less significant association with sulphide or sulphate mineral.

Table 3.5 Person correlation and p-value between the element concentration and geochemical groups.

	Phosphate		Sulphur		Al+Na+K		Zr+Hf		Ca+Mg		Ti	
	r	*p-value*	*r*	*p-value*	*r*	*p-value*	*R*	*p-value*	*r*	*p-value*	*r*	*p-value*
Al	0.196	0.393	0.128	0.580	0.992**	<0.001	-0.267	0.242	-0.320	0.1577	-0.373	0.096
Ca	0.239	0.298	-0.323	0.153	-0.398	0.074	0.666**	<0.001	0.909**	<0.001	0.225	0.328
Fe	0.406	0.068	0.487	0.025	0.364	0.105	-0.615	0.003	-0.154	0.505	-0.233	0.309
K	0.194	0.400	-0.046	0.843	0.892**	<0.001	-0.245	0.284	-0.113	0.626	-0.064	0.783
Mg	0.028	0.904	-0.379	0.090	-0.170	0.461	0.291	0.201	0.973**	<0.001	0.104	0.653
Na	0.153	0.509	0.251	0.272	0.589**	0.005	-0.357	0.112	0.150	0.517	-0.680	<0.001
P	1.000	<0.000	0.281	0.217	0.204	0.375	0.130	0.575	0.109	0.639	-0.580	0.802
S tot	0.281	0.217	1.000	<0.000	0.113	0.627	-0.481	0.027	-0.378	0.091	-0.510*	0.018
Ti	-0.058	0.802	-0.510	0.018	-0.361	0.108	0.200	0.385	0.155	0.502	1.000	<0.000
Mn	0.274	0.230	-0.389	0.082	-0.423	0.056	0.550*	0.010	0.882**	<0.001	0.213	0.353
Ag	0.237	0.300	0.023	0.922	-0.090	0.699	0.510*	0.018	-0.142	0.539	0.039	0.866
As	0.231	0.314	0.173	0.454	0.288	0.206	-0.262	0.251	-0.244	0.287	0.052	0.823
Ba	0.201	0.381	-0.162	0.483	0.698**	<0.001	-0.301	0.184	-0.014	0.952	-0.014	-0.173
Be	0.224	0.329	-0.264	0.247	-0.223	0.330	0.422	0.057	0.460*	0.036	0.481	0.027
Bi	0.313	0.168	0.080	0.730	0.347	0.124	-0.123	0.596	-0.320	0.157	0.248	0.278
Cd	0.298	0.190	-0.021	0.930	-0.227	0.322	0.359	0.110	0.695**	<0.001	-0.088	0.704
Co	0.269	0.238	-0.302	0.183	-0.374	0.095	0.575**	0.006	0.879**	<0.001	0.010	0.967
Cr	0.104	0.654	-0.314	0.166	0.107	0.645	0.022	0.923	0.657**	<0.001	0.349	0.121
Cs	0.058	0.801	0.364	0.105	0.817**	<0.001	-0.489*	0.024	-0.538*	0.012	-0.349	0.122
Cu	0.414	0.062	0.055	0.813	-0.055	0.812	0.150	0.515	0.693**	<0.001	-0.305	0.178
Ga	0.440*	0.046	0.183	0.427	0.742**	<0.001	-0.397	0.075	-0.265	0.246	-0.253	0.268
Hf	0.078	0.738	-0.472*	0.031	-0.148	0.523	0.971**	<0.001	0.407	0.067	0.068	0.771
In	-0.183	0.427	0.205	0.372	-0.106	0.646	-0.297	0.192	-0.128	0.581	0.373	0.096
Li	0.499*	0.021	-0.231	0.315	0.119	0.609	0.546*	0.010	0.476*	0.029	-0.165	0.474

* Significantive correlation at level $p<0.05$ * *Significative correlation at level $p<0.01$

Phosphate
Sulphur
Al+Na+K
Zr+Hf
Ca+Mg
Ti

	Phosphate		Sulphur		Al+Na+K		Zr+Hf		Ca+Mg		Ti	
	r	*p-value*	*r*	*p-value*	*r*	*p-value*	*R*	*p-value*	*r*	*p-value*	*r*	*p-value*
Mo	0.396	0.076	0.313	0.167	-0.051	0.826	0.105	0.649	-0.381	0.088	-0.284	0.213
Nb	0.077	0.740	-0.388	0.082	-0.376	0.093	0.081	0.726	0.091	0.696	0.891**	<0.001
Ni	0.308	0.174	-0.308	0.175	-0.272	0.233	0.556**	0.009	0.910**	<0.001	-0.004	0.987
Pb	0.098	0.672	0.033	0.888	-0.105	0.651	0.286	0.209	-0.414	0.062	0.379	0.090
Rb	0.293	0.198	0.243	0.289	0.887**	<0.001	-0.211	0.358	-0.372	0.097	-0.434*	0.050
Re	0.098	0.673	0.195	0.397	0.286	0.209	-0.086	0.712	-0.152	0.510	-0.241	0.293
Sb	0.374	0.095	-0.005	0.981	0.249	0.277	-0.076	0.745	0.433*	0.050	0.015	0.949
Sc	0.291	0.201	0.205	0.373	0.787**	<0.001	-0.436*	0.048	-0.055	0.813	-0.568**	0.007
Se	0.226	0.325	0.065	0.780	-0.434*	0.049	0.177	0.443	-0.102	0.661	0.090	0.699
Sn	0.333	0.140	0.051	0.827	0.250	0.274	-0.454*	0.038	-0.005	0.983	0.287	0.207
Sr	0.290	0.202	0.349	0.121	0.547*	0.010	-0.579**	0.006	0.010	0.966	-0.487*	0.025
Ta	0.030	0.898	-0.305	0.179	-0.209	0.364	0.176	0.445	0.015	0.948	0.782**	<0.001
Te	-0.264	0.247	-0.204	0.374	-0.004	0.998	0.080	0.732	-0.083	0,719	-0.274	0.229
Th	0.389	0.081	0.259	0.256	0.792**	<0.001	-0.227	0.322	-0.116	0.616	-0.667**	<0.001
Tl	0.100	0.666	-0.303	0.182	-0.520*	0.016	0.759**	<0.001	0.276	0.226	0.254	0.267
U	0.540*	0.011	-0.270	0.236	0.032	0.892	0.805**	<0.001	0.427	0.054	-0.049	0.831
V	0.155	0.504	-0.088	0.705	0.540*	0.011	-0.345	0.126	-0.049	0.831	0.183	0.426
W	0.103	0.657	-0.124	0.592	0.118	0.612	-0.319	0.158	0.295	0.194	0.251	0.273
Y	0.214	0.351	-0.107	0.643	0.280	0.218	0.604**	0.004	0.192	0.405	-0.469*	0.032
Zn	0.324	0.153	-0.073	0.753	-0.252	0.271	0.276	0.227	0.841**	<0.001	-0.020	0.932
Zr	0.131	0.571	-0.481*	0.027	-0.289	0.204	1.000**	<0.001	0.448*	0.042	0.203	0.377
ΣLREE	0.284	0.212	0.336	0.137	0.786**	<0.001	-0.374	0.095	-0.151	0.515	-0.683**	<0.001
ΣHREE	0.398	0.074	-0.059	0.799	0.484*	0.026	0.384	0.086	0.194	0.400	-0.512*	<0.018

* Significative correlation at level $p<0.05$

* *Significative correlation at level $p<0.01$

Phosphate
Sulphur
Al+Na+K
Zr+Hf
Ca+Mg
Ti

Following the association in Table 3.5, ternary diagrams were constructed to illustrate further the geochemical relationships among major element groups, specifically aluminosilicates, carbonates, oxides, sulphides, phosphates, and minerals such as zircon and rutile (Ti). These diagrams provide a visual representation of the relative proportions of these groups within the different coal waste samples, allowing for a more apparent distinction between group affinities.

In addition to Pearson correlation analysis, geochemical associations of major and trace, elements were evaluated using cluster analysis. Before clustering, the concentration data were normalised to ensure comparability across all aspects. The study was conducted using a dataset of 21 samples, and the most optimal dendrograms were obtained by applying Pearson's regression distance and the Ward method.

The results, presented in Figure 3.10, illustrate the hierarchical clustering structure. The analysis revealed two statistically significant groups characterised by distinct geochemical signatures. The cluster on the left predominantly comprises unburned coal mining waste (UCW), except for sample BCW5. In contrast, the right-side cluster represents burned coal mining waste and the burned mixed material, highlighting the geochemical differentiation induced by combustion processes.

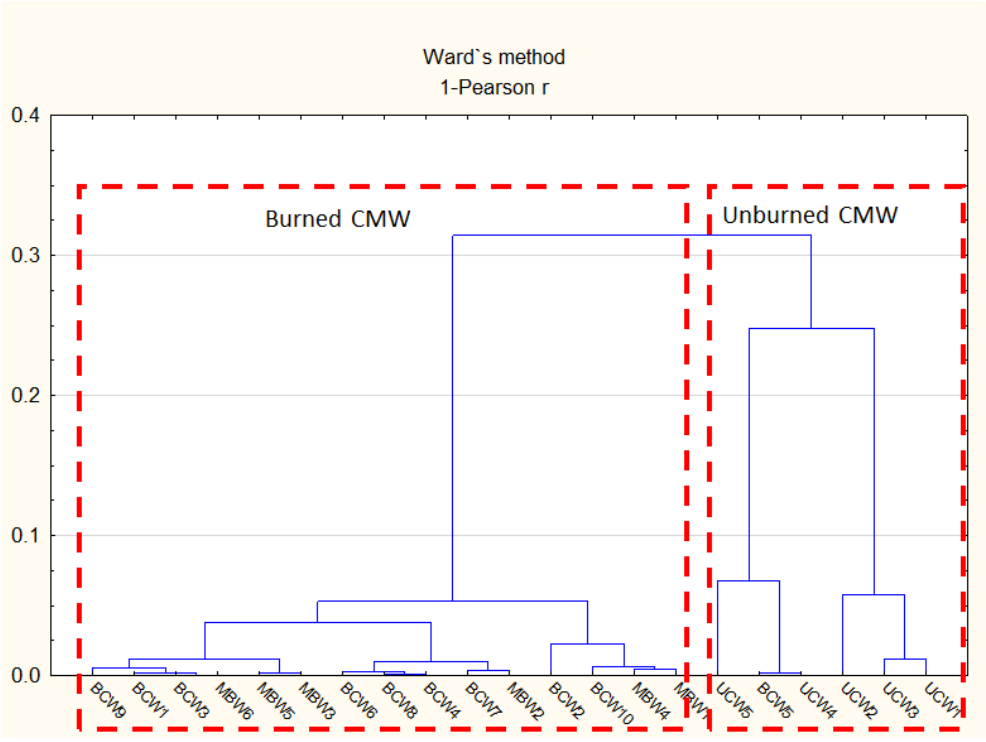

Figure 3.10 Hierarchical cluster analysis performance with a clear separation between unburned (BCW) and burned (BCW, MBW) coal mining waste from Fojo mine.

A second cluster analysis was conducted to further assess the geochemical associations among major, trace, and rare earth elements (REE) based on their chemical similarities. The analysis identified two primary groups at the first hierarchical level (Figure 3.11). However, due to the complexity of the elemental associations at this level, the dataset was further classified into five distinct sub-clusters: A, B, C, D, and E.

The clustering was performed using 59 variables and 21 cases, revealing that elemental groupings varied according to their geochemical behaviour and affinity for specific mineral phases. The most optimal dendrograms were obtained using Pearson's regression distance and the Ward method, ensuring a robust classification of geochemical associations.

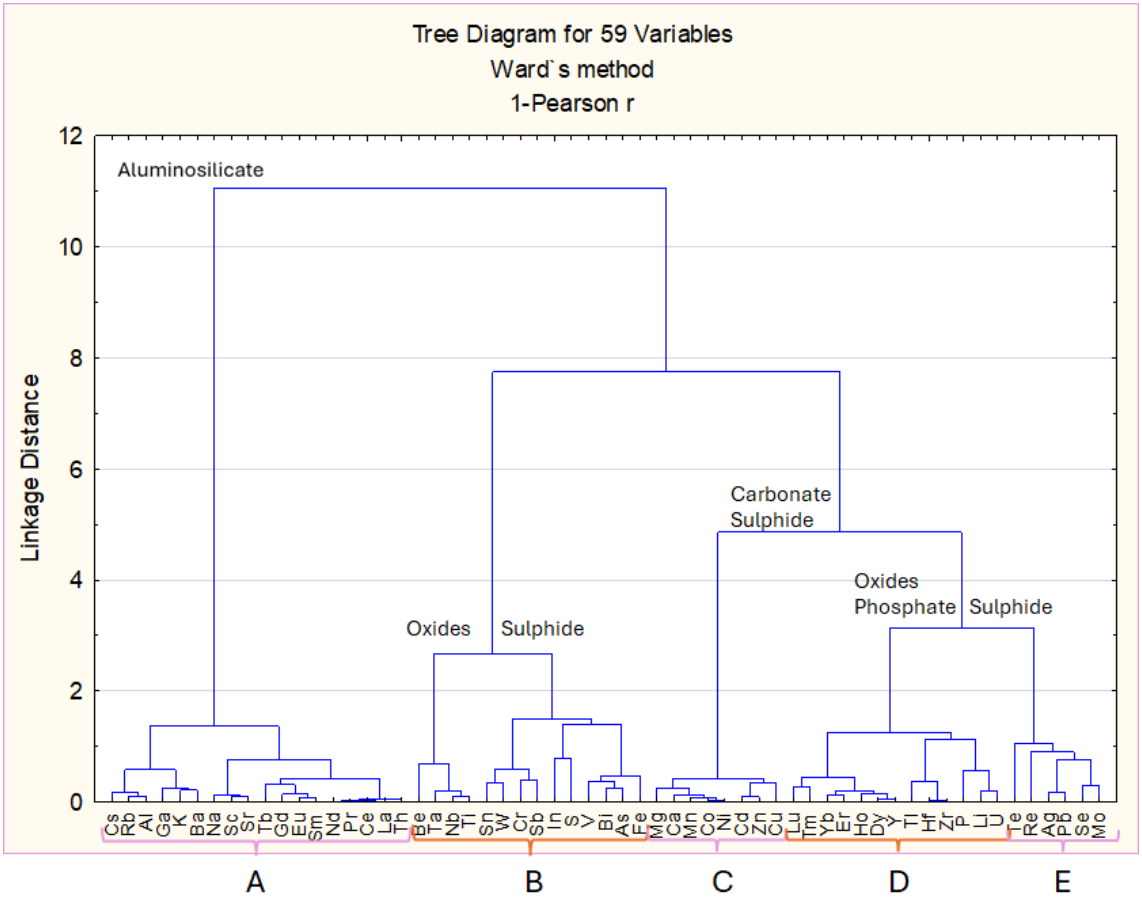

Figure 3.11 Dendrogram for the element geochemical association of the Fojo coal mining waste.

Cluster analysis classified the elements into five distinct groups based on their geochemical associations. Cluster A includes Cs, Rb, Al, Ga, K, Ba, Na, Sc, Sr, Tb, Gd, Eu, Sm, Nd, Pr, Ce, La, and Th. The presence of Al, K, Na, Cs, Rb, Ba, and Sr are associated with aluminosilicates, principally feldspar, micas, and clays. The REE (Tb, Gd, Eu, Sm, Nd, Pr, Ce, and La), are typically found in phosphate (monazite, xenotime)

or aluminosilicate (clays). Cluster B comprises Be, Ta, Nb, Ti, Sn, W, Cr, Sb, In, S, V, Bi, As, and Fe. Titanium (Ti) appears to be one of the dominant elements, indicating a strong association with oxide minerals (rutile). On the other hand, the presence of S could represent sulphide-rich minerals (pyrite, arsenopyrite, etc)

Cluster C consists of Mg, Ca, Mn, Co, Ni, Cd, Zn, and Cu. Calcium (Ca) and magnesium (Mg) suggest this group is primarily associated with carbonate phases and/or base-metal sulphides. These metals are often mobile under acidic conditions. Cluster D includes Lu, Tm, Yb, Er, Ho, Dy, Y, Tl, Hf, Zr, P, Li, and U. This cluster is dominated by heavy rare earth elements (HREE) along with zirconium (Zr) and hafnium (Hf), indicating an affinity for silicate phases. However, the presence of P induces a possible association with REE (Lu, Tm, Yb, Er, Ho, Dy, Y), forming phosphate minerals such as monazite and xenotime, or adsorbing onto Fe-oxides and clays. Cluster E comprises Te, Re, Ag, Pb, Se, and Mo. This cluster likely represents elements enriched in hydrothermal or metalliferous environments. Te, Re, Ag, Pb suggest a metallic signature, possibly from sulphide oxidation or secondary enrichment processes. Se and Mo may indicate redox-sensitive behaviour, potentially mobilised under changing pH/Eh conditions. These elements could be highly mobile in acidic and reducing conditions, influencing environmental risks.

After the cluster analysis, a PCA was performed with all the samples from the coal waste (UCW, BCW, MBW). The PCA biplot (Figure 3.12) reveals a clear separation between unburned waste (UCW, red ellipse) and burned waste (BCW, MBW, green ellipse) samples. This pattern suggests that combustion processes significantly alter the geochemical composition of coal waste residues. Principal component analysis (PCA) was performed to investigate the geochemical variability among coal waste samples and to identify associations between major, trace, and rare earth elements (REE). The first two principal components (PC1 and PC2) account for 47.4 % of the total variance, providing insight into the primary geochemical controls of the samples studied.

The distribution of elements along the principal components highlights distinct groupings. Notably, UCW1 and UCW2 are strongly associated with Mg, Zn, U, Ni, Cd, Co, Mn, Ca, Hf, Zr, and Be, indicating that these elements could be bound to carbonate phases or other mineralogical components preserved in unburned samples. UCW3, UCW4, and UCW5 are primarily represented by Se, Ag, Nb, Ta, and Pb, suggesting a different geochemical signature that may reflect the influence of trace element-rich phases or detrital minerals.

A subset of burned and partially burned samples (BCW2, MBW3, MBW4, and MBW1) shows a closer proximity to UCW samples, indicating that these residues may not have

undergone complete combustion, potentially preserving some of their original coal waste's unburned mineralogical features. The remaining burned waste samples are grouped (BCW, MBW), showing strong associations with Na, Th, Ba, Sc, Sr, LREE, K, Al, Ga, V, Rb, and Cs, elements typically enriched in aluminosilicate phases or refractory mineral fractions following combustion. Samples BCW5, MBW6, BCW10, and BCW9 were associated with the chemical elements As, S, and Bi. This relation could indicate that these samples contain a sulphur phase with minerals such as arsenopyrite, or may be impurities in Fe or Cu sulphides.

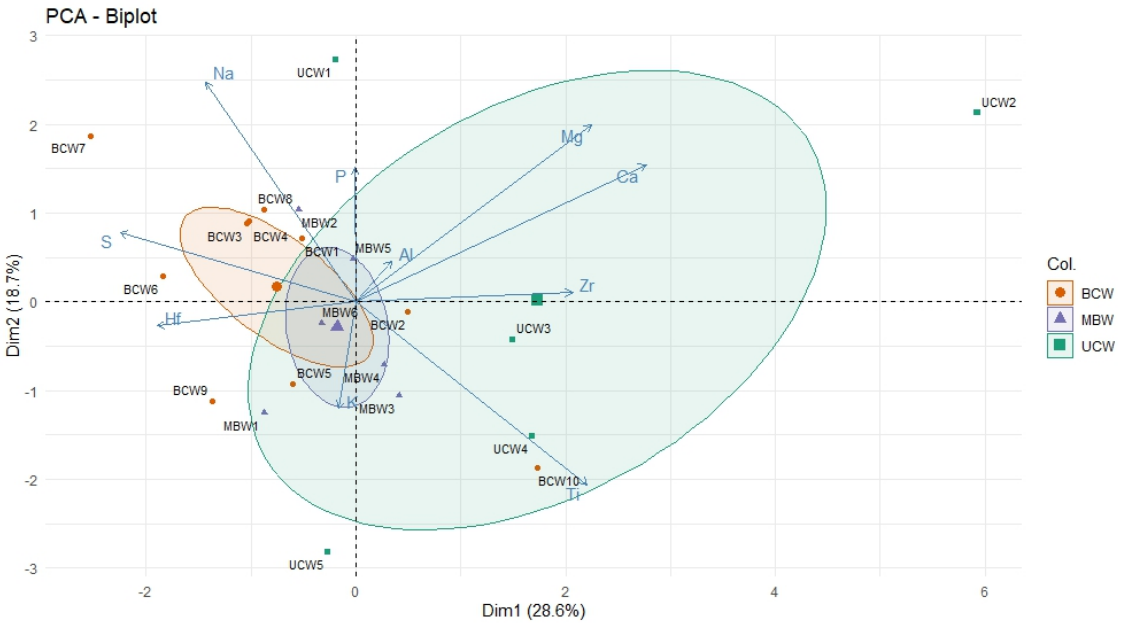

Figure 3.12 PCA biplot for the coal waste samples with chemical group elements.

These results highlight the impact of combustion on the redistribution of elements, with preferential retention of refractory elements and depletion of volatile or carbonate-associated elements in burned residues. The intermediate position of MBW samples reinforces the heterogeneous nature of mixed burned waste, which combines features of both burned and unburned materials.

3.2.3 Geochemical Comparison of Fojo Mine and Other Douro Coalfield Wastes

The mean inorganic geochemical composition of burned and unburned coal mining waste was compared. Element concentrations in unburned waste (UCW) were used as a baseline against which those in burned waste (BCW) and mixed burned waste (MBW) were evaluated. The results, presented in Figure 3.13, indicate that BCW and MBW exhibit nearly identical elemental variations, suggesting similar geochemical behaviour.

Among the three coal waste types—unburned (UCW), burned (BCW), and mixed burned waste (MBW)—several elements show lower concentrations following combustion, including Ca, Mg, P, Ag, Be, Cd, Co, Hf, Li, Mn, Mo, Ni, Pb, Se, Ta, Te, Tl, U, Y, Zn, and Zr. In contrast, Fe, Na, S, As, Bi, Cs, In, Sc, Sr, Th, and ∑LREE concentrations increase after combustion, indicating their relative enrichment in burned residues.

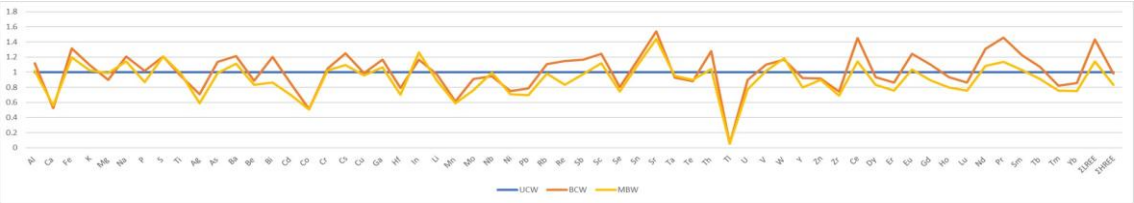

Figure 3.13 Relationship between the element's concentration in the unburned coal waste and the burned coal waste, and the mixed material.

At the same time, the enrichment factor (EF) was calculated using the mean aluminium (Al) concentration from UCW and BCW as the reference element, as its concentration remained unchanged after combustion (Barbieri 2016).

The enrichment factor is expressed as follow:

$EF = (Metal/RE)_{soil} / (Metal/RE)_{background}$

Where RE is the value of the metal, adopted as the reference element.

For EF interpretation, values between 0.97 and 1.04 were used to indicate no enrichment or depletion, while EF > 1 signified enrichment, EF < 1 indicated depletion and EF = 1 indicated no variation. The results, presented in Figure 3.14, show the most depleted elements in the following order: Tl <Co < Ca < Mn < Ag < Pb < Hf < Se < Cd < Be < Mg < Y < Mo < Zn < Ta < Ti < ∑HREE < Cu < P < Cr. The enriched elements were Sr > ∑LREE > Fe > Th > Sc = Cs > Ba > Na > S > Bi > Sn > Sb. Elements that maintained their concentrations after combustion included As, V, Al, K, W, Rb, Ga, In, and Re.

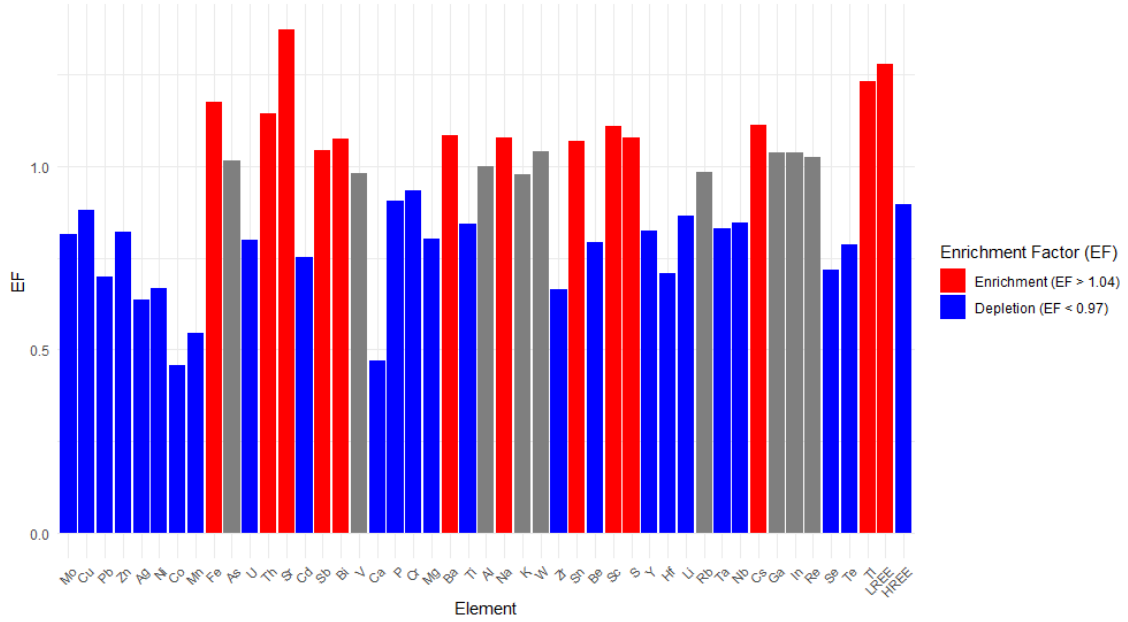

Figure 3.14 Enrichment factors for major and trace elements in the coal waste after combustion.

After this, the elemental concentrations of coal waste that did not undergo combustion in the Douro Coalfield were compared to those of UCW from the Fojo coal waste site. The mean concentration of non-burned coal waste from the Douro Coalfield (including Serrinha, Midões, and São Pedro da Cova) was used as the baseline (Ribeiro et al. 2010a,b; 2011). The results in Figure 3.15 reveal distinct variations in elemental concentrations. Lower concentrations were observed for Al, Na, Ti, Ba, Bi, Cd, Cr, Cs, Hf, Li, Nb, Sc, Sr, Ta, U, W, Zr, and ∑HREE, while Ca, Fe, Mg, P, S, As, Co, Cu, Mn, Mo, Pb, Sb, Th, and Zn exhibited higher concentrations. The remaining elements maintained consistent concentrations.

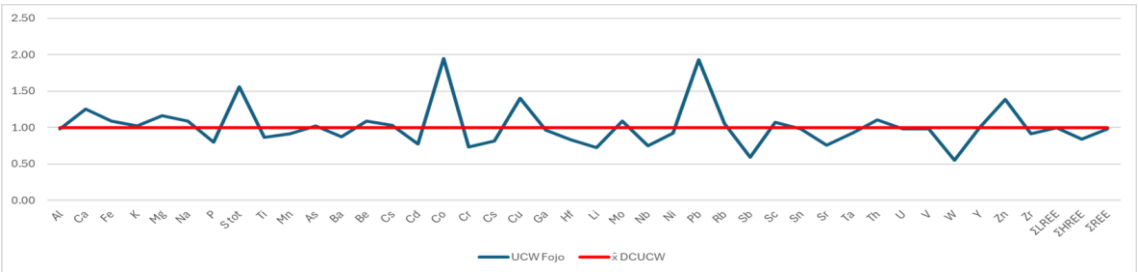

Figure 3.15 Fojo unburned coal mining waste element relationship compared with the non-burned baseline from the DC.

Figure 3.16 compares the average enrichment coefficients of elements in burnt coal mining waste from the Douro Coalfield (Lomba, Midões, and São Pedro da Cova) and the Fojo coal mining waste (BCW and MBW). The mean concentrations of major, trace, and rare earth elements (REE) in non-burnt coal mining waste from the Douro Coalfield

were used as a reference to calculate the enrichment coefficients in burnt and mixed coal waste samples.

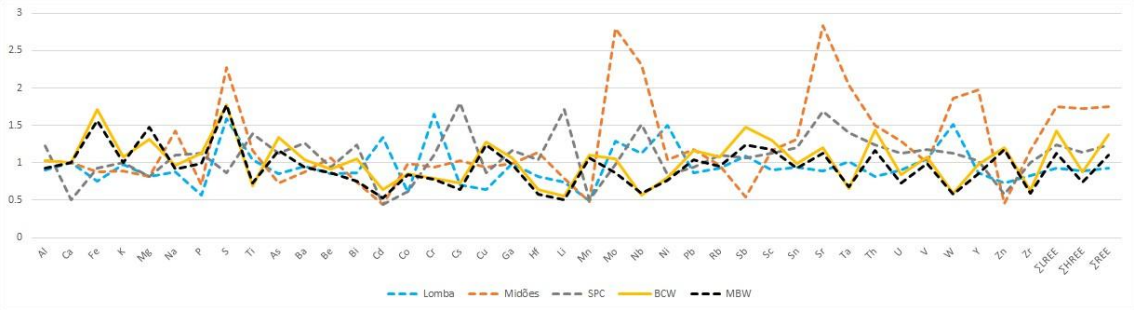

Figure 3.16 Comparing media enrichment coefficient for burned coal mining waste for different mine wastes in the Douro Coalfield and from Fojo mine (BCW, MBW).

The BCW and MBW samples exhibited similar behaviour, distinct from other burnt coal waste in the Douro Coalfield. Fojo burnt and mixed coal waste showed higher concentrations of several elements, including Fe, Mg, P, S, As, Cu, Mn, Pb, Sb, Sc, Sr, Th, Zn, and ∑HREE, while displaying lower concentrations of Na, Ti, Be, Cd, Co, Cr, Cs, Hf, Li, Nb, Ni, Sn, Ta, U, W, Zr, and ∑LREE.

3.2.4 Polycyclic Aromatic Hydrocarbons (PAH)

The environmental fate and behaviour of PAH have received considerable attention due to their potential toxicity and genotoxicity (Mukerjee et al. 1998; Wang et al. 2009). PAH are abundant on the earth and have two main sources of PAH in the environment: i) natural sources are related to the incomplete combustion of organic matter, pyrogenic PAH; ii) PAH can also be produced geologically when organic sediments are chemically transformed into fossil fuels such as oil and coal, petrogenic PAH (Achten and Andersson 2015; Abdel-Shafy and Mansour 2016; Li et al. 2019).

For this study, ten coal waste samples were analysed: four coal wastes affected by combustion (BCW1, BCW5, BCW7, BCW9), two unburned coal waste (UCW1, UCW4), two mixed materials (MBW1, MBW5), one from the uphill soil without coal waste influence (US4), and one from soil from the downhill soil (DS2), as illustrated in Figure 3.17.

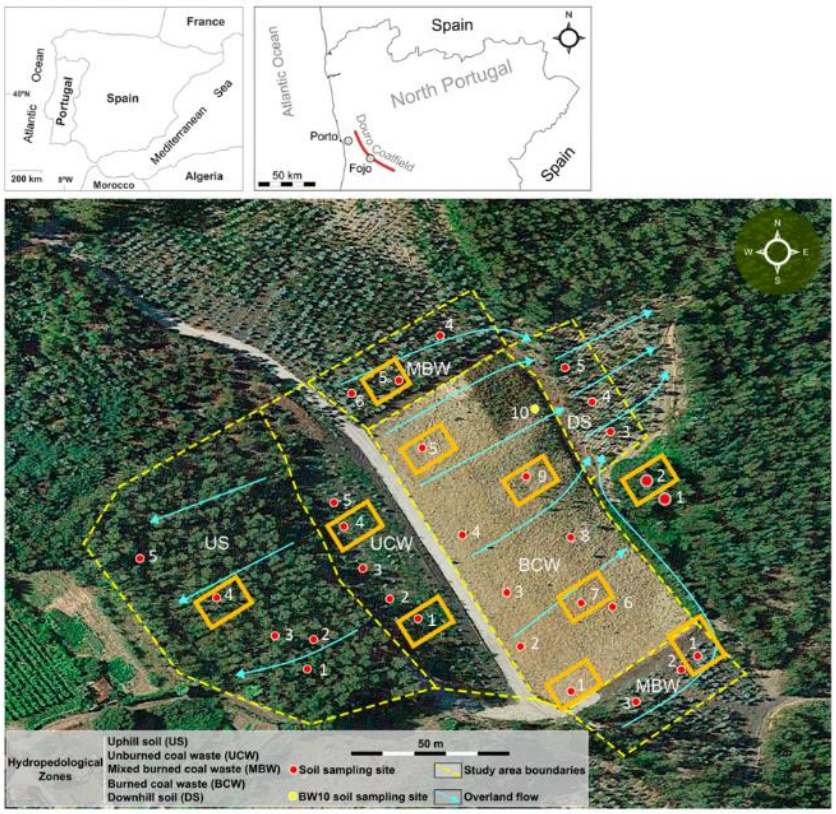

Figure 3.17 Coal waste sample's location from the three different sites (UCW, BCW, MBW), the uphill soil (US), and the downhill soil (DS), for PAH analysis.

The mean concentration and the standard deviation of the 16 PAH were analysed in the CMW samples (Table 3.6). The results indicated that the total PAH concentration is higher in BCW9 (1155.5 µg/kg) and lower for UCW1 (92.8 µg/kg). The lower concentration is expected to be in the uphill (US4) soil or the downhill (DS2) soil, as these soils are located near coal waste. Still, both sites have shown higher concentration than the coal waste without combustion (UCW1, UCW4), the mixed material (MB1, MBW5), and two burned coal wastes (BCW1, BCW7). The most abundant PAH in the samples is phenanthrene (Phe), followed by naphthalene (Nap), with minor concentrations of acenaphthylene (UCW, MBW), anthracene (UCW, BCW), benz[a]anthracene (UCW, MBW), and chrysene (UCW, MBW). Phe and Nap were detected in all the samples analysed.

Table 3.6 PAH concentration in µg/kg for ten samples of unburned (UCW1, UCW4), burned (BCW1, BCW5, BCW7, BCW9), and mixed coal mining waste (MBW1, MBW5) for the Fojo mine, as well as soils without coal mining waste (US4, DS2).

		US4		UCW1		UCW4		BCW1		BCW5		BCW7		BCW9		MBW1		MBW5		DS2	
		Media	SD	Media	SD	Media	SD	Media	SD	Media	SD	Media	SD	Media	SD	Media	SD	Media	SD	Media	SD
LMW	Nap	35.3	0.3	50.7	0.2	30.4	0.6	45.6	0.2	71.5	0.4	80.9	0.4	81.3	0.4	93.0	0.6	44.3	1.1	22.7	0.2
PAH	Acy	16.1	0.5	3.40	0.1	30.9	0.8	U	-	U	-	U	-	U		2.3	0.1	1.9	-	279.9	1.4
	Ace	2.1	0.0	U	-	U	-	U	-	U	-	R	-	R		R	-	R	-	U	-
	Flu	15.7	0.2	R	-	R	-	R	-	11.0	2.2	11.2	1.6	11.9	2.8	R	-	R	-	R	-
	Phe	42.4	1.5	23.9	0.1	20.2	1.2	172.4	7.1	492.6	10.5	100.5	1.4	994.2	23.3	80.1	4.1	28.6	0.2	60.0	5.3
	Ant	R	-	0.20	0.1	U	-	6.8	1.2	R	-	1.9	0.3	U	-	R	-	R	-	R	
HMW	Flt	9.1	0.4	R	-	5.8	1.6	52.1	2.7	51.1	4.5	7.4	0.5	R	-	R	-	R	-	21.2	2.3
PAH	Pyr	2.2	0.1	R	-	R	-	31.5	1.9	25.4	1.4	2.1	0.0	68.1	2.9	R	-	R	-	11.5	1.1
	BaA	0.5	0.1	3.10	1.0	0.1	0.3	R	-	R	-	R	-	R	-	R	-	7.2	1.4	4.9	0.9
	Chr	3.6	0.2	11.1	1.0	3.5	0.6	R	-	R	-	R	-	R	-	R	-	10.7	0.7	10.3	1.1
	Bbf	10.5	1.1	U	-	R	-	R	-	R	-	R	-	R	-	R	-	R	-	U	-
	BkF	38.1	1.5	U	-	R	-	R	-	R	-	R	-	R	-	R	-	R	-	U	-
	BaP	5.1	0.5	R	-	6.1	0.2	R	-	R	-	R	-	R	-	R	-	R	-	U	-
	DahA	12.4	0.2	R	-	R	-	R	-	R	-	R	-	R	-	R	-	R	-	R	-
	BghiP	R	-	R	-	R	-	R	-	R	-	R	-	R	-	R	-	R	-	R	-
	Ind	R	-	U	-	R	-	R	-	U	-	U	-	U	-	U	-	R	-	R	-
	∑PAH	193.1		92.3		97.0		308.4		651.5		204.0		1155.5		175.4		92.8		410.5	

U: Under the minimum similarity index
R: The ratio of the reference ion does not match

The PAH were classified into low molecular weight (LMW) and high molecular weight (HMW), based on the number of condensed aromatic rings. Two to three aromatic rings characterise LMW PAH, while HMW PAH possess four to six aromatic rings (Achten and Hofmann 2009; Ribeiro et al. 2012). The sum of the LMW PAH and HMW PAH in each sample indicates the predominant compound among the LMW PAH in both the burned and unburned samples. Indeed, the concentration of LMW PAH and HMW PAH was found to increase in the burning samples (BCW, MBW) compared to the unburning samples (UCW). On the other hand, the concentration of HMW PAH was observed to be lower than the LMW PAH in all samples. However, a slight increase in the concentration of HMW PAH was noted in the coal waste samples, specifically in BCW and MBW (Figure 3.18).

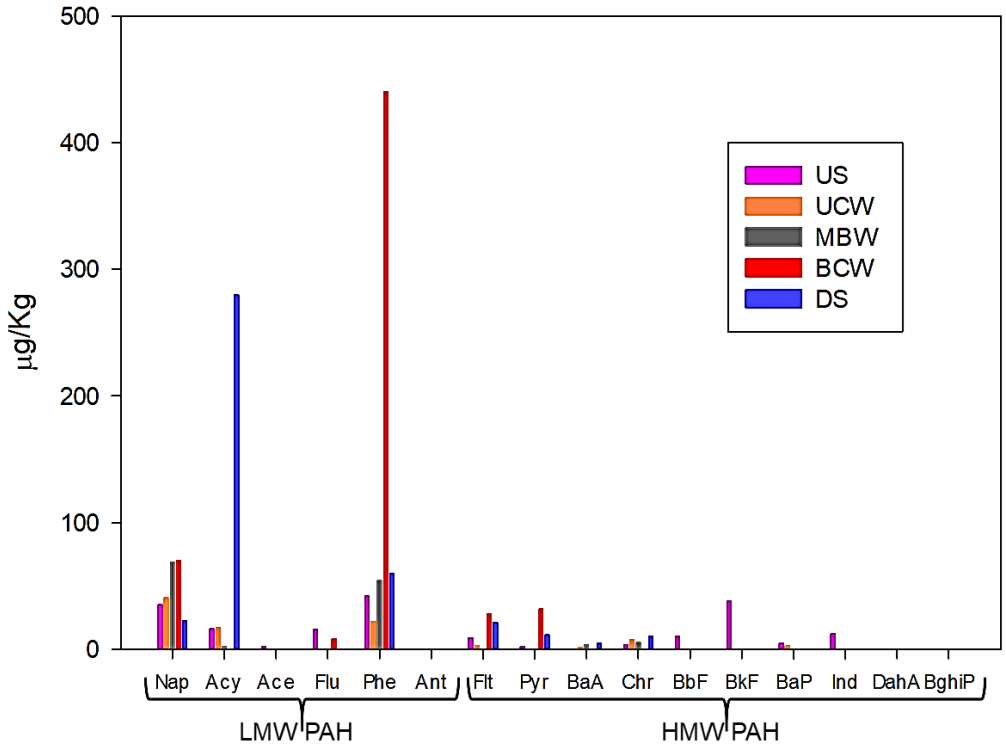

Figure 3.18 Mean concentration of LMW and HMW PAH in the coal mining waste without combustion (UCW) and with heat influence (BCW, MBW).

Figure 3.19 provides a more detailed review of the PAH results for Fojo coal mining waste for all the sites. It shows that the percentage composition of LMW is higher than that of HMW in all the samples. The uphill soil (US4) has a higher rate of HMW than the coal waste passed through the combustion process (BCW, MBW), and follows the subsequent order: B4 > BCW1 > MBW5 > UCW4 > UCW1 > BCW5 > DS2 > BCW7 > BCW9 > MBW1. The highest percentage of LMW is for

MBW1>BCW7>BCW9>DS2>UCW1>UCW4>MBW5>BCW1>B4.

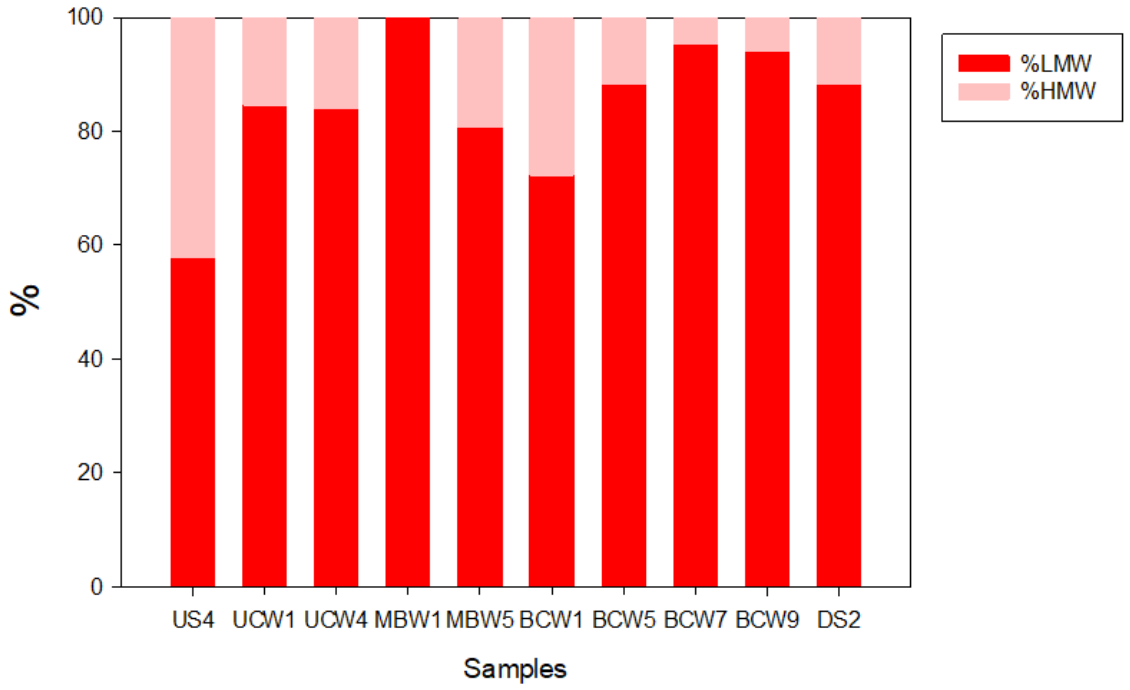

Figure 3.19 The Fojo coal mining waste percentage of LMW and HMW for each sample analysed in different soil types.

The relationship between Phe and Ant was calculated to understand the petrological and/or pyrolytic source of the PAH. Table 3.7 presents the type of sample, the percentage of LMV and HMV PAH, and the Phe/Ant. The results show that the unburned coal waste (UCW1) presented the highest value. Samples UCW4, BCW5, BCW9, MBW1, and MBW5 did not have anthracene in the PAH composition, so the relation could not be calculated. BCW1 and BCW7 had values lower than 100.

Table 3.7 Percentage of LMW PAH and HMW PAH, and Phe/Ant ratio of samples from the Fojo Coal mining waste

	Sample	%LMV PAH	%HMV PAH	Phe/Ant
Uphill soil (US)	US4	58	42	-
Unburned CMW (UCW)	UCW1	85	15	119.5
	UCW4	84	16	-
Burned CMW (BCW)	BCW1	73	27	25
	BCW5	88	12	-
	BCW7	95	5	62
	BCW9	94	6	-
Mixed CMW (MBW)	MBW1	100	0	-
	MBW5	81	19	-
Downhill soil (DS)	DS2	88	12	-

3.3 Discussion

3.3.1 Petrographic and Mineralogic Assessment

The petrographic qualitative characteristics of the organic and mineral matter indicate that vitrinite is the predominant maceral group, occurring in the forms of collotelinite and collodetrinite. Additionally, the presence of inertinite was detected as fusinite and semifusinite, a finding that is in concordance with the observations made by Ribeiro et al. (2010a) on the DC coal waste material in SPC, Lomba, and Midões.

The random vitrinite reflectance was found to be higher in the UCW than in the samples subjected to self-burning, BCW, and MBW. This observation corroborates the findings of previous studies (Taylor et al. 1998; Ribeiro et al. 2010a; Ribeiro et al. 2022) that have documented a lowering in vitrinite reflectance in samples exhibiting combustion effects. On the other hand, areas in DC with unburned coal waste exhibit similar values to those obtained in this study (Marques et al. 2009; Ribeiro et al. 2010b). The values obtained by UCW indicate that the coal mining waste sample is classified as Anthracite A, following the ISO 11760:2005 standard.

The dark reaction rims with lower reflectance (Figure 3.5 A, B, C, and D) occur when the original coals are of high rank (Taylor et al. 1998), as is the case with the DC coals. This behaviour is also observed at high combustion temperatures, as inferred by minerals neoformed during combustion (Ribeiro et al. 2010a, 2013, 2015). Concurrently, cracks, reaction rims, framboidal pyrite oxidation, and devolatilisation vacuoles are clear indicators of the combustion process at higher temperatures (Ribeiro et al. 2010a).

However, the identification of brighter reaction rims with higher reflectance is associated with lower combustion temperatures (Alpern and Maume 1969; Misz-Kennan et al. 2020). This could be caused by the application of the cooling agent during fire extinction, which may provide evidence of the consequences of using this product.

The selected samples were analysed using SEM, which revealed the presence of minerals such as florence, acanthite (silver sulphide), and arsenopyrite (Figure 3.9). These minerals were found to be associated with UCW, as well as pyrite and iron oxides (Figure 3.7d). In the case of BCW and MBW, the minerals included zircon, rutile, xenotime, monazite, pyrite, iron oxide, cinnabar, and galena. The reddish hue observed in the coal mining waste samples indicates thermal influence and is associated with iron oxides (Figure 3.3 B, C, and D).

In other studies, in the DC, it was demonstrated that this type of sample, with self-burning, represents iron oxides in minerals such as magnetite, hematite, and maghemite (Ribeiro et al. 2015). Furthermore, Ribeiro et al. (2022) reported the presence of abundant aluminosilicates and iron oxides in coal waste from the Peijão area, as well as framboidal pyrite and secondary iron oxides that enclose organic matter.

3.3.2 Geochemical Association and Affinities

3.3.2.1 Coal Ash Yield, pH, and Electrical Conductivity

As illustrated in Table 3.2, the ash yield rate was higher for burnt and mixed coal mining waste materials (BCW and MBW) than for unburned coal waste (UCW). Ash yield values are directly related to self-burning processes and higher temperatures (Ribeiro et al. 2022).

The sample most affected by thermal processes was BCW10, which exhibited a reddish color due to the presence of iron oxides, as mentioned previously. This sample also demonstrated the highest ash yield, indicating that the organic matter was more intensely affected during combustion (Ribeiro et al. 2022). In contrast, samples UCW1 and UCW4 exhibited the lowest ash yield.

The findings indicated that the main ash yield was lower in samples that did not undergo combustion. Similar observations have been reported regarding ash yield in the DC (Ribeiro and Flores 2021; Ribeiro et al. 2022). These values were elevated for burnet samples, indicating partial consumption of carbon (C) and an increase in the concentration of inorganic matter. As expected, the ash yield is in concordance with the observed reduction in C in BCW and MBW (Ribeiro et al. 2022).

The elevated ash yield of the Fojo coal mining wastes may suggest that the majority of the chemical elements are associated with the mineral phase (Gentzis and Goodarzi 1995; Ward 2016). The burning process of coal is a destructive oxidation reaction that alters the macerals and minerals of coal (Gentzis and Goodarzi 1995). During combustion, the elemental composition of coal undergoes a series of changes, with elements that are associated with coal macerals volatilising and becoming depleted, while inorganically associated elements become enriched in the ash (Gentzis and Goodarzi 1995).

A comparison of the ash yield results with other studies on anthracite coal material from DC, revealed that the ash yield for Lomba ranged from 50.6 % to 98.1 %, for Midões from 71.2 % to 84.6 %, SPC from 75.4 % to 91.2 % (Ribeiro et al. 2010a), and in Pejão from 63.17 % to 99.24 % (Ribeiro et al. 2022). These findings appear to align with the

results obtained in the present study. The observed ash yield of anthracite from the DC was found to be higher than that of anthracite from other parts of the world. For instance, the ash yield of anthracite from DPR Korea was found to be between 8 % and 20 % (Hu et al. 2006), while in Qinshui, China, it ranged from 13.2 % to 93.3 % (Zhao et al. 2019). The range was 11.1 % to 40.8 % in Korea (Kim et al. 2023) and 2.76 % to 28.29 % in Pennsylvania, USA (Agioutantis et al. 2023).

The pH values for the coal waste increase in acidity during the combustion process, ranging from 3.50 to 5.23 in UCW and from 3.63 to 4.63. In other samples from Fojo coal waste, the same behaviour is observed between burned and unburned coal waste (Çelebi and Ribeiro 2023); for SPC, the pH varies between 3.8 and 5.4 (Ribeiro and Flores 2020). The increased acidity in coal waste is associated with pyrite and jarosite (Abfertiawan et al. 2020; Li et al. 2007; Ludwing et al. 1999). In the case of pyrite, the oxidation of sulphide to sulphate leads to the formation of sulphuric acid. Self-combusting coal waste piles can accelerate these reactions, thereby contributing to the generation of acid drainage. pH could be higher in UCW because of the presence of carbonates, such as calcite, aragonite, and siderite. These minerals are reported to have the potential to neutralise acid (Alhamed 2015; Pope et al. 2010). The burned zones showed slightly lower acid-forming potential than unburned zones, as combustion leads to the oxidation of sulphides and potential volatilisation of sulphur compounds (Xu et al. 2022; Yan et al. 2001).

The highest EC was observed for UCW4, BCW7, and UCW5, but in general, BCW exhibited higher EC than UCW, except for UCW4 and UCW5 (Table 3.2). The BCW samples may be related to the increased release of soluble salts and metal ions from oxidation reactions resulting from the combustion process (Ribeiro et al. 2010a). At the same time, the lower values of EC in UCW1, UCW2, and UCW3 could be related to the retention of primary silicate minerals and organic material in unburned samples, which also limits ionic dissolution. On the other hand, low EC values in samples that underwent combustion could suggest that leaching of elements may have occurred.

A negative correlation was observed between pH and EC in the coal waste (Figure 3.20). The heat generated by the combustion process benefits the acidification process, increasing the solubility of metal ions and sulphate compounds, which in turn contributes to elevated conductivity. In contrast, unburned samples (UCW1, UCW2, UCW3) showed less acidic pH values and correspondingly lower EC due to lower sulphide oxidation and sulphate dissolution.

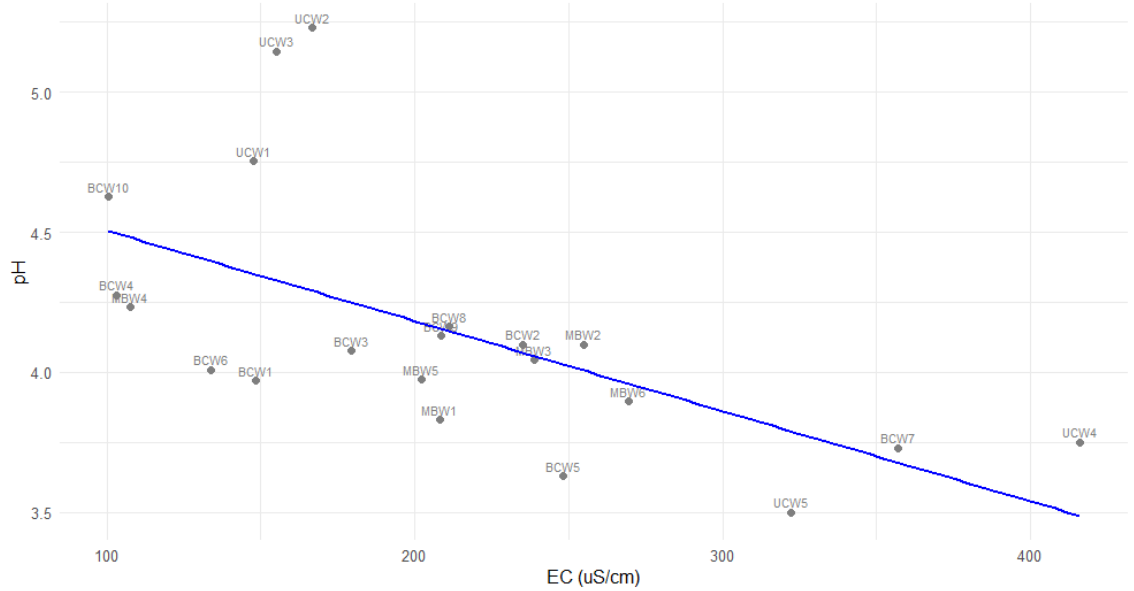

Figure 3.20 Correlation diagram between pH and electrical conductivity (EC) for the three types of coal mining waste, UCW, BCW, MBW.

3.3.2.2 Major and trace elements composition

The concentration of elements in the coal mining waste in the study area is within the respective range of each element when compared with the data reported for two samples analysed by Ribeiro et al. (2022). The most abundant elements in all samples are Al, Fe, and K, which reflect the dominant mineralogical composition of the Fojo CMW, namely, llite, kaolinite, feldspar, and Fe oxides (Espinha Marques et al. 2024; Ribeiro et al. 2022).

It is seen that the major elements have a concentration greater than 0.1% and include elements inorganically predominant as Al, Fe, Mg, Ca, Mn, Na, K, Ti, S and P (Dai et al. 2021). Trace element data indicate high to medium variability, as evidenced by the standard deviation (SD) values (±169 to ±6.06) for Mn, Zn, Pb, Cu, ∑LREE, Co, As, Cr, Ba, Ni, Sr, and V (Table 3.3). In contrast, the remaining elements exhibit low variability, with a standard deviation (SD) value of up to ±2.26. However, the elements indicating high variability in concentration values are considered to have diverse affinities, including both organic and inorganic, as well as multiple types (Finkelman 1994; Saha et al. 2016; Vejahati et al. 2010;).

The combustion process significantly affected the distribution of various elements, with some showing enrichment in BCW due to mineral transformations, while others exhibited depletion, likely due to volatilisation or leaching (Vejahati et al. 2010). The inorganic element concentrations between samples UCW, BCW, and MBW reveal a depletion of certain elements and an enrichment of others. This indicates that when the

decomposition temperature is reached, as in the case of depletion, part of the element concentration is lost to the atmosphere. During coal combustion, several parameters influence their transformation, such as volatilisation, the kinetics of release from particles, and their competitive affinity to active atoms like H, O, and S (Yan et al. 2001).

The decrease in the concentration of Ca, Mg, P, Ti, Ag, Be, Co, Hf, Li, Mn, Mo, Ni, Pb, Se, Te, Tl, Zn, and Zr is primarily attributed to volatilisation at elevated temperatures, resulting in their presence in the vapor phase (Gentzis and Goodarzi 1995; Ribeiro et al. 2022; Yan et al. 2001). Some elements are faster to volatilize (Sn, Se, Tl, Te, Cd, Sb, and Pb) than others (Cu, Ni, Zn, Cr, Co, and Mn), depending on the type of chemical bond and heating rate during combustion (Wang and Tomita 2003). At the same time. It is considered that lixiviation could have an important role in the element depletion.

Iron, Na, S, As, Ba, Bi, Cs, Ga, In, Rb, Re, Sb, Sc, Sr, Th, W, and ∑LREE were the elements that exhibited enrichment in burned and mixed coal mining waste. Arsenic, Cs, Ga, Rb, and Th were reported in the Serrinha waste pile as elements with significant enrichment and slightly higher content (Ribeiro et al. 2010b) compared with unburned samples from the DC. In general, some chemical elements (e.g., Ti, Al, Fe, Mg, Ca, Mn, Na, K, S, and P) are the dominant components of minerals in coal and the major components of the ash resulting from coal combustion (Dai et al. 2021).

The concentration increase is associated with the contribution of other minerals from the lithology source. For example, Ribeiro et al. (2010a) state that the enrichment in Cs, Li, and Rb in DC mining waste was attributed to the contribution of granitic rocks ocorring in the area. On the other hand, Clarke (1993) states that chemical elements undergoing combustion tend to concentrate, e.g., Fe, Sc, Sr, Th, and ∑LREE. Conversely, As, S, Se, Pb, Ni, and Mo are reported to volatilise between 277 °C and 1200 °C (Yan et al. 2001).

According to Goldschmid's (1956) classification of chemical elements, the chalcophile elements, which have a strong affinity for sulphur, are often associated with sulphide minerals and undergo either complete or significant volatilisation (Gentzis and Goodarzi, 1995). In contrast, the lithophile elements, which have a strong affinity for oxygen and are associated with the aluminosilicate minerals (clays and feldspars), are often concentrated in the coal ashes (Gentzis and Goodarzi 1995). Some authors have attributed the observed decrease in element concentration to the high combustion temperatures, which vary depending on the element type. In the case of certain elements, volatilisation can occur in the coal mining waste, indicating that the

temperature has reached the point of partial evaporation (Yan et al. 2001; Ribeiro et al. 2022).

A comparative analysis of the depletion of elements between CMW from Fojo mine with Lomba and SPC reveals a similar behaviour in Fojo and Lomba for P, Be, Co, Hf, Mn, Zn, and Zr. At the same time, in SPC coal waste, this is observed only for Zn and Zr. Indeed, a comparison of the enrichment of elements in the waste pile of Fojo and Lomba indicates similarities for S, Cs, Ga, Sr, W, and LREE.

In contrast, Fojo and SPC waste exhibit similarities in the concentrations of As, Ba, Sr, and LREE. Ribeiro et al. (2010b) state that coal waste is a mixture of carbonaceous shales and lithic arenites with a variable amount of disseminated coal. The chemical composition will depend on the chemical composition of the Douro Coalfield lithologies and coal. From this point of view, each CMW pile could have similar and different features for inorganic elements because coal mining waste is a heterogeneous material with trace element variation (Gluskoter 1977).

The major and trace elements concentration results obtained for UCW, BCW, and MBW were compared with those from other studies (Ribeiro et al. 2010a, 2010b, 2011, 2022), using the average chemical element concentration of unburnt coal mining waste from the DC as the baseline. This enables an understanding of the relationship between samples from different coal waste piles. The results demonstrated that the samples analysed in this study exhibited identical geochemical characteristics to those from Pejão coal mining waste material studied by Ribeiro et al. (2022). However, they highlighted that the waste deposited in the Fojo CMW pile, which was not influenced by the combustion process, has a geochemical signature distinct from the CMW deposited in the SPC and Lomba CMW piles.

The observed variation in the geochemical composition of these residues can be attributed to the heterogeneity associated with the different areas of DC and the varied lithological contributions related to each area of the sedimentary basin. The SPC and Lomba CMW piles presented a concentration of Mg, Mn, Co, and Zn, lower than the average amount of the waste deposited in the Fojo CMW pile. On the other hand, the waste from the Fojo CMW pile showed the highest enrichment in Ca, Mg, S, Mn, Co, Cu, Pb, and Zn when compared to the remaining coal waste from the DC.

The geochemical composition of samples that pass through a combustion process from CMW piles in different DC mines exhibits notable differences. The concentration of the principal elements studied in the Fojo CMW pile is closer to the average concentration of these elements in the baseline when compared with the concentration observed in

SPC, Midões, and Lomba. In the case of SPC, there is a significant enrichment in Cs, Li, Nb, and Ta, which the compositional variation within the DC can explain. This is because these same elements are present in greater concentration in the samples that were not affected by pyrogenic effects and were studied in SPC.

3.3.2.3 Elements Mode of Occurrence in the Coal Waste Material

Understanding how elements are present in coal, their chemical bonds, and the dissemination within the coal are critical because their concentration and chemical state influence their weathering and combustion behaviour (Finkelman 1981ab; Dai et al. 2014; Finkelman et al. 2018; Dai et al. 2021). At the same time, the mode of occurrence is essential because metal(loid)s is associated with both inorganic phases and organic matter complexes, and depending on the binding, they could be more easily bioavailable (Finkelman 1994; Sahoo et al. 2014; Swaine 2013; Ward 2016).

Statistical techniques, such as correlation coefficients, cluster analysis, and principal component analysis (PCA), are widely used to infer the modes of element occurrence (Dai et al. 2005; Dai et al. 2021; Eskenazy et al. 2010; Finkelman 1981ab; Finkelman et al. 2019; Goodarzi 1990; Qin et al. 2018; Ribeiro et al. 2022; Spears and Zheng 1999). Table 3.7 summarises the relationship between each element and ash yield, their association with chemical groups, their similarity with other elements in the cluster analysis, their significance as key factors (PCA), and the enrichment factor (EF) results. Pearson correlation analysis suggests the presence of distinct geochemical groups with strong associations. Aluminium, Ba, Cs, Ga, K, Na, Rb, Sc, Sr, Th, V, and ∑LREE exhibit a positive correlation with ash yield and a strong positive correlation with Al + Na + K ($p < 0.05$). For the cluster analysis, these elements are grouped in Cluster A due to their affinity as lithophile elements and a high positive correlation between them.

Principal component analysis results indicate a stronger association with coal waste subjected to combustion (BCW, MBW), suggesting their presence in the ashes as elements with combustion resistance and, for some of them, enrichment (e.g., Th, Sr, V, Ba, Na, Sc, Cs, and ∑LREE). These elements primarily represent the aluminosilicate fraction of the mineral matrix. Most elements are more than 60 % reported as silicates; only Sr and REEs have 20 % because their principal mode of occurrence is phosphate (Dai et al. 2023; Finkelman et al. 2018). For the DC, it is reported that Cs and Rb are associated with granitic rocks, which could explain the enrichment in the ashes (Ribeiro et al. 2022).

Another group of elements, Cd, Cr, Cu, Mg, Sb, and Zn, also show a positive correlation with ash yield and a significant positive correlation with the carbonate phase ($p < 0.05$)

in the mineral fraction. The cluster analysis classifies Cr and Sb within the sulphide phase (Cluster B). Finkelman et al. (2018) noted that the Cr mode of occurrence is primarily in the silicate fraction (75 %), but a lower percentage (10 %) may also be present in the sulphide fraction. Sb is related more to sulphide (55 %). Magnesium is associated with the carbonate and silicate fraction (Dai et al. 2023).

On the other hand, Cd, Cu, and Zn are also grouped in cluster C (carbonate phase). Due to their chalcophile characteristic, Cd, Cu, Sb, and Zn are reported as principally associated with the sulphide fraction. However, they can also occur in macerals, pyrite, and copper in chalcopyrite (Finkelman et al. 2018; Parzentny and Róg 2021). However, it is reported that these elements can be hosted by macerals such as fusinite, mainly with the inclusion of pyrite and carbonate sand and clay (Parzentny and Róg 2021).

The correlation between the elements' concentration and S did not show a significant association; however, with the carbonate group (Ca+Mg), it is very high ($p < 0.01$). PCA results suggest that these elements are primarily associated with unburned coal waste (UCW) and coal waste with a partial heat process, particularly BCW2, MBW3, MBW4, and BCW1. Indeed, this suggestion implies that the elements from cluster C, during combustion, are mobilised through volatility into the environment and are depleted in the ashes.

Elements such as As, Bi, Fe, In, Nb, S, Sn, and W are also positively correlated with ash yield but show no clear association with aluminosilicates, carbonates, or zircon-bearing minerals. However, Fe exhibits a positive correlation with S ($r = 0.487$; $p = 0.025$), while Nb correlates with Ti ($r = 0.891$; $p < 0.001$), suggesting that Fe is primarily present as pyrite and Nb is associated with mineral rutile.

In Cluster B, As, Bi, and Fe are grouped, indicating that As and Bi may be hosted by pyrite or other sulphide minerals, such as arsenopyrite. Likewise, In, W, and S cluster together, likely forming additional sulphide phases. PCA shows that As, Bi, Fe, In, S, Sn, and W are components for BCW and MBW, but Nb is more associated with coal without the combustion process (UCW).

In contrast, Ag, Ca, Co, Hf, Li, Mn, Ni, Tl, U, Y, and Zr exhibit a negative correlation with ash yield and a strong positive correlation with Zr+Hf ($p < 0.05$), suggesting that these elements are likely incorporated or hosted in mineral zircon (e.g., Hf, Zr, Li, U, and Y in Cluster D). The anomalous behaviour of zirconium observed in the self-combusted coal mining residues suggests that Zr did not behave as a strictly conservative, refractory element during the combustion process. Under typical combustion of anthracitic coal,

zirconium is expected to remain associated with the mineral fraction and to become enriched in the ash, owing to the extreme thermal stability and very low solubility of zircon ($ZrSiO_4$). However, the negative correlation between Zr and ash content observed in this study indicates that alternative processes affected its post-combustion distribution.

During self-combustion, locally high temperatures, combined with an atmosphere enriched in sulphur-bearing gases (SO_2 and SO_3) derived from the oxidation of sulphide minerals and organic sulphur, may have promoted the partial destabilisation of zircon. Under such conditions, zircon can undergo thermal and chemical alteration, leading to the formation of zirconium sulphate ($Zr(SO_4)_2$) or related sulphated species. Unlike $ZrSiO_4$, zirconium sulphate is readily soluble in water, fundamentally altering the mobility of zirconium within the residue (Ayers and Zhu 2025; Bernini et al. 2013; Kovalenko and Ryzhenko 2009).

$$ZrSiO_4+2H_2SO_4 \rightarrow Zr(SO_4)_2+SiO_2+2H_2O$$

Following the combustion phase, secondary processes such as rainfall infiltration and internal water circulation within the waste pile could have facilitated the dissolution and downward transport of these newly formed, water-soluble Zr phases. This secondary lixiviation would result in the progressive depletion of zirconium from the solid combustion residues, rather than its retention within the ash fraction. Consequently, zirconium would be preferentially removed from the system or redistributed into finer fractions or leachates, producing the observed decoupling between Zr and ash content.

Therefore, the combined effects of high-temperature sulphate-rich combustion conditions and post-combustion aqueous leaching provide a plausible explanation for the unexpected loss of zirconium from the ash fraction. This finding indicates that, under self-combustion conditions, zirconium may lose its conservative character and become susceptible to secondary mobilisation, challenging its conventional use as an immobile lithogenic tracer in thermally altered coal mining wastes.

Additionally, Co, Ca, Mn, Ni, and Li show a strong positive correlation with carbonates ($p < 0.05$) and are classified within Cluster C. These last elements are considered key components of unburned coal waste (UCW). Unlike these elements, Ag does not cluster with them but is more closely associated in Cluster E, likely forming phosphate and/or sulphide minerals.

The final elements exhibiting a negative correlation with ash yield include Be, Mo, P, Pb, Re, Se, Ta, Te, Ti, and ∑HREE. Berilium and Ta show a strong correlation with Ti,

indicating an association with mineral rutile, and are grouped with Ti in Cluster B. However, Mo, P, Pb, Re, Se, and Te do not correlate strongly with aluminosilicates, carbonates, zircon-bearing minerals, rutile, or sulphides. Instead, ∑HREE are grouped within Cluster D, alongside zircon-bearing minerals and P.

Indeed, for the mineralogy observed by the SEM image, it is reported that REE minerals are associated with P, as seen in xenotime, monazite, and florencite. In contrast, Mo, Pb, Re, and Se form a distinct group in Cluster E, suggesting a potential association with phosphate and/or sulphide phases due to the presence of mineral galena (PbS), aconthite (AgS) in the samples burned coal waste (BCW10, BCW7), and unburned coal waste (UCW2, UCW5).

Table 3.8 presents a summary of the relationships between the major and trace elements, with the ash percentage, chemical groups, clusters, PCA, and enrichment factor. These associations and relationships denote the possible mode of occurrence for each element in the coal mining waste.

Table 3.8 Pearson correlation values for major, trace and REEs elements with the ash yield and geochemical groups, highlighting their affinity based on cluster association, key component elements (PCA), and enrichment factor. * denote $p < 0.05$

	Ash yield		Chemical groups						Cluster					PCA		EF		
	positive	negative	P	S	Al+Na+K	Zr+Hf	Ca+Mg	Ti	A	B	C	D	E	PC1	PC2	Enrichment	Depletion	no change
Ag	-	x*	-	-	-	x	-	-	-	-	-	-	x	-	-	-	**x**	**-**
Al	x	-	-	-	x	-	-	-	x	-	-	-	-	**x**	**-**	-	-	**x**
As	x	-	-	-	-	-	-	-	-	x	-	-	-	-	-	-	-	**x**
Ba	x*	-	-	-	x	-	-	-	x	-	-	-	-	-	-	**x**	**-**	-
Be	-	x	-	-	-	-	x	x	-	x	-	-	-	-	-	-	**x**	**-**
Bi	x	-	-	-	-	-	-	-	-	x	-	-	-	-	-	**x**	**-**	-
Ca	-	x	-	-	-	x	x	-	-	-	x	-	-	-	**x**	**-**	**x**	**-**
Cd	x	-	-	-	-	-	x	-	-	-	x	-	-	-	**x**	**-**	**x**	**-**
Cr	x*	-	-	-	-	-	x	-	-	x	-	-	-	-	-	-	**x**	**-**
Cs	x	-	-	-	x	-	-	-	x	-	-	-	-	**x**	**-**	**x**	**-**	-
Co	-	x	-	-	-	x	x	-	-	-	x	-	-	-	**x**	**-**	**x**	**-**
Cu	x	-	-	-	-	-	x	-	-	-	x	-	-	-	**x**	**-**	**x**	**-**
Fe	x	-	-	x	-	-	-	-	-	x	-	-	-	-	-	**x**	**-**	-
Ga	x*	-	x	-	x	-	-	-	x	-	-	-	-	**x**	**-**	-	-	**x**
In	x	-	-	-	-	-	-	-	-	x	-	-	-	-	-	-	-	**x**
Hf	-	x*	-	-	-	x	-	-	-	-	-	x	-	-	-	-	**x**	**-**
K	x	-	-	-	x	-	-	-	x	-	-	-	-	**x**	**-**	-	-	**x**
Li	-	x	x	-	-	x	x	-	-	-	-	x	-	-	**x**	**-**	**x**	**-**
Mg	x	-	-	-	-	-	x	-	-	-	x	-	-	-	**x**	**-**	**x**	**-**
Mn	-	x	-	-	-	x	x	-	-	-	x	-	-	-	**x**	**-**	**x**	**-**
Mo	-	x	-	-	-	-	-	-	-	-	-	-	x	-	-	-	**x**	**-**
Na	x	-	-	-	x	-	-	-	x	-	-	-	-	-	-	**x**	**-**	-
Nb	x	-	-	-	-	-	-	x	-	x	-	-	-	-	-	-	**x**	**-**

	Ash yield		Chemical groups						Cluster					PCA		EF		
	positive	negative	P	S	Al+Na+K	Zr+Hf	Ca+Mg	Ti	A	B	C	D	E	PC1	PC2	Enrichment	Depletion	no change
Ni	-	x	-	-	-	x	x	-	-	-	x	-	-	-	**x**	**-**	**x**	**-**
P	-	x	x	-	-	-	-	-	-	-	-	x	-	-	-	-	**x**	**-**
Pb	-	x*	-	-	-	-	-	-	-	-	-	-	x	-	-	-	**x**	**-**
Rb	x	-	-	-	x	-	-	-	x	-	-	-	-	**x**	**-**	-	-	**x**
Re	-	x	-	-	-	-	-	-	-	-	-	-	x	-	-	-	-	**x**
S	x	-	-	x	-	-	-	-	-	x	-	-	-	-	-	**x**	**-**	-
Sb	x	-	-	-	-	-	x	-	-	x	-	-	-	-	-	**x**	**-**	-
Sc	x*	-	-	-	x	-	-	-	x	-	-	-	-	**x**	**-**	**x**	**-**	-
Se	-	x	-	-	-	-	-	-	-	-	-	-	x	-	-	-	**x**	**-**
Sn	x*	-	-	-	-	-	-	-	-	x	-	-	-	-	-	**x**	**-**	-
Sr	x*	-	-	-	x	-	-	-	x	-	-	-	-	**x**	**-**	**x**	**-**	-
Ta	-	x	-	-	-	-	-	x	-	x	-	-	-	-	-	-	**x**	**-**
Te	-	x	-	-	-	-	-	-	-	-	-	-	x	-	-	-	**x**	**-**
Ti	-	x	-	-	-	-	-	x	-	x	-	-	-	-	-	-	**x**	**-**
Th	x	-	-	-	x	-	-	-	x	-	-	-	-	**x**	**-**	**x**	**-**	-
Tl	-	x*	-	-	-	-	-	-	-	-	-	x	-	-	-	-	**x**	**-**
V	x*	-	-	-	x	-	-	-	x	x	-	-	-	-	-	-	-	**x**
U	-	x	x	-	-	x	-	-	-	-	-	x	-	-	**x**	**-**	**x**	**-**
W	x*	-	-	-	-	-	-	-	-	x	-	-	-	-	-	-	-	**x**
Y	-	x	-	-	-	x	-	-	-	-	-	x	-	-	-	-	**x**	**-**
Zn	x	-	-	-	-	-	x	-	-	-	x	-	-	-	**x**	**-**	**x**	**-**
Zr	-	x*	-	-	-	x	x	-	-	-	-	x	-	-	-	-	**x**	**-**
LREE	x	-	-	-	x	-	-	-	x	-	-	-	-	**x**	**-**	**x**	**-**	-
HREE	-	x	-	-	x	-	-	-	-	-	-	x	-	-	x	-	**x**	-

Besides interpreting each element and its mode of occurrence, it was observed that certain elements (e.g., Be, Ca, Co, Ga, Li, Mn, and Ni) exhibited more than one strong positive correlation within the geochemical groups. The element is associated with the group that showed the highest correlation across multiple mineral phases; however, this association depends on the strength of the correlation, geochemical behaviour, mineralogy, phase identification, as well as environmental and post-combustion processes (Arnold 2023; Dai et al. 2021; Vejahati et al. 2010).

Iron, Th, Sr, Sb, Bi, Ba, Na, Sn, Sc, S, Cs, and LREE showed enrichment after the combustion process. The enrichment of elements depends on various factors, such as the parent coal's geochemical composition, lithology, combustion temperature, element volatility, weathering, and post-depositional processes. Except for Sb, these elements are classified as lithophile elements. They are the fundamental source of rock-forming minerals of the earth´s crust. The principal occurrence modes of Ba, Cs, Sc, and Na are silicates (Dai et al. 2021, 2023; Finkelman et al. 2018). Sb and Fe are associated with the sulphide phase, but only Fe shows a clear correlation with S; Sb has an association with the carbonate phase, but the cluster analysis shows an affinity with S. LREE and Sr have more affinity with the phosphate phase, but Sr showed an association with silicate (plagioclase) (25 %) (Dai et al. 2023; Finkelman et al. 2018).

Conversely, the concentrations of Mo, Cu, Pb, Zn, Ag, Ni, Co, Mn, U, Cd, Ca, P, Cr, Mg, Ti, Zr, Be, Y, Hf, Li, Ta, Nb, Se, Te, Tl, and HREE decreased after the combustion process. Some of these elements, including Cu, Mo, Tl, Se, Zn, Cr, Pb, Te, Ag, and Cd, are classified as chalcophile, indicating their association with sulphur. However, in this study, Ag and Tl are more closely associated with zircon minerals, while Cd, Cr, Zn, and Cu are primarily linked to the carbonate phase. Similarly, Mn, Co, and Ni, which are siderophile elements, predominantly occur within the carbonate phase. The lithophile elements Li, Be, Mg, Ca, Y, HREE, Ti, Zr, Nb, Hf, Ta, and P exhibit a primary mode of occurrence in both zircon minerals and the carbonate phase.

The depletion of these elements occurs mainly due to volatilisation, phase transformation, and leaching. The extent of depletion depends on the element's volatility, combustion temperature, and mineral association (Ribeiro et al. 2022). The tendency trends of trace element volatilisation and temperature value for coal combustion under oxidation condition reported are: Hg (below 27 ^{o}C) > come Te, Tl (27-227 ^{o}C) > Cd, Se, most Te (277-527 ^{o}C) > Pb, Sn, half As (427-627 ^{o}C) > Zn, half As (627-927 ^{o}C) > Cu, Ni (727-1227 ^{o}C) > Co (1227-1427 ^{o}C) > V (1227-1527 ^{o}C) > Mn (1227-above 1527 ^{o}C)

> Cr (above 1527 ºC) (Yan et al. 2001). Elements such as Se, Zn, Pb, and Cd are released into the atmosphere at temperatures between 200 °C and 800 °C.

The geochemical behaviour of the studied elements reflects their affinity with specific mineral phases and their response to the combustion process. Elements can be classified into different geochemical groups based on their associations. Understanding these affinities provides insight into the mobility, stability, and enrichment patterns of major, trace, and rare earth elements (REE) in the studied samples. The ternary diagrams indicate that the principal geochemical groups appear to be sulphide, phosphate, carbonate, and aluminosilicate.

3.3.3 Polycyclic Aromatic Hydrocarbons Composition

Polycyclic aromatic hydrocarbons (PAH) comprise many carcinogenic substances and are ubiquitous in the environment (Achen and Hofmann 2009). The total PAH concentration was higher for the pyrogenic-origin coal waste (BCW and MBW) than for the petrogenic-origin coal waste (UCW), and LMW PAH was higher than HMW PAH (Figure 3.21) due to the concentration of phenanthrene (Phe) and naphthalene (Nap). Some authors state that increasing temperature increases HMWPAH yield, while LMW PAH decrease through volatilisation or degradation (Hayashi et al. 1993; Peng et al. 2016; Yu et al. 1998). However, it is not a linear association; a maximum PAH concentration is shown at 800 °C, and then the concentration decreases at higher temperatures, between 900 °C and 1200 °C (Lui et al. 2012; Dong et al. 2013).

The evolution of the heating and pyrolysis processes increases the formation of PAH at temperatures between 500 ºC and 800 ºC in coal waste. At these temperatures, the aromatic structure starts to crack, and two competitive reactions occur: PAH formation and PAH decomposition (Dong et al. 2013). Below 800 °C, the rates of cracking and condensation are low, so the former reaction is dominant (Dong et al. 2013).

The lowest values of the sum of PAH for the Fojo coal waste were found for the unburned coal waste in contrast with what was observed by Ribeiro et al. (2012), where the unburned coal waste from Lomba and SPC had the highest concentration. However, as shown in Figure 3.21, there is a low formation of HMW PAH and a high dominance of LMW PAH (Phe and Nap). It is suggested that in temperatures above 600 ºC and below 800 ºC (Peng et al. 2016), the rate of two- and three-ring PAH formation is favourable, due to the breaking of the C-C bonds in large aromatic hydrocarbons (Dong et al. 2013; Ledesma et al. 2000; Liu et al. 2012). LMW compounds are bonded to the coal macromolecular structure by hydrogen bonds and Van Der Waals forces (Liu et al. 2012). The weak bonds in coal began to rupture at low temperatures, and some PAH were

formed, increasing the LMW PAH (Peng et al. 2016). Phe and Nap are the most abundant PAH at 500 ºC and are more abundant until 800 ºC (Peng et al. 2016). These compounds, with 2-3 rings, dominate regardless of coal rank or origin (Laumann et al. 2011).

Anthracite coal has less volatile matter than other coals (e.g., bituminous), and the LMW components with three rings are reported to be predominant in burning modes, especially in the gaseous phase (Liu et al. 2009; Neff et al. 2004; Peng et al. 2016). On the other hand, it is expected to obtain HMW PAH at higher temperatures (Ribeiro et al. 2012); the cyclisation reaction of LMW PAH during pyrolysis increases, leading to a reduction in LMW PAH (Peng et al. 2016). These authors reported that at 900 ºC, HMW PAH reach their maximum value, and they implied that PAH formation is dominated by decomposition reactions at lower temperatures (LMW PAH) and formation reactions at higher temperatures (HMW PAH) (Peng et al. 2016). In this study, the concentration of HMW PAH is much lower than LMW PAH (Table 3.5), implying that a higher temperature was not achieved. This low combustion temperature could have been caused by the use of the cooling agent in the fire extinguisher in 2017, which inhibited the formation of HMW PAH.

When the results of LMW and HMW from Fojo coal mining waste dump are compared with other coal dumps in the DC, specifically SPC, Lomba, and Midões, the percentage of HMW is higher, indicating that higher temperatures were achieved in the self-burning process and also indicating the pyrolytic origins of the PAH (Ribeiro et al. 2012; Santos et al. 2023). In the case of the Fojo coal dump, these temperatures were not reached due to the fire extinguishing process conducted by Empresa de Desenvolvimento Mineiro using water and an unidentified cooling agent.

The level of PAH in soil is reported to depend on the distance from the emissions source (Yuan et al. 2014). The spatial dispersal of PAH compounds in soils is also affected by dissipation processes, such as sorption-desorption, abiotic degradation, volatilisation, biodegradation, leaching, and bioaccumulation (Li et al. 2010; Su and Zhu 2008). The higher percentage of HMW found in the uphill soil at site US4, where no coal waste has been deposited, appears to be related to the extinction process. When the combustion was being extinguished with water and an unknown cooling agent, a large amount of smoke was generated, in which HMW could be released in the particulate phase. Due to the effect of the wind, these particles may have been transported and subjected to different wet/dry deposition patterns (De La Torre-Roche et al. 2009; Hayakawa et al.

2019; Tobiszewski and Namiesnik 2012). PAH are often highly concentrated in post-wildfire soil and ash (Kieta et al. 2023).

The molecular index value of Phe/Ant radio for unburned (UCW) and burned coal samples (BCW and MBW) is presented in Table 3.5. The ratio of parent phenanthrene to parent anthracene has been extensively used to differentiate between petrogenic and pyrogenic PAH pollution in sediments (Guo et al. 2007; Stogiannidis and Laane 2014). Ribeiro et al. (2012) state that when the Phe/Ant ratio is lower than 10%, there is a pyrolytic contribution for the PAH, which is associated with combustion sources (Stogiannidis and Laane 2014). Depending on the different PAH sources (e.g., crude, Anthracite, asphalt, coke, low-rank coal) Phe/Ant ratio.

In this study, all Phe/Ant ratio ranges are higher than 10, indicating the petrogenic origins of the PAH. This fact is true in the case of unburned coal waste (UCW1 and UCW4) and mixed material (MBW1 and MBW5), where the origin of PAH is coal without a combustion or heat process. However, in the case of coal waste that undergoes a combustion process (BCW), the increase in LMW PAH, specifically phenol (Phe), is associated with the breakdown of organic matter heated to high temperatures, resulting in the formation of smaller organic molecules, carbon dioxide, and water (Neff et al. 2004). Polycyclic aromatic hydrocarbons formed during combustion are called pyrogenic PAH and are often abundant in exhaust vapour and particulate phases. Two- and 3-ring PAH are most abundant in the vapour phase (Neff et al. 2004; Liu et al. 2009; Peng et al. 2016). Stogiannidis and Laane (2014) state that, to a lesser extent, Phe is abundant and has a pyrolytic source. These authors suggest that when the Phe/Ant ratio ranges from 10 to 30, a mixed source profile is present. Indeed, Anthracite is reported to have a pyrogenic source for Phe/Ant over 10 (Chen et al. 2005).

3.4 Final Remarks

Coal mining waste from the Fojo mine was studied from the petrographic, mineralogical, and geochemical points of view. The petrographic characterisation of the organic constituents indicates vitrinite as the predominant group, and higher values of random vitrinite reflectance were observed for the unburned coal mining waste (UCW) than for the samples with combustion (BCW and MBW). Cracks and reaction rims, framboidal pyrite oxidation, and devolatilisation vacuoles indicate the combustion process at elevated temperatures. However, brighter reaction rims and higher reflectance were associated with lower combustion temperatures, indicating the effect of the cooler agent.

Using the SEM technique, the principal minerals obtained in the unburned coal waste (UCW) were florencite, acanthite, arsenopyrite, pyrite, and iron oxides. For burned and

mixed coal waste, the minerals were zircon, rutile, xenotime, monazite, pyrite, iron oxide, cinnabar, and galena.

Aluminium, Fe, and K dominate the concentration of the major elements in coal mining waste. The other elements, Ca, Mg, Na, S, and Ti, have concentrations of <1.0%. Fe, Th, Sr, Sb, Bi, Ba, Na, Sn, Sc, S, Cs and ∑LREE elements increase concentration in the burned and mixed coal waste (BCW and MBW), while there is a decrease for the elements: Mo, Cu, Pb, Z n, Ag, Ni, Co, Mn, U, Cd, Ca, P, Cr, Mg, Ti, Zr, Be, Y, Hf, Li, Ta, Nb, Se, Te, Tl, and HREE.

The mode of occurrence for major and trace chemical elements was evaluated indirectly using the Pearson correlation between the ash yield and element concentration, cluster analysis, and PCA. The aluminosilicates fraction comprised the following elements: Al, Ba, Cs, Ga, K, Na, Rb, Sc, Sr, Th, V, LREE. The carbonate fraction is associated with Ca, Cd, Co, Cu, Mg, Mn, Ni, and Zn. The phosphate phase is formed by the following elements: U, Li, and HREE. The sulphur fraction is integrated by Fe, As, Bi, V, In, Sb, Cr, W, and Sn. The elements associated with rutile minerals are Ti, Nb, Ta, and Be. The aluminosilicate fraction, zircon mineral, and sulphide fraction involved burned waste and some mixed coal waste. The other fraction, like the carbonate group, is associated with unburned coal waste (UCW).

The concentration of the 16 priority PAH was determined in the organic fraction of the coal mining waste from burnt, mixed, and unburned coal waste from the Fojo waste pile. ∑PAH are higher in the burning of coal waste. LMW PAH are the dominant compounds for burned (BCW) and unburned samples (UCW). Phe is the most abundant PAH, followed by Nap. LMW PAH in unburned coal waste have a petrological source. Regarding burnet coal waste, the origin of LMW PAH is petrological and pyrolytic, despite the radio Phe/Ant being higher than 10. Burnt coal waste passes through a combustion process at lower temperatures due to the use of a cooler agent during the fire extinguishing in 2017. Through this process, HMW from the gas phase passes to a particulate phase and, by wind-driven processes, is enriched in the uphill soil.

Chapter 4. Hydropedological Characterisation of the Fojo Coal Mining Waste Deposition Area

4.1. Introduction

Hydropedology seeks to investigate two fundamental questions: (1) How does soil architecture control the partitioning of hydrologic fluxes (and related biogeochemical and ecological functions) in heterogeneous landscapes? Moreover, (2) How does landscape hydrology influence soil genesis, variability, and function over space and time? Therefore, unlike traditional Soil Science and Hydrology, Hydropedology emphasises the two-way interactions between pedological and hydrological processes (Lin 2012; Ma et al. 2017).

Knowledge of hydropedological characteristics in areas where coal mining waste was deposited can be used to understand the behaviour of soil leachates and their influence on the surrounding soils and water bodies. Features such as hydraulic conductivity, infiltration capacity, and soil texture could explain how water moves through the waste material with potential environmental pollution effect by: i) facilitating the rapid transport of leachates, enhancing the dispersion of Potentially Toxic Elements and major constituents; ii) determining the extent to which water percolates through the waste, influencing the dissolution and migration of pollutants; and iii) promoting faster water movement and contaminant leaching as coarse-grained materials (e.g., sandy fractions), whereas finer-grained components (e.g., clay) may retain metals through adsorption processes, potentially leading to localised accumulation.

The current chapter examines the soils of the Fojo coal mining waste deposition area. In the study area, a network of points was selected for soil sampling and field characterisation, encompassing soils without waste deposition (uphill and downhill soils from the waste pile) and soils from the waste deposition area (unburned, burned, and mixed burned coal waste).

The research aims to assess changes in the hydropedological conditions of soils from areas affected by the deposition of coal mining waste that underwent self-burning. The study area was evaluated through an integrative approach, combining aspects of hydrology, geology, soil science, mineralogy, geochemistry, and hydrogeochemistry.

The first step involved defining hydropedological zones based on field observations of soil formation factors, such as parent material, topography, biological activity, human influence, and time (Amundson 2021; Jenny 1994). These factors were then analysed

in relation to local hydrological processes, including rainfall interception, infiltration, percolation, surface runoff, and interflow. One of the identified zones represents the conditions before the commencement of coal mining activities. In contrast, the others reflect human-induced changes, particularly the deposition of coal mining waste and, to a lesser extent, the effects of intensive forestry.

4.2. Materials and Methods

The study area location is presented in Figure 4.1, which illustrates the hydropedological zoning, sampling, and field characterisation sites. Twenty-nine samples were selected as follows: five samples located uphill from the coal waste pile (Uphill Soil – US), five samples in the Unburned Coal Waste site (UCW), six samples in the Mixed Burned Coal Waste site (MBW), 10 samples in the Burned Coal Waste site, (including the Cover Layer – CL – and the burned coal waste itself – BCW), and three samples located downhill from the coal waste pile site (Downhill Soil – DS).

Figure 4.1 Location of the samples for the hydropedological study sites in the Fojo CMW disposal site.

4.2.1 Field Procedures

Between 2021 and 2023, hydropedological studies were conducted. First, local hydrological conditions and processes, such as interception, infiltration, percolation, overland flow, and interflow, were observed. Next, the soil morphology was described in each hydropedological zone, according to the FAO (2006) guidelines, in terms of: i) the formation of soil horizons, ii) soil horizon depth and thickness, iii) the type of soil horizon boundaries, iv) soil structure, v) soil texture, vi) soil colour, vii) accumulation of humified organic matter, viii) soil porosity, and ix) biological activity. Samples from the upper mineral horizons were collected and analysed for mineralogy and potentially toxic element (PTE) geochemistry. Field evaluations included unsaturated hydraulic conductivity (K), volumetric soil water content, and hydrophobicity (Al Majou et al. 2008). Finally, the hydrogeochemistry of leachates was examined to assess the soil leaching potential.

The sampling methods included manual collection using stainless steel tools. For all soil types, the uppermost mineral horizon was sampled to a depth of 20 cm. In the case of the burned coal waste (BCW) covered with a cover layer (CL), it was necessary to remove the cover layer, which was approximately 5-7 cm thick, after the burned coal waste samples were collected. Figure 4.2 shows the collection of soil from the forest located uphill from the waste dump, burned coal waste, and the layer of material used to extinguish the fire.

Figure 4.2 Field sampling of soil from the uphill (US, a and b) and coal waste materials from the combustion (BCW, c and d) site covered with an unknown material (CL).

The mixed coal waste (MBW), unburned coal waste (UCW), and downhill soil (DS) were clearly superficial; it was not necessary to dig deeply, clean the area of leaves (Figure 4.3). In addition to the other samples, up to 10 cm were taken. An attempt was made to avoid samples with large rocks; the collection included small particle sizes. All samples were labelled, sealed, and stored in polyethene bags.

Figure 4.3 Unburned (a), mixed coal waste (b), and downhill (c) soil sampling at the study site,

The unsaturated hydraulic conductivity expresses the rate at which water can move through the soil porous medium and is a function of the soil water potential and content. Water movement through soil can occur under both saturated and unsaturated conditions.

The assessment of the unsaturated hydraulic conductivity (K) was performed using the mini disk infiltrometer (MDI), (e.g., Gadi et al. 2017; Naik et al. 2018; Schacht and Marschner 2015). Macropore flow is prevented by applying a negative potential during infiltration measurements (Minasny and George 1999). The MDI method provides better K results (Reynolds 2008; METER 2020; Zhang 1997) compared to those of other methods, such as the Warrick method (Warrick 1992) and Haverkamp's method

(Haverkamp et al. 1994), and in validation with small-scale rainfall simulations (Li et al. 2005).

The MDI comprises a single tube divided into two chambers (Figure 4.4). The lower chamber serves as a water reservoir, with a capacity of 95 cm^3. It is sealed at the base with a porous sintered stainless-steel disk that has a thickness of 0.3 cm and a diameter of 4.5 cm. The upper chamber is employed to establish the pressure head, which is the primary factor determining the occurrence of infiltration. The pressure head can be adjusted within −7 cm to −0.5 cm. Refer to the user manual for a more detailed description of the device (Decagon 2005).

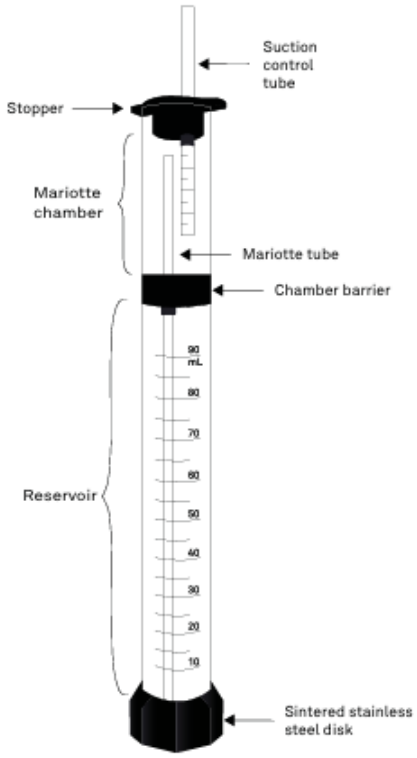

Figure 4.4 Mini Disk Infiltrometer components diagram and measurement design (METER 2020).

The measurement was taken by selecting a flat area on the soil surface (Figure 4.5). The starting water volume was recorded at the beginning of the test. Then, the infiltrometer was placed on the soil surface, and the declining water volume was recorded at regular intervals as the water infiltrated. The recording continued until at least 30-40 mL of water had infiltrated. All tests were performed applying a suction rate of −1 cm. The measured infiltration data were then analysed using the steady-state data analysis method proposed by Zhang (1997) and recommended in the user manual (Decagon 2005). The cumulative infiltration data were then fitted to the Philip infiltration equation (Philip 1957):

$$I = C1 + C2\sqrt{t}$$

where $C1$(LT^{-1}) and $C2$ (LT$^{-1/2}$) are parameters related to soil hydraulic conductivity and sorptivity, respectively; *I* (L) represent the cumulative infiltration and *t* (T) denotes time.

The hydraulic conductivity, *K(h)*, is then calculated as follows:

$$K(h) = \frac{C1}{A}$$

where $C1$ is the slope of the cumulative infiltration versus the square root of time curve, and A is a parameter that denotes the van Genuchten soil texture parameters (for 12 soil classes) corresponding to the disk radius and applied pressure head. For silty clay loam (α = 0.01, n =1.23), the A parameter can be determined using the following equation or obtained directly from a table in the user manual. A revised version of the user manual (Decagon 2005) presents slightly corrected values of parameter A. However, it is important to note that these values are derived from the USDA soil database, which is based on soils from the United States (Rawls et al. 1982).

$$A = 11.65\ (n^{0.1} - 1)\exp[7.5(n - 1.9)\alpha h](\alpha r_d)^{0.91}, n < 1.9$$

Additionally, a study by Dohnal et al. (2010) found that the original procedure fails to provide accurate results for soils with a van Genuchten parameter $n < 1.35$. For such soils, a modified equation is recommended to obtain more reliable $K(h)$ values:

$$K(h) = C1\ (\alpha r_0)^{0.61} 11.65(n^{0.82} - 1)\exp[34.65(n - 1.19)\alpha h_0],\ \ n < 1.35$$

Figure 4.5 Unsaturated hydraulic conductivity measurement in the field with the mini disk infiltrometer (MDI).

The volumetric water content was quantified with a capacitance probe (ThetaProbe, model ML3, from Delta T Devices, Figure 4.6). The electronic components of the probe are contained in a sealed plastic body attached to four sensing rods, which are inserted directly into the soil for taking the readings. A data logger converts the soil moisture output signal to moisture using the supplied general soil calibrations.

Figure 4.6 The ThetaProbe model ML3 for the measurement of the soil volumetric water content.

The ML3 works when power is applied. This creates a 100 MHz waveform that is used to an array of stainless steel rods, which transmit an electromagnetic field into the soil (Borges 2024; Sing et al. 2020). The water content of the soil surrounding the rods dominates its permittivity. The measurement is a response to the polarisation in an electromagnetic field. Water has a permittivity ≈ 81, compared to soil ≈ 4 and air ≈ 1.

The soil's permittivity (ϵ) strongly influences the applied field, which the ML3 detects. This results in a stable voltage output that serves as a sensitive and straightforward measurement of soil moisture content (Figure 4.7). The soil moisture output signal is a differential analogue DC voltage. A data logger or meter converts this to soil moisture using the supplied general soil calibrations (for mineral and organic soils). The depth is always constant and depends on the length of the rods. At the same time, the hole diameter is approximately 45 mm and is angled about 10 ° to the vertical. The rods must be fully inserted to ensure good soil contact (Delta-T Devices Ltd 2017).

Figure 4.7 Measuring the volumetric soil water content in the study area using the ML3 ThetaProbe.

Soil hydrophobicity refers to soils that develop water repellence. A quick and reliable method for the determination of this feature is the so-called Water Drop Penetration Time (WDPT) (Bisdom et al. 1993; Dekker and Ritsema 1994; Dekker et al. 2009; Tinebra et al. 2019; van Woudt 1959; Veneris and Farid 2024). Generally, organic compounds are responsible for this behaviour, as they accumulate on and between soil particles and cause soil water repellence when they form a specific molecular arrangement near or at the critical water content (Roy and McGill 2000).

Above the critical soil water content, the soil behaves as a wettable porous medium and below as a water-repellent one. This change in the state of the soil has a drastic impact on flow and transport processes, resulting in significantly different hydrological behaviours for wettable versus water-repellent soils (Dekker et al. 2009). Generally, soil is considered water-repellent if the WDPT exceeds 5 s. Dekker and Jungerius (1990) described an index that allows a quantitative classification of the persistence of soil water repellence.

A WDPT was conducted in the field for each type of soil (Figure 4.8). Dekker et al. (2009) defined the following seven classes of hydrophobicity based on the time it takes for water drops to penetrate the soil: class 0, wettable and non-water repellent (infiltration within 5 s); class 1, slightly water repellent (5 – 60 s); class 2, strongly water repellent (60 – 600 s); class 3, severely water repellent (600 – 3600 s); and extremely water repellent (>1 h), further subdivided into class 4 (1 – 3 h); class 5 (3– 6 h); and class 6 (> 6 h).

Figure 4.8 Water Drop Penetration Time test (WDPT) in the field.

A drop of distilled water is placed on the smoothed surface of the soil sample using a standard pipette dropper, and the time elapsed before the drop is absorbed is determined.

4.2.2. Laboratory Methods

Inorganic major and trace elements analysed for soil geochemistry were performed according to what was described in Chapter 3 (see Materials and Methods). The soil mineralogy was characterized by X-ray diffraction (XRD). Samples were dried at approximately 50 °C and then disaggregated. The fine fractions (<2 µm particle size) were separated by sedimentation. Mineralogical analyses of fractions under 63 µm and 2 µm were carried out using a Panalytical X´Pert-Pro MPD, Kα Cu (λ = 1.5405 Å) radiation on random-oriented powders (total sample) and oriented aggregates (<2 µm). Oriented aggregates were treated with glycerol and exposed to heat treatment at 500 °C. The mineral composition was assessed using (hkl) peaks (on random power mounts)

for nonclay minerals and (001) peaks (on orientated aggregates) for clay minerals. The mineral phases were identified using the criteria recommended by Schultz (1964), Brown and Brindley (1980), and the Joint Committee for Powder Diffraction Standards.

The USGS Field Leach Test (USGS FLT) was conducted to evaluate the leaching potential of major ions, potentially toxic elements (PTE), and Fe in soils (Hageman 2007). The extraction ratio of 20:1 ensured that the readily soluble components were leached without surpassing saturation limits while providing sufficient leachates for all analyses. A 50 g portion of the fine-earth fraction (<2 mm) from each soil sample was placed in a 1L wide-mouthed borosilicate glass bottle. Then, 1L of deionized water (pH 5.7) was carefully added to prevent dust loss. The bottle was capped and shaken for 5 minutes, then allowed to settle for 10 minutes. Additionally, pH, electrical conductivity (EC), and alkalinity were measured. The leachates were filtered through 0.45 µm filters and preserved for further analysis (American Public Health Association [APHA] 2017; Rodier and Legube 2016).

The pH and EC values were measured using a Crison MultiMeter MM 41. Total alkalinity and bicarbonate (HCO_3) were analysed by titration. Total organic carbon (TOC) was studied in a Shimadzu TOC-V (TOC-ASI-V, Shimadzu Corporation, Kyoto, Japan); Potentially Toxic Elements (Cr, Mn, Ni, Cu, Zn, As, Al, Cd, and Pb) and Fe, were analysed on a Varian AA240 Atomic Absorption Spectrometer (Varian Inc, Palo Alto, CA, USA). The major ions (Na, K, Mg, Ca, Cl, NO_3^-, and SO_4^{-2}) were analysed by ion chromatography (DionexTM system DX-120/ICS-1000, Dionex Corporation, Sunnyvale, CA, USA).

4.2.3. Statistical Analysis

A Principal Component Analysis (PCA) was performed to relate soil types in each hydropedological zone with the composition of soil leachates. Before initiating the multivariate analysis, the data were standardised to mitigate high variability in parameter values and to eliminate redundant variables, thereby optimising the analysis process. Subsequently, a principal component analysis (PCA) was performed using CANOCO for Windows version 4.5 software.

4.3 Results and Discussion

The results of hydropedological parameters provide critical insights into the movement and retention of contaminants derived from coal waste in soils. Key properties such as soil permeability, porosity, and water retention capacity influence the extent to which pollutants are transported through the soil matrix. High permeability and low water

retention facilitate the downward migration of contaminants, thereby increasing the risk of groundwater contamination (Pérez-Lucas et al. 2018; You et al. 2020).

Conversely, soil with higher retention capacities can act as temporary sinks for pollutants, potentially leading to prolonged contamination in localised areas (Rate 2022). Understanding these parameters is essential for assessing the environmental impact of coal waste and predicting the mobility of potentially toxic elements (PTE) within different soil profiles (Espinha Marques et al. 2021, 2024; Santos et al. 2023ab; Teodoro et al. 2021).

Leachates from coal waste play a crucial role in determining the availability and mobility of contaminants in soils (Ribeiro and Flores 2021). These leachates, enriched with dissolved metal(loid)s and other pollutants, can alter soil chemistry by modifying pH, ionic strength, and redox conditions, thereby influencing the solubility and transport of PTE. The release of acidic leachates can enhance metal mobility, increasing their bioavailability and toxicity to soil biota (Ashworth 2005; Di Palma and Mecozzi 2010).

Additionally, interactions between leachates and soil minerals, such as adsorption onto clay particles or complexation with organic matter, can either enhance or limit the spread of contaminants (Kowalska et al. 1994; Warith and Yong 1991; Weissmahr et al. 1998). Evaluating the composition and behaviour of these leachates is essential for understanding their long-term environmental impact and guiding remediation strategies.

Beyond saturated hydraulic conductivity (K), volumetric water content, and hydrophobicity, several other hydropedological factors significantly influence contaminant dynamics in soils. Soil aggregation and structural stability significantly impact water infiltration and pollutant dispersion, as well-structured soils may facilitate preferential flow pathways, leading to rapid contaminant transport (Basset et al. 2023; Kodešová et al. 2009).

4.3.1 Hydropedological Zoning, Soil Morphology, and Structure of the Unsaturated Zone

The hydropedological characteristics and flow dynamics of the soil refer to the interactions between soil properties and the movement of water through it (Ma et al. 2017). These characteristics are crucial to understanding water retention, infiltration, drainage, and the movement of nutrients and contaminants (Lin 2012). In this context, the hydropedological zoning was done through a brief description of each type of soil:

(i) The Uphill Soil (US) represents the natural geological and hydropedological conditions before the deposition of coal mining waste. The morphological characteristics are shown

in Table 4.1. Located at the highest point of the study area, this zone remains unaffected by the deposition of coal mining waste. Its parent material consists of Carboniferous metasedimentary rocks, while the vegetation cover primarily comprises *Eucalyptus globulus*, *Acacia melanoxylon*, *Acacia dealbata*, and *Pinus pinaster*. The soil profile follows the O-Ah-C-R sequence. The analytical results and field measurements concern the Ah horizon

Table 4.1 Soil morphological characteristics of the uphill soil (US) hydropedological zone

Soil feature	O horizon	Ah horizon	C horizon
Colour	–	10YR4/4 (dark yellowish brown)	–
Texture	–	silt loam	–
Structure (morphology/distinctiveness/ size)	–	subangular blocky/strong/fine	–
Thickness	10−15 cm	15−25 cm	20−50 cm
Lower boundary (distinctness/topography)	clear/smooth	gradual/wavy	–
Organic matter (presence/abundance/ humification)	present/abundant/ none to incipient	present/abundant/ humified	mostly absent/none to very scarce/humified
Porosity (size/abundance)	–	very fine/common, fine/few, medium/ very few	–
Biological activity (roots: diameter/abundance)	–	very fine/common, fine/common medium/very few	very fine/none, fine/none medium/very few coarse/very few

(ii) The Unburned Coal Waste Pile (UCW) consists of typical coal mining waste that has not undergone self-burning. The morphological characteristics are shown in Table 4.2. Its vegetation cover is relatively recent, primarily composed of *Acacia dealbata* and *Eucalyptus globulus*. The dominant soil profile follows the O-A-C sequence, with only an incipient accumulation of humified organic matter in the A horizon, which is absent in some areas of the hydropedological zone. Analytical results and field measurements are focused on the C horizon.

Table.4.2 Soil morphological characteristics of the Unburned Coal Waste Pile (UCW) hydropedological zone

Soil feature	O horizon	Incipient A horizon	C horizon
Colour	–	5Y3/1 (very dark gray)	–
Texture	–	silt loam/sandy loam	–
Structure (morphology/distinctiveness/ size)	–	apedal	–
Thickness	1−5 cm	2−8 cm	> 100 cm
Lower boundary (distinctness/topography)	gradual/wavy	gradual/wavy	–
Organic matter (presence/abundance/ humification)	present/abundant/ none to incipient	present/scarce/ humified	mostly absent/none to very scarce/humified
Porosity (size/abundance)	–	very fine/common, fine/common, medium/few coarse/few	very fine/common, fine/common, medium/few coarse/few
Biological activity (roots: diameter/abundance)	–	very fine/few, fine/very few medium/very few coarse/very few	very fine/none, fine/none medium/very few coarse/very few

(iii) The Burned Coal Waste Pile (BCW) consists of coal mining waste that has undergone self-burning. The morphological features are shown in Table 4.3. The waste is protected by a 30–40 cm layer, known as the Cover Layer (CL), which is composed of mixed material primarily derived from the C and R horizons of nearby soils with various metasedimentary parent materials. Vegetation is largely absent in this area. The soil profile consists of two horizons: C1, corresponding to the CL protective layer, and C2, representing the BCW layer. Analytical results and field measurements focus on both the C1 and C2 horizons.

Table.4.3 Soil morphological characteristics of the Burned Coal Waste Pile (BCW) hydropedological zone

Soil feature	C1 horizon (cover layer, CL)	C2 horizon (burned material, BCW)
Colour	7.5YR7/6 (reddish yellow)	5Y3/1 (very dark grey)
Texture	silt loam/sandy loam/loam	silt loam
Structure (morphology/distinctiveness/size	apedal	apedal
Thickness	30−40 cm	> 100 cm
Lower boundary (distinctness/topography)	clear/wavy	–
Organic matter (presence/abundance/ humification)	present/scarce/ humified	absent
Porosity (size/abundance)	very fine/few, fine/common medium/common coarse/few	very fine/common, fine/common, medium/few
Biological activity (roots: diameter/abundance)	–	–

(iv) The Mixed Burned Coal Waste (MBW) consists of a blend of materials from U

phill Soil (US), Unburned Coal Waste (UCW), and Burned Coal Waste (BCW). The morphological feature is shown in Table 4.4. *Eucalyptus globulus* was planted in 2020, forming the current vegetation cover. The soil profile follows a C-R sequence, where C corresponds to the mixed material and the R horizon to Carboniferous metasedimentary rocks. Analytical results and field measurements focus on the C horizon.

Table 4.4 Soil morphological characteristics of the Mixed Burned Coal Waste (MBW) hydropedological zone

Soil feature	C horizon
Colour	5Y2.5/1 (black)
Texture	silt loam/loamy sand
Structure (morphology/distinctiveness/ size)	apedal
Thickness	> 100 cm
Lower boundary (distinctness/topography)	–
Organic matter (presence/abundance/ humification)	absent
Porosity (size/abundance)	very fine/common, fine/common, medium/few coarse/few
Biological activity (roots: diameter/abundance)	medium/very few coarse/very few

(v) The downhill soil (DS) primarily represents the original geological and pedological conditions before the deposition of coal mining waste. The soil morphological characteristics are presented in Table 4.5. Nevertheless, due to its location at the lowest part of the study area, this soil is influenced by the uphill coal waste through debris input and water movement via overland flow and interflow. The vegetation cover is primarily composed of *Eucalyptus globulus*. The soil profile follows an O-Ap-C-R sequence, with analytical results and field measurements focusing on the Ap horizon.

Table 4.5 Soil morphological characteristics of the Downhill Soil (DS) hydropedological zone

Soil feature	O horizon	Ap horizon	C horizon
Colour	–	10YR3/2 (very dark greyish brown)	–
Texture	–	silt loam	–
Structure (morphology/distinctiveness/size	–	subangular blocky/moderate to weak/very fine to fine	–
Thickness	5−8 cm	35−45 cm	50−100 cm
Lower boundary (distinctness/topography)	clear/smooth	gradual/wavy	–
Organic matter (presence/abundance/ humification)	present/abundant/ none to incipient	present/moderately abundant/ humified	mostly absent/none to very scarce/humified
Porosity (size/abundance)	–	very fine/few, fine/common, medium/common	–
Biological activity (roots: diameter/abundance)	–	very fine/very few, fine/few medium/few	very fine/none, fine/none medium/very few coarse/very few

The structure of the unsaturated zone varies considerably across the hydropedological zones identified in the study area, as summarised in Table 4.6. Each zone presents a distinct sequence of layers, reflecting differences in material composition and hydrological features. For example, both the uphill soil (US) and downhill soil (DS) exhibit a four-layer profile, starting with an organic debris layer (O horizon), followed by a mineral topsoil horizon (Ah or Ap), and transitioning into weathered and weakly weathered rock (C and R horizons, respectively).

In contrast, the profiles associated with coal waste zones — unburned (UCW), mixed burned (MBW), and burned (BCW) — are predominantly characterised by layers of coal mine waste, with variations in thickness and horizon development. The MBW and BCW profiles tend to have thicker coal waste deposits and fewer identifiable horizons. Water circulation in the upper layers is mainly through porous media, whereas in the deeper layers it occurs through fractures within the rock massif. These structural differences directly affect water retention, flow pathways, and the potential mobility of contaminants in the unsaturated zone across different land covers and substrate conditions.

Table 4.6 Typical structure of the unsaturated zone according to the hydropedological zoning

Hydropedological zone	Unsaturated zone structure	Depth (cm)	Type of material	Type of water circulation medium
Uphill Soil (US)	Layer 1	–	organic debris (O horizon)	–
	Layer 2	0 (top) 12 (bottom)	mineral particles and humified organic matter (Ah horizon)	porous
	Layer 3	12 (top) 150 (bottom)	weathered rock (C horizon)	fractured
	Layer 4	> 150 (top)	weakly weathered rock (R horizon and underlying rock massif)	fractured
Unburned Coal Waste (UCW)	Layer 1	–	organic debris (O horizon)	–
	Layer 2	0 (top) 5 (bottom)	coal mine waste and humified organic matter (incipient A horizon)	porous
	Layer 3	5 (top) 100-250 (bottom)	coal mine waste (C horizon)	porous
	Layer 4	> 100-250 (top)	weakly weathered rock (underlying rock massif)	fractured
Mixed Burned Coal Waste (MBW)	Layer 1	0 (top) 150 (bottom)	(C horizon)	porous
	Layer 2	> 150 (top)	weakly weathered rock (underlying rock massif)	fractured
Burned Coal Waste (BCW)	Layer 1	0 (top) 35 (bottom)	mostly rock fragments (cover layer – C1 horizon)	porous
	Layer 2	35 (top) 150-5000 (bottom)	coal mine waste (C2 horizon and underlying coal mine waste)	porous
	Layer 3	> 150-5000 (top)	weakly weathered rock (underlying rock massif)	fractured
Downhill Soil (DS)	Layer 1	–	organic debris (O horizon)	–
	Layer 2	0 (top) 40 (bottom)	mineral particles and humified organic matter (Ap horizon)	porous
	Layer 3	40 (top) 150-200 (bottom)	weathered rock (C horizon)	fractured
	Layer 4	> 100-200 (top)	weakly weathered rock (R horizon and underlying rock massif)	fractured

The Figure 4.9 illustrates some aspects of the study area, such as the features of the land surface, vegetation cover, and soil profile. Soils with a parent material consisting of coal mining waste (UCW, MBW and BCW) are classified as Technosols (Espinha Marques et al. 2021, 2024). According to the available soil mapping and the criteria of the World Reference Base for Soil Resources (Agroconsultores and Geometral, 1995; FAO, 2015), soil types from the US and DS hydropedological zones exhibit Regosol characteristics.

Figure 4.9 The Fojo coal mining waste and soil from the surrounding area: a) vegetation cover in the forest from the uphill soil (US); b) soil profile in the uphill soil; c) unburned coal waste (UCW=; d) mixed coal waste (MBW); e) burned coal waste and cover layer

4.3.2 Hydropedological Field Measurement

The results of unsaturated hydraulic conductivity (K), volumetric water content, and hydrophobicity measurements are shown in Table 4.7. The MDI test values show that, across all soils, the order of magnitude of K remains the same in both the wet and dry seasons, indicating that volumetric water content is not a critical factor controlling this hydropedological property.

In the Ah horizon (US zone), the measured K is 0.00 cm/s in the wet and dry seasons because of the high hydrophobicity, while most of the remaining K average values are around 10^{-4} cm/s. In the UCW zone (C horizon), K values range from $1.39x10^{-4}$ cm/s to $1.79x10^{-3}$ cm/s.

In the BCW zone, K values range from $3.05x10^{-5}$ cm/s to $1.90x10^{-3}$ cm/s in the C1 horizon (CL material) and from $1.76x10^{-4}$ cm/s to $5.50x10^{-3}$ cm/s in the C2 horizon (BCW material). For the MBW zone (C horizon), K values range from $2.42x10^{-4}$ cm/s to $1.83x10^{-3}$ cm/s. However, sample BCW10, which consists of material from the deepest part of the burned waste pile, has K values similar to those of the lower C2 horizon in the BCW zone (i.e., 10^{-4} cm/s). The DS zone (Ap horizon) has K values ranging from 3.74×10^{-5} cm/s to 5.94×10^{-4} cm/s.

In several soils from the Fojo coal mining site (e.g., UCW, MBW, BCW-C2, BCW10), the unsaturated hydraulic conductivity (K) remained within the same order of magnitude between the wet (March 2022) and dry (July 2023) seasons. This stability occurred despite notable decreases in volumetric water content (VWC). These findings indicate that VWC does not predominantly control K in these samples. Instead, intrinsic factors such as soil structure, porosity, texture, or pore connectivity are likely the dominant controls (Jarvis et al. 2013; Nimmo 1997; Schuh and Cline 1990). This is especially evident in the BCW-C2 horizon, where K remained constant despite VWC dropping from 34.2% to 14.4%, highlighting a structurally stable, conductive pore network.

Table 4.7 Unsaturated hydraulic conductivity (K), volumetric water content, and hydrophobicity mean values in soils from the Fojo coal mining waste disposal site and the surrounding area.

Hydropedological zone/Soil sample	Horizon/ number of measurements	March 2022		July 2023		Hydrophobicity
		K (cm/s)	VWC (%)	K (cm/s)	VWC (%)	
US	Ah (n = 5)	0.00	8.5	0.00	6.5	Severely water-repellent
UCW	C (n = 5)	$8.59x10^{-4}$	15.6	$7.47x10^{-4}$	12.1	Wettable
MBW	C (n = 6)	$8.12x10^{-4}$	24.4	$6.97x10^{-4}$	10.3	Wettable
BCW	C1 (n = 9)	$7.45x10^{-4}$	19.2	$5.90x10^{-4}$	8.8	Wettable
	C2 (n = 9)	$1.10x10^{-3}$	34.2	$1.10x10^{-3}$	14.4	Wettable
DS	Ap (n = 3)	$1.65x10^{-4}$	25.3	$6.78x10^{-4}$	7.2	Wettable
BCW10	C2 (n = 1)	$9.19x10^{-4}$	15.3	$7.83x10^{-4}$	5.4	Wettable

MDI suction rate: -1 cm; hydrophobicity classification according to Dekker et al. (2009)

On the other hand, the US samples show no hydraulic conductivity at all in either season, despite having some moisture. That's a clear example of hydrophobicity being a limiting factor, where even existing moisture doesn't translate into flow. Regarding hydrophobicity, all soils are wettable throughout the year except for the US zone soil, which is usually severely hydrophobic, except perhaps during exceptionally wet periods.

4.3.3 Soil Mineralogy

The overall mineralogical composition of the fine earth fraction is shown in Table 4.8. Silicates, with an absolute predominance of quartz, followed by phyllosilicates (mainly muscovite and kaolinite) and feldspars (potassic and calc-sodic), are the main minerals in the samples. Iron oxides (hematite and, in some samples, goethite) and titanium oxides (anatase) are present in almost all samples, as well as sulphates, namely jarosite and alunites. Siderite, the only detected carbonate, is relatively common but in small amounts (Espinha Marques et al. 2024).

Table 4.8 Mean Mineralogical Composition (%) of the fine-earth fraction of soils of the Fojo coal mine waste pile and its surrounding area.

	Hydropedological zones						
				BCW			
Minerals	US (n = 2)	UCW (n = 2)	MBW (n = 2)	CL (n = 5)	BCW (n = 5)	DS (n= 2)	BCW10 (n = 1)
Quartz	85.8	52.8	69.0	58.0	55.5	82.5	55.0
K Feldspar	1.3	3.3	1.3	5.5	5.2	3.5	5.5
Plagioclase	4.3	7.3	5.0	5.6	5.8	3.0	4.5
Opal C/CT	0.0	0.0	0.0	0.0	0.0	traces	0.0
Zeolites	0.0	0.0	0.0	0.0	0.0	traces	0.0
Muscovite	4.5	13.0	9.5	12.9	12.4	4.3	13.5
Kaolinite	2.0	3.5	2.5	4.1	2.5	1.0	1.5
Chlorite	0.0	2.8	0.0	1.0	0.0	0.0	0.0
Pyrophyllite	0.0	0.0	0.0	0.0	0.0	traces	0.0
Hematite	0.0	1.5	3.8	0.9	6.5	0.0	8.0
Goethite	0.0	1.0	1.0	1.4	0.0	0.0	0.0
Anatase	2.3	4.5	2.5	3.7	3.6	2.0	3.5
Siderite	0.0	2.5	1.3	1.5	0.8	0.8	0.5
Pyrite	0.0	4.0	0.0	0.0	0.0	0.0	0.0
Jarosites	0.0	2.5	2.8	2.8	4.8	2.3	5.0
Alunites	0.0	2.0	1.5	2.8	3.3	1.0	3.5
Gypsum/ Anhydrite	0.0	0.0	0.0	0.6	0.0	0.0	0.0

The fine-earth fraction also shows some mineralogical differences among the hydropedological zones. The US soil is almost monomineralic, given the predominance of quartz (85.8 %). The UCW soil is characterised by the presence of some accessory minerals, notably higher chlorite, siderite, and pyrite values. The MBW soil is indistinct, reflecting the mixture of US, UCW, and BCW materials. In the case of the CL layer (C1 horizon of the BCW soil), quartz is much less abundant than in the US soil (58 %), offset by more significant amounts of muscovite, kaolinite, and chlorite. In addition to containing

less quartz (55.8%), the BCW layer (C2 horizon of the BCW soil) is significantly enriched in hematite, jarosite, and alunite.

The presence of siderite and pyrite in the UCW soil may be related to the reducing environment in the coal mine rock massif. Siderite ($FeCO_3$) and pyrite (FeS_2) typically form in anoxic (oxygen-poor) and reducing conditions, which are common in coal-forming environments. These conditions facilitate the precipitation of iron with carbonate (siderite) or sulphur (pyrite). If the rock massif in the coal mine has been historically part of a reducing environment, it could have provided the necessary geochemical conditions (low oxygen, availability of Fe, CO_2, and sulphides) for siderite and pyrite to form (Mclennan et al. 2000; Shen et al. 2023).

On the other hand, jarosite and alunite in the BCW layer reflect the oxidising environment of the waste pile, which is affected by self-burning (Çelebi and Ribeiro, 2023). The DS soil, despite having a similar amount of quartz as the US soil (82.5%), is characterised by the presence of some accessory minerals, namely, the only one in which the ubiquitous, although always discreet, presence of opal C/CT, zeolites, and pyrophyllite is observed. The fine-earth mineralogical composition of the BCW10 sample is quite similar to that of the BCW material.

As shown in Chapter 3, aluminosilicate minerals are the principal mode of occurrence for many major and trace elements in the unburned, mixed, and burned coal waste samples. To understand the complete mineralogical composition, the clay fraction was analysed (Table 4.9), revealing that illite is dominant in all soils, followed by kaolinite. Smectite and chlorite are also common, while pyrophyllite is somewhat less common (Espinha Marques et al. 2024).

Table 4.9 Mean mineral composition (%) of the clay fraction of soils from the Fojo coal mine waste pile and its surrounding area.

	Hydropedological zones						
				BCW			
Minerals	US (n = 2)	UCW (n = 2)	MBW (n = 2)	CL (n = 5)	BCW (n = 5)	DS (n= 2)	BCW10 (n = 1)
Smectite	27.5	0.0	2.8	7.8	0.0	10.0	9.0
Chlorite	0.0	7.0	0.0	5.4	0.0	8.5	6.0
Illite	53.5	72.0	83.5	65.0	88.0	55.0	65.0
Pyrophyllite	0.0	5.0	0.0	1.8	0.0	15.5	10.0
Kaolinite	19.0	16.0	14.0	20.0	12.0	11.0	10.0

The clay fraction results also reveal distinct characteristics according to the hydropedological zones. US soil is characterised by a very significant smectite content at the expense of a relative decrease in illite. The UCW soil shows a relative enrichment

in chlorite and pyrophyllite. In addition to illite and kaolinite, the MBW soil is characterised by smectite.

In the BCW soil, the CL layer is essentially characterised by the presence of accessory minerals, notably smectite, chlorite, and pyrophyllite. An almost monomineralic composition, such as the predominance of illite, characterises the BCW layer. However, the BCW10 sample has a more diverse clay mineralogy, including smectite, chlorite, and pyrophyllite, like the DS soil, which is rich in these minerals and depleted in illite.

4.3.4. Hydrogeochemistry of Soil Leachates and Interflow

The results of the soil leaching tests showed that the water-soil interaction with major ions, Fe, and PTE differed considerably across hydropedological zones. Similar contrasts were observed in the pH and EC of leachates. In March 2022, interflow was observed at the base of the waste pile after a rainy period. A water sample was collected to conduct a hydrogeochemical characterisation similar to that of the leachates. The mean values of pH, EC, TOC, and major ions in leachates are presented in Table 4.10.

Table 4.10 Major ion content, pH, EC, and TOC of soil leachates and interflow from the Fojo coal mine waste pile and its surrounding area

Hydropedological zone/Soil sample/ Interflow	pH	EC	TOC	HCO_3^-	Cl^-	SO_4^{-2}	Na^+	K^+	Ca^{+2}	Mg^{+2}	∑ major ions
US (n = 5)	5.7	11	6.15	2.95	1.14	0.78	1.76	0.52	0.62	0.17	7.94
UCW (n = 5)	4.7	67	3.33	1.05	0.58	20.27	0.42	0.88	4.05	1.67	28.92
MBW (n = 6)	4.1	65	0.90	0.05	0.35	19.49	0.89	0.77	5.02	1.26	27.83
BCW-CL (n = 9)	5.0	23	1.04	1.64	0.60	7.11	0.75	0.60	1.30	0.88	12.85
BCW-BCW (n = 9)	4.2	61	0.67	<0.05	0.34	19.25	0.73	0.70	2.90	1.42	25.35
DS (n = 3)	4.7	49	1.72	0.71	0.60	17.61	1.23	0.96	2.00	2.26	25.37
BCW10 (n = 1)	4.7	28	0.62	<0.05	0.37	8.98	0.57	1.16	1.81	0.61	13.50
Interflow (n = 1)	3.7	2690	12.20	<0.05	10.20	2635.00	83.00	11.00	301.50	206.50	3247.20

Mean values: EC (electric conductivity) in µS/cm; central ion and total organic carbon (TOC) content in mg/L. Analytical detection limits (LD) for leachates: 0.05 mg/L for HCO_3^-; 0.03 mg/L for Cl^-, SO_4^{2-}, Na^+, K^+, Ca^{2+}, Mg^{2+}.

The pH values are higher in samples without coal mining influence, specifically, 5.7 in US and 5.0 in CL. In samples with coal mining influence, pH values are more acidic, especially in self-burning materials: 4.2 in BCW and 4.1 in MBW. These results agree with other studies, which have shown that pH values are generally lower in samples influenced by coal mining (Dick et al. 1983; Eychaner 1999; Ivanova et al. 2023).

The soil EC also reflects the influence of coal mining, as the lower values were measured in the US and CL samples (11 µS/cm and 22 µS/cm, respectively). Compared to other tests, the highest values were measured in UCW, BCW, and MBW (67 µS/cm, 58 µS/cm, and 65 µS/cm, respectively). Intermediate pH and EC values were measured in the DS

samples. Soil EC has been identified as a key factor driving changes in soil properties in mining-affected areas, due to the high metal content (Ma et al. 2019).

Regarding major ion content, US and CL leachates exhibit significantly lower mineralisation compared to those of UCW, BCW, MBW, and DS, consistent with the EC results. The hydrogeochemical facies of the leachates are shown in Figures 4.10 and 4.11. Both diagrams, Piper and Stiff, yield the same results. In the case of US and CL, the principal facies are Na-HCO_3 and Mg-SO_4, respectively. The dominant facies are Ca-SO_4 for UCW, BCW, and MBW, and Mg-Ca-SO_4 for DS.

The leachate characteristics of BCW10 are similar to those of BCW, except for the lower SO_4 content. Common dominant major elements in anthracite coal waste leachates reported include Ca, Mg, Na, and S (Ribeiro and Flores 2021). Leachates are often classified as acid high-metal, with elements such as Cd, Co, Mn, Ni, and Zn readily mobilised and associated with water-soluble and exchangeable compounds (Komonweeraket et al. 2015; Mudd et al. 2004; Ribeiro and Flores 2021).

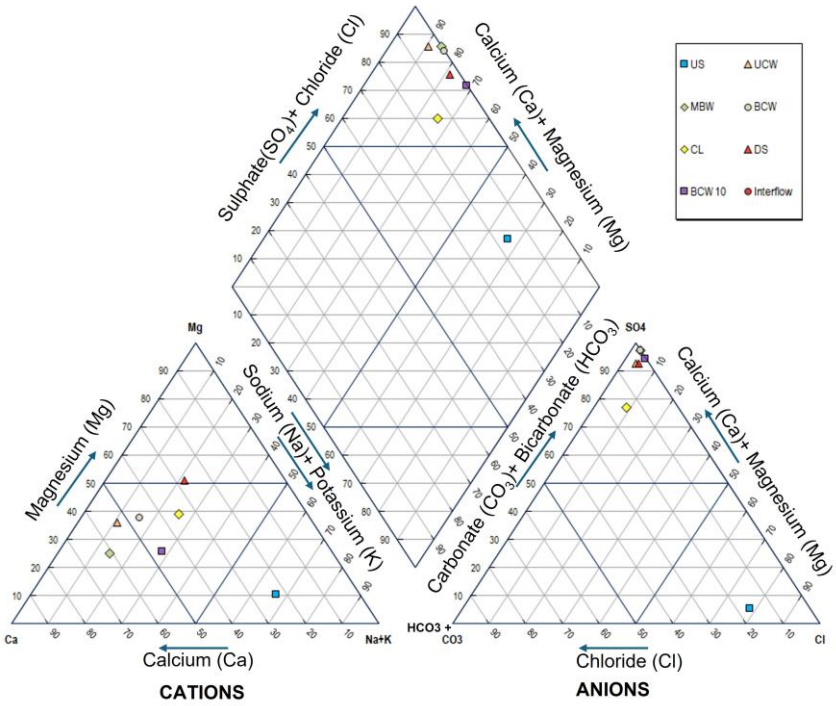

Figure 4.10 Piper diagram of soil leachates and interflow from the Fojo coal mine waste pile and the surrounding area

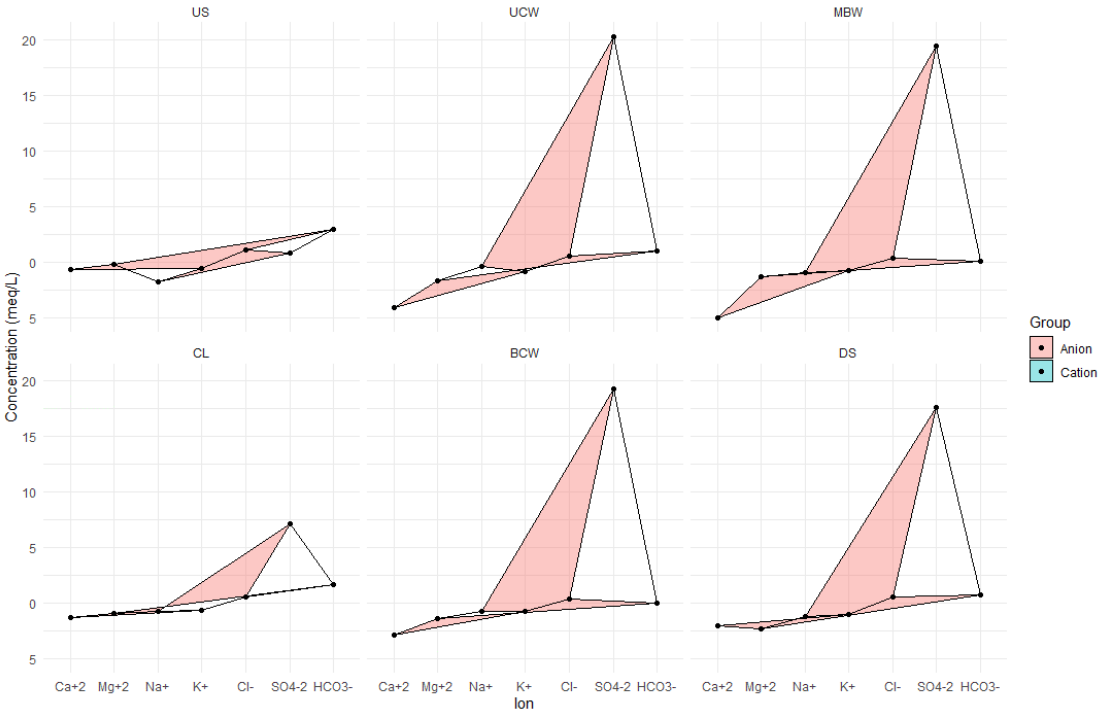

Figure 4.11 Stiff diagram of soil leachates and interflow from the Fojo coal mine waste pile and the surrounding area

The comparison of the hydrogeochemistry of soil leachates with soil geochemistry in Table 4.11 shows different leaching potentials for PTE and Fe. For Mn and Zn, higher hydrogeochemical concentrations correspond to significant geochemical concentrations. In contrast, this relationship is not apparent for Fe, Al, As, Cd, Ni, Cu, Cr, and Pb.

Table 4.11 Potentially Toxic Elements and Fe content of soil leachates, soil, and interflow from the Fojo coal mine waste pile and surrounding area

Hydropedological zone/Soil sample/ Interflow		Fe	Al	Mn	As	Cd	Ni	Cu	Cr	Zn	Pb
US	Leachate	77.78	64.36	1.00	1.17	n.d.	0.91	1.70	0.38	n.d.	0.20
(n = 5)	Soil	1.97	5.71	18.20	17.16	0.01	9.52	10.16	49.60	14.32	22,61
UW	Leachate	66.51	97.19	170.45	0.48	0.04	7.58	2.52	n.d.	35.60	1.05
(n = 5)	Soil	4.55	8.37	230.00	53.62	0.17	29.44	51.52	87.40	74.44	68,37
MBW	Leachate	21.81	441.88	62.42	0.23	0.15	9.72	9.42	0.36	8.00	2.76
(n = 6)	Soil	5.46	8.53	135.50	52.98	0.12	20.82	49.20	89.33	66.65	47,76
BCW-CL	Leachate	77.55	43.02	59.88	0.21	0.03	5.59	1.83	0.06	0.22	1.03
(n = 9)	Soil	5.59	12.53	83.78	39.04	0.07	33.37	58.17	100.89	37.68	46.16
BCW-BCW	Leachate	32.23	276.57	84.18	0.32	n.d.	8.92	2.43	n.d.	39.78	n.d.
(n = 5)	Soil	5.94	9.37	134.67	58.94	0.15	22.13	51.79	90.22	68.86	52.55
DS	Leachate	24.27	154.93	385.57	0.57	0.07	9.20	4.70	n.d.	7.33	n.d.
(n = 3)	Soil	3.01	9.12	334.33	35.90	0.02	22.57	24.97	82.67	42.10	31,75
BCW10	Leachate	77.28	29.63	78.70	<LD	n.d.	3.83	n.d.	n.d.	126.00	n.d.
(n = 1)	Soil	6.44	9.33	196.00	79.60	0.12	20.80	41.3	102.00	64.2	62.58
Interflow (n =1)		2948.00	1002.00	14600.00	2.70	12.00	137.20	110.00	6.45	n.a.	n.d.

Mean values: concentrations in leachates and interflow in µg/L; concentrations in soil in mg/kg; n.a.–not analysed; n.d.–not detected. Limit of detection (LD) for leachates: 1 µg/L for Cd, As, Pb, Ni, Cu, Zn, Al, and Cr; 25 µg/L for Fe and Al.

The results also showed different distribution patterns of PTE (Al, Mn, As, Cd, Ni, Cu, Cr, Zn, Pb) and Fe across the hydropedological zones. The concentrations of PTE and Fe in leachates are presented in Figure 4.12, where it can be observed that the values tend to be higher in soil samples with coal mining influence (UCW, MBW, and BCW) than in US and CL.

In fact, UCW and BCW leachates have similar total concentrations of PTE and Fe, with more expressive differences in Al, Fe, Mn, and Zn. Compared to the BCW material, the BCW10 sample contains more Fe (compatible with pyrite weathering in a more intense self-burning environment) and Zn. In contrast, this sample is relatively depleted in Al and, to a lesser extent, Mn, Ni, and Cu.

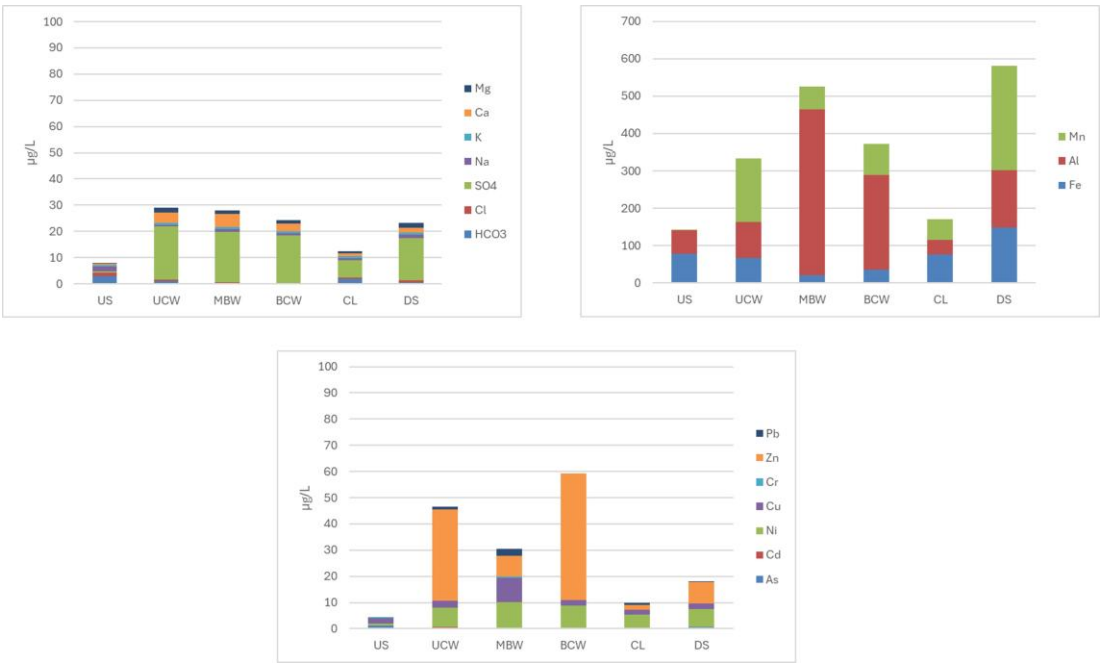

Figure 4.12 Mean contents of the major ions, potential toxic elements, and Fe of soil leachates from the Fojo coal mining waste and the surrounding area

The hydrogeochemistry of soil leachates indicates that water-soil interaction in the upper unsaturated zone is more intense in soils with mining influence, resulting in higher concentrations of soluble major ions and PTE. In addition, the DS soils exhibit signs of coal mining influence, as indicated by their relatively high concentrations of SO_4^{-2}, Ca, Mg, Al, Mn, Ni, Cu, and Zn. This influence results from the overland flow and interflow in the coal mine waste pile. It has probably occurred for decades since the waste was first deposited, but has intensified since the self-burning event.

During heavy rainfall, overland flow was observed in the BCW and MBW hydropedological zones (Figure 4.1). It promoted the transport of solid particles and dissolved chemical compounds to the DS zone. In addition, the interflow water that emerges at the base of the waste pile, with high concentrations of major ions, PTE, and Fe (Table 4.10 and Table 4.11), also reaches the DS material, contributing to changes in its geochemical and hydrogeochemical signature.

The interflow hydrogeochemistry results from a longer and deeper flow path, along which the fluid becomes progressively more acidic due to pyrite weathering, promoting interaction with the mine waste and resulting in much more intense leaching of major ions, PTE, and Fe. The pH and EC values are 3.7 and 2690 µS/cm, respectively; the mineralisation is higher than in the soil leachates, and the hydrogeochemical facies are Ca-SO_4. Similarly, Fe and some PTE concentrations are higher in interflow than in the soil leachates: Al, Mn, As, Cd, Ni, Cu, and Cr.

A Pearson's test was carried out, which showed a positive moderate correlation between SO_4 and Ca (r = 0.549; p < 0.001); and Cd (r = 0.508; p < 0.001) and a strong correlation with Mg (r = 0.876; p < 0.001), and Ni (r = 0.708; p < 0.001). On the other hand, Cr, Cu, Pb, Cd, and Al showed a strong positive correlation, suggesting they may have originated from a common source. In addition, Cl^- showed moderate positive correlations with As (r = 0.594; p < 0.001), Fe (r = 0.565; p < 0.001), and Na (r = 0.686; p < 0.001). For HCO_3^- a weak positive correlation was presented for Na (r = 0.380; p = 0.017), and a moderate positive correlation for Fe (r = 0.453; p = 0.004), and As (r = 0.410; p = 0.010). Indeed, a weak negative correlation was observed for K (r = -0.391; p = 0.014), and Ca (r = -0.319; p = 0.047), and a moderate negative correlation for Mg (r = -0.489; p = 0.002), Al (r = -0.554; p < 0.001), Ni (r = -0.520; p < 0.001), and Zn (r = -0.483; p = 0.002).

The one-way ANOVA test results showed significant differences for all variables using the different sites as a factor, except for NO_3^-, NH_4^+, Ca, and Ni (Table 4.12).

Table 4.12. One-way ANOVA results for the lixiviate parameters in the different coal mining waste.

ANOVA					
	Sum of Squares	df	Medium Square	F	Sig.
pH	2,605	5	0,521	3,981	0,006
Conductivity	193978,891	5	38795,778	6,801	0,000
MO	973,552	5	194,710	20,307	0,000
Turbidity	1,101	5	0,220	2,850	0,030
TOC	128,083	5	25,617	15,831	0,000
Alcalinity	27,432	5	5,486	15,250	0,000
HCO_3^-	40,824	5	8,165	15,249	0,000
Cl	2,411	5	0,482	17,556	0,000
SO_4^{-2}	1987,990	5	397,598	6,515	0,000
F	0,005	5	0,001	7,059	0,000
NO_3^-	0,945	5	0,189	1,720	0,157
NO_2^-	0,000	5	0,000	5,117	0,001
NH_4^+	1927,175	5	385,435	0,546	0,740
Na	5,794	5	1,159	8,677	0,000
K	0,679	5	0,136	5,697	0,001
Ca	84,602	5	16,920	2,072	0,094
Mg	11,343	5	2,269	3,967	0,006
Fe	20072,680	5	4014,536	3,785	0,008
Al	761538,986	5	152307,797	5,803	0,001
Mn	601350638,340	5	120270127,668	3,168	0,019
As	3,591	5	0,718	3,446	0,013
Cd	0,100	5	0,020	3,380	0,014
Ni	294,858	5	58,972	2,328	0,065
Cu	0,000	5	0,000	4,978	0,002
Cr	0,987	5	0,197	3,264	0,017
Zn	0,016	5	0,003	10,003	0,000
Pb	33,637	5	6,727	8,798	0,000

The post hoc Dunnett test indicates significant differences between US and DS for TOC, HCO_3^-, SO_4^{-2}, K, Mg, and Mn. In the case of US and UW, the significant differences are observed in OM, pH, Conductivity, TOC, HCO_3^-, SO_4^{-2}, Na, K, and Mg. The significant differences between the US and the mixed material (MBW) are for pH, EC, TOC, F, Na, K, Fe, Al, Ni, As, Cd, and Pb.

4.3.5 Hydropedological Setting and Soil Leaching

Field observations and measurements, along with mineralogical, geochemical, and hydrogeochemical results, indicate that coal mining has produced severe changes in the hydropedological conditions of the study area. The US hydropedological zone corresponds to pre-coal mining waste disposal and represents the least favourable conditions for soil leaching.

In this case, interception of rainfall by the abundant vegetation cover, which has existed at this site for decades, if not centuries, reduces the amount of water reaching the ground surface and can reduce infiltration. In addition, the infiltration capacity of the Ah horizon is also reduced by its hydrophobic nature (derived from soil organic matter, e.g., Dekker et al. 2009), which appears to persist for most of the year (Table 4.7) and can increase overland flow (e.g., Butzen et al. 2015; Leighton-Boyce et al. 2007). Under these conditions, the unsaturated hydraulic conductivity in the Ah horizon is very low or even zero, and water infiltration and percolation in the upper soil horizons can occur mainly during the wettest events of the year, generating hydropedological conditions less favourable to leaching. Water percolation is also limited to greater depths, particularly from the R horizon downwards, due to the lower permeability of the fractured metasedimentary rocks.

Another relevant feature of the US zone is that pedological evolution and soil leaching have been ongoing for centuries or even longer. Under these conditions, the topsoil has become geochemically depleted of leachable compounds and enriched in minerals less susceptible to leaching. This explains the lower concentration of major ions, PTE, and Fe in soil leachates.

In contrast, conditions in the mining-influenced hydropedological zones, as well as in the DS zone, are more favourable for water infiltration and percolation in the upper horizons, which could induce solute transport to the deepest part of the unsaturated zone and the water table aquifer. In the UCW and MBW hydropedological zones, the vegetation cover is more recent and less dense than in the US zone, and the A horizon is incipient and very shallow (in part of the UCW zone) or absent (in the remainder of the UCW zone and the entire MBW zone).

In these circumstances, not only is interception much less effective than in the US zone, but the soil hydrophobicity is much lower due to the scarcity or absence of humified organic matter, giving way to higher infiltration and percolation in a more permeable

porous medium, especially during the rainy season, when most precipitation occurs, and evapotranspiration is lower.

This situation is even more extreme in the BCW zone, where vegetation is almost absent, the soil is hydrophilic, and K is an order of magnitude higher in the C2 horizon (Table 4.7). In addition, the more permeable porous medium in the burned coal waste allows a transition to the fractured medium only at greater depths than in the other hydropedological zones, creating a longer flow path that favours leaching.

Furthermore, the mineral composition of the UCW and MBW soils reflects incipient pedogenetic evolution, with a more diverse and abundant suite of leachable compounds. In the case of the BCW soil, the self-burning process induced significant mineralogical transformations, primarily through oxidising processes that promoted the destruction of pyrite and siderite, followed by the formation of hematite, jarosite, and alunite. As a result of pyrite weathering, the water percolating through the BCW material becomes increasingly acidic and more capable of promoting leaching, resulting in highly mineralised interflow water.

DS soils, similar to those in the US, have been influenced by coal mine waste piles for decades. This influence encompasses the transport of solid particles (ranging in size from clay to gravel), particularly during overland flow in the BCW and MBW hydropedological zones, as well as dissolved chemical constituents from interflow through the deepest part of the burned waste pile in an acidic environment. The hydrogeochemical signature of this influence includes higher levels of SO_4, Ca, Mg, Al, Mn, Ni, Cu, and Zn than the US soil.

The chemical composition of soil leachates reflects hydropedological zoning, and PCA analysis confirms these contrasts, as highlighted in Figure 4.13. The PCA plot distinguishes soil samples from different hydropedological zones and shows their relationships with major and trace elements, pH, and TOC.

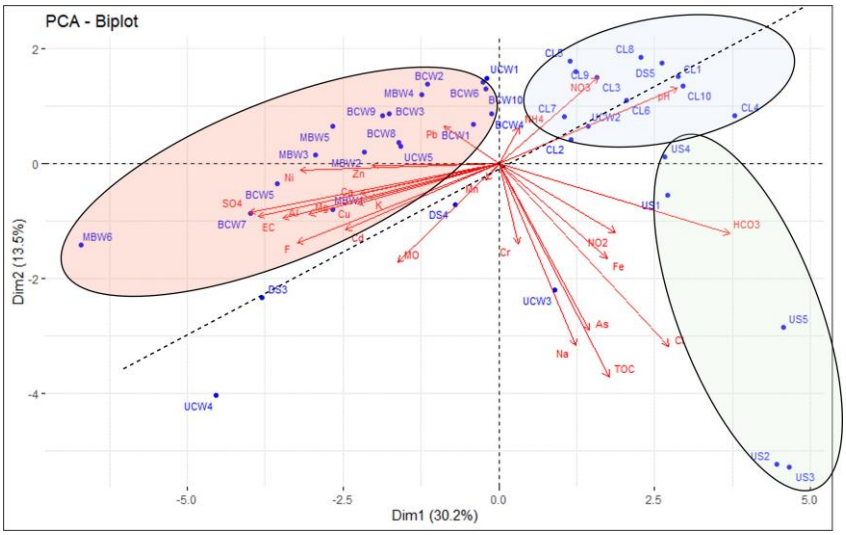

Figure 4.13 PCA analysis of chemical parameters in soil leachates from the Fojo waste pile and the surrounding area; Uphill Soil (US) cluster in green; Burned Waste (BCW) and Mixed Burned Waste (MBW) cluster in red; Cover layer (CL) cluster in blue; the dashed line marks the boundary defined by the downhill soil (DS) samples.

The US soils, represented by the green cluster, appear clearly separated from all other samples. These soils exhibit lower electrical conductivity (EC) and metal concentrations, reflecting natural background conditions with minimal influence from mining residues. BCW and MBW are grouped in the orange cluster, suggesting similar behaviour characterised by elevated EC, higher pH, and increased concentrations of various trace elements. The CL samples, forming the blue cluster, are distinctly different from the other samples, suggesting they may originate outside the study area.

The DS soil samples are plotted along a line that separates those with mining influence (UCW, BCW, and MBW) from those without (US). It exhibits variability, likely due to heterogeneous leaching and mixing from the overlying coal waste materials (BCW, MBW, and UCW), as well as the influence of both natural soils and waste leachates. The UCW (Unburned Coal Waste) is associated with elements such as sulphur (S) or possibly moderate electrical conductivity (EC) and pH. It reflects material with less transformation than BCW, but still with contaminant potential.

The PCA shows a clear distinction between the chemical signatures of natural soils (US), mining waste soils (BCW, MBW, UCW), covering layer (CL), and potentially affected downhill soil (DS). Burned wastes (BCW and MBW) are associated with elevated concentrations of trace elements, higher EC, and lower pH, whereas US soils exhibit low-impact profiles. The downhill soil (DS) exhibits intermediate behaviour, suggesting influence from waste-derived leachates.

4.4 Final Remarks

The environmental impacts of coal mining on soil and water bodies are well known. In coal mining areas, landscapes and ecosystems often undergo significant changes, accompanied by alterations in hydrology and pedology. The local hydrological cycle is disrupted by changes in rainfall interception, overland flow, infiltration, and percolation. In addition, the local soil system is altered by waste disposal in landfills, often large in volume and area, resulting in the creation of new soil types classified as Technosols.

A hydropedological perspective (encompassing the definition of hydropedological zones) is valuable for understanding water-soil interactions in this environment. It also provides a basis for an integrative scientific approach for evaluating changes in processes and features in the upper unsaturated zone.

This study employed an integrative approach to assess changes in the hydropedological conditions of an area with coal mining waste deposition and self-burning: the Fojo waste pile, in the Douro Coalfield, Northwest Portugal. The first research task was to define the hydropedological zoning of the waste pile and the surrounding area based on soil formation factors. Next, the soils in each hydropedological zone were characterised by morphological features. Samples were collected from the most superficial mineral horizons for mineralogical (fine and clay fraction) and geochemical analysis. Unsaturated hydraulic conductivity, soil water content, and hydrophobicity were measured on these soil horizons. The hydrogeochemistry of the leachates (including major ions, PTE, and Fe) was characterised, and finally, the soil leaching potential was evaluated.

The research results showed clear contrasts between the hydropedological zones in all aspects studied, from soil morphology to soil leaching. Indeed, the hydropedological conditions favour rainfall infiltration, percolation, and leaching of major ions and PTE in the upper soil horizons of the hydropedological zones with mining influence (UCW, MBW, BCW) rather than in the original soil, free from mining impact (US). In addition, the leaching potential in the US zone is expected to be lower due to soil mineralogy and percolation into the deepest part of the soil profile (C horizon and, especially, R horizon), which occurs in a fractured medium corresponding to a material with lower permeability and lower specific surface than in the case of UCW, BCW and MBW zones. Also, based on the morphological characteristics of the soil profile, hydropedological field measurements, and the structure of the unsaturated zone, it is expected that the transport of pollutants to greater depths and eventually to the water table aquifer will be more effective in the UW, MBW, and BW hydropedological zones.

Leachates from mining-affected soils are more acidic, especially those with self-burning properties. They also have higher major-ion content (Ca-SO_4 hydrogeochemical facies) and higher PTE content. The influence of self-burning enables differentiation of the soil in the UCW zone from the BCW layer. The BCW layer is characterised by a higher K value, a different mineral composition (both in the fine soil fraction and in the clay fraction), leachates with a slightly more acidic pH, and different concentrations of some PTE.

Although the DS soil was similar to the US soil before waste deposition, it currently shows an apparent mining influence, as evidenced by leachate composition closer to that of mining-influenced soils.

In summary, the hydropedological setting in mining-influenced hydropedological zones corresponds to soils that are more susceptible to the leaching of major ions and PTE and have a more pronounced ability to disperse environmental pollutants in groundwater.

The Fojo coal mine waste pile study exemplifies the growing interest in applying hydropedological concepts, methods, and techniques to evaluate the environmental impacts of coal mining. Such an approach can be highly valuable for decision-making related to environmental management in coal-mining areas. It can also be applied to the exploitation of many other geological resources.

Chapter 5. Ecotoxicological Effects of the Coal Mining Waste Elutriate in Aquatic and Terrestrial Species.

5.1 Introduction

Mining activities significantly alter the landscape's outline, chemistry, and biology (Sonter et al. 2018). The acidic nature of water circulating in coal mine waste is usually due to the oxidation of pyrite, and the low pH increases the dissolution of PTE, favouring their transport in leachates (Costa and Duarte 2005; Nyström et al. 2021). The chemical mobility of pollutants is fundamental to understand toxicity, bioavailability, and geochemical behaviour (Dang et al. 2002; Ribeiro et al. 2010a). Indeed, a wide range of significant effects, including increased morbidity and mortality, reduced numbers of plant and animal species, decreased plant growth, and loss of visual aesthetic landscape characteristics, can result from this phenomenon (Cehlár et al. 2016).

Ecotoxicological tools have been proven to be a sensitive and appropriate approach for assessing toxicity and estimating the environmental risk of contaminants (Alvarenga et al. 2021) since chemical methods need to be complemented with a biological procedure to explain the effects on the ecosystem's biota (Abd Aziz et al. 2019; Lee et al. 2015). However, research on toxicology in coal mines and CMW is scarce, and the impact of PTE-enriched effluents on terrestrial and aquatic biota is poorly known (Martin and Black 1998; Shylla et al. 2021).

Previous studies on the assessment of the environmental impact of coal mining waste in the Douro Coalfield (North of Portugal) have mainly focused on geochemical analysis and characterisation (Ribeiro et al. 2010a, 2011, 2020; Ribeiro and Flores 2021), leaving room for an ecotoxicology-based environmental risk assessment. The present research adopted an ecotoxicological approach, and the main goal is to assess the potential toxicity of soil elutriates from coal mining waste (both burned and unburned areas) in the aquatic ecosystem. To achieve this goal, a set of bioassays was conducted using aquatic model species from different trophic levels, and several endpoints were evaluated: Microtox assays, bioluminescence inhibition of the bacterium *Aliivibrio fischeri*; acute assays, including mortality of *Daphnia magna*, and growth inhibition of *Lemna minor* and seed germination for *Lactuca sativa*. Additionally, sub-individual parameters were also evaluated in *L. minor* and *L. sativa* [total chlorophyll content, catalase (CAT) activity, and malondialdehyde (MDA) content] after exposure to the different soil elutriates.

5.2 Materials and Methods

The presented research was conducted in elutriates from 25 soil samples representative of the heterogenic pedological zones, arranged as follows: three (3) samples in US (US1, US4, US5), three (3) samples for UCW (UCW1, UCW3, UCW5), five (5) samples BCW (BCW3, BCW4, BCW8, BCW9, BCW10), five (5) samples of CL (CL3, CL4, CL8, CL9, CL10), six (6) samples in MBW (MBW1, MBW2, MBW3, MBW4, MBW5, MBW6), and three (3) samples for DS (DS1, DS3, DS5) (*see* Figure 2.2 and Table 2.1 in Chapter 2). The ecotoxicological effects of elutriates of these soils were conducted in three aquatic species: i) *Aliivibrio fisheri* (bacteria bioluminescence inhibition assay); ii) *Lemna minor* (macrophyte growth inhibition assay, with additional measured endpoints: total chlorophyll content, catalase (CAT) activity, and lipid peroxidation levels) and iii) *Daphnia magna* (microcrustacean acute assay); and one terrestrial species *Lactuca sativa* (lettuce germination assay, with additional measured endpoints: morphologic alterations, total chlorophyll content, CAT activity, and lipid peroxidation levels).

Figure 5.1 The location of the CMW used to obtain the leached samples was tested in the species.

5.2.1. Physicochemical Parameters, Nutrients, and Metals Determination

For soil physical and chemical determinations [pH, conductivity (µS/cm), water-holding capacity (%), and organic matter content (%)], samples were air-dried for 1 week,

homogenised, and sieved through a 4 mm mesh. Soil pH and conductivity were measured in a soil-water suspension (extraction ratio 1:5 w/v) according to the method described in FAO (1984). Each soil replicate (10 g) was mechanically shaken with 50 mL of deionised water for 15 min. After the mixtures had stood for 1 h, the solution pH was measured with a multiparametric probe. The soil-water suspension was left to rest overnight, and the following day, the conductivity of the samples was measured using a multiparametric probe (FAO, 1984). Water holding capacity (WHC) was determined in each soil, where the soil was placed in plastic bottles (where the background was replaced by filter paper) and immersed in water for 3 h (ISO 2008). After this period, the samples were drained for 2 h by rejecting excess water with absorbent paper. The WHC was determined by weighing each replicate before and after drying at 105 °C until the weight stabilised (ISO 2008). Organic matter (OM) content was determined using the percentage of the initial dry weight of the sample (three replicates per elutriate) and the dry ash after igniting in a muffle furnace at 450 °C for 8 h (SPAC, 2000).

To evaluate the bioavailability of metals and nutrients in the leachates of each soil, several methodologies were carried out as described in Espinha Marques et al. (2021). Bicarbonate (HCO_3^-) and oxidability were analysed by titration. The major inorganic ions (Na, K, Mg, Ca, Li, Cl, NO_3^-, F, and SO_4^{-2}) were analysed by ion chromatography, CI (DionexTM system DX-120/ICS-1000, Dionex Corporation, Sunnyvale, CA, USA), and the potential toxic elements (Cr, Mn, Ni, Cu, Zn, As, Cd, and Pb) in a Varian AA240 Atomic Absorption Spectrometer (Varian Inc., Palo Alto, CA, USA). Other components, such as Al, Fe, NO_2^-, and NH_4^+, were analysed and put in a Continuous Segmented Flow Instrument (CSF) (San-Plus Skalar, Skalar Analytical, Breda, The Netherlands).

5.2.2 Soil Elutriates.

Elutriates were prepared using a ratio of 1:4 (w/v) of each soil with a respective culture medium of each species: distilled water for Microtox® assay with *Aliivibrio fisheri* and *Lactuca sativa* germination assay, ASTM hard-water medium for *D. magna* acute assay, and Steinberg medium for *L. minor* growth assay. (ASTM 1989; OECD 2004). The soil suspension was mechanically stirred for 12 hours at room temperature, followed by a period of deposition of 12 hours. After this period, the elutriate was collected by decantation. All the assays were performed using the direct elutriate, without dilution, and used within 48 h.

5.2.3 *Aliivibrio fischeri* – Microtox® Toxicity Assay

Standard Microtox® assays were performed using liquid phase (elutriates) procedures according to standardized protocols (Microbics 1992). Lyophilized luminescent marine

bacteria *A. fischeri* (NRRL strain number B-11177) was used for this assay after rehydration with a reconstitution solution before starting the assay. Bioluminescence evaluation was performed 5 minutes after exposure, at 9 dilutions of each elutriate (dilution factor of 2), using the Microtox Model 500 toxicity system with an automatic luminescence recording, following the protocol of the Microtox® Acute Toxicity Basic Test Procedures manual – Modern Water. EC20 values were achieved and used to report toxicity values for the elutriates.

5.2.4 *Daphnia magna* – Acute Immobilisation Assay

Daphnia magna acute immobilisation assay was performed according to the standard guideline OECD 202 (OECD 2004), with six-well microplate adaptation. Each elutriate was assessed with six replicates containing 12.5 mL of elutriate and five neonates (less than 24 h old born between the 3rd and the 5th broods). A negative control was conducted with *D. magna* neonates exposed to the ASTM medium. The assay was performed under controlled temperature conditions (20 ± 2 ºC) and photoperiod (16 h^{L}:8 h^{D}). After 48 h of elutriate exposure, the organisms were observed, and immobilised organisms were counted to assess the percentage of mortality induced by each elutriate.

5.2.5 *Lemna minor* – Growth Inhibition Assay

Lemna minor growth inhibition assays were conducted according to standard guidelines (OECD 2006), with microplate adaptation (Diogo et al. 2023a). Four replicates per elutriate were used, and 12.5 mL of elutriate and four fronds of *L. minor* were added to each replicate. The control group was exposed to the Steinberg medium.

The assays were conducted for 7 days, and the microplates were maintained under controlled conditions of light (24 h, ~ 7000 lux) and temperature (23 ± 2 ºC). At the final exposure period (7 days), the number of fronds was counted, and the results were expressed as a percentage of growth inhibition (OECD 2006). The fronds were washed with distilled water, dried with absorbent paper, weighed, and stored in Eppendorf microtubes at -80 ºC for quantification of the total chlorophyll content and biochemical determinations [catalase (CAT) activity and malondialdehyde (MDA) content].

The total chlorophyll content was quantified according to the method defined by Lichtenthaler (1987). Pigment extraction occurred overnight in 1 mL of 96 % ethanol at 4 ºC. After this period, the absorbance was measured through spectrophotometry at 644.2 and 648.6 nm (GenesysTM 10 Series Thermo Spectronic). Chlorophyll results were expressed in mg/mg fresh weight. For the CAT activity determinations, samples (~ 5 mg of fronds per replicate) were sonicated in 1 mL of ice-cold phosphate buffer (50

mM, pH 7.0) with 0.1 % Triton X-100. Catalase is an antioxidant defence enzyme responsible for the decomposition of hydrogen peroxide into water and molecular oxygen (Alkimin et al. 2020) and was quantified according to Aebi (1984), adapted to a 96-well plate. CAT activity was expressed as millimoles of H_2O_2 consumed per minute, per mg fresh weight. For MDA quantification, biological samples (~ 5 mg of fronds per replicate) were sonicated in 500 µL of 0.1 % trichloroacetic acid.

MDA is a final product of lipid peroxidation in plant cells. Its content was determined by the thiobarbituric acid method, as described by Elkahoui et al. (2005). Moreover, it is expressed as µM MDA equivalents per mg fresh weight. The supernatant's specific and non-specific absorbance was measured at 532 and 600 nm, respectively. The concentration of MDA was calculated by subtracting the non-specific absorbance and using the molar extinction coefficient ε=155 mM^{-1} cm^{-1}.

5.2.6 *Lactuca sativa* – Germination Assay

The germination assay was conducted according to OECD guidelines (2006) with a few adaptations. Seeds of *Lactuca sativa* (Vilmorin, France) were sterilised in a bath of 5 % sodium hypochlorite (NaClO) for 5 minutes, followed by 3 washes in sterile deionised water. After that, in a flow chamber, ten (10) seeds were placed in a sterile square Petri dish containing solid Iqland's solution (Hoagland and Arnon 1950) with 1.5 % agar and 10 mL of each soil elutriate. Four square Petri dishes were prepared per soil elutriate (4 biological replicates). 10 mL of sterile deionised water was added to the Petri dish with solid Hoagland's solution on the control plates.

The plates were placed vertically under controlled conditions of temperature (20 ± 2 ºC), photoperiod (16 h^L:8 h^D), and luminosity (~ 6000 lux). At the end of the exposure period (fourteen days after 50 % of seed emergence in the control group), the percentage of seed emergence as well as the biometric parameters of the seedlings [e.g., aerial part and root size, and fresh biomass (OECD 2006)] were evaluated. Additionally, morphologic alterations in early plant development were recorded (e.g., damage/deformations, chlorosis, wilting).

Additionally, several sub-individual effects were evaluated. Aerial parts were weighed and stored at -80 °C to further quantify total chlorophyll concentration and to conduct biochemical determinations of CAT activity and MDA content. The total chlorophyll (> 5 mg of aerial part, n=3) content was extracted in 1 mL of 96 % ethanol at 4 ºC overnight and determined according to Lichtenthaler (1987). After the extraction period, the absorbance at 644.2 and 648.6 nm was determined using a spectrophotometer

(GenesysTM 10Series Thermo Spectronic). Results were expressed in mg/mg fresh weight.

For the determinations of CAT activity, samples (> 30 mg of aerial part per replicate, n=3) were sonicated in 1 mL of ice-cold phosphate buffer (50 mM, pH 7.0) with 0.1% Triton X-100. Catalase is an antioxidant defence enzyme that decomposes hydrogen peroxide (H_2O_2) into water and molecular oxygen (Alkimin et al. 2020). CAT was quantified according to Aebi (1984), and the results were expressed as micromoles of H_2O_2 consumed/minute/mg fresh weight. Regarding MDA quantifications, the samples (> 10 mg of aerial part, n=3) were sonicated in 500 µL of 0.1 % trichloroacetic acid. The thiobarbituric acid method described by Elkahoui et al. (2005) was used to determine MDA content, and the results were expressed as µM MDA equivalents/mg fresh weight.

5.2.7 Statistical Analysis

The PCA was performed to relate soil physical and chemical properties to the composition of soil elutriates. For ecotoxicological assay results, the Pearson test was used to discriminate ecotoxicological assay for each parameter responsible for biological effects. All the evaluated endpoints (germination inhibition, fresh biomass, size, pigments, and biochemical quantifications) were checked for normality by the Shapiro-Wilk test and for homogeneity of variances by Levene's test to verify compliance with the ANOVA assumptions. To determine significant differences between soil elutriates and the control elutriates, an analysis of variance (one-way ANOVA), followed by a Dunnett's test, was performed to discriminate differences between the control group. The software SPSS Statistics v29 was used for all the statistical analyses, considering a significance level of $\alpha = 0.05$.

5.3. Results and Discussion

5.3.1 Soil and Elutriates: Physical and Chemical Characterisation.

In the study area, soils composed of technogenic materials (coal mining wastes) were classified as Technosols (Espinha Marques et al. 2021; FAO 2015). Table 5.1 presents the nutrients and trace metal concentrations recorded in the soil elutriates. At the same time, Figure 5.1 shows the PCA results regarding the matrix of physical and chemical parameters measured in each soil elutriate. Soil electric conductivity (EC) ranged between 33-366 µS/cm. The lowest EC values were observed in soil US5 and CL4, and the highest in UCW5, MBW6, and DS3 soils. However, DS3 and DS1 (downhill soils) have very high EC values, 366 µS/cm and 168 µS/cm, respectively, compared with US soils.

This fact could demonstrate that the leachates from burned material present an enrichment of ions' bioavailability. Despite that, none of the Fojo coal waste samples' EC values exceed the reference value limits for EC (475 µS/cm) proposed by the Portuguese Environment Agency for agricultural soils (APA 2019). Moreover, compared with values detected in other coal waste piles from North Portugal, the here-obtained results were lower than those in the Serrinha mine (86.9-1410 µS/cm) (Ribeiro et al. 2010b), and similar to the São Pedro da Cova mine (22-475 µS/cm) (Santos et al. 2023).

The WHC defines the ability of soil to hold water at a particular time (Adhikari et al. 2022). The studied samples showed a lower WHC for US soils and the highest values for CL samples. Regarding the remaining samples, the WHC was similar, ranging between 23 % and 35.8 %. Increased soil WHC is mainly associated with higher infiltration rates and lower runoff; thus, it could decrease the potential for soil erosion. Chapter 4 describes the soil features and indicates that soils with lower water-holding capacity (WHC) have a lower infiltration range due to their granulometric characteristics and the presence of organic material, which renders them water repellent, making it difficult for water to be taken up by the pores.

Soil with low WHC loses a significant portion of rainwater by deep percolation, leaching nutrients from the root zone, leading to inefficient use of resources and adverse environmental problems (AbdAllah et al. 2021). The burned coal waste samples (BCW) and mixed burned coal waste (MBW) correspond to soils in which pollutants are more leachable and potentially transported to downhill soil (DS). According to the measured pH, all soils are acidic. The lowest pH value was measured in UCW5 (pH = 3.5) and the highest in US5 (pH = 5.15). Ribeiro and Flores (2021) suggested that this pH range could promote significant acid mine drainage (AMD) of PTE for similar areas in the Douro Coalfield. It is necessary to understand the mineralogy of the coal residues that incentivise AMD production by minerals such as pyrite and jarosite, and the concentration of the minerals that work as neutralisers: calcite, aragonite, and siderite (Çelebi and Ribeiro 2023). However, the release of PTE will depend on the exposure leaching time and the pH (Li et al. 2022; Liu et al. 2023).

Table 5.1 Physical and chemical parameters for major and trace elements measured in soil and coal mining waste elutriates. EC in µS/cm; central ion, total organic carbon (TOC), Cu and Zn content in mg/L, OM in %, and trace elements in µg/L

sample	pH	EC	MO	TOC	HCO3	Cl	SO4	F	NO3	NO2	NH4	Na	K	Ca	Mg	Fe	Al	Mn	As	Cd	Ni	Cu	Cr	Zn	Pb
US1	4.31	59	9.95	4.39	2.52	0.74	0.90	0.01	0.52	0.00	0.22	0.81	0.52	0.79	0.21	67.62	39.24	2.70	0.50	0.00	1.45	0.002	0.85	0.000	1.00
US4	4.43	53	10.22	3.35	2.02	0.85	0.44	0.01	0.43	0.00	0.16	1.07	0.49	0.53	0.15	44.49	33.69	0.50	0.35	0.01	1.30	0.000	0.00	0.000	0.00
US5	4.53	43	7.21	5.24	3.28	1.31	0.95	0.01	0.70	0.01	0.16	1.73	0.52	0.46	0.15	63.44	59.68	0.00	1.85	0.02	0.10	0.002	0.10	0.000	0.00
UCW1	4.75	147	19.44	1.60	0.69	0.34	12.83	0.01	0.88	0.01	0.04	0.39	0.78	2.68	1.3	20.7	08.10	118.3	0.00	0.03	11.6	0,000	0.00	0.032	1.60
UCW3	5.15	155	24.92	4.74	2.33	0.84	15.92	0.03	0.54	0.01	0.00	0.49	1.06	4.44	1.74	79.66	49.52	160.7	1.15	0.04	4.70	0.003	0.00	0.025	0.00
UCW5	3.50	322	24.51	1.48	0.00	0.34	17.15	0.01	0.31	0.00	0.04	0.25	0.51	0.87	0.54	82.59	199.3	51.30	0.00	0.05	3.70	0.006	0.00	0.028	1.70
MBW1	3.83	208	9.03	0.87	0.00	0.47	15.94	0.03	0.51	0.00	0.03	0.95	0.81	1,00	0.72	45.66	617.2	27.90	0.20	0.20	6.85	0.014	1.25	0.015	3.40
MBW2	4.10	255	12.94	0.59	0.00	0.27	20.14	0.03	0.68	0.00	0.20	1.04	0.57	2.64	1.59	27.80	300.9	69.35	0.55	0.00	8.80	0.007	0.65	0.012	4.00
MBW3	4.04	238	9.87	1.35	0.32	0.42	20.39	0.02	0.80	0.00	0.34	1.20	0.68	18.33	1.74	25.78	187.6	77.25	0.00	0.20	9.90	0.004	0.00	0.000	3.50
MBW4	4.23	108	11.24	0.60	0.00	0.28	10.79	0.04	0.23	0.00	0.01	0.58	0.93	1.49	0.56	0.00	171.0	20.70	0.60	0.00	6.80	0.004	0.00	0.000	2.95
MBW5	3.97	202	11.64	0.97	0.00	0.33	17.47	0.04	0.56	0.00	0.02	0.75	0.85	2.11	0.98	20.67	412.1	56.40	0.00	0.10	8.45	0.010	0.00	0.000	2.70
MBW6	3.90	270	11.52	1.03	0.00	0.30	32.23	0.08	0.72	0.00	0.06	0.81	0.80	4.56	1.96	10.97	962.5	122.9	0.00	0.40	17.5	0.018	0.25	0.021	0.00
BCW3	4.08	179	7.77	0.59	0.00	0.34	17.85	0.03	0.54	0.00	0.12	0.69	0.70	2.62	1.24	32.45	365.5	50.80	0.00	0.00	11.4	0.004	0.00	0.037	0.00
BCW4	4.28	103	11.36	0.68	0.00	0.36	11.08	0.03	0.63	0.00	0.00	0.61	0.75	1.51	0.77	22.03	165.6	44.30	0.75	0.00	5.45	0.003	0.00	0.024	0.00
BCW8	4.16	211	7.23	0.64	0.00	0.34	18.93	0.03	0.45	0.00	0.00	0.91	0.81	3.25	1.22	27.13	323.1	72.20	0.60	0.00	7.95	0.000	0.00	0.053	0.00
BCW9	4.13	209	4.49	0.68	0.00	0.28	21.06	0.04	0.28	0.00	0.01	0.77	0.74	3.88	1.67	27.04	221.9	99.15	0.25	0.00	7.95	0.000	0.00	0.051	0.00
BCW10	4.63	101	4.69	0.62	0.00	0.37	8.98	0.01	0.22	0.00	0,00	0.57	1.16	1.81	0.61	77.28	29.63	78.70	0.25	0.00	3.83	0.000	0.00	0.126	0.00
CL3	4.79	75	3.70	0.53	2.21	0.57	4.86	0.01	1,00	0.00	0.03	0.80	0.55	0.92	0.64	100.68	9.192	38.00	0.15	0.00	23.7	0.002	0.00	0.000	0.95
CL4	5.08	33	6.57	1.49	2.02	0.73	1.23	0.01	0.79	0.01	0.06	0.71	0.51	0.54	0.25	178.58	2.232	5.85	0.00	0.00	0.65	0.001	0.00	0.000	1.60
CL8	4.78	56	4.04	0.87	1.512	0.48	3.53	0.01	0.43	0.00	0.03	0.55	0.57	0.87	0.53	60.10	11.50	45.40	0.00	0.00	0.95	0.000	0.00	0.000	0.00
CL9	4.62	142	5.14	1.62	0.00	0.60	11.82	0.02	1.19	0.01	0.16	0.84	0.56	2.28	1.13	45.79	130.1	101.1	0.25	0.00	5.95	0.000	0.00	0.002	0.00
CL10	4.99	46	5.61	1.77	3.15	0.49	3.12	0.01	0.89	0.00	0.11	0.57	0.77	0.93	0.37	58.80	12.14	21.50	0.40	0.00	2.10	0.000	0.00	0.016	0.20
DS1	4.11	168	19.44	2.12	0.95	0.62	10.71	0.01	0.58	0.00	0.16	0.95	0.71	1.56	0.70	59.88	171.1	136.3	0.80	0.00	0.10	0.005	0.70	0.014	0.40
DS3	4.21	366	6.07	1.93	0.00	0.70	33.18	0.03	0.22	0.00	0.33	1.69	1.12	3.36	4.32	36.08	342.9	368.9	0.90	0.20	17.1	0.000	0.00	0.019	0.00
DS5	4.76	68	5.08	1.52	2.14	0.54	4.74	0.01	1.48	0.01	0.11	0.67	0.83	1.03	0.63	19.19	14.02	350.6	0.00	0.00	3.60	0.000	0.00	0.000	0.00

The PCA analysis indicates a clear separation between soils from burned (dashed line) and unburned coal mining wastes (Figure 5.2). The soil samples from each site appear to be replicated, as indicated by the closeness recorded (oval dotted lines; Figure 5.2). On the other hand, the unburned coal waste samples (UCW) and downhill soil samples (DS) showed individual behaviour (appeared not clustered). PCA analysis also indicates that the uphill soils (US) do not relate to the measured physical and chemical parameters. At the same time, the cover layer (CL) and unburned coal waste (UCW) were characterised by high WHC, NH_4^+, NO_2^-, NO_3^-, As, and Fe. Higher concentrations of trace elements (Zn, Ni, Cd, Cu, Pb, and Cr), soluble cations (K, Na, Mg, Ca), macronutrients (Al, Mn), inorganic ions (SO_4^{-2}, F) appear associated with the burned coal wastes areas (MBW and BCW, Figure 5.2), which is in line with other studies that report that elements leaching can be heat-dependent (Espinha Marques et al. 2021; Ribeiro and Flores 2021).

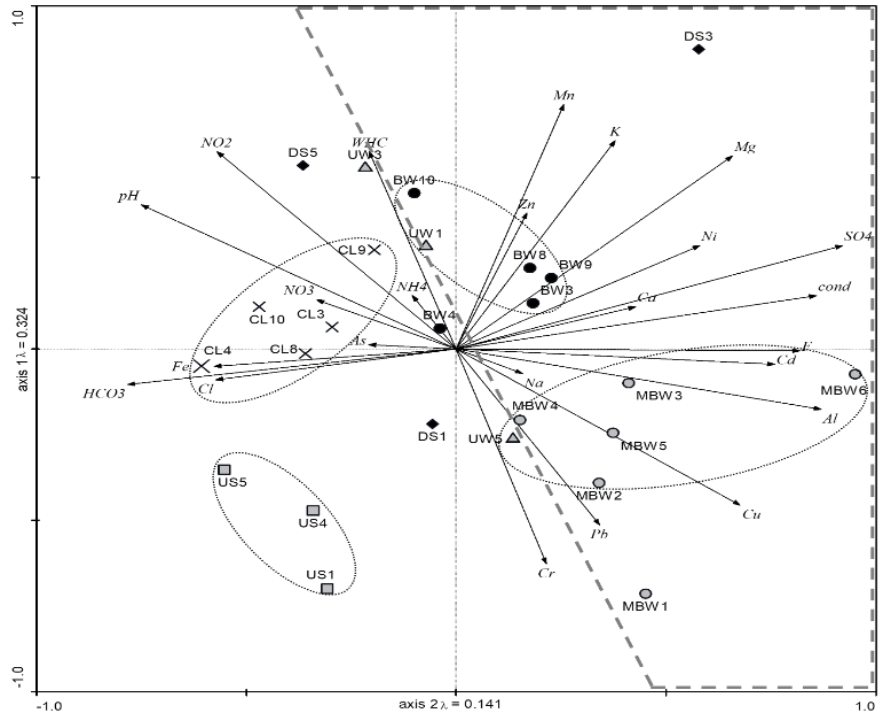

Figure 5.2 Principal component analysis (PCA) results from physical and chemical parameters, nutrients, metals, data from each soil elutriate, and sample sites - Dashed line evidence burned areas; oval dotted lines showed soil sampling areas (Narayan et al. 2024).

5.3.2 *Alivibrio fischeri* Bioluminescence Inhibition

The Table 5.2 presents the EC20 values for the bioluminescence inhibition of the bacterium *Allivibrio fischeri* after exposure to soil elutriates. All the elutriates revealed toxicity to *A. fischeri*, with CL8 (EC20 = 0.88 %) being the most toxic, while CL4 was

the least toxic (EC20 = 55.9 %). For CL8 soil elutriate acid, pH values were recorded (pH = 4.78), as well as high values of HCO_3 and Fe. Berglind et al. (2010) already showed that light production was highly pH dependent and concluded that the optimal pH for the growth of *A. fischeri* is 6.8 (higher than recorded in CL8 elutriate). Below this value, the luminescence rate was significantly lower (Silva et al. 2021). In addition, high concentrations of Fe > 3.1 mg/L affected the stability of the bioluminescence capacity of this species (Futra et al. 2014; Teixeira et al. 2014). Conversely, Haygood and Nealson (1985) reported that extremely low concentrations of Fe (0.16 mg/L) also inhibited this bacterium's luminescence.

The EC20 toxicity endpoint showed a positive and significant correlation with macronutrient Fe (r = 0.544, p = 0.005), the inorganic ion NO_2^- (r = 0.447, p = 0.025), and pH (r = 0.443; p = 0.027). Indeed, Scheerer et al. (2006) already showed that the bioluminescence of *A. fischeri* could be affected by temperature, pH, ionic strength, nitrogen, and carbon source. In the present study, and according to physical and chemical results, *A. fischeri* bioluminescence seems to be affected by low values of pH, WHC, and NH_4^+, parameters that characterise the CL elutriates (Table 5.1).

Table 5.2 Results of ecotoxicity effects on *Allivibrio fisheri*, *Lemna minor*, *Daphnia magna* and *Lactuca sativa* after exposure to the different soil elutriates

Soil Elutriates	***A. fischeri*** EC_{20} (%)	***L. minor*** Growth inhibition (%)	***D. magna*** Acute effects (%)	***L. sativa*** Germination inhibition (%)
US1	8.70	**61.8 ± 6.6**	**100 ± 0.00**	2.50
US4	**2.48**	**47.2 ± 4.9**	**70.0 ± 12.9**	27.5
US5	8.72	**55.0 ± 5.2**	5.00 ± 5.00	17.5
UCW1	7.81	8.30 ± 3.8	10.0 ± 5.80	17.5
UCW3	55.8	0.10 ± 4.0	0.00 ± 0.00	**45.0**
UCW5	**2.19**	**85.0 ± 4.1**	**100 ± 0.00**	**37.5**
MBW1	13.2	-3.20 ± 3.0	0.00 ± 0.00	2.50
MBW2	3.37	27.5 ± 1.3	**75.0 ± 25.0**	20.0
MBW3	15.4	31.5 ± 6.6	20.0 ± 8.20	5.00
MBW4	12.8	14.2 ± 3.7	0.00 ± 0.00	10.0
MBW5	5.41	27.8 ± 3.8	20.0 ± 8.20	15.0
MBW6	3.39	32.3 ± 4.2	15.0 ± 5.00	17.5
BCW3	6.80	42.7 ± 8.0	0.00 ± 0.00	15.0
BCW4	**1.42**	16.6 ± 2.7	0.00 ± 0.00	22.5
BCW8	9.93	16.2 ± 3.2	0.00 ± 0.00	15.0
BCW9	**1.97**	9.20 ± 3.6	5.00 ± 5.00	**35.0**
BCW10	**1.51**	9.10 ± 4.0	0.00 ± 0.00	10.0
CL3	**1.53**	3.10 ± 3.7	0.00 ± 0.00	20.0
CL4	55.9	7.20 ± 2.7	0.00 ± 0.00	12.5
CL8	**0.88**	4.50 ± 2.2	0.00 ± 0.00	17.5
CL9	8.04	4.50 ± 1.6	0.00 ± 0.00	22.5
CL10	**1.61**	7.70 ± 2.8	0.00 ± 0.00	**40.0**
DS1	4.99	6.90 ± 6.6	5.00 ± 5.00	20.0
DS3	6.02	4.00 ± 7.8	15.0 ± 15.0	30.0
DS5	3.69	7.80 ± 3.4	0.00 ± 0.00	**37.5**

5.3.3 Daphnia magna Acute Toxicity

Daphnia magna acute toxicity results are shown in Table 5.2. Elutriates from soils US1 and UCW5 proved to be the most toxic, causing 100 % mortality of *D. magna* in less than 24 h. Elutriates from soils US4 and MBW2 caused more than 70 % of the mortality, while the remaining soil elutriates induced less than 20 % *D. magna* mortality. A negative and significant correlation between *D. magna* and pH (r = -0.416; p = 0.039), WHC (r = -0.620; p < 0.001), and K (r = -0.442; p = 0.027), and a positive correlation with OM (r = 0.437; p = 0.029) was observed. These results could be explained by the low pH and/or the PTE concentration recorded in the soil elutriates (Table 5.1). Overall, for this species, elutriates from burned coal wastes (BCW, MBW) seem to be less toxic than the unburned soils (US, CL, DS); this could be explained by the higher OM content and the potential association with metals (Adusei-Gyamfi et al. 2019; Fan et al. 2016). Indeed, there is competition among cations for binding sites in OM, with preferences for cations depending on the organic radical and pH (Adusei-Gyamfi et al. 2019). Moreover, soils with lower water-holding capacity (WHC) appear to increase toxicity to D. magna, as these soils are unable to retain nutrients, and metals become bioavailable in the elutriates (Abdullah et al. 2022). US soils should serve as potential reference soils since they have not been exposed to the impact of coal mining waste, and trace metal concentration is lower than that of the burned and unburned coal waste (Table 5.1). However, the results indicate that US soils have physical and chemical properties, as well as types of vegetation (e.g., *Pinus pinaster*, *Arbutus unedo*, *Eucalyptus*, and Bryophyta), which can confer high acidity levels.

Several studies have already demonstrated that a mixture of chemical components with changes in pH, OM, WHC, and K values could induce acute toxicity to *D. magna* (e.g. Alvarenga et al. 2008; De Schamphelaere and Janssen 2002; Loureiro et al. 2005; Maisto et al. 2011; Pukalchick et al. 2017; Yim et al. 2006). The UCW5 elutriate showed a high concentration of metallic elements (Al, and Pb), while MBW2 showed high concentrations of Cr and Ni (Table 5.1). Some studies suggested that Cd and Cu were more toxic to D. magna than Pb and Cr (Khangarot and Ray 1989; Okamoto et al. 2015), depending on PTE concentration and exposure time (Peng et al. 2022). Aluminium appears to be toxic to *D. magna*. However, the concentration of Al recorded in the UCW5 and US1 (more toxic soil elutriates; 0.199 mg/L and 0.039 mg/L, respectively) was lower than the EC_{50} reported by the literature [EC_{50} (48 h) = 0.586 mg/L, at 5.10-6.40 pH] (Fikirdeşici-Ergen et al. 2018). To ensure protection against acute toxicity to aquatic species, vertebrates, and invertebrates, the United States Environmental Protection Agency (USEPA 1998) criteria recommend that the average

concentration of aluminium in water samples must not exceed 0.087 mg/L more than once every three years when pH is between 6.5 and 9. However, in the present study, several elutriates (e.g., UCW5, MBW, BCW, CL9, DS1, and DS3) exceed this reference value (e.g., the maximum concentration detected was 0.963 mg/L in MBW6 elutriate). Despite the reported Al concentration, the high toxicity can be attributed to the complex mixture of PTE detected in soil elutriates (Peng et al. 2022), as well as to the low pH and low water hardness (resulting from Ca and Mg ions) observed in the elutriates.

Furthermore, Pb and Cr showed toxicity to *D. magna* at 0.10 mg/L Pb and 0.12 mg/L Cr; however, when combined in a metal mixture, an increase in toxicity was observed (0.062 mg/L for Pb and 0.015 mg/L for Cr) (Jeong et al. 2001; Mansour et al. 2015). Other studies also report acute toxicity *of D. magna to Ni and Zn at 0.1-1 mg/L and to* Cd and Cu at <0.1 mg/L (e.g., Okamoto et al. 2015), and Meyer et al. (2015) reported a *D. magna* EC_{50} value for Cu of 0.103 mg/L.

5.3.4 Lemna minor

The results obtained in the *L. minor* growth inhibition assay after exposure to soil elutriates are shown in Table 5.2. *Lemna minor* is recognised as an important bioindicator with ecological relevance for monitoring different pollution sources (Garnczarska and Ratajczak 2000). The highest growth inhibition (> 85 %) was observed when *L. minor* was exposed to UCW5. The soil elutriates exhibited an acidic pH, higher electrical conductivity (EC), and elevated metal concentrations (Al and Pb). The growth inhibition can be associated with the low pH (3.5) recorded, since the optimal pH value for *L. minor* growth is 6 to 8 (Chong et al. 2003; Iqbal and Baig 2016; Kaur et al. 2012). In addition, the concentration of Al is commonly considered an abiotic stress factor under acidic conditions (Su et al. 2019), and it is a potential growth-limiting factor for plant development in acidic soils (Rout et al. 2001). Moreover, it has already been reported that 0.196 mg/L of Al causes a toxic effect in *L. minor* after 48 h of exposure (Fikirdeşici-Ergen et al. 2018). The authors demonstrated that when Al is in solution, it hydrolyses, and at low pH, the increase in H^+ ions cause damage to the species and contributes to mortality (Satizábal et al. 1999). Su et al. (2019) demonstrated that Al is toxic to root growth, interfering with mechanisms such as cell elongation and division, and competing with K, Ca, Mn, Cu, and Mg for binding sites, thereby disrupting multiple biological processes and oxidative stress pathways. *L. minor* was also highly affected after exposure to US1, US4, US5, and BCW3 (growth inhibition between 40 % and 60 %). Indeed, significant negative correlations were

observed between *L. minor* growth inhibition and pH (r = -0.504; p = 0.010), WHC (r = -0.672; p < 0.001), and K (r = -0.462; p = 0.020).

A low concentration of K in plants reduces photosynthetic CO_2 fixation, followed by membrane and chlorophyll damage, thus altering leaf anatomy, decreasing the chloroplast surface area, and increasing antioxidant activities (Johnson et al. 2022). Radić et al. (2010) studied the ecotoxicological assessment of industrial effluent using *L. minor*. They demonstrated that metals are toxic (Zn > Ni > Fe > Cu > Cr > Pb) to L. minor tissues, causing varying degrees of damage (e.g., Pb exposure increases proline content and inhibits *L. minor* growth). Dirilgen (2011) studied the effects of Pb on *L. minor* growth inhibition during 4 and 7 days, and the EC50 values for Pb were estimated as 6.8 mg/L to 5.5 mg/L (higher values than those detected in soil elutriates in the present study, such as for MBW2 = 0.004 mg/L). Van Dyck et al. (2023) studied the effects of Mn and observed a decrease in *L. minor* growth at concentrations above 70 mg/L, which is higher than the values observed in the here-elutriates (Table 5.1). Moreover, *L. minor* showed growth reduction in the presence of As above 2 mg/L (Duester et al. 2011), with a value up to the present study (Table 5.1). Trace elements, such as Cd, cause visible damage to *L. minor* at 0.5 mg/L (Khellaf and Zerdaoui 2010), consistent with values observed in the soil elutriates (Table 5.1). On the other hand, several studies showed low toxicity for *L. minor* after exposure to some metals, namely Mn at 25 mg/L (Van Dyck et al. 2023), Fe at 22.6 mg/L (Teixeira 2014), Zn at 15 mg/L (Van Dyck et al. 2023), Ni at 2.5 mg/L (Nogueira et al. 2020) where no significant effects in the growth rate were recorded. Despite the low metal toxicity for *L. minor*, mentioned above, the physical and chemical parameters such as pH, hardness, and the presence of several metals may have contributed to the observed effects.

Total chlorophyll and biochemical biomarkers (CAT activity and MDA content) of *L. minor* have also been used as sensitive tools to assess the toxicity of soil elutriates (Figure 5.3). A significant increase in the concentration of total chlorophyll was recorded for *L. minor* after exposure to BCW3 soil elutriate, while a significant decrease was observed in BCW9 soil elutriate (both burned coal mining wastes; Figure 5.3). Indeed, both elutriates showed a similar concentration of Mg, Al, Ni, Mn, and Zn. For BCW3, the increase in chlorophyll content could be explained by the possibility that PTE exposure can induce a plant response, leading to an increase in chlorophyll (Chandra and Kang 2016). This response is often a defence mechanism that helps counteract stress and maintain photosynthetic activity. Chandra and Kang (2016) studied mixed PTE (Cd, Cu, Cr, and Zn) stress on photosynthesis, transpiration rate, and chlorophyll content in poplar hybrids, and observed a decrease in chlorophyll content; however, an

increase was also detected in higher potential toxic elements concentrations (200 mg/L to 500 mg/L). This fact may be explained by the biological accumulation of potentially toxic elements, which could contribute to induced effects at high concentrations. The BCW9 soil elutriate sample could affect the photosynthetic process of *L. minor*, possibly due to PTE concentrations recorded [Al (0.222-0.365 mg/L), Mn (0.05-0.09 mg/L), Ni (0.007-0.011 mg/L), Zn (0.04-0.05 mg/L)] that could be incorporated in the chlorophyll molecule during the process.

Indeed, the excess PTE accumulated could be used in this pigment biosynthesis, altering the functional properties (Jmii and Dewez 2021). Hou et al. (2007) already showed that total chlorophyll decreases in *L. minor* with the increase of PTE concentration (Cu > 10 mg/L; Cd > 0.5 mg/L), due to the peroxidation of chloroplast membranes mediated by or replacing Mg in chlorophyll molecules by PTE. Radić et al. (2011), also suggested that Mg substitution in chlorophyll molecules by metal ions such as Cu, Zn, Cd, Hg, Pb, or Ni (recorded in the soil elutriates, *see* Table 5.1) could be the reason for the breakdown of photosynthesis in *L. minor*. Regarding the correlation analysis, only a positive significant correlation between Ca (r = 0.403; p = 0.046) and total chlorophyll content was observed. Pal and Laloraya (1972) already suggest that calcium seems to exert an effect on chlorophyll formation through its control of the uptake of minerals essential for chlorophyll biosynthesis.

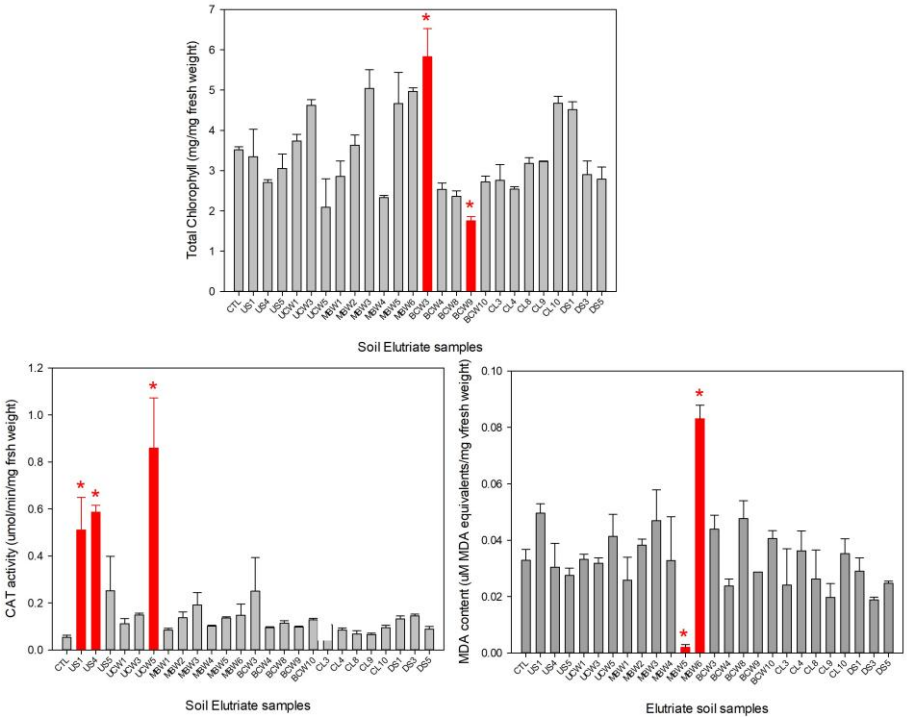

Figure 5.3 Total chlorophyll content and biochemical markers CAT and MDA for each soil elutriate for *L. minor*. * Stands for significant difference when compared to CTL (Dunnett test, p < 0.05)

A significant increase in CAT activity was observed after exposure to the unburned soil elutriates from US1, US4, and UCW5 (the most toxic samples for *L. minor* growth inhibition and D. magna mortality; Figure 5.3 and Table 5.2). These results suggest that the soil elutriate induced a significant increase in CAT activity to counteract the oxidative stress caused by elutriate exposure. CAT belongs to the most important enzymes that scavenge reactive oxygen species in plant cells (Dvořák et al. 2021; Tuzet et al. 2019). CAT participates in the main defence system against the accumulation and toxicity of hydrogen peroxide, controlling the levels in cells and converting them to water and oxygen (Msttés 2000). CAT activity of *L. minor* exposed to PTE mainly displayed biphasic responses with increased metal concentration (Hou et al. 2007). Moreover, CAT activity increased when *L. minor* was exposed to soil elutriates with low pH, WHC, nutrient K, and trace metals Pb, Cu, and Cr values (Table 5.1). Despite the low concentration of trace metals observed in the elutriates (Table 5.1), Gwóźdź et al. (1997) already reported that CAT increases in the presence of PTE at low concentration. Indeed, a negative and significant correlation between CAT activity and WHC (r = -0.582; p = 0.002), K (r = -0.409; p = 0.042), and pH (r = -0.400; p = 0.048), while a positive and significant correlation was observed with OM (r = 0.460; p = 0.021).

The MDA content is an indicator of the cell damage endpoint and was determined to indicate the level of lipid peroxidation of *L. minor* fronds (Nunes et al. 2014). The results indicate a significant increase in MDA content after exposure to MBW6, while a significant decrease was recorded for the MBW5 elutriate (Figure 5.3; burned coal wastes). After exposure to the MBW5 elutriate, *L. minor* response suggested that the antioxidative system could prevent oxidative damage (Foyer and Noctor 2005; Varga et al. 2013). On the other hand, MBW6 showed the highest concentration of toxic elements, F- (0.08 mg/L), Al (0.962 mg/L), Cr (0.002 mg/L), and Cd (0.004 mg/L), compared to MBW5. MDA is a decomposition product of polyunsaturated fatty acids (PUFA) of biomembranes, and its increase shows that plants are under high-level antioxidant stress (Balen et al. 2011). The content of MDA in *L. minor* shows a positive and significant correlation between F^- (r = 0.428; p = 0.033), Al (r = 0.410; p = 0.042), Cd (r = 0.415; p = 0.039), and Cu (r = 0.398; p = 0.049).

Radić et al. (2018) showed that Cd concentrations between 0.0016 and 0.003 mg/L increase the MDA concentration in *L. minor*, after exposure for 16 h to aqueous soil extracts from coal combustion. Cd is a non-essential metal and is known to interfere with plant growth and metabolic processes (Hou et al. 2007; Radić et al. 2013, 2018). Miras-Moreno et al. (2022) showed that Cu causes inhibition of plant growth, induces

oxidative damage, and negatively affects photosynthetic activity, chlorophyll biosynthesis, and plant mineral nutrition at up to 10 mg/L. Other studies with Ni and Zn have shown that these metals induce cell division and, consequently, plant growth, causing genotoxicity and oxidative damage effects (e.g., Rout and Das 2003).

5.3.5 *Lactuca sativa*

The results from the germination assays regarding fresh biomass and growth of *L. sativa* (roots and aerial parts) after exposure to soil elutriates are presented in Table 5.3. All the soil elutriates inhibited the seeds' germination. However, only a set of 6 soils (UCW3, UCW5, BCW9, CL10, DS3, and DS5) caused a significant inhibition (> 30 %) relative to the control group ($F_{[25, 111]} = 3.252$, $p < 0.001$). Despite the different physical and chemical characteristics of the soil elutriates (Table 5.1), it is important to emphasise that the chemical composition includes several elements that have already been shown to cause deleterious effects in plant growth, namely Fe, Cr, Cu, Mn, and Zn. Seneviratne et al. (2019) suggested that the inhibition of seeds' physiological and metabolic activities leads to a decrease in germination due to the presence of PTE exposure (e.g., Cu, Zn, Cd, As). Some of these PTE act as micronutrients and participate in several metabolic reactions in plant development. However, when the threshold concentrations are exceeded, they become toxic (Angulo-Bejarano et al. 2021).

Although the chemical elements detected in the soil elutriates appear in concentrations lower than those considered capable of affecting 50 % of the individuals exposed (EC_{50}) [e.g., the maximum [Ni] in the soil elutriates was 23.8 µg/L in CL3 and the EC_{50} (10 days) = 148 µg/L, (Lyu et al. 2018). The fact is that this soil elutriates are complex samples and, possibly, more toxic than expected (Houshmandfar and Moraghebi 2011). Furthermore, Shafiq et al. (2010), showed that exposure to PTE mixtures decreases plant seed germination, changes cell membrane permeability, and reduces seed reserves.

Table 5.3 Result for germination inhibition (%), fresh biomass (g), size (cm) in the aerial and roots of *Lactuca sativa*, and morphological alteration (%) after exposure to soil elutriates. * stands for discriminant significance compared to the control group (Dunnett test, $p < 0.05$)

Soil Samples	Germination inhibition (%)	Fresh Biomass (g)		Size (cm)		Morphological alterations (%)	
		Aerial part	Roots	Aerial part	Roots	Aerial part	Roots
CTL	1.7	0.39 ± 0.02	0.023 ± 0.003	5.22 ± 0.32	4.57 ± 0.04	0.0	0.0
US1	2.5	0.41 ± 0.03	0.018 ± 0.002	4.23 ± 0.14	1.87 ± 0.30*	5.0	10.0
US4	27.5	0.31 ± 0.02	0.017 ± 0.002	3.93 ± 0.44	1.38 ± 0.14*	35.0*	47.5*
US5	17.5	0.29 ± 0.03	0.025 ± 0.003	4.39 ± 0.39	1.88 ± 0.19*	22.5	25.0
UCW1	17.5	0.21 ± 0.02*	0.012 ± 0.001	3.27 ± 0.74*	1.77 ± 0.48*	35.0*	50.0*
UCW3	45.0*	0.08 ± 0.03*	0.005 ± 0.001*	2.52 ± 0.23*	0.84 ± 0.15*	65.0*	65.0*
UCW5	37.5*	0.19 ± 0.02*	0.008 ± 0.001*	3.63 ± 0.48*	2.70 ± 0.35*	42.5*	45.0*
MBW1	2.5	0.29 ± 0.03	0.010 ± 0.001*	5.30 ± 0.32	3.28 ± 0.41	2.5	7.5
MBW2	20.0	0.19 ± 0.03*	0.006 ± 0.002*	4.15 ± 0.49	1.80 ± 0.26*	27.5	32.5
MBW3	5.0	0.29 ± 0.03	0.007 ± 0.002*	5.59 ± 0.58	2.14 ± 0.49*	7.5	10.0
MBW4	10.0	0.31 ± 0.03	0.014 ± 0.002	4.94 ± 0.35	2.45 ± 0.56*	12.5	17.5
MBW5	15.0	0.18 ± 0.03*	0.012 ± 0.003	3.42 ± 0.65*	1.34 ± 0.29*	22.5	37.5*
MBW6	17.5	0.27 ± 0.02	0.017 ± 0.003	5.10 ± 0.47	1.87 ± 0.16*	17.5	30.0
BCW3	15.0	0.32 ± 0.03	0.034 ± 0.004	4.45 ± 0.23	2.80 ± 0.75*	20.0	27.5
BCW4	22.5	0.29 ± 0.03	0.033 ± 0.004	4.04 ± 0.59	2.21 ± 0.54*	22.5	42.5*
BCW8	15.0	0.14 ± 0.04*	0.007 ± 0.003*	2.33 ± 0.60*	1.11 ± 0.26*	42.5*	62.5*
BCW9	35.0*	0.17 ± 0.03	0.010 ± 0.003*	4.31 ± 0.18	2.01 ± 0.26*	35.0*	47.5*
BCW10	10.0	0.37 ± 0.02	0.027 ± 0.002	4.30 ± 0.53	2.10 ± 0.33*	7.5	27.5
CL3	20.0	0.22 ± 0.02*	0.021 ± 0.003	3.49 ± 0.50*	2.00 ± 0.46*	27.5	42.5*
CL4	12.5	0.28 ± 0.02*	0.027 ± 0.003	4.56 ± 0.30	1.64 ± 0.43*	5.0	17.5
CL8	17.5	0.30 ± 0.02	0.027 ± 0.003	4.07 ± 0.33	2.12 ± 0.31*	20.0	30.0
CL9	22.5	0.22 ± 0.04*	0.012 ± 0.002	3.53 ± 0.31*	1.39 ± 0.23*	30.0*	42.5*
CL10	40.0*	0.20 ± 0.04*	0.020 ± 0.003	4.51 ± 0.43	2.31 ± 0.25*	47.5*	45.0*
DS1	20.0	0.44 ± 0.04	0.003 ± 0.003*	3.33 ± 0.58*	1.97 ± 0.28*	32.5*	32.5
DS3	30.0*	0.16 ± 0.03*	0.024 ± 0.003	2.96 ± 0.53*	2.04 ± 0.40*	40.0*	45.0*
DS5	37.5	0.20 ± 0.04*	0.012 ± 0.002	3.00 ± 0.81*	2.04 ± 0.50*	50.0*	65.0*

L. sativa exposure to soil elutriates UCW3 and UCW5 (unburned coal waste) caused also a significant decrease of fresh biomass and size in the aerial part ($F_{[25, 111]} = 6.063$, $p < 0.001$; $F_{[25, 111]} = 4.037$, $p < 0.001$, respectively) and roots ($F_{[25, 111]} = 6.437$ p < 0.001; $F_{[25, 111]} = 6.822$, $p < 0.001$, respectively) (Table 5.3). Despite not causing significant changes in seed germination, some soil elutriates were able to reduce plant height, root length, and fresh weight of the aerial part and roots of *L. sativa* (e.g., burned coal waste: BCW2, BCW5, BCW8, and BCW9; unburned coal waste: CL3 and CL9; and downhill soils: DS1, DS3, and DS5). Moreover, all the soil elutriates (except burned coal waste BCW1) caused a significant reduction in root length. Lyu et al. (2018) reported the success of root elongation tests with *L. sativa* to assess the toxicity of phenolic compounds, pure chemicals, and complex effluent materials. Although the mechanisms involved in inhibiting root growth are not well established, as they are the first to come into contact with the contaminated medium, they are generally more sensitive (Gangwar and Singh 2011).

The inhibition of root growth may be related to the ability of PTE present in the samples to affect physiological, biochemical, and molecular processes (e.g., changes in nutrient

flux and action, cell cycle interruption) (Geremias et al. 2012). Furthermore, the literature suggests that root growth inhibition (caused by PTE) alters water balance and nutrient absorption, affecting their transportation to the aerial parts and negatively impacting the shoot growth (Singh et al. 2016). In addition to the endpoints proposed by the guideline, the visual phytotoxicity assessment is also recommended (OECD, 2006). However, it is rarely done or described. Therefore, an evaluation of morphological alterations observed during the early stage of plant development was recorded (Table 5.3 and Figure 5.4). Figure 5.4 exhibits and describes some alterations observed in the aerial part and roots after *L. sativa* exposure to soil elutriates (e.g., deformations, atrophy, reduced growth), as well as in the control plants. Severe toxicity symptoms (necrotic lesions, chlorosis, senescence, inhibition of growth) have already been reported in plants exposed to PTE (e.g., Cd, Cr, Pb, and Al) even at very low concentrations (mg/L) (Angulo-Bejarano et al. 2021).

Singh et al. (2016) reported several symptoms observed in leaves, namely chlorosis, senescence, low biomass accumulation, and growth inhibition after exposure to potential toxic elements (e.g., Cd, Zn, Fe, and Cu) at concentrations of mg/L. Moreover, soil elutriates that induced significant alterations, with more than 30% of morphological alterations, were also identified in Table 5.3. A higher percentage of morphological alterations was observed in the aerial part ($F_{[25, 111]} = 5.592$, $p < 0.001$) and roots ($F_{[25, 111]} = 5.452$, $p < 0.001$) of *L. sativa* exposed to soil elutriates UCW (unburned coal waste) and DS (downhill soils). The results demonstrated that these elutriates, characterised by higher NH_4^+, NO_3^-, NO_2^-, and PTE concentrations (Figure 5.1 and Table 5.1), inhibit L. sativa germination and growth (in terms of size and biomass, Table 5.3) and induce morphological phytotoxicity (Figure 5.3, Table 5.3). Other studies have already described the toxicity symptoms of *L. sativa* exposed to PTE, inorganic ions, and other components detected in the soil elutriates (Angulo-Bejarano et al. 2021; Singh et al. 2016). Gangwar and Singh (2011) reported that typical symptoms of Cr toxicity include slight leaf chlorosis, wilting, and stunted root growth. Moreover, Gangwar and Singh (2011) showed that the accumulation of NH_4^+ leads to nutrient deficiency and chlorosis in plants. Kohli et al. (2019) demonstrated that Pb also affects the physiological characteristics of plants, resulting in reduced seed germination rates, stunted root growth, as well as necrotic lesions and leaf chlorosis.

According to the Pearson correlation coefficient, seed germination inhibition, fresh biomass of aerial parts and roots, as well as morphological alterations in both organs (Table 5.3), show a positive correlation with NO_2^- and Mn concentrations (Table 5.1) ($p < 0.05$). These results suggest that NO_2^- and Mn may be the main contributors to the

observed toxicity in *L. sativa*. NO_2^- is a substance that induces toxic effects on plant growth, reducing parameters such as plant height, the number of leaves, and fresh biomass yield. It can also cause severe leaf necrotic spots and increase chlorosis symptoms (Bowsher et al. 2007; Hoque et al. 2007).

Some authors explained that nitrite toxicity is a result of interference with various physiological processes such as photosynthesis (inhibiting enzyme activity, leading to reduced carbon fixation, decrease in sugars and other organic compounds production), ATP production, disruption membrane integrity, and permeability, inhibition of NO_3^- uptake and induction of oxidative stress (Castro et al. 2009; Foyer et al. 1994; Hoque et al. 2007). On the other hand, Mn in high concentrations is considered an environmental pollutant that can cause toxic effects in plants (Mourato et al. 2015; Nagajyoti et al. 2010). Studies have already demonstrated that Mn at concentrations higher than 1000 µM induces a significant reduction in root length during the germination process (Di Salvatore et al. 2008; Marichali et al. 2014; Moreira et al. 2020). The decrease in root length may be related to the interference of the metal with cell division, proliferation, and elongation (Moreira et al. 2020).

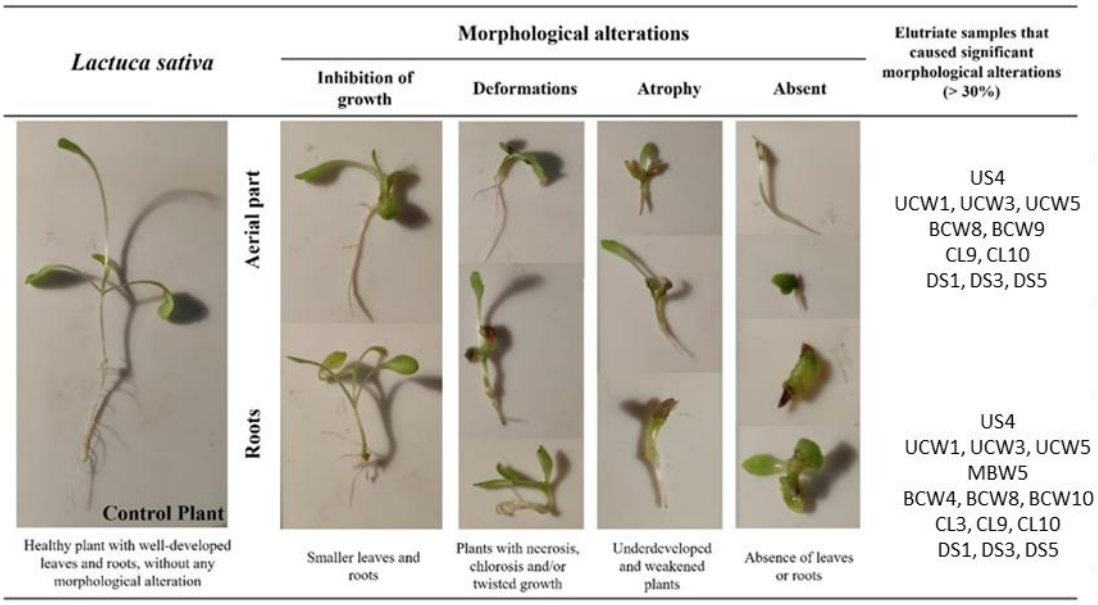

Figure 5.4 Identification and morphological alteration description of *Lactuca sativa* individuals after exposure to different soil elutriates (Adapted from Diogo et al. 2023a)

Although not included in standardised protocols, other endpoints (e.g., total chlorophyll content, catalase activity, and malondialdehyde content) were also used to assess the toxicity of soil elutriates on sub-individual effects on seed germination and seedling development (Figure 5.4). Significant alterations in total chlorophyll content were recorded, though not relative to the control group (Figure 5.4). Total chlorophyll content

was not a responsive endpoint in the present study. However, it has already been considered a sensitive indicator of toxicity, being used as an indicator of the physiological stage of different species (e.g., Diogo et al. 2023b; Gavina et al. 2013). Moreover, several authors reported changes in pigment content in different plants (e.g., *Phaseolus vulgaris*, *Zea mays*, *Lactuca sativa*) exposed to soils and soils elutriate samples with PTE (e.g., Cu, Ni, Pb, Zn, and Cd) (Alengebawy et al. 2021; Pereira et al. 2009; Seneviratne et al. 2019). These metals are considered destructive substances for photosynthesis, contributing to the declines, either causing structural damage to chloroplasts, preventing photosynthetic light harvesting, affecting the photosynthetic electron transport, or inhibiting chlorophyll biosynthesis (Seneviratne et al. 2019; Sethy and Ghosh 2013; Sharma and Agrawal 2005).

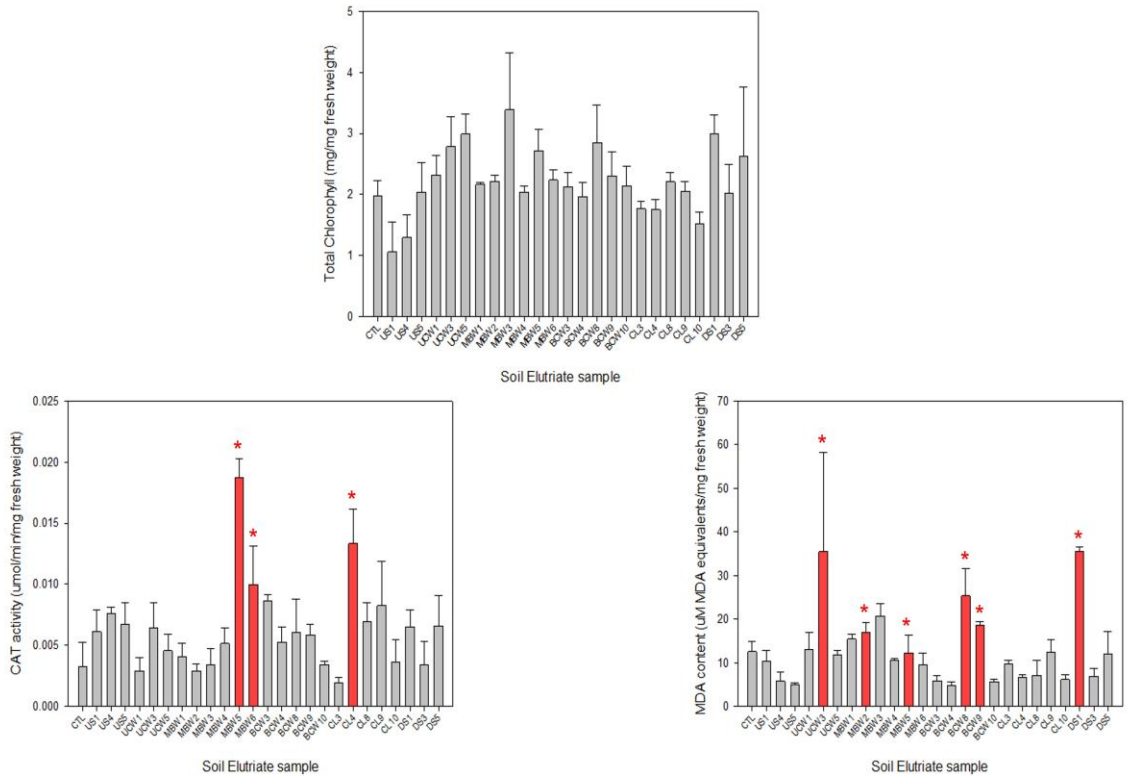

Figure 5.5 Results of *Lactuca sativa* pigments (total chlorophyll) and biochemical biomarkers CAT and MDA measured in the aerial part, after exposure to the different soil elutriates. * Stands for significant differences when compared to CTL (Dunnett test, $p < 0.05$)

Regarding CAT activity, a significant increase was observed in the aerial part after exposure to soil elutriates MBW5, MBW6, and CL4 (Figure 5.5), suggesting that these soils may have induced a pro-oxidative perturbation in *L. sativa*. One of the typical defence mechanisms against toxic elements is the enhanced activity of antioxidant enzymes, which play an essential role in the adaptation/survival of plants exposed to stress conditions (Zhang and Farahbakhsh 2007). CAT activity changes (inductions

and inhibitions) in plants exposed to PTE (e.g., Cu, Cr, Pb, Zn) have already been shown to be directly related to metal concentrations. Gwóźdź et al. (1997) reported that CAT activity decreases in the presence of high concentrations of PTE (e.g., Pb, Cb, and Cu) and increases in the presence of low concentrations, corroborating what was observed in the present study for *Lactuca sativa* (in soil elutriates CL4, MBW5, and MBW6). According to the results obtained here, CAT demonstrated the ability to neutralise reactive oxygen species production and prevent oxidative damage, possibly caused by MBW6 and CL4, as these samples did not affect the MDA content. In contrast, the same did not happen for the MBW5 sample, which caused an increase in CAT activity and a significant increase in MDA content (Figure 5.4).

MDA levels also increased after exposure to the soil elutriates of UCW3, MBW2, MBW5, BCW8, BCW9, and DS1 in the aerial part (Figure 5.5). The excessive formation of ROS and the consequent increase in MDA content in the aerial part and roots of plants exposed to different PTE (e.g., Cd, Cr, Pb, and Zn) were previously reported by several authors (Ding et al. 2021; Sethy and Ghosh 2013). MDA is a by-product of lipid peroxidation, used as an indicator of oxidative stress (Zhang and Farahbakhsh 2007). In this study, MDA was demonstrated to be a sensitive parameter, as it allowed the identification of samples that can affect the metabolic and physiological pathways of *L. sativa*, despite no significant inhibition of seed germination occurring (Zhang and Farahbakhsh 2007).

5.4 Final Remarks

Elutriates from burned, mixed, and unburned coal mining wastes, when tested on non-target model species, demonstrated the potential toxicity of these residues. The most sensitive species were the bacterium *Aliivibrio fischeri* and *Lactuca sativa*, whereas *Daphnia magna* and *Lemna minor* showed lower sensitivity. In *A. fischeri*, bioluminescence inhibition was primarily associated with low pH, elevated concentrations of Fe, NH_4^+, and high WHC. For *L. sativa*, toxicity was mainly attributed to NO_2^- and Mn, which appear to play a key role in inducing biological stress in environments impacted by coal mining wastes.

Root length inhibition in *L. sativa* is considered an early indicator of metal-induced toxicity. The most toxic samples across all tested species were UCW5, US1, US4, and US5, followed by MBW2, MBW3, MBW5, MBW6, BCW9, CL10, DS1, and DS3. These findings underscore the potential of coal mining waste elutriates to act as sources of environmental contamination. The mobilisation and percolation of bioavailable organic and inorganic pollutants from these wastes pose a serious threat to plant survival. They

can significantly disrupt terrestrial and aquatic ecosystems by affecting their biotic components and overall ecological balance.

This research highlights the importance of assessing the toxicity of coal mining waste elutriates to raise awareness within both the scientific community and society regarding the potential impacts of contaminants dispersed through percolation and surface runoff into adjacent soil and aquatic systems. The observed ecotoxicological response also emphasises species-specific sensitivity to environmental pollutants. Variation in pH, trace metal concentrations, and inorganic ion levels in the elutriates played a critical role in modulating toxicity, with results indicating the presence of multiple stressors acting simultaneously. Notably, adverse effects were observed even at relatively low concentrations of trace elements, indicating potential synergistic interactions and the influence of additional toxicants, such as polycyclic aromatic hydrocarbons (PAH) or other organic compounds.

Overall, these findings indicate a significant risk posed by coal mining waste to various environmental compartments, including soil, water, and biota, particularly when they are exposed to leachates generated by rainfall infiltration or self-burning. The toxicity of the elutriates from unburned coal residues and adjacent soils (e.g., UCW and DS) further reinforces the need for targeted risk assessments and long-term monitoring of impacted sites.

To mitigate these environmental impacts, remediation strategies should prioritise the isolation and stabilisation of coal mining waste to prevent leachate formation, enhance site drainage to reduce infiltration, and promote revegetation with tolerant native species to restore ecosystem functionality. Furthermore, a deeper understanding of the role of organic toxicants and their interactions with trace metals is essential for developing more effective and comprehensive risk management strategies.

Chapter 6. Conclusions

6.1 Final Comments

This doctoral research aimed to evaluate the environmental impacts of self-combusted coal mining wastes (CMW) at the Fojo coal waste dump (DC, Portugal) through an integrated approach encompassing geochemical, pedological, and ecotoxicological methodologies. The study provides new insights into the transformations induced by combustion and cooling procedures, their impacts on soil systems, and the potential ecotoxicological risks associated with the leaching of coal mining waste, both with and without combustion. By studying these three dimensions in tandem, it was possible to link the thermal alteration of materials (due to combustion and firefighting actions) to the generation of reactive mineral phases, the modification of soil physical and chemical properties, and the subsequent environmental risks associated with pollutant mobility and bioavailability.

The Fojo coal mining waste showed apparent differences in petrographic features among unburned, burned, and mixed materials. Vitrinite dominated the organic fraction, with higher reflectance in unburned materials, while combustion features such as framboidal pyrite oxidation and devolatilisation vacuoles were evident in burned samples. The use of a cooling agent to extinguish the fire in 2017 modified combustion signatures, resulting in lower-temperature indicators in the burned materials.

The mineralogical composition of unburned coal waste (UCW) contains minerals as florencite, acanthite, arsenopyrite, pyrite, and iron oxides. These features changed significantly after combustion, with minerals such as zircon, rutile, and monazite present in both burned and mixed samples (BCW, MBW).

The geochemical signature of UCW is dominated by elements typically associated with aluminosilicate, such as: Al, K, Na, Rb, Ga, Ba, Cs, Sc, Th, V, and ∑LREE. Carbonate-related elements (Ca, Mg, Mn, Zn, Cu, Co, Cd, Ni) and petrogenic elements (Mo, Pb, Zn, U, Cr) are also present, while phosphate-associated (Li, U, ∑HREE) and rutile-related elements (Ti, Nb, Ta, Be) are less abundant. The burnet waste shows an enrichment in Fe, Th, Sr, Sb, Bi, Ba, Na, Sn, Sc, S, Cs, and ∑LREE. Decline in many carbonate and phosphate elements, such as Ca, Mg, Cd, Cr, Mn, U, and ∑HREE, due to the thermal volatilisation and mineral transformation. Higher association with aluminosilicate and sulphide fraction, and a stronger presence of zircon and rutile minerals were observed. Elemental associations were inferred using multivariate

statistical methods, confirming combustion-related redistribution and the mineral-phase affinities of trace elements.

The geochemical variability aligns with the mineralogical transformation observed under SEM and XRD, confirming thermal alteration. The mode of occurrence of elements supports the association of specific geochemical groups (e.g. sulphides, aluminosilicates, carbonates) with each type of waste. These differences provide insight into the environmental behaviour of each waste type, including the mobility of trace elements and potential ecotoxicological risks. Compared to other coal mining waste disposal sites in the DC, the petrographic, mineralogical, and geochemical characteristics of the Fojo coal waste dump do not fully align with the other CMW sites.

The principal distinguishing feature of coal mining waste is the presence of burned, mixed waste exhibiting clear evidence of high-temperature alteration. This includes a broader range of minerals, notably high-temperature neoformed phases, distinct patterns of trace elements enrichment and depletion, and increased elemental mobility in leachates, particularly in BCW and MBW, associated with combustion processes and fire suppression activities. These findings underline the importance of site-specific assessment in coal mining waste management, particularly where thermal alteration has occurred.

The concentration of 16 priority PAH is highest in the burned coal mining waste. Low-molecular-weight (LMW) PAH dominate both burned and unburned waste, but their origins differ. In UCW, PAH are primarily petrogenic, originating from the organic matter in coal. In BCW, both petrogenic and pyrolytic origins are present, resulting from the combustion process. Although the Phe/Ant radio exceeds 10, indicating a predominantly petrogenic signature, the combustion process (especially under the influence of cooling agents) allowed the condensation of high molecular weight PAH into the particulate phase. These compounds were likely dispersed by wind and deposited in the uphill soils, a forest component, as observed in the US.

The hydropedological study of the Fojo Coal mining waste dump shows that the disposal and self-burning of the coal waste led to significant alterations in the soil´s hydropedological properties. The changes were evident in the soil morphology, mineral composition, infiltration capacity, leaching behaviour, and the mobility of PTE. The definition of different hydropedological zones (e.g. US, UCW, BCW, MBW, CL, DS) enabled a detailed characterisation of unsaturated hydraulic conductivity, soil water content, hydrophobicity, and leaching potential across the waste disposal site and the surrounding area.

The Fojo site revealed more pronounced hydrogeochemical differentiation with the formation of Ca-SO_4 hydrogeochemical facies and greater contrasts in leachate pH and element concentrations among the defined hydropedological units. Compared with findings from other coal waste piles in the Douro Carboniferous Basin, key similarities and some distinctions emerge. On both sides, combustion-affected soils exhibit substantial transformations in the unsaturated zone, including the loss of organic matter, formation of new mineral phases (e.g., jarosite, hematite, smectite), and increased concentration of potentially toxic elements. The development of technogenic and the disruption of natural soil structure contribute to enhanced vertical movement of water and contaminants, thereby increasing the risk of groundwater pollution. Furthermore, while both sites exhibited an increase in the leachability of PTE and major ions in burned zones, the Fojo site revealed a more pronounced hydrogeochemical differentiation.

Although Fojo and SPC share similar combustion-induced alterations, the Fojo study takes it a step further by integrating a spatially explicit hydropedological framework. This approach enhances the understanding of water-soil interactions in post-mining environments.

Leachates, or elutriates, derived from coal mining waste (CMW) have demonstrated clear toxic effects on both aquatic and terrestrial organisms, even at relatively low metal concentrations. The findings from the ecotoxicological studies provide compelling evidence that CMW elutriates are a significant source of environmental contamination, capable of disrupting key physiological and biochemical processes in standard species. Bioassays with four standard species, *Alivibrio fischeri* (bacteria), *Daphnia magna* (aquatic invertebrate), *Lemna minor* (aquatic plant), and *Lactuca sativa* (terrestrial plant), revealed different sensitivities to CMW elutriates. *A. fischeri* showed marked bioluminescence inhibition, likely due to the low pH, nitrite (NO_2^-), and elevated Fe concentrations. *D. magna* responded to low pH, low K, and the presence of Al, Pb, Cr, and Ni. *L. minor* exhibited growth and chlorophyll inhibition, primarily associated with low pH, Al, and mixed metals, which induced oxidative stress. *L. sativa* was also affected, particularly in terms of root growth inhibition, despite the relatively low concentration of metals in the elutriates. The sub-lethal exposures can interfere with early developmental processes.

Both chemical and physical parameters affect toxicity. Acidic conditions enhance the solubility and bioavailability of metals, thereby increasing the toxicity. PTE, particularly Al, Pb, Cd, NI, Zn, Cr, all of which are known to affect cellular function, disrupt

membranes, inhibit enzymes, and generate oxidative stress. Nitrite (NO_2^-), toxic to aquatic species, particularly affecting respiration and metabolic regulation. Macronutrient imbalance, low K and high Fe levels impair osmoregulation and other essential physiological functions. The most toxic elements and mechanisms of action show that Al is strongly toxic to all studied species. It disrupts nutrient uptake, induces oxidative stress, and interferes with root elongation and photosynthesis, effects observed in *L. minor*. Lead and Cd interfere with cellular metabolism, photosynthetic pathways, and enzyme activities, while Ni and Cr are linked to DNA damage, oxidative stress, and growth inhibition in plants and invertebrates. Zinc is essential in trace amounts but toxic at elevated levels, particularly affecting aquatic biota. The mechanisms involved include metal-induced oxidative stress, enzyme inhibition, membrane disruption, and interference with hormonal and developmental pathways.

The ecotoxicological study demonstrates that these species are potential indicators of the toxicity of the CMW leachates. *A. fischeri* is highly sensitive and useful for early warning of aquatic toxicity. *L. sativa* is sensitive to a wide range of contaminants, and root length inhibition serves as a reliable and early indicator of metal toxicity. *L. minor* responds visibly to waterborne contaminants, particularly in chlorophyll content and growth rates. *D. magna* was the least sensitive species in this study, but still a valid model for chronic aquatic toxicity testing. These species serve as bioindicators of environmental contamination by coal mining waste, offering practical tools for ecological risk assessment and environmental monitoring.

Coal mining waste elutriates pose a tangible ecological threat to aquatic and terrestrial biota, primarily due to their acidic nature and the presence of bioavailable metals and inorganic ions. This toxicity is evident not only in standard bioassays but also in specific biochemical and morphological responses, underscoring the importance of incorporating bioindicators into environmental assessment frameworks. Further studies across broader trophic levels and longer exposure times are warranted to understand the long-term ecological implications of these pollutants.

In summary, and focused on the results here-obtained, this doctoral research demonstrates that unburned coal mining waste (UCW) can exert toxic effects primarily due to its content of low-molecular-weight polycyclic aromatic hydrocarbons (PAH), despite showing a lower concentration of trace metals in elutriates. These compounds, particularly phenanthrene and naphthalene, may interfere with early developmental stages and cellular processes, as evidenced by toxicity responses in *L. sativa* and A. *fischeri*. Conversely, burned and mixed waste (BCW and MBW) are toxic largely due to

acidic leachates enriched in trace metals such as Al, Pb, Cr, Ni, and Cd. These elutriates cause oxidative stress, inhibit root elongation, and affect aquatic primary producers, as observed in *Lemna minor* bioassays. These findings underscore distinct toxicological mechanisms: organic-phase toxicity, primarily due to low-molecular-weight PAH in unburned waste, and metal-associated toxicity in burned waste. This highlights the complex environmental risk profile of coal mining residues and the need for tailored remediation strategies.

6.2 Recommendations and Future Research

This study underscores the complex environmental risk posed by self-burning coal mining waste (CMW), highlighting the interplay between combustion processes, geochemical transformations, hydropedological dynamics, and ecotoxicological effects. In light of these findings, the following recommendations and directions for future research are proposed:

6.2.1 Investigation of Cooling Agents and Firefighting Residues

The impact of firefighting substances on mineral formation and pollutant behaviour warrants further attention. Analytical identification of the cooling agents used and their potential role in altering PAH condensation or mineral assemblages could refine our understanding of the reactivity and toxicity of post-combustion residue.

6.2.2 Monitoring of Atmospheric Transport and Soil Deposition of PAH

The potential for windborne transport of PAH from combustion zones to surrounding soils, as observed in uphill soils, warrants atmospheric dispersion modelling and monitoring. This would aid in understanding off-site contamination pathways and assessing risk to terrestrial ecosystems and human receptors.

6.2.3 Development and Testing of Remediation Strategies

Given the distinct mechanisms of toxicity between unburned (organic-phase) and burned (metal-rich acidic) wastes, remediation approaches should be adapted accordingly. Future work should explore passive and active treatments such as phytoremediation, amendments with alkaline materials, or engineered covers to stabilise or detoxify CMW.

6.2.4 Integration of Bioindicators into Routine Monitoring Protocols

The proven sensitivity of species such as *Lemna minor*, *Lactuca sativa*, and *Alivibrio fisheri* supports their inclusion in standardised monitoring frameworks. The development of ecotoxicological indices based on these bioassays could enhance early detection of environmental hazards at CMW sites.

6.2.5 Policy and Regulatory Implications

Findings from this study should inform national and EU-level guidelines on coal waste management, particularly concerning self-burning risks. Establishing thresholds for PAH and metal concentrations in elutriates, as well as enforcing regular ecotoxicological testing, could contribute to more effective environmental protection.

6.2.6 Interdisciplinary Collaboration for Post-Mining Landscape Rehabilitation

Addressing the legacy of CMW requires an interdisciplinary approach that involves geoscientists, ecotoxicologists, hydrologists, and land-use planners. Future initiatives should integrate scientific insights into sustainable land management practices, aligning rehabilitation efforts with the restoration of ecosystem services and climate resilience objectives.

6.3 Research Products and Presentations

6.3.1 Articles in Journals

Espinha Marques, J., Narayan, A., Santos, P., Ribeiro, J., Antunes, S.C., Melo, A., Rocha, F., Flores, D., Mansilha, C., (2024). Hydropedological Characterization of a Coal Mining Waste Deposition Area Affected by Self-Burning. Hydrology. 11(5), 62. DOI: 10.3390/hydrology11050062

Narayan, A., Diogo, B.S., Mansilha, C., Espinha Marques, J., Flores, D., Antunes, S.C. (2024). Assessment of ecotoxicological effects of Fojo coal mine waste elutriate in aquatic species (Douro Coalfield, North Portugal). Frontiers in Toxicology. 6. art. no. 1334169. DOI: 10.3389/ftox.2024.1334169

Diogo, B.S., **Narayan, A.,** Mansilha, C., Marques, J.E., Flores, D., Antunes, S.C., (2023). Phytotoxicity of coal waste elutriates (Douro Coalfield, North Portugal) in Lactuca sativa. Environmental Science and Pollution Research. 30, 107650-107660. DOI: 10.1007/s11356-023-29868-w

6.3.2 Presentation at Congresses

Rajnauth, A., Diogo B.S., Espinha Marques, J., Flores, D., Antunes S.C. (2023). Ecotoxicological effects of elutriates from coal mining waste in Lactuca sativa seed germination. Trabalho apresentado no III Congresso Internacional TOXRUN, Porto, 2024

Rajnauth, A., Diogo, B.S., Espinha Marques, J., Flores D., Antunes S.C. (2023). Efeitos ecotoxicológicos de lixiviados das escombreiras da mina do Fojo (Pejão, Norte de Portugal) em espécies-modelo aquáticas. Trabalho apresentado em XI Congresso Nacional de Geologia 2023, Universidade de Coimbra, Coimbra, 16-20 de julho, Livro de Resumos: 523-524pp.

Costa, M., **Rajnauth, A.,** Santos, P., Ribeiro, J., Flores, D. (2023). Estudo de resíduos mineiros de carvão afetados termicamente: Especificidades petrográficas e mineralógicas. Trabalho apresentado em XI Congresso Nacional de Geologia 2023, Universidade de Coimbra, Coimbra, 16-20 de julho, Livro de Resumos: 497-498pp.

Santos, P., **Rajnauth, A.,** Espinha Marques, J., Ribeiro, J., Flores, D. (2023). Caraterização ambiental dos solos da envolvente da escombreira da mina do Fojo complexo mineiro do Pejão. Trabalho apresentado em XI Congresso Nacional de Geologia 2023, Universidade de Coimbra, 16-20 de julho, Livro de Resumos: 529-530pp.

Santos, P. **Rajnauth, A.,** Espinha Marques, J., Ribeiro, J., Costa, M., Flores, D. (2023). Caraterização geoquímica dos resíduos de carvão afetados por combustão nas escombreiras da mina do Fojo complexo mineiro do Pejão, Norte de Portugal. Trabalho apresentado em XI Congresso Nacional de Geologia 2023, Universidade de Coimbra, 16-20 de julho, Livro de Resumos: 355-356pp.

Costa, M., **Rajnauth, A.,** Santos, P., Flores, D. (2023). Petrographic and mineralogical new data from a burnt coal waste pile, Pejão Mining Complex. Trabalho apresentado em Jornadas do ICT, Universidade do Minho, Braga, 2 e 3 de fevereiro., Braga, 2023.

Santos, P., **Rajnauth, A.,** Ribeiro, J., Espinha Marques, J., Flores, D. (2023). Soil Geochemical Assessment Surrounding a Coal Mine Waste Pile Affected by Self-combustion Pejão Mining Complex. Trabalho apresentado em Jornadas do ICT, Universidade do Minho, Braga, 2023.

Costa, M**., Rajnauth, A**., Santos, P., Ribeiro, J., Flores, D. (2022). Petrographic and geochemical characterization of a coal waste pile affected by self-burning in the Douro Coalfield, Portugal. Trabalho apresentado em 73rd Annual Meeting of the International Committee for Coal and Organic Petrology (ICCP 2022), Symposium on Recent trends on coal utilization for sustainable development and energy security, New Delhi, India. p. 1-2.

.

References

AbdAllah AM, Mashaheet AM, Burkey KO (2021) Super absorbent polymers mitigate drought stress in corn (*Zea mays* L.) grown under rainfed conditions. *Agricultural Water Management,* 254, 106946. https://doi.org/10.1016/j.agwat.2021.106946

Abfertiawan MS, Palinggi Y, Handajani M, Pranoto K, Atmaja A (2020) Evaluation of Non-Acid-Forming material layering for the prevention of acid mine drainage of pyrite and jarosite. *Heliyon*, *6*(11). https://doi.org/10.1016/j.heliyon.2020.e05590

Achten C, Hofmann T (2009) Native polycyclic aromatic hydrocarbons (PAH) in coal – A hardly recognized source of environmental contamination. *Science of The Total Environment*, 407. 2461-2473. https://doi.org/10.1016/j.scitotenv.2008.12.008

Adeniyi AG, Emenike EC, Iwuozor KO, Okoro HK, Ige OO (2022) Acid mine drainage: The footprint of the Nigeria mining industry. *Chemistry Africa*, *5*(6), 1907-1920. https://doi.org/10.1007/s42250-022-00493-3

Adhikari S, Timms W, Mahmud MAP (2022) Optimising water holding capacity and hydrophobicity of biochar for soil amendment – A review. *Science of The Total Environment*, 851, 158043. https://doi.org/10.1016/j.scitotenv.2022.158043

Adusei-Gyamfi J, Ouddane B, Rietveld L, Cornard JP, Criquet J (2019) Natural organic matter-cations complexation and its impact on water treatment: A critical review. *Water research*, 160, 130-147. https://doi.org/10.1016/j.watres.2019.05.064

Aebi H (1984) Catalase in vitro. *Methods in enzymology*, 6(C), 105–121. https://doi.org/10.1016/S0076-6879(84)05016-3

Agioutantis Z, Schobert HH, Hower JC (2023) On the interactions between strength and petrology of Pennsylvania anthracite. *International Journal of Coal Geology*, *277*, 104339. https://doi.org/10.1016/j.coal.2023.104339

Agroconsultores and Geometral (1995) Carta de Solos e Carta de Aptidão da Terra de Entre Douro e Minho, Escala 1: 100 000. Direção Regional da Agricultura e Entre Douro e Minho, Braga.

Al Majou H, Bruand A, Duval O (2008) The use of in situ volumetric water content at field capacity to improve the prediction of soil water retention properties. *Canadian Journal of Soil Science*, *88*(4), 533-541.https://doi.org/10.4141/CJSS07065

Alengebawy A, Abdelkhalek ST, Qureshi SR, Wang MQ (2021) Heavy metals and pesticides toxicity in agricultural soil and plants: Ecological risks and human health implications. *Toxics* 9, 42. https://doi.org/10.3390/toxics9030042

Alhamed M (2015) Identification of geochemical processes controlling the neutralization of abandoned coal mine drainage using integration of geochemical modelling, geochemical analysis, and batch test: an example from the south of Bochum, Germany. *Arabian Journal of Geosciences*, *8*(10), 8009-8025. https://doi.org/10.1007/s12517-015-1830-7

Alkimin GD de, Santos J, Soares AMVM, Nunes B (2020) Ecotoxicological effects of the azole antifungal agent clotrimazole on the macrophyte species *Lemna minor* and *Lemna gibba*. *Comparative Biochemistry and Physiology Part C: Toxicology & Pharmacology*, 237, 108835. https://doi.org/10.1016/J.CBPC.2020.108835

Alpern B, Maume F (1969) Etude pétrographique de l'oxydation naturelle et artificielle des houilles. *Rev. Ind. Min*, *51*(11), 979-996.

Alvarenga P, Guerreiro N, Simões I, Imaginário MJ, Palma P (2021) Assessment of the environmental impact of acid mine drainage on surface water, stream sediments, and macrophytes using a battery of chemical and ecotoxicological indicators. *Water*, *13*(10), 1436. https://doi.org/10.3390/w13101436

Alvarenga P, Palma P, Gonçalves AP, Fernandes RM, De Varennes A, Vallini G, Cunha-Queda AC (2008) Evaluation of tests to assess the quality of mine-contaminated soils. *Environmental Geochemistry and Health*, *30*(2), 95-99. https://doi.org/10.1007/s10653-008-9147-z

American Public Health Association [APHA] (2017) Standard Methods for the Examination of Water and Wastewater (SMEWW), 23rd Edition; Rice, E.W., Baird, R.B., Eaton, A.D., Eds.; American Public Health Association, American Water Works Association, Water Environment Federation: Washington, DC, USA; p. 168.

Amrani M, Taha Y, El Haloui Y, Benzaazoua M, Hakkou R (2020) Sustainable reuse of coal mine waste: Experimental and economic assessments for embankments and pavement layer applications in Morocco. *Minerals*, *10*(10), 851. https://doi.org/10.3390/min10100851

Amundson R (2021) Factors of soil formation in the 21st century. *Geoderma*, 391, 114960. https://doi.org/10.1016/j.geoderma.2021.114960

Angulo-Bejarano P, Puente-Rivera J, Cruz-Ortega R (2021) Metal and metalloid toxicity in plants: An overview on molecular aspects. *Plants* 10, 635. https://doi.org/10.3390/plants10040635

APA (2019) Solos Contaminados—Guia Técnico, Valores de Referência Para o Solo [Contaminated Soils—Technical Guide, Soil Reference Values]; Agência Portuguesa do Ambiente: Lisbon, Portugal

Arnold BJ (2023) A review of element partitioning in coal preparation. *International Journal of Coal Geology*, *274*, 104296.https://doi.org/10.1016/j.coal.2023.104296

Ashworth SC (2005) Metal speciation and mobility as influenced by landfill disposal practices. *Water Encyclopedia*, *1*, 723-728. https://doi.org/10.1002/047147844X.ww126

ASTM (1989) Standard practice for conducting acute toxicity tests with fishes, macroinvertebrates, and amphibians. In: Reports E 729-80.

Atlas do Ambiente (1985) ArcGIS REST Services Directory. https://sniambgeoogc.apambiente.pt/getogc/rest/services/Atlas/Atlas_Ambiente/MapServer

Ayers JC, Zhu C (2025) Zircon solubility, metamict ZrSiO4 replacement, and hydrothermal zircon formation at upper crustal pressures. *Geochemistry, Geophysics, Geosystems*, *26*(3), e2024GC011925. https://doi.org/10.1029/2024GC011925

Balen B, Tkalec M, Šikić S, Tolić S, Cvjetko P, Pavlica M, Vidaković-Cifrek Ž (2011) Biochemical responses of *Lemna minor* experimentally exposed to cadmium and zinc. *Ecotoxicology*, 20(4), 815–826. https://doi.org/10.1007/s10646-011-0633-1

Banerjee D (2014) Acid drainage potential from coal mine wastes: Environmental assessment through static and kinetic tests. *International Journal of Environment Science and Technology, 11*, 1365–1378. https://doi.org/10.1007/s13762-013-0292-2

Barbieri M (2016) The Importance of Enrichment Factor (EF) and Geoaccumulation Index (Igeo) to Evaluate the Soil Contamination. J Geol Geophys 5: 237. https://doi.org/10.4172/2381-8719.1000237

Basset C, Abou Najm M, Ghezzehei T, Hao X, Daccache A (2023) How does soil structure affect water infiltration? A meta-data systematic review. *Soil and Tillage Research*, *226*, 105577. https://doi.org/10.1016/j.still.2022.105577

Belmer N, Tippler C, Davies PJ, Wright IA (2014) Impact of a coal mine waste discharge on water quality and aquatic ecosystems in the Blue Mountains World Heritage Area. In *Proceedings of the 7th Australian Stream Management Conference, Townsville, Queensland* (pp. 385-391).

Berglind R, Leffler P, Sjöström M (2010) Interactions between pH, potassium, calcium, bromide, and phenol and their effects on the bioluminescence of Vibrio fischeri. *Journal of Toxicology and Environmental Health, Part A*, *73*(16), 1102-1112. https://doi.org/10.1080/15287394.2010.482918

Bernini, D, Audétat A, Dolejš D, Keppler H (2013) Zircon solubility in aqueous fluids at high temperatures and pressures. *Geochimica et Cosmochimica Acta*, *119*, 178-187.

Bisdom EBA, Dekker LW, Schoute JFT (1993) Water repellency of sieve fractions from sandy soils and relationships with organic material and soil structure, *Geoderma*, 56, 105 – 118, https://doi/10.1016/0016-7061(93)90103-R

Blinova S, Dobrydina T (2017) Influence of coal industry enterprises on biodiversity (on the example of Formicidae). In *E3S Web of Conferences* (Vol. 21, p. 02011). EDP Sciences. https://doi.org/10.1051/e3sconf/20172102011

Borges B, Armindo M, Ferreira IMPLVO, Mansilha C (2018) Dispersive liquid–liquid microextraction for the simultaneous determination of parent and nitrated polycyclic aromatic hydrocarbons in water samples. *Acta Chromatographica* 30,119–126

Borges IB (2024) Protótipo de sensor de umidade do solo.

Bott TL, Jackson JK, McTammany ME, Newbold JD, Rier ST, Sweeney BW, Battle JM (2012) Abandoned coal mine drainage and its remediation: impacts on stream ecosystem structure and function. *Ecological applications*, *22*(8), 2144-2163. https://doi.org/10.1890/11-1735.1

Bowsher CG, Lacey AE, Hanke GT, Clarkson DT, Saker LR, Stulen I, Emes MJ (2007) The effect of Glc6P uptake and its subsequent oxidation within pea root plastids on nitrite reduction and glutamate synthesis. *Journal of experimental botany*, *58*(5), 1109-1118. https://doi.org/10.1093/jxb/erl269

Brown G, Brindley GW (1980) X-ray diffraction procedures for clay mineral identification. Monograph No. 5; Mineralogical Society of Great Britain and Ireland: London, England; pp. 1-495, https://doi/10.1180/mono-5

Butzen V, Seeger M, Marruedo A, Jonge L, Wengel R, Ries JB, Casper MC (2015) Water repellency under coniferous and deciduous forest — Experimental assessment and impact on overland flow. *Catena,* 133, 255-265, https://doi.org/10.1016/j.catena.2015.05.022

Cardoso A, Madeira M, Ribeiro C (2015) Soil classification and typology in Portugal. *Catena*, 135, 290–303. https://doi.org/10.1016/j.catena.2014.12.002

Castro E, Manas MP, De Las Heras J (2009) Nitrate content of lettuce (*Lactuca sativa L.*) after fertilization with sewage sludge and irrigation with treated wastewater. *Food Additives and Contaminants*, *26*(2), 172-179.

Cehlár M, Domaracká L, Šimko I, Puzder M (2015) Mineral resource extraction and its political risks. In *Production Management and Engineering Sciences–Scientific Publication of the International Conference on Engineering Science and Production Management, ESPM* (pp. 39-43).

Çelebi EE, Ribeiro J (2023) Prediction of acid production potential of self-combusted coal mining wastes from Douro Coalfield (Portugal) with integration of mineralogical and chemical data. *International Journal of Coal Geology*, *265*, 104152. https://doi.org/10.1016/j.coal.2022.104152

Chaminé HI, Gama Pereira LC, Fonseca PE, Moço LP, Fernandes JP, Rocha F, Flores D, Pinto de Jesus A, Gomes C, Soares de Andrade AA (2003) Tectonostratigraphy of middle and upper Palaeozoic black shales from Porto–Tomar–Ferreira do Alentejo shear zone (W Portugal): New perspectives on the Iberian Terrane. *Geobios*, *36*, 649–663, ISSN 0016-6995. https://doi.org/10.1016/j.geobios.2003.03.002

Chandra R, Kang H (2016) Mixed heavy metal stress on photosynthesis, transpiration rate, and chlorophyll content in poplar hybrids. *Forest Science and Technology*, 12(2), 55–61. https://doi.org/10.1080/21580103.2015.1044024

Chen Y, Sheng G, Bi X, Feng Y, Mai B, Fu J (2005) Emission factors for carbonaceous particles and polycyclic aromatic hydrocarbons from residential coal combustion in China. *Environmental Science and Technology* 39:1861–1867

Chinh LD, Gheewala SH, Bonnet S (2007) Integrated environmental assessment and pollution prevention in Vietnam: the case of anthracite production. *Journal of Cleaner Production*, *15*(18), 1768-1777. https://doi.org/10.1016/j.jclepro.2006.03.006

Chong Y, Hu H, Qian Y (2003) Effect of inorganic nitrogen compounds and pH on the growth of duckweed. *Huan jing ke xue Huanjing kexue*, 24(4), 35—40. http://europepmc.org/abstract/MED/14551954

Christopher R, Kinney O, Fiori A, Congdon J (1996) Oral deformities in tadpoles (Ranacatesbeiana) associated with coal ash deposition: effects on grazing ability and

growth. *Freshwater Biology*, *36*(3), 723-730. https://doi.org/10.1046/j.1365-2427.1996.00123.x

Civeira MS, Pinheiro RN, Gredilla A, de Vallejuelo SFO, Oliveira ML, Ramos CG, Silva, LF (2016) The properties of the nano-minerals and hazardous elements: Potential environmental impacts of Brazilian coal waste fire. *Science of the Total Environment*, *544*, 892-900. https://doi.org/10.1016/j.scitotenv.2015.12.026

Clarke LB (1983) The fate of trace elements during combustion and gasification: An overview. *Fuel* 72:731-736. https://doi.org/10.1016/0016-2361(93)90072-A

Correia PAP (2016) *Contribution to the knowledge of the fossil flora and fauna of the Douro Carboniferous Basin (NW of Portugal)* (Doctoral dissertation, Universidade do Porto (Portugal)).

Costa M, Moura H, Pinto de Jesus A, Suárez-Ruiz I, Flores D (2022) Effects of magmatic fluids in coals of São Pedro da Cova Coalfield, Douro Carboniferous Basin, Portugal: insights from inorganic geochemistry. *Minerals*, *12*(2), 275. https://doi.org/10.3390/min12020275

Custódio J (2004) Museu do Carvão & das Minas do Pejão. Programa Museológico, Castelo de Paiva. 87 pp.

Dai S, Finkelman RB, French D, Hower CJ, Graham IT, Zhao F (2021) Modes of occurrence of elements in coal: A critical evaluation. *Earth-Science Reviews,* 222.103815. https://doi.org/10.1016/j.earscirev.2021.103815

Dai S, Finkelmam RB, Hower JC, French D, Graham IT, Zhao L (2023) *Inorganic geochemistry of coal*. Elsevier.

Dai S, Ren D, Tang Y, Yue M, Hao L (2005) Concentration and distribution of elements in Late Permian coals from western Guizhou Province, China. *International Journal of Coal Geology*, 61. 119-137. https://doi.org/10.1016/j.coal.2004.07.003

Dai S, Seredin VV, Ward CR, Jiang J, Hower JC, Song X, Jiang Y, Wang X, Gornostaeva T, Li X, Liu H, Zhao L, Zhao C (2014) Composition and modes of occurrence of minerals and elements in coal combustion products derived from high-Ge coals. *International Journal of Coal Geology,* 121 (1), 79–97. https://doi.org/10.1016/j.coal.2013.11.004

Dang Z, Liu C, Haigh MJ (2002) Mobility of heavy metals associated with the natural weathering of coal mine spoils. *Environmental pollution*, *118*(3), 419-426. https://doi.org/10.1016/S0269-7491(01)00285-8

De La Torre-Roche RJ, Lee,W-Y, Campos-Diaz SI (2009) Soil-borne polycyclic aromatic hydrocarbons in El Paso, Texas: analysis of a potential problem in the United States/Mexico border region. *Journal of Hazardous Materials***,** 163: 946–958. http://doi.org/10.1016/j.jhazmat.2008.07.089

de Schamphelaere KA, Janssen CR (2002) A biotic ligand model predicting acute copper toxicity for *Daphnia magna*: the effects of calcium, magnesium, sodium, potassium, and pH. *Environmental science & technology*, 36(1), 48-54. https://doi.org/10.1021/es000253s

Decagon D (2005) Inc. Minidisk Infiltrometer User's Manual; Decagon Devices. *Inc.: Pullman, WA, USA*.

Dekker LW, Jungerius PD (1990) Water repellency in the dunes with particular reference to the Netherlands. *Catena Supplement*, 18, 173 – 183.

Dekker LW, Ritsema CJ (1994) Uneven moisture patterns in water repellent soils, *Geoderma,* 70, 87 – 99, https://doi.org/10.1016/0016-7061(95) 00075-5

Dekker LW, Ritsema CJ, Oostindie K, Moore D, Wesseling JG (2009) Methods for determining soil water repellency on field-moist samples. *Water Resources Research*, 45(4). https://doi.org/10.1029/2008wr007070

Delta-T Devices Ltd (2017) ML3 ThetaProbe. https://delta-t.co.uk/wp-content/uploads/2017/02/ML3-user-manual-version-2.1.pdf

Dias R, Araújo AA, Terrinha P, Kullberg JC (2013) *Geologia de Portugal, Volume I, Geologia Pré-mesozóica de Portugal*. Escolar Editora.

Dick WA, Bonta JV, Haghiri F, Page JR (1983) Stream water quality of two small watersheds as affected by surface coal mining. *American Society of Agronomy, Crop Science Society of America, and Soil Science Society of America*. (Vol. 12, No. 3, pp. 351-358). https://doi.org/10.2134/jeq1983.00472425001200030011x

Ding Z, Fang Q, Daraz U, Sun Q (2021) Physiological responses and metal distributions of different organs of *Phragmites australis* shoots under acid mine drainage stress. *Environmental Science and Pollution Research* 28, 3375–3385. https://doi.org/10.1007/s11356-020-10700-8

Diogo BS, Narayan A, Mansilha C, Marques JE, Flores D, Antunes, SC (2023a) Phytotoxicity of coal waste elutriates (Douro Coalfield, North Portugal) in Lactuca sativa. *Environmental Science and Pollution Research*, *30*(49), 107650-107660. https://doi.org/10.1007/s11356-023-29868-w

Diogo BS, Rodrigues S, Lage OM, Antunes SC (2023b) Are the ecotoxicological tools viable to evaluate the effectiveness of wastewater treatment plant effluents? *International Journal of Environmental Science and Technology*. https://doi.org/10.1007/s13762-023-04791-2

Di Palma L, Mecozzi R (2010) Batch and column tests of metal mobilization in soil impacted by landfill leachate. *Waste Management*, *30*(8-9), 1594-1599. https://doi.org/10.1016/j.wasman.2010.04.003

Di Salvatore M, Carafa AM, Carratu G (2008) Assessment of heavy metals phytotoxicity using seed germination and root elongation tests: A comparison of two growth substrates. *Chemosphere*, *73*(9), 1461-1464. https://doi.org/10.1016/j.chemosphere.2008.07.061

Dirilgen N (2011) Mercury and lead: Assessing the toxic effects on growth and metal accumulation by *Lemna minor*. *Ecotoxicology and Environmental Safety*, 74(1), 48–54. https://doi.org/10.1016/j.ecoenv.2010.09.014

Dohnal M, Dusek J, Vogel T (2010) Improving hydraulic conductivity estimates from minidisk infiltrometer measurements for soils with wide pore-size distributions. *Soil Science Society of America Journal*, 74(3), 804-811. https://doi.org/10.2136/sssaj2009.0099

Domingos LCG, Freire JLS, Gomes da Silva F, Gonçalves F, Pereira E, Ribeiro A (1983) The structure of the intramontane Upper Carboniferous basins in Portugal. *Memórias dos Serviços Geológicos de Portugal*, (29), 187-194.

Dong J, Cheng Z, Li F (2013) PAHs emission from the pyrolysis of Western Chinese coal. *Journal of Analytical and Applied Pyrolysis,* 502-507. http://dx.doi.org/10.1016/j.jaap.2013.05.020

Duester L, Van Der Geest HG, Moelleken S, Hirner AV, Kueppers K (2011) Comparative phytotoxicity of methylated and inorganic arsenic and antimony species to *Lemna minor*, *Wolffia arrhizal* and *Selenastrum capricornutum*. *Microchemical Journal*, 97 (1), 30-37. https://doi.org/10.1016/j.microc.2010.05.007

Dutta M, Khare P, Chakravarty S, Saikia D, Saikia BK (2018) Physico-chemical and elemental investigation of aqueous leaching of high sulfur coal and mine overburden from Ledo coalfield of Northeast India. *International Journal of Coal Science and Technology*, *5*, 265–281. https://doi.org/10.1007/s40789-018-0210-9

Dvořák P, Krasylenko Y, Zeiner A, Šamaj J, Takáč T (2021) Signaling toward reactive oxygen species-scavenging enzymes in plants. *Frontiers in Plant Science*, 11. https://doi.org/10.3389/fpls.2020.618835

Eagar RMC (1983) The non-marine bivalve fauna of the Stephanian C of North Portugal. In: M. J. LEMOS DE SOUSA & J. T. OLIVEIRA, Eds, The Carboniferous of Portugal. *Memórias dos Serviços Geológicos do Portugal*, Lisboa, 29: 179-185.

Elkahoui S, Hernández JA, Abdelly C, Ghrir R, Limam F (2005) Effects of salt on lipid peroxidation and antioxidant enzyme activities of *Catharanthus roseus* suspension cells. *Plant Science*, 168(3), 607–613. https://doi.org/10.1016/j.plantsci.2004.09.006

Eskenazy G, Finkelman RB, Chatterjee S (2010) Some considerations concerning the use of correlation coefficients and cluster analysis in interpreting coal geochemistry

data. *International Journal of Coal Geology*, *83*(4), 491-493. https://doi.org/10.1016/j.coal.2010.05.006

Espinha Marques J, Martins V, Santos P, Ribeiro J, Mansilha C, Melo A, Flores D (2021) Changes induced by self-burning in technosols from a coal mine waste pile: a hydropedological approach. *Geosciences*, *11*(5), 195. https://doi.org/10.3390/geosciences11050195

Espinha Marques J, Narayan A, Santos P, Ribeiro J, Antunes SC, Melo A, Rocha F, Flores D, Mansilha C (2024) Hydropedological characterization of a coal mining waste deposition area affected by self-burning. *Hydrology*, 11, 62. https://doi.org/10.3390/hydrology11050062

Eychaner JH (1999) Progress of environmental studies in coal mining areas of western Pennsylvania and central West Virginia. In *Twentieth Annual West Virginia Surface Mine Drainage Task Force Symposium, 1999, Proceedings: Morgantown, W. Va*.

Fan W, Peng R, Li X, Ren J, Liu T, Wang X (2016) Effect of titanium dioxide nanoparticles on copper toxicity to *Daphnia magna* in water: role of organic matter. Water Research, 105, 129-137. https://doi.org/10.1016/j.watres.2016.08.060

FAO (2006) Food and Agriculture Organization of the United Nations. *Guidelines for Soil Description*, 4th ed.; Food and Agriculture Organization of the United Nations (FAO): Rome; pp. 67–71

FAO (2015) Food and Agriculture Organization of the United Nations. IUSS Working Group WRB. World Reference Base for Soil Resources 2014, Update 2015, International Soil Classification System for Naming Soils and Creating Legends for Soil Maps; World Soil Resources Reports No. 106, Rome; 192p.

FAO (1984) Agriculture Organization of the United Nations - Physical and chemical methods of soil and water analysis.

Feio M, Daveau S (2004) O Relevo de Portugal. Associação Portuguesa de Geomorfólogos, Coimbra

Fernandes JP, Pinto de Jesus A, Teixeira F, Sousa MJL (1997) Primeiros resultados palinológicos na Bacia Carbonífera do Douro (NO de Portugal). In: Grandal 'Angale, A., Gutiérrez-Marco, J.C., Santos Fidalgo, L. (Eds.), XIII Jornadas de Paleontologia "Fósiles de Galicia" y V Reunión Internacional Proyecto 351 PICG "Paleozoico inferior del Noroeste de Gondowana", A Coruna, 1997, Libro de Resúmenes y Excursiones, Sociedade Espanola de Paleontologia, pp. 176–179

Ferreira AB (1996) Geomorphology of Portugal: long-term evolution and tectonic setting. In: Ferreira AB, Vieira GT (eds) Fifth European Intensive Course on Applied Geomorphology. Mediterranean and urban areas, ERASMUS ICO-91-96-I-1226/07, publ 9, pp 15–25

Ferreira D (1981) Carte Géomorphologique du Portugal. Centro de Estudos Geográficos, Memórias 6, Lisboa

Fikirdeşici-Ergen Ş, Üçüncü-Tunca E, Kaya M, Tunca E (2018) Bioremediation of heavy metal contaminated medium using *Lemna minor*, *Daphnia magna* and their consortium. *Chemistry and Ecology*, 34(1), 43–55. https://doi.org/10.1080/02757540.2017.1393534

Finkelman RB (1981a) The origin, occurrence, and distribution of the inorganic constituents in low-rank coals. In: Proceedings of the Basic Coal Science Workshop. H.H. Schobert, compiler. Grand Forks Energy Tech, Center, Grand Forks, N.D., pp. 70–90.

Finkelman RB (1981b) Modes of Occurrence of Trace Elements in Coal: USGS Open-File Report 81–99. 322 p.

Finkelman RB (1994) Modes of occurrence of potentially hazardous elements in coal: levels of confidence. *Fuel Processing Technology*, 39:21–34. https://doi.org/10.1016/0378-3820(94)90169-4

Finkelman RB, Gross P (1999). The types of data needed for assessing the environmental and human health impacts of coal. *International Journal of Coal Geology*, *40*, 91–101. https://doi.org/10.1016/S0166-5162(98)00061-5

Finkelman RB, Dai S, French D (2019) The importance of minerals in coal as the hosts of chemical elements: A review. *International Journal of Coal Geology*, *212*, 103251. https://doi.org/10.1016/j.coal.2019.103251

Finkelman RB, Palmer CA, Wang P (2018). Quantification of the modes of occurrence of 42 elements in coal. *International Journal of Coal Geology, 185.* 138-160. https://doi.org/10.1016/j.coal.2017.09.005

Flores D, Teodoro AC, Melo A, Mansilha C, Viveiros D, Ribeiro J, Ferreira J, Espinha Marques J, Santos JL, Batista JM, Duarte L, Santos P (2024) Escombreiras em autocombustião na Bacia Carbonífera do Douro: Processos, impactes ambientais e monitorização. Memórias da Academia das Ciências de Lisboa: Bacia Carbonífera do Douro: Novos Desenvolvimentos.

Fomin A, Moser H, Pickl C (2000) Ecotoxicological investigations of extremely acidic mining lakes using bioassays suitable for testing at low pH. *Toxicological & Environmental Chemistry*, *76*(3-4), 237-254. https://doi.org/10.1080/02772240009358932

Foyer CH, Noctor G (2005) Oxidant and antioxidant signalling in plants: a re-evaluation of the concept of oxidative stress in a physiological context. *Plant, Cell, and Environment*, 28(8), 1056–1071. https://doi.org/10.1111/j.1365-3040.2005.01327.x

Foyer CH, Noctor G, Lelandais M (1994) Short-term effects of nitrate, nitrite and ammonium assimilation on photosynthesis, carbon partitioning and protein phosphorylation in maize. *Planta* **192**, 211–220. https://doi.org/10.1007/BF01089037

Frankel TE, Crowell C, Giancarlo L, Hydorn D, Odhiambo BK (2023) Investigating the potential impacts of coal ash runoff on the freshwater Seminole ramshorn snail (Planorbella duryi) under laboratory conditions. *Chemosphere*, *310*, 136815. https://doi.org/10.1016/j.chemosphere.2022.136815

Futra D, Heng L, Surif S, Ahmad A, Ling T (2014) Microencapsulated *Aliivibrio fischeri* in alginate microspheres for monitoring heavy metal toxicity in environmental waters. *Sensors*, 14(12), 23248–23268. https://doi.org/10.3390/s141223248

Gadi VK, Tang YR, Das A, Monga C, Garg A, Berretta C, Sahoo L (2017) Spatial and temporal variation of hydraulic conductivity and vegetation growth in green infrastructures using infiltrometer and visual technique. *Catena*,155, 20–29. https://doi.org/10.1016/j.catena.2017.02.024

Gangwar S, Singh VP (2011) Indole acetic acid differently changes growth and nitrogen metabolism in *Pisum sativum* seedlings under chromium (VI) phytotoxicity: Implication of oxidative stress. *Scientia Horticulturae* 129, 321–328. https://doi.org/10.1016/j.scienta.2011.03.026

Gao Y, Xiao W, Yu Y, Xu LJ, Shao F, Zeng JY (2014) Comprehensive treatment of coal waste piles with spontaneous combustion. *Applied Mechanics and Materials*, *533*, 384–389. https://doi.org/10.4028/www.scientific.net/AMM.533.384

García Giménez R, Vigil de la Villa R, Frías M (2016) From coal-mining waste to construction material: a study of its mineral phases. *Environmental Earth Sciences*, 75, 1-8. https://doi.org/10.1007/s12665-016-5494-8

Garnczarska M, Ratajczak L (2000) Metabolic responses of *Lemna minor* to lead ions II. Induction of antioxidant enzymes in roots. *Acta Physiologiae Plantarum*, 22(4), 429–432. https://doi.org/10.1007/s11738-000-0084-4

Gavina A, Antunes SC, Pinto G, Claro MT, Santos C, Gonçalves F, Pereira R (2013). Can physiological endpoints improve the sensitivity of assays with plants in the risk assessment of contaminated soils? *PLoS One* 8, e59748. https://doi.org/10.1371/journal.pone.0059748

Gentzis T, Goodarzi F (1995) Enrichment and Depletion of Elements in a Subbituminous Coal and in Its 120°C, 400°C and 800°C Ashes. *Energy Sources,* 17(1), 41–55. https://doi.org/10.1080/00908319508946070

Geremias R, Bortolotto T, Wilhelm-Filho D, Pedrosa RC, de Fávere VT (2012). Efficacy assessment of acid mine drainage treatment with coal mining waste using *Allium cepa*

as a bioindicator. *Ecotoxicological Environmental Safety* 79, 116–121. https://doi.org/10.1016/j.ecoenv.2011.12.010

Giri K, Mishra G, Pandey S, Verma PK, Kumar R, Bisht NS (2014) Ecological degradation in northeastern coal fields: Margherita Assam. *International Journal of Science, Environment and Technology*, *3*(3), 881-884.

Gluskoter HJ (1977) Trace elements in coal: occurrence and distribution. Circular no. 499.

Goldschmidt VM (1956) Geochemistry. Clarendon Press, Oxford, 730 p.

Gomes A, Chaminé HI (2005) Cartografia geológica e geomorfológica para a caracterização de riscos naturais a escala do planeamento regional: Aplicação ao concelho de Castelo de Paiva (NW de Portugal). *Xeografica*, Santiago de Compostela, 5:85-105.

Gonçalves EJ (2013) *Hidrogeologia das áreas de Valongo, de Paredes e de Arouca, no context do Anticlinal de Valongo* (Tese de doutoramento, Universidade do Porto).

Goodarzi F (1990) Variation of elements in self-burning coal seam from Coalspur, Alberta Canada. *Energy Sources* 12, 345–361. https://doi.org/10.1080/00908319008960209

Green Plan (2011) Estudo de Impacte Ambiental Área de Acolhimento Empresarial e Logistica “Cruz da Carreira”. http://hdl.handle.net/10400.11/5692

Guha-Roy PK (1991) Coal mining in Meghalaya and its impact on environment. *Exposure*, *4*, 31-33.

Guo Z, Lin T, Zhang G, Zheng M, Zhang Z, Hao Y, Fang M (2007) The sedimentary fluxes of polycyclic aromatic hydrocarbons in the Yangtze River Estuary coastal sea for the past century. *Science of the Total Environment,* 386:33–41. https://doi.org/10.1016/j.scitotenv.2007.07.019

Gwóźdź EA, Przymusiński R, Rucińska R, Deckert J (1997) Plant cell responses to heavy metals: molecular and physiological aspects. *Acta Physiological Plant* 19:459–465. https://doi.org/10.1007/s11738-997-0042-5

Hageman PL (2007) U.S. Geological Survey field leach test for assessing water reactivity and leaching potential of mine wastes, soils, and other geologic and environmental materials. In U.S. Geological Survey Techniques and Methods; USGS: Reston, USA; Book 5, Chapter D3, p. 14.

Hall LW, Burton DT, Ward BJ (1982) Effects of power plant coal pile and coal waste runoff and leachate on aquatic biota: an overview with research recommendations. CRC Critical Reviews in Toxicology, 10(4), 287-301. https://doi.org/10.3109/10408448209003369

Hasii O, Gasii G (2024) Coal mining and water resources: impacts, challenges, and strategies for sustainable environmental management. In *IOP Conference Series: Earth and Environmental Science* (Vol. 1348, No. 1, p. 012017). IOP Publishing. https://doi.org/10.1088/1755-1315/1348/1/012017

Haverkamp R, Ross PJ, Smettem KRJ, Parlange JY (1994) Three-dimensional analysis of infiltration from the disc infiltrometer: 2. Physically based infiltration equation. *Water Resource Research*, 3011, 2931–2935. https://doi.org/10.1029/94WR01788

Hayakawa K, Tang N, Nagato EG, Toriba A, Aoki K (2019) Identification of long-range transported polycyclic aromatic hydrocarbons in snow at Mt. Tateyama, Japan. *Aerosol and Air Quality Research* 19: 1252–1258. https://doi.org/10.4209/aaqr.2018.05.0153

Hayashi J, Kawakami T, Taniguchi T, Kusakabe K, Morooka S, Yumura M (1993) Control of molecular composition of tar by secondary reaction in fluidized-bedpyrolysis of a subbituminous coal. *Journal of Energy and Fuel*, 7. 57–66.

Haygood MG, Nealson KH (1985) The effect of Iron on the growth and luminescence of the symbiotic bacterium *Vibrio fischeri*. Symbiosis.

Hoagland D, Arnon D (1950) The water-culture method for growing plants without soil. *Circular. California agricultural experiment station* 347, 32.

Hoque MM, Ajwa HA, Smith R (2007) Nitrite and ammonium toxicity on lettuce grown under hydroponics. *Communications in soil science and plant analysis*, *39*(1-2), 207-216. https://doi.org/10.1080/00103620701759194

Hou W, Chen X, Song G, Wang Q, Chi Chang C (2007) Effects of copper and cadmium on heavy metal polluted waterbody restoration by duckweed (*Lemna minor*). *Plant Physiology and Biochemistry*, 45(1), 62–69. https://doi.org/10.1016/j.plaphy.2006.12.005

Houshmandfar A, Moraghebi F (2011) Effect of mixed cadmium, copper, nickel and zinc on seed germination and seedling growth of safflower. *African Journal of Agricultural Research* 6, 1182–1187. https://doi.org/10.5897/AJAR10.1033

Hu J, Zheng B, Finkelman RB, Wang B, Wang M, Li S, Wu D (2006) Concentration and distribution of sixty-one elements in coals from DPR Korea. *Fuel*, *85*(5-6), 679-688. https://doi.org/10.1016/j.fuel.2005.08.037

ICCP (1998) The new vitrinite classification (ICCP System 1994). *Fuel* 77, 349–358.

ICCP (2001) The new inertinite classification (ICCP system 1994). *Fuel* 80, 459–471.

Instituto Nacional de Meteorologia e Geofísica (1990) O Clima de Portugal - Normais Climatológicas Entre o Douro e Minho e Beira Litoral, I.N.M.G., Lisboa.

Instituto Português de Mar e Atmosfera (2023). Normal Climatologica-Porto/Pedras Rubras 1981-2010. https://www.ipma.pt/bin/file.data/climate-normal/cn_81-10_PORTO_PEDRAS_RUBRAS.pdf

Iqbal J, Baig MA (2016) Effect of nutrient concentration and pH on growth and nutrient removal efficiency of duckweed (Lemna minor) from natural solid waste leachate. *Int. J. Health Med*, *1*(3), 1-7.

ISO (2008) ISO 17512-1: Soil quality — Avoidance test for determining the quality of soils and effects of chemicals on behavior — Part 1: Test with earthworms (*Eisenia fetida* and *Eisenia andrei*).

ISO 1171 (2010) Solid mineral fuels — Determination of ash. International Organization for Standarization

ISO 11760 (2005) Classification of coals, 1st edition. International Organization for Standardization, Geneva, Switzerland. 9 pp.

ISO 589 (2008) Hard Coal — Determination of Total Moisture. International Organization

ISO 7404-5 (2009) Methods for the Petrographic Analysis of Coals – Part 5: Method of Determining Microscopically the Reflectance of Vitrinite. International Organization for Standardization, p. 14. Geneva, Switzerland.

ISO 7407-2 (2009) Methods for the Petrographic Analysis of Coals - Part 2: Methods of Preparing Coal Samples. International Organization for Standardization, p. 12. Geneva, Switzerland.

IUSS Working Group WRB (2022) World Reference Base for Soil Resources. International Soil Classification System for Naming Soils and Creating Legends for Soil Maps (4th ed.). FAO, Rome.

Ivanova S, Vesnina A, Fotina N, Prosekov A (2023) Influence of Coal Mining Activities on Soil's Agrochemical and Biochemical Properties. *Qubahan Academic Journal*, *3*(4), 387-399. https://doi.org/10.48161/qaj.v3n4a229

Jarvis N, Koestel J, Messing I, Moeys J, Lindahl A (2013) Influence of soil, land use and climatic factors on the hydraulic conductivity of soil. *Hydrology and Earth System Sciences*, *17*(12), 5185-5195. https://doi.org/10.5194/hess-17-5185-2013

Jenny H (1994) Factors of soil formation: a system of quantitative pedology. Courier Corporation.

Jeong JW, Cha MS, Jo SJ, Lee SJ (2001) Acute and chronic toxicity of heavy metals to *Daphnia magna*. *Journal of Environmental Science International*, 10(4), 293-298.

Jmii S, Dewez D (2021) Toxic responses of palladium accumulation in duckweed (*Lemna minor*): Determination of biomarkers. *Environmental Toxicology and Chemistry*, 40(6), 1630–1638. https://doi.org/10.1002/etc.5011

Johnson R, Vishwakarma K, Hossen MdS, Kumar V, Shackira AM, Puthur JT (2022) Potassium in plants: Growth regulation, signaling, and environmental stress

tolerance. *Plant Physiology and Biochemistry*, 172, 56–69. https://doi.org/10.1016/j.plaphy.2022.01.001

Kaur L, Gadgil K, Sharma S (2012) Role of pH in the accumulation of lead and nickel by common duckweed (*Lemna minor*). *International Journal of Bioassays*, 1(12), 191–195.

Khangarot BS, Ray PK (1989) Investigation of correlation between physicochemical properties of metals and their toxicity to the water flea *Daphnia magna* straus. *Ecotoxicology and Environmental Safety*, 18(2), 109–120. https://doi.org/10.1016/0147-6513(89)90071-7

Khellaf N, Zerdaoui M (2010) Growth response of the duckweed Lemna minor to heavy metal pollution.

Kieta KA, Owens PN, Petticrew EL (2023) Post-wildfire contamination of soils and sediments by polycyclic aromatic hydrocarbons in north-central British Columbia, Canada. *International Journal of Wildland Fire*, *32*(7), 1071-1088.https://doi.org/10.1071/WF22211

Kim S, Lee SE, Baek SH, Choi U, Bae HJ (2023) Preparation of Activated Carbon from Korean Anthracite: Simultaneous Control of Ash Reduction and Pore Development. *Processes*, *11*(10), 2877. https://doi.org/10.3390/pr11102877

Kodešová R, Vignozzi N, Rohošková M, Hájková T, Kočárek M, Pagliai M, Šimůnek J (2009) Impact of varying soil structure on transport processes in different diagnostic horizons of three soil types. *Journal of Contaminant Hydrology*, *104*(1-4), 107-125. https://doi.org/10.1016/j.jconhyd.2008.10.008

Kohli SK, Handa N, Bali S, Khanna K, Arora S, Sharma A, Bhardwaj R (2019) Current scenario of Pb toxicity in plants: Unraveling plethora of physiological responses. *Reviews of Environmental Contamination and Toxicology,* 249 pp. 153–197. https://doi.org/10.1007/398_2019_25

Komnitsas K, Paspaliaris I, Zilberchmidt M, Groudev S (2001) Environmental impacts at coal waste disposal sites-efficiency of desulfurization technologies. *Global Nest: the International Journal*, *3*(2), 135-142.

Komonweeraket K, Cetin B, Benson CH, Aydilek AH, Edil TB (2015) Leaching characteristics of toxic constituents from coal fly ash mixed soils under the influence of pH. *Waste Management*, *38*, 174-184. https://doi.org/10.1016/j.wasman.2014.11.018

Kovalenko NI, Ryzhenko BN (2009) Comparative study of the solubility of zircon and baddeleyite. Geochemistry International, 47(4), 405-413. https://doi.org/10.1134/S0016702909040077

Kowalska M, Güler H, Cocke D L (1994) Interactions of clay minerals with organic pollutants. *Science of the total environment*, *141*(1-3), 223-240. https://doi.org/10.1016/0048-9697(94)90030-2

Laboratório Nacional de Energia e Geologia [LNEG] (2013) Mapa mineralógico de Portugal. Escala 1:200.000 (Shapfile). Used 18 of May 2025 from https://geoportal.lneg.pt/mapa/?Mapa=CartaDepositosMinerais_Norte

Lair GJ, Gerzabek MH, Haberhauer G (2007) Sorption of heavy metals on organic and inorganic soil constituents. *Environmental Chemistry Letters*, *5*, 23–27. https://doi.org/10.1007/s10311-006-0059-9

Lanctôt C, Wilson SP, Fabbro L, Leusch FD, Melvin SD (2016) Comparative sensitivity of aquatic invertebrate and vertebrate species to wastewater from an operational coal mine in central Queensland, Australia. *Ecotoxicology and Environmental Safety*, *129*, 1-9.https://doi.org/10.1016/j.ecoenv.2016.03.003

Larsson M, Lam MM, van Hees P, Giesy JP, Engwall M (2018) Occurrence and leachability of polycyclic aromatic compounds in contaminated soils: Chemical and bioanalytical characterization. *Science Total Environment*, 622–623, 1476–1484, ISSN 0048-9697. https://doi.org/10.1016/j.scitotenv.2017.12.015

Laumann S, Micic V, Kruge MA, Achten C, Sachsenhofer RF, Schwarzbauer J, Hofmann T (2011). Variations in concentrations and compositions of polycyclic aromatic

hydrocarbons (PAHs) in coals related to the coal rank and origin. *Environmental Pollution*, 159. 2690-2697. https://doi.org/10.1016/j.envpol.2011.05.032

Ledesma EB, Kalish MA, Nelson PF, Wornat MJ, Mackie JC (2000) Formation and fate of PAH during the pyrolysis and fuel-rich combustion of coal primary tar. *Fuel*, 79.1801-1814. https://doi.org/10.1016/S0016-2361(00)00044-2

Leighton-Boyce G, Doerr SH, Shakesby RA, Walsh RPD (2007) Quantifying the impact of soil water repellency on overland flow generation and erosion: a new approach using rainfall simulation and wetting agent on in situ soil. *Hydrological Processes*, 21: 2337-2345. https://doi.org/10.1002/hyp.6744

Lemos de Sousa MJ (1984) Carta Geológica de Portugal na escala de 1/50000. Notícia Explicativa da Folha 9-D - Penafiel. Aditamento relativo ao Carbonífero. 3 pp. Serviços Geológicos de Portugal, Lisboa.

Lemos de Sousa MJ, Wagner RH (1983) General description of the terrestrial Carboniferous basins in Portugal and history of investigations. In: M. J. LEMOS DE SOUSA & J. T. OLIVEIRA, Eds, The Carboniferous of Portugal. *Memórias dos Serviços Geológicos de Portugal*, 29: 117-126.

Li A, Chen C, Chen J, Lei P (2021) Environmental investigation of pollutants in coal mine operation and waste dump area monitored in Ordos Region, China. *RSC Advances*, *11*(17), 10340-10352. https://doi.org/10.1039/D0RA10586D

Li F, Yu T, Huang Z, Jiang T, Wang L, Hou Q (2022) Leaching experiments and risk assessment to explore the migration and risk of potentially toxic elements in soil from black shale. *Science of The Total Environment*, 844, 156922. https://doi.org/10.1016/j.scitotenv.2022.156922

Li H, Chen J, Wu W, Piao X (2010) Distribution of polycyclic aromatic hydrocarbons in different size fractions of soil from a coke oven plant and its relationship to organic carbon content. *Journal of Hazardous Materials* 176, 729–734. https://doi.org/10.1016/j.jhazmat.2009.11.095

Li J, Smart RSC, Schumann RC, Gerson AR, Levay G (2007) A simplified method for estimation of jarosite and acid-forming sulfates in acid mine wastes. *Science of the Total Environment*, *373*(1), 391-403. https://doi.org/10.1016/j.scitotenv.2006.11.012

Li XY, González A, Solé-Benet A (2005) Laboratory methods for estimating infiltration rate of soil crusts in the Tabernas Desert badlands. *Catena*, 603, 255-266. https://doi.org/10.1016/j.catena.2004.12.004

Li Z, Ma Z, Van der Kuijp TJ, Yuan Z, Huang LA (2014) Review of soil heavy metal pollution from mines in China: Pollution and health risk assessment. *Science of the Total Environment*, *468–469*, 843–853, ISSN 0048-9697. https://doi.org/10.1016/j.scitotenv.2013.08.090

Lichtenthaler HK (1987) Chlorophylls and carotenoids: Pigments of photosynthetic biomembranes. *Methods in Enzymology*, 148(C), 350–382. https://doi.org/10.1016/0076-6879(87)48036-1

Lilić J, Cupać S, Lalević B, Andrić V, Gajić-Kvasčev M (2014) Pedological characteristics of open-pit Cu wastes and post-flotation tailings (Bor, Serbia). *Journal of Soil Science and Plant Nutrition*, 14, 161–175. http://dx.doi.org/10.4067/S0718-95162014005000013

Lin H (2012) Hydropedology*. Hydropedology, 3–39.* https://doi.org/10.1016/b978-0-12-386941-8.00001-0

Liu S, Wang C, Zhang S, Liang J, Chen F, Zhao K (2012) Formation and distribution of polycyclic aromatic hydrocarbons (PAHs) derived from coal seam combustion: a case study of the Ulanqab lignite from Inner Mongolia, northern China. *International Journal of Coal Geology*. 90-91, 126–134. https://doi.org/10.1016/j.coal.2011.11.005

Liu WX, Dou H, Wei ZC, Chang B, Qiu WX, Liu Y, Tao S (2009) Emission characteristics of polycyclic aromatic hydrocarbons from the combustion of different residential coals in North China. *Science of the total environment*, *407*(4), 1436-1446. https://doi.org/10.1016/j.scitotenv.2008.10.055

Liu Y, Molinari S, Dalconi MC, Valentini L, Ricci G, Carrer C (2023) The leaching behaviors of lead, zinc, and sulfate in pyrite ash contaminated soil: mineralogical assessments and environmental implications. *Journal of Environmental Chemical Engineering*, 11(3), 109687. https://doi.org/10.1016/j.jece.2023.109687

Loureiro S, Ferreira AL, Soares AM, Nogueira AJ (2005) Evaluation of the toxicity of two soils from Jales mine (Portugal) using aquatic bioassays. *Chemosphere*, 61(2), 168-177. https://doi.org/10.1016/j.chemosphere.2005.02.070

Ludwig B, Khanna P, Balkenhol R, Friedrich G, Dohrmann R (1999) Pyrite oxidation in a sediment sample of an open-cut brown coal mine: mineral formation, buffering of acidity and modeling of cations and sulfate. *Journal of Plant Nutrition and Soil Science*, *162*(5), 499-509. https://doi.org/10.1002/(SICI)1522-2624(199910)162:5<499::AID-JPLN499>3.0.CO;2-4

Lyu J, Park J, Kumar Pandey L, Choi S, Lee H, De Saeger J, Depuydt S, Han T (2018) Testing the toxicity of metals, phenol, effluents, and receiving waters by root elongation in *Lactuca sativa* L. *Ecotoxicology Environmental Safety* 149, 225–232. https://doi.org/10.1016/j.ecoenv.2017.11.006

Ma K, Zhang Y, Ruan M, Guo J, Chai T (2019) Land subsidence in a coal mining area reduced soil fertility and led to soil degradation in arid and semi-arid regions. *International Journal of Environmental Research and Public Health*, *16*(20), 3929. https://doi.org/10.3390/ijerph16203929

Ma Y, Li X, Guo L, Lin H (2017) Hydropedology: Interactions between pedologic and hydrologic processes across spatiotemporal scales. *Earth-Science Reviews,* 171, 181–195. https://doi.org/10.1016/j.earscirev.2017.05.014

Maisto G, Manzo S, De Nicola F, Carotenuto R, Rocco A, Alfani A (2011) Assessment of the effects of Cr, Cu, Ni and Pb soil contamination by ecotoxicological test. *Journal of Environmental monitoring*, 13(11), 3049-3056

Maltby L, Booth R (1991) The effect of coal-mine effluent on fungal assemblages and leaf breakdown. *Water Research*, *25*(3), 247-250. https://doi.org/10.1016/0043-1354(91)90003-9

Mansour SA, Abdel-Hamid AA, Ibrahim AW, Mahmoud NH, Moselhy WA (2015) Toxicity of some pesticides, heavy metals, and their mixtures to *Vibrio fischeri* bacteria and *Daphnia magna*: comparative study. *Journal of Biology Life Science*, 6(2), 221-240. http://dx.doi.org/10.5296/jbls.v6i2.8174

Marichali A, Dallali S, Ouerghemmi, S, Sebei H, Hosni K (2014) Germination, morpho-physiological and biochemical responses of coriander (*Coriandrum sativum L*.) to zinc excess. *Industrial Crops and Products*, *55*, 248-257. https://doi.org/10.1016/j.indcrop.2014.02.033

Marques M, Suárez-Ruiz I, Flores D, Guedes A, Rodrigues S (2009) Correlation between optical, chemical and micro-structural parameters of high-rank coals and graphite. *International Journal of Coal Geology*, *77*(3-4), 377-382. https://doi.org/10.1016/j.coal.2008.06.002

Martins A, Figueiredo T (2009) Spatial variability of soil properties and erosion risk in a Portuguese mountainous watershed. *Revista de Ciências Agrárias*, 32(1), 122–139.

Martin Jr, LK, Black MC (1998) Biomarker assessment of the effects of coal strip-mine contamination on channel catfish. *Ecotoxicology and Environmental Safety*, *41*(3), 307-320. https://doi.org/10.1006/eesa.1998.1714

McLennan AR, Bryant GW, Bailey CW, Stanmore BR, Wall TF (2000) An experimental comparison of the ash formed from coals containing pyrite and siderite mineral in oxidizing and reducing conditions. *Energy & Fuels*, *14*(2), 308-315.

Medeiros AC, Pilar L, Fernandes AP (1964) Carta geológica de Portugal, na escala de 1/50000. Notícia Explicativa da Folha 13-B (Castelo de Paiva). Serviços geológicos de Portugal, Lisboa. 61 pp

Meegoda JN, Gao S, Al-Joulani NMA, Hu L (2011) Solid waste and ecological issues of coal to energy. *Journal of Hazardous, Toxic, and Radioactive Waste*, *15*(2), 99-107. https://doi.org/10.1061/(ASCE)HZ.1944-8376.0000071

METER Group (2020) Mini Disk Infiltrometer; Meter Group, Inc.: Court Pullman, WA, USA, pp. 1–15.

Meyer JS, Ranville JF, Pontasch M, Gorsuch JW, Adams WJ (2015) Acute toxicity of binary and ternary mixtures of Cd, Cu, and Zn to *Daphnia magna*. *Environmental toxicology and chemistry*, 34(4), 799-808. https://doi.org/10.1002/etc.2787

Meyer W, Seiler TB, Reininghaus M, Schwarzbauer J, Püttmann W, Hollert H, Achten C (2013) Limited waterborne acute toxicity of native polycyclic aromatic compounds from coals of different types compared to their total hazard potential. *Environmental science & technology*, *47*(20), 11766-11775.

Microbics M (1992) Microtox manual - a toxicity handbook (Vol. I–VI). Microbics Corporation.

Minasny B, George BH (1999) The measurement of soil hydraulic properties in the field. *Science*, 22, 26th

Miras-Moreno B, Senizza B, Regni L, Tolisano C, Proietti P, Trevisan M, Del Bouno D (2022) Biochemical Insights into the ability of *Lemna minor* extract to counteract copper toxicity in maize. *Plants*, 11(19), 2613. https://doi.org/10.3390/plants11192613

Misz M, Fabiańska M, Ćmiel S (2007) Organic components in thermally altered coal waste: Preliminary petrographic and geochemical investigations. *International Journal of Coal Geology*, *71*(4), 405–424. https://doi.org/10.1016/j.coal.2006.08.009

Misz-Kennan M, Kus J, Flores D, Avila C, Büçkün Z, Choudhury N, Christanis K, Hower JC, Joubert JP, Kalaitzidis S, Karayigit AI, Malecha M, Marques M, Martizzi P, O'Keefe J, Panaitescu C, Pickel W, Predeanu G, Pusz S, Ribeiro J, Rodrigues S, Singh A, Suárez-Ruiz I, Sýkorová I, Wagner N, Zivotic D (2020) Development of a petrographic classification system for organic particles affected by self-heating in coal waste (An ICCP Classification System, Self-heating Working Group–Commission III). *International Journal of Coal Geology*, *220*, 103411. https://doi.org/10.1016/j.coal.2020.103411

Modarres A, Rahmanzadeh M, Ayar P (2015) Effect of coal waste powder in hot mix asphalt compared to conventional fillers: Mix mechanical properties and environmental impacts. *Journal of Cleaner Production,* 91, 262–268. https://doi.org/10.1016/j.jclepro.2014.11.078

Monteiro M, Santos P, Marques JE, Flores D, Pereira CM, Ribeiro JA, Azenha M (2024) Assessment of mobile mercury concentration in soils of an abandoned coalfield waste pile in Douro region: the Fojo waste pile (Portugal) study case. *Journal of Soils and Sediments*, *24*(5), 2068-2077. https://doi.org/10.1007/s11368-024-03786-x

Mora C, Vieira G (2020) The Climate of Portugal. In: Vieira, G., Zêzere, J., Mora, C. (eds) Landscapes and Landforms of Portugal. World Geomorphological Landscapes. Springer, Cham. https://doi.org/10.1007/978-3-319-03641-0_2

Moreira IN, Martins LL, Mourato MP (2020) Effect of Cd, Cr, Cu, Mn, Ni, Pb and Zn on seed germination and seedling growth of two lettuce cultivars (*Lactuca sativa* L.). *Plant Physiology Reports*, *25*(2), 347-358.

Mourato M, Moreira I, Leitão I, Pinto F, Sales J, Martins L (2015) Effect of heavy metals in plants of the genus Brassica. *International Journal of Molecular Sciences,16*(8), 17975.

Msttés JM (2000) Effects of antioxidant enzymes in the molecular control of reactive oxygen species toxicology. *Toxicology*, 153(1–3), 83–104. https://doi.org/10.1016/S0300-483X(00)00306-1

Mudd GM, Weaver TR, Kodikara J (2004) Environmental geochemistry of leachate from leached brown coal ash. *Journal of Environmental Engineering*, *130*(12), 1514-1526. https://doi.org/10.1061/(ASCE)0733-9372(2004)130:12(1514)

Nádudvari Á, Fabiańska MJ, Marynowski L, Kozielska B, Konieczyński J, Smołka-Danielowska D, Ćmiel S (2018) Distribution of coal and coal combustion related organic pollutants in the environment of the Upper Silesian Industrial Region. *Science of the Total Environment*, *628*, 1462-1488. https://doi.org/10.1016/j.scitotenv.2018.02.092

Nagajyoti P, Lee K, Sreekanth T (2010) Heavy metals, occurrence and toxicity for plants: A review. *Environmental Chemistry Letters,8*(3), 199–216.

Naik AP, Ghosh B, Pekkat S (2018) Estimating soil hydraulic properties using mini disk infiltrometer. ISH *Journal of Hydraulic Engineering*, 25(1), 62–70. https://doi.org/10.1080/09715010.2018.1471363

Narayan A, Diogo BS, Mansilha C, Espinha Marques J, Flores D, Antunes SC (2024) Assessment of ecotoxicological effects of Fojo coal mine waste elutriate in aquatic species (Douro Coalfield, North Portugal). *Frontiers in Toxicology*, *6*, 1334169. https://doi.org/10.3389/ftox.2024.1334169

Neff JM, Stout SA, Gunster DG (2004) Ecological Risk Assessment of Polycyclic Aromatic Hydrocarbons in Sediments: Identifying Sources and Ecological Hazard. *Integrated Environmental Assessment and Management,* 1. 22-33. https://doi.org/10.1897/IEAM_2004a-016.1

Nimmo JR (1997) Modeling structural influences on soil water retention. *Soil Science Society of America Journa*l, 61(3), 712-719. https://doi.org/10.2136/sssaj1997.03615995006100030002x

Nogueira V, Sousa CT, Araujo JP, Pereira R (2020) Evaluation of the toxicity of nickel nanowires of freshwater organisms at concentration and short-term exposures compatible with their application in water treatment. *Aquatic Toxicology*, 227: 105595. https://doi.org/10.1016/j.aquatox.2020.105595

Nunes B, Pinto G, Martins L, Gonçalves F, Antunes SC (2014) Biochemical and standard toxic effects of acetaminophen on the macrophyte species *Lemna minor* and *Lemna gibba*. *Environmental Science and Pollution Research*, 21(18), 10815–10822. https://doi.org/10.1007/s11356-014-3059-5

Nunes JP, Almeida AC, Sequeira MM, Bugalho MN (2019) Forest soils in Portugal: Diversity, classification and ecosystem functions. *Revista de Ciências Agrárias*, 42(1), 159–176

Nyström E, Thomas H, Wanhainen C, Alakangas L (2021) Occurrence and release of trace elements in pyrite-rich waste rock. *Minerals*, *11*(5), 495. https://doi.org/10.3390/min11050495

OECD (2004) Test No. 202: *Daphnia* sp. acute immobilisation test. https://doi.org/10.1787/9789264069947-en

OECD (2006) Test No. 221: *Lemna* sp. growth inhibition test. https://doi.org/https://doi.org/10.1787/9789264016194-en

Ofori P, Hodgkinson J, Khanal M, Hapugoda, Yin J (2023) Potential resource from coal mining and combustion waste: Australian perspective. *Environment, Development and Sustainability*, 25:10351-10368. https://doi.org/s10668-022-02492-3

Okamoto A, Yamamuro M, Tatarazako N (2015) Acute toxicity of 50 metals to *Daphnia magna*. *Journal of Applied Toxicology*, 35(7), 824–830. https://doi.org/10.1002/jat.3078

Pactwa K, Woźniak J, Dudek M (2020) Coal mining waste in Poland in reference to circular economy principles. *Fuel*, *270*, 117493.

Pais J, Cunha P, Legoinha P, Dias RP, Pereira D, Ramos A (2013) Cenozóico das Bacias do Douro (sector ocidental), Mondego, Baixo Tejo e Alvalade. In: Dias R, Araújo A, Terrinha P, Kullberg JC (eds) Geologia de Portugal, vol II, Geologia Meso-cenozóica de Portugal. Escolar Editora, Lisboa, pp 461–532

Pal RN, Laloraya MM (1972) Effect of calcium levels on chlorophyll synthesis in peanut and linseed plants. *Biochemie und Physiologie der Pflanzen*, 163(5), 443–449. https://doi.org/10.1016/S0015-3796(17)31269-6

Parzentny HR, Róg L (2021) Distribution and mode of occurrence of Co, Ni, Cu, Zn, As, Ag, Cd, Sb, Pb in the feed coal, fly ash, slag, in the topsoil and in the roots of trees and undergrowth downwind of three power stations in Poland. *Minerals*, *11*(2), 133. https://doi.org/10.3390/min11020133

Peng N, Li Y, Liu Z, Liu T, Gai C (2016) Emission, distribution and toxicity of polycyclic aromatic hydrocarbons (PAHs) during municipal solid waste (MSW) and coal co-

combustion. *Science of the Total Environment,* 565. 1201-1207. https://doi.org/10.1016/j.scitotenv.2016.05.188

Peng W, Liu Y, Lin M, Liu Y, Zhu C, Sun L, Gui H (2022) Toxicity of coal fly ash and coal gangue leachate to *Daphnia magna*: Focusing on typical heavy metals. *Journal of Cleaner Production*, 330, 129946. https://doi.org/10.1016/j.jclepro.2021.129946

Pereira R, Marques CR, Ferreira MJS, Neves MFJV, Caetano AL, Antunes SC, Mendo S, Gonçalves F (2009) Phytotoxicity and genotoxicity of soils from an abandoned uranium mine area. *Applied Soil Ecology* 42, 209–220. https://doi.org/10.1016/j.apsoil.2009.04.002

Pérez-Lucas G, Vela N, El Aatik, A, Navarro S (2018) Environmental risk of groundwater pollution by pesticide leaching through the soil profile. In *Pesticides-use and misuse and their impact in the environment*. IntechOpen. https://doi.org/10.5772/intechopen.82418

Philip JR (1957) The theory of infiltration: 4. Sorptivity and algebraic infiltration equations. *Soil science*, *84*(3), 257-264.

Pinto de Jesus A (1987) Bassin Houiller du Douro (NW du Portugal); Stratigraphie et contrôle tectonique de la genèse et de l'évolution. Ann. Soc. géol. Nord, 106: 209-217.

Pinto de Jesus A (2001) Génese e Evolução da Bacia Carbonífera do Douro (Estefaniano C inferior, NW de Portugal): Um Modelo. 2 Volumes [Texto 232 pp., 4 anexos; Atlas 71pp]. Universidade do Porto. (Tese de Doutoramento)

Pinto de Jesus A (2003) Evolução sedimentar e tectónica da Bacia Carbonífera do Douro (Estefaniano C inferior, NW de Portugal). Cad. Lab. xeol. Laxe, Coruña, 28: 107-125.

Pinto de Jesus A, Lemos de Sousa MJ (2003) Sedimentary and tectonic evolution of the Douro Basin (Lower Stephanian C - NW of Portugal). In: Abstracts of the XVth International Congress on the Carboniferous and Permian Stratigraphy, Utrecht, Netherlands, 405-408.

Pinto de Jesus A, Rocha F, Gomes C, Lemos de Sousa MJ (1997) Mineralogical parameters used as lithostratigraphic markers: Serrinha formation of the Douro Carboniferous Basin (Portugal). *Boletin de la Sociedad Espanola de Mineralogia*, *20*, 119–120

Pinto de Jesus A, Rocha F, Gomes C, Lemos de Sousa MJ (2003) Mineralogia e cristaloquímica de minerais argilosos de sedimentos da bacia carbonífera do Douro (Estefaniano C inferior—NW Portugal). In *Ciências da Terra*; UNL: Lincoln, NE, USA, 2003; Volume Especial 5.

Pone JDN, Hein KAA, Stracher GB, Annegarn HJ, Finkelman RB, Blake DR, McCormack JK, Schroeder P (2007) The spontaneous combustion of coal and its by-products in the Witbank and Sasolburg coalfields of South Africa. *International Journal of Coal Geology*, *72*(2),124–140. https://doi.org/10.1016/j.coal.2007.01.001

Pope J, Weber P, Mackenzie A, Newman N, Rait R (2010) Correlation of acid base accounting characteristics with the Geology of commonly mined coal measures, West Coast and Southland, New Zealand. *New Zealand Journal of Geology and Geophysics*, *53*(2-3), 153-166. https://doi.org/10.1080/00288306.2010.498404

Priac A, Poupeney A, Druart C, Crini G (2014) Ecotoxicity evaluation of industrial discharge waters and metallic solutions using two organisms (Lactuca sativa and Daphnia magna). *Journal of Pollution Effects & Control*, *2*(117), 2. https://doi.org/10.4172/2375-4397.1000117

Pukalchik M, Mercel F, Panova M, Brendová K, Terekhova VA, Tlustos P (2017) The improvement of multicontaminated sandy loam soil chemical and biological properties by the biochar, wood ash, and humic substances amendments. *Environmental pollution*, 229, 516-524. https://doi.org/10.1016/j.envpol.2017.06.021

Qin S, Lu Q, Li Y, Wang J, Zhao Q, Gao K (2018) Relationships between trace elements and organic matter in coals. *Journal of Geochemical Exploration*, *188*, 101-110. https://doi.org/10.1016/j.gexplo.2018.01.015

Querol X, Zhuang X, Font O, Izquierdo M, Alastuey A, Castro I, van Drooge BL, Moreno T, Grimalt JO, Elvira J, Cabañas M, Bartroli R, Hower JC, Ayora C, Plana F, López-Soler A (2011) Influence of soil cover on reducing the environmental impact of spontaneous coal combustion in coal waste gobs: A review and new experimental data. *International Journal of Coal Geology*, *85*(1), 2–22. https://doi.org/10.1016/j.coal.2010.09.002

Radić S, Gregorović G, Stipaničev D, Cvjetko P, Šrut M, Vujčić V (2013) Assessment of surface water in the vicinity of fertilizer factory using fish and plants. *Ecotoxicology and Environmental Safety*, 96, 32–40. https://doi.org/10.1016/j.ecoenv.2013.06.023

Radić S, Medunić G, Kuharić Ž, Roje V, Maldini K, Vujčić V, Krivohlavek A (2018) The effect of hazardous pollutants from coal combustion activity: Phytotoxicity assessment of aqueous soil extracts. *Chemosphere*, 199, 191–200. https://doi.org/10.1016/j.chemosphere.2018.02.008

Radić S, Stipaničev D, Cvjetko P, Mikelić IL, Rajčić MM, Širac S (2010) Ecotoxicological assessment of industrial effluent using duckweed (*Lemna minor* L.) as a test organism. *Ecotoxicology*, 19(1), 216–222.

Radić S, Stipaničev D, Cvjetko P, Rajčić MM, Širac S, Pevalek-Kozlina B, Pavlica M (2011) Duckweed *Lemna minor* as a tool for testing toxicity and genotoxicity of surface waters. *Ecotoxicology and Environmental Safety*, 74(2), 182–187. https://doi.org/10.1016/j.ecoenv.2010.06.011

Radić S, Vujčić V, Cvetković Ž, Cvjetko P, Oreščanin V (2014) The efficiency of combined CaO/electrochemical treatment in removal of acid mine drainage induced toxicity and genotoxicity. *Science of the total environment*, *466*, 84-89. https://doi.org/10.1016/j.scitotenv.2013.07.011

Ramos C, Ramos-Pereira A (2020) Landscapes of Portugal: paleogeographic evolution, tectonics and geomorphology. In *Landscapes and Landforms of Portugal* (pp. 3-31). Cham: Springer International Publishing.

Rate A (2022) Urban soil as a source and sink. *Urban Soils: Principles and Practice*, 293-317. https://doi.org/10.1007/978-3-030-87316-5_9

Rawls WJ, Brakensiek DL, Saxtonn KE (1982) Estimation of soil water properties. *Transactions of the ASAE*, *25*(5), 1316-1320. https://doi.org/10.13031/2013.33720

Reynolds WD (2008) Unsaturated Hydraulic Properties: Field Tension Infiltrometer. In Soil Sampling and Methods of Analysis, 2nd ed.; Carter, M.R., Gregorich, E.G., Eds.; CRC Press: Boca Raton, FL, USA, pp. 1–22.

Ribeiro DA (2020a) Energia territorialização: o sistema carbonífero do douro. In *Património Industrial Ibero-americano: recentes abordagens* (p. 6). Publicações do Cidehus.

Ribeiro J (2020b) Escombreiras de carvão em autocombustão. *Revista de Ciência Elementar*, *8*(1). http://doi.org/10.24927/rce2020.007

Ribeiro J, Ferreira da Silva E, de Jesus AP, Flores D (2011) Petrographic and geochemical characterization of coal waste piles from Douro Coalfield (NW Portugal). *International Journal of Coal Geology*, *87*(3–4), 226–236. https://doi.org/10.1016/j.coal.2011.06.014

Ribeiro J, Ferreira da Silva E, Flores D (2010a) Burning of coal waste piles from Douro Coalfield (Portugal): Petrological, geochemical and mineralogical characterization. *International Journal of Coal Geology*, *81*(4), 359–372. https://doi.org/10.1016/j.coal.2009.10.005

Ribeiro J, Ferreira da Silva E, Li Z, Ward C, Flores D (2010b) Petrographic, mineralogical and geochemical characterization of the Serrinha coal waste pile (Douro Coalfield, Portugal) and the potential environmental impacts on soil, sediments and surface waters. *International Journal of Coal Geology*, *83*(4), 456–466. https://doi.org/10.1016/j.coal.2010.06.006

Ribeiro J, Flores D (2021) Occurrence, leaching, and mobility of major and trace elements in a coal mining waste dump: The case of Douro Coalfield, Portugal. Energy

Geoscience, 2. 121-128. https://doi.org/10.1016/j.engeos.2020.09.005
Ribeiro J, Flores D, Ward CR, Silva LFO (2010c) Identification of nanominerals and nanoparticles in burning coal waste piles from Portugal. *Science of the Total Environment*, *408*(23), 6032–6041. https://doi.org/10.1016/j.scitotenv.2010.08.046
Ribeiro J, Moura R, Flores D, Lopes DB, Gouveia C, Mendonça S, Frazão O (2013) The Douro Coalfield Fires of Portugal. In *Coal and Peat Fires: A Global Perspective* (Vol. 2, pp. 313–337). Elsevier Inc. https://doi.org/10.1016/B978-0-444-59412-9.00016-8
Ribeiro J, Sant'Ovaia H, Gomes C, Ward C, Flores D (2015) Mineralogy and magnetic parameters of materials resulting from mining and coal consumption from Douro Coalfield (NW Portugal). In: Stracher, G.B., Prakash, A., Sokol, E.V. (Eds.), Coal and Peat Fires: A Global Perspective, vol. 3. Elsevier, pp. 493–507. Case Studies - Coal Fires. https://doi.org/10.1016/j.coal.2022.103941
Ribeiro J, Silva T, Mendonça Filho JG, Flores D (2012) Polycyclic aromatic hydrocarbons (PAHs) in burning and non-burning coal waste piles. *Journal of Hazardous Materials*, 199, 105-110. https://doi.org/10.1016/j.jhazmat.2011.10.076
Ribeiro J, Suárez-Ruiz I, Flores D (2016) Geochemistry of self-burning coal mining residues from El Bierzo Coalfield (NW Spain): Environmental implications. *International Journal of Coal Geology*, *159*, 155–168. https://doi.org/10.1016/j.coal.2016.04.006
Ribeiro J, Suárez-Ruiz I, Flores D (2020) Self-burning coal mining residues – an environmental issue or a source of raw materials? *EGU General Assembly*. https://doi.org/10.5194/egusphere-egu2020-20018
Ribeiro J, Suárez-Ruiz I, Flores D (2022) Coal-related fires in Portugal: New occurrences and new insights on the characterization of thermally affected and non-affected coal waste piles. *International Journal of Coal Geology*, *252*. https://doi.org/10.1016/j.coal.2022.103941
Rivas-Martínez S (1985) Biogeografía y vegetación: Publicación de la Real Academia de las Ciencias Exactas, Físicas y Naturaleza 1-103. Madrid.
Rodier J, Legube B (2016) Eaux Naturelles, Eaux Residuaires, Eau de Mer, 10th ed.; De L'Eau, L., Ed.; DUNOD: Mala-koff; ISBN 9782100754120.
Rouhani A, Newton RA, Al Souki KS, Quattrini G, Gusiatin MZ (2024) A 6-year review status on soil pollution in coal mining areas from Europe. *Environmental Geochemistry and Health* **46**, 392. https://doi.org/10.1007/s10653-024-02179-w
Rouhani A, Skousen J, Tack FM (2023) An overview of soil pollution and remediation strategies in coal mining regions. *Minerals*, *13*(8), 1064. https://doi.org/10.3390/min13081064
Rout G, Samantaray S, Das P (2001) Aluminium toxicity in plants: a review. *Agronomie*, 21(1), 3-21. https://doi.org/10.1051/agro:2001105
Rowe CL (2014) Bioaccumulation and effects of metals and trace elements from aquatic disposal of coal combustion residues: Recent advances and recommendations for further study. In *Science of the Total Environment* (Vols. 485–486, Issue 1, pp. 490–496). Elsevier. https://doi.org/10.1016/j.scitotenv.2014.03.119
Roy JL, McGill WB (2000) Investigation into mechanisms leading to the development, spread and persistence of soil water repellency following contamination by crude oil. *Canadian Journal of Soil Science*, *80*(4), 595-606. https://doi.org/10.4141/S99-091
Saha D, Chakravarty S, Shome D, Raviathul Basariya M, Kumari A, Kundu AK, Chatterjee D (2016) Distribution and affinity of trace elements in Samaleswari coal, Eastern India. *Fuel,* 181, 376–388. https://doi.org/10.1016/j.fuel.2016.04.134
Sahoo PK, Equeenuddin SM, Powell MA (2016) Trace Elements in Soils around Coal Mines: Current Scenario, Impact and Available Techniques for Management. *Current Pollution Report*, *2*, 1–14. https://doi.org/10.1007/s40726-016-0025-5
Sahoo PK, Tripathy MK, Panigrahi, Equeenuddin S (2014) Geochemical characterization of coal and waste rocks from a high sulphur bearing coalfield, India: Implication for

acid and metal generation. *Journal of Geochemical Exploration, 145*, 135-147. https://doi.org/10.1016/j.gexplo.2014.05.024

Santos P, Espinha Marques J, Ribeiro J, Mansilha C, Melo A, Fonseca R, Sant'Ovaia H, Flores D (2023a) Geochemistry of Soils from the Surrounding Area of a Coal Mine Waste Pile Affected by Self-Burning (Northern Portugal). *Minerals* 13(1), 28. https://doi.org/10.3390/min13010028

Santos P, Ribeiro J, Espinha Marques J, Flores D (2023b) Environmental and health risk assessment of soil adjacent to a self-burning waste pile from an abandoned coal mine in Northern Portugal. *Environments*, *10*(3), 53. https://doi.org/10.3390/environments10030053

Santos R (2008) Caracterização Hidrogeológica e Hidroquimica da Área Mineira de Germunde, Pejão. Tese de Doutoramento. Universidade do Porto. Portugal

Satizábal AC, Andrade BM, Zuñiga M del C (1999) Toxicidad aguda del aluminio sobre *Daphnia magna* en aguas con diferentes niveles de dureza. *Actualidades Biológicas*, 21(71), 131–142. https://doi.org/10.17533/udea.acbi.329742

Saxby JD (2000) Minerals in coal. In: Glikson M, Mastalerz M, editors. Organic Matter and Mineralisation. Kluwer Academic Publishers; 2000. p. 314–26.

Schacht K, Marschner B (2015) Treated wastewater irrigation affects soil hydraulic conductivity and aggregate stability of loamy soils in Israel. *Journal of Hydrology and Hydromechanics*, 631, 47–54. https://doi.org/10.1515/johh-2015-0010

Scheerer S, Gomez F, Lloyd D (2006) Bioluminescence of *Vibrio fischeri* in continuous culture: Optimal conditions for stability and intensity of photoemission. *Journal of Microbiological Methods*, 67(2), 321–329. https://doi.org/10.1016/j.mimet.2006.04.010

Schuh WM, Cline RL (1990) Effect of soil properties on unsaturated hydraulic conductivity pore-interaction factors. *Soil Science Society of America Journal*, *54*(6), 1509-1519. https://doi.org/10.2136/sssaj1990.03615995005400060001x

Schultz LG (1964) Quantitative interpretation of mineralogical composition from X-ray and chemical data for the Pierre Shale (No. 391-C).

Seneviratne M, Rajakaruna N, Rizwan M, Madawala HMSP, Ok YS, Vithanage M (2019) Heavy metal-induced oxidative stress on seed germination and seedling development: a critical review. *Environmental Geochemistry and Health* 41, 1813–1831. https://doi.org/10.1007/s10653-017-0005-8

Sethy S, Ghosh S (2013) Effect of heavy metals on germination of seeds. *Journal of Natural Science, Biology and Medicine* 4, 272. https://doi.org/10.4103/0976-9668.116964

Shafiq M, Iqbal M, Mohammad A (2010) Effect of lead and cadmium on germination and seedling growth of *Leucaena leucocephala*. *Journal of Applied Sciences and Environmental Management* 12. https://doi.org/10.4314/jasem.v12i3.55497

Shankar U, Boral L, Pandey HN, Tripathi RS (1993) Degradation of land due to coal mining and its natural recovery pattern. *Current Science*, 680-687. http://www.jstor.org/stable/24095947

Sharma RK, Agrawal M (2005) Biological effects of heavy metals: An overview. *Journal of Environment Biology* 301–313

Shen M, Dai S, French D, Graham IT, Spiro BF, Wang N, Tian X (2023) Geochemical and mineralogical evidence for the formation of siderite in Late Permian coal-bearing strata from western Guizhou, SW China. *Chemical Geology*, *637*, 121675. https://doi.org/10.1016/j.chemgeo.2023.121675

Shylla L, Barik SK, Behera MD, Singh H, Adhikari D, Upadhyay A, Joshi SR (2021) Impact of heavy metals on water quality and indigenous Bacillus spp. prevalent in rat-hole coal mines. *3 Biotech*, *11*(5), 253. https://doi.org/10.1007/s13205-021-02808-6

Silva AR, Sousa C, Exner D, Schwaiger R, Alves MM, Petrovykh DY, Pereira L (2021) pH-induced modulation of *Vibrio fischeri* population life cycle. *Chemosensors*, 9(10), 283. https://doi.org/10.3390/chemosensors9100283

Silva CS (2024) A vegetação de Portugal continental e ilhas: descrição e localização https://storymaps.com/stories/0a9838bf9c6d4d9289a455e89777757d

Simonin M, Rocca JD, Gerson JR, Moore E, Brooks AC, Czaplicki L, Bernhardt ES (2021) Consistent declines in aquatic biodiversity across diverse domains of life in rivers impacted by surface coal mining. *Ecological Applications*, *31*(6), e02389. https://doi.org/10.1002/eap.2389

Singh A, Gaurav K, Meena GK, Kumar S (2020) Estimation of soil moisture applying modified dubois model to Sentinel-1; a regional study from central India. *Remote Sensing*, *12*(14), 2266. https://doi.org/10.3390/rs12142266

Singh S, Parihar P, Singh R, Singh VP, Prasad SM (2016) Heavy metal tolerance in plants: Role of transcriptomics, proteomics, metabolomics, and ionomics. *Fronteirs of Plant Science* 6. https://doi.org/10.3389/fpls.2015.01143

Skarzyńska KM (1995) Reuse of coal mining wastes in civil engineering - Part 1: Properties of minestone. *Waste Management*, *15*(1), 3–42. https://doi.org/10.1016/0956-053X(95)00004-J

Smoliński A, Dombek V, Pertile E, Drobek L, Gogola K, Żechowska SW, Magdziarczyk M (2021) An analysis of self-ignition of mine waste dumps in terms of environmental protection in industrial areas in Poland. Scientific Reports, 11(1), 1-10. https://doi.org/10.1038/s41598-021-88470-7

Sonter LJ, Ali SH, Watson JE (2018) Mining and biodiversity: key issues and research needs in conservation science. *Proceedings of the Royal Society B*, *285*(1892), 20181926. https://doi.org/10.1098/rspb.2018.1926

SPAC (2000) Soil and Plant Analysis - Council Handbook of Reference Methods. Florida.

Spears DA, Zheng Y (1999) Geochemistry and origin of elements in some UK coals. *International Journal of Coal Geology,* 38, 161–179. https://doi.org/10.1016/S0166-5162(98)00012-3

Stogiannidis E, Laane R (2014) Source Characterization of Polycyclic Aromatic Hydrocarbons by Using Their Molecular Indices: An Overview of Possibilities. *Reviews of Environmental Contamination and Toxicology,* 49–133. http://doi.org/10.1007/978-3-319-10638-0_2

Su C, Jiang Y, Yang Y, Zhang W, Xu Q (2019) Responses of duckweed (*Lemna minor* L.) to aluminum stress: Physiological and proteomics analyses. Ecotoxicology and Environmental Safety, 170, 127–140. https://doi.org/10.1016/j.ecoenv.2018.11.113

Su YH, Zhu YG (2008) Uptake of selected PAH from contaminated soils by rice seedlings (Oryza sativa) and influence of rhizosphere on PAH distribution. *Environment pollution*, 155(2), 359-365. https://doi.org/10.1016/j.envpol.2007.11.008

Suárez-Ruiz I, Crelling JC (Eds.) (2008) Applied coal petrology. The role of petrology in coal utilization. Elsevier. 388 pp.

Swaine DJ (1990) Trace Elements in Coal. Butterworth, London. 278 pp

Swaine DJ (2013) Trace elements in coal. Butterworth-Heineman.

Swaine DJ, Goodarzi F. (Eds.). (1995). Environmental Aspects of Trace Elements in Coal.
Kluwer Academic Publishers, the Netherlands. 312 pp.

Taylor GH, Teichmüller M, Davis A, Diessel CFK, Littke R, Robert P (1998) Organic Petrology. Gerbrüder Borntraeger, Berlin, Stuttgart, p. 704.

Teixeira S, Vieira MN, Espinha Marques J, Pereira R (2014) Bioremediation of an iron-rich mine effluent by *Lemna minor*. *International journal of phytoremediation*, 16(12), 1228-1240. https://doi.org/10.1080/15226514.2013.821454

Teodoro A, Santos P, Espinha Marques J, Ribeiro J, Mansilha C, Melo A, Flores D (2021) An integrated multi-approach to environmental monitoring of a self-burning coal waste pile: The São Pedro da Cova mine (Porto, Portugal) study case. *Environments*, 8(6), 48. https://doi.org/10.3390/environments8060048

Tinebra I, Alagna V, Iovino M, Bagarello V (2019) Comparing different application procedures of the water drop penetration time test to assess soil water repellency in

a fire-affected Sicilian area. *Catena*, 177, 41–48. https://doi.org/10.1016/j.catena.2019.02.005

Tiwary RK, Dhar BB (1994) Environmental pollution from coal mining activities in Damodar river basin, India. *Mine water and the environment*, 13(1), 1-10.

Tiwary RK (2001) Environmental impact of coal mining on water regime and its management. *Water, Air, and Soil Pollution*, *132*, 185-199. https://doi.org/10.1023/A:1012083519667

Tobiszewski M, Namie´snik J (2012) PAH diagnostic ratios for the identification of pollution emission sources. *Environment Pollution* 162: 110–119. https://doi.org/10.1016/j.envpol.2011.10.025.

Tuzet A, Rahantaniaina MS, Noctor G (2019) Analyzing the function of catalase and the ascorbate–glutathione pathway in H_2O_2 processing: insights from an experimentally constrained kinetic model. *Antioxidants & Redox Signaling*, 30(9), 1238–1268. https://doi.org/10.1089/ars.2018.7601

USEPA (1996) EPA method 3540 C, Soxhlet extraction. Available from: https://www.epa.gov/sites/default/files/2015-12/documents/3540c.pdf

USEPA (1996) EPA method 3630 C, Silica gel cleanup; 1996. Available from: https://www.epa.gov/sites/default/files/2015-12/documents/3630c.pdf

USEPA (1996) EPA method 3660 B, Sulphur cleanup; 1996. Available from: https://www.epa.gov/sites/default/files/2015-12/documents/3660b.pdf

USEPA (1998) Great Lakes dredged material testing and evaluation manual.

Van Dyck I, Vanhoudt N, Batle JV, Horemans N, Van Gompel A, Nauts R, Vangronseveld j (2023) Uptake of Co, Cs, Mn, Ni and Zn by *Lemna minor* and their effects on physiological and biochemical functions. *Environmental and Experimental Botany*, 213, 105440. https://doi.org/10.1016/j.envexpbot.2023.105440

van Woudt BD (1959) Particle coatings affecting the wettability of soils, *Journal of Geophysical Research*, 64, 263 – 267, https://doi.org/10.1029/JZ064i002p00263

Varga M, Horvatić J, Čelić A (2013) Short term exposure of *Lemna minor* and *Lemna gibba* to mercury, cadmium and chromium. *Open Life Sciences*, 8(11), 1083–1093. https://doi.org/10.2478/s11535-013-0238-1

Vejahati F, Zhenghe X, Gupta R (2010) Trace elements in coal: associations with coal minerals and their behavior during coal utilization – a review. *Fuel*, 89:904–11. https://doi.org/10.1016/j.fuel.2009.06.013

Veneris M, Farid A (2024) Finer Measurement Scales for Induced Hydrophobicity Using the Water Droplet Penetration Test. *Geotechnics*, *4*(2), 581-603. https://doi.org/10.3390/geotechnics4020032

Vo TL, Nash W, Del Galdo M, Rezania M, Crane R, Nezhad MM, Ferrara L (2022) Coal mining wastes valorization as raw geomaterials in construction: A review with new perspectives. *Journal of Cleaner Production*, 336, 130213. https://doi.org/10.1016/j.jclepro.2021.130213

Wagner RH, Lemos de Sousa MJ (1983) The Carboniferous Megafloras of Portugal - A revision of identifications and discussion of stratigraphic ages. In: M. J. LEMOS DE SOUSA & J. T. OLIVEIRA, Eds, The Carboniferous of Portugal. *Memorias do Serviço Geologico do Portugal*, 29: 127-152.

Wagner RH, Ribeiro A, Lemos de Sousa MJ (1984) Bacia Carbonífera do Douro. Reinterpretação da Geologia do sector Germunde-Choupelo. Recomendações para a investigação geológico-mineira deste sector e de sectores anexos. Fornelo. 17 pp. (Relatório inédito).

Wang J, Tomita A (2003) A chemistry on the volatility of some trace elements during coal combustion and pyrolysis. *Energy & fuels*, *17*(4), 954-960. https://doi.org/10.1021/ef020251o

Ward CR (2016) Analysis, origin and significance of mineral matter in coal: An updated review. *International Journal of Coal Geology*, *165*, 1-27. https://doi.org/10.1016/j.coal.2016.07.014

Warith MA, Yong RN (1991) Landfill leachate attenuation by clay soil. *Hazardous Waste and Hazardous Materials*, *8*(2), 127-141. https://doi.org/10.1089/hwm.1991.8.127

Warrick AW (1992) Models for disc infiltrometers. *Water Resources Research*, *28*(5), 1319-1327. https://doi.org/10.2136/sssaj1993.03615995005700030001x

Weissmahr KW, Haderlein SB, Schwarzenbach RP (1998) Complex formation of soil minerals with nitroaromatic explosives and other π-acceptors. *Soil Science Society of America Journal*, *62*(2), 369-378. https://doi.org/10.2136/sssaj1998.03615995006200020012x

Welch C, Barbour SL, Hendry MJ (2021) The geochemistry and hydrology of coal waste rock dumps: A systematic global review. *Science of the Total Environment*, *795*, 148798. https://doi.org/10.1016/j.scitotenv.2021.148798

Xu F, Chu M, Hao C, Zhou L, Sun X, Gu Z (2022) Volatilization characteristics and relationship of arsenic and sulphur during coal pyrolysis. *Fuel*, *315*, 123223. https://doi.org/10.1016/j.fuel.2022.123223

Yan R, Gauthier D, Flamant G (2001) Volatility and chemistry of trace elements in a coal combustor. *Fuel*, *80*(15), 2217-2226. https://doi.org/10.1016/S0016-2361(01)00105-3

Yim, Jin Hee, Kyoung W. Kim, and Sang D. Kim (2006). Effect of hardness on acute toxicity of metal mixtures using Daphnia magna: Prediction of acid mine drainage toxicity. *Journal of hazardous materials* 16-21. https://doi.org/10.1016/j.jhazmat.2005.11.107

You X, Liu S, Dai C, Guo Y, Zhong G, Duan Y (2020) Contaminant occurrence and migration between high-and low-permeability zones in groundwater systems: A review. *Science of the total environment*, *743*, 140703. https://doi.org/10.1016/j.scitotenv.2020.140703

Younger PL (2002) Coalfield closure and the water environment in Europe. *Mining Technology*. https://doi.org/10.1179/mnt.2002.111.3.201

Younger PL (2004) Environmental impacts of coal mining and associated wastes: a geochemical perspective. *Geological Society, London, Special Publications*, *236*(1), 169-209. https://doi.org/10.1144/GSL.SP.2004.236.01.12

Yu LE, Hildemann LM, Niksa S (1998) Trends in Aromatic ring number distributions of coal tars during secondary pyrolysis. *Journal of Energy and Fuel* 12. 450–456.

Yuan H, Li T, Ding X, Zhao G, Ye S (2014) Distribution, sources and potential toxicological significance of polycyclic aromatic hydrocarbons (PAHs) in surface soils of the Yellow River Delta, China. *Marine Pollution Bulletin* 83, 258–264. https://doi.org/10.1016/j.marpolbul.2014.03.043

Zhang K, Farahbakhsh K (2007) Removal of native coliphages and coliform bacteria from municipal wastewater by various wastewater treatment processes: Implications to water reuse. *Water Resource* 41, 2816–2824. https://doi.org/10.1016/j.watres.2007.03.010

Zhang R (1997) Infiltration models for the disk infiltrometer. *Soil Science Society of America Journal*, 616,1597–1603.

Zhao L, Dai S, Nechaev VP, Nechaeva EV, Graham IT, French D (2019) Enrichment origin of critical elements (Li and rare earth elements) and a Mo-U-Se-Re assemblage in Pennsylvanian anthracite from the Jincheng Coalfield, southeastern Qinshui Basin, northern China. *Ore Geology Reviews*, *115*, 103184. https://doi.org/10.1016/j.oregeorev.2019.103184